Characterisation of dysregulated proteins in macrophages infected with *Mycobacterium smeg*matis focusing on matrix metalloproteases and their effectors

Palesa Pamela Seele
SLXPAL001

SUBMITTED TO THE UNIVERSITY OF CAPE TOWN
In fulfilment of the requirements for the degree:

Doctor of Philosophy

Faculty of Health Sciences
Department: Integrative Biomedical Sciences
Division: Chemical and Systems Biology
UNIVERSITY OF CAPE TOWN

Supervisor: Professor Edward Sturrock
Co-Supervisor: Professor Jonathan Blackburn

Declaration

I, ***Palesa Pamela Seele***, hereby declare that the work on which this dissertation/thesis is based is my original work (except where acknowledgements indicate otherwise) and that neither the whole work nor any part of it has been, is being, or is to be submitted for another degree in this or any other university.

I empower the university to reproduce for the purpose of research either the whole or any portion of the contents in any manner whatsoever.

Signature: Signed by candidate

Date: …04 June 2019…

Dedications

I dedicate this work to my beloved

'ntatemoholo' Edmund Kaunyane Seele for being the inspiring, loving and kind spirit.

And to

Professor Bongani Mayosi

For embodying excellence and instilling hope.

Acknowledgements

My sincere appreciation to my supervisor Prof. Edward Sturrock and co-supervisor Prof. Jonathan Blackburn for affording me the opportunity to work on this project and in their labs. Thanks for all your efforts.

Thank you to everyone in the Sturrock's Lab, especially Sylva, Dr. Lubbe and Vinasha, for your motivation, advice and support. I learned a lot from you. Your contribution did not go unnoticed especially during lab meetings. Thanks to Sylva for proof-reading my draft.

Thank you to the Blackburn Lab and a special thanks to Dr. Calder, Dr. Hermann and Dr. Nel for helping with the preparation and running of my samples. Thanks to Dr. Calder for going through my data analysis and proof-reading my draft. Thank you to Dr. Mlamla for listening and always willing to help.

I would like to acknowledge Dr. Kevin Dzobo for the encouraging talks, the MMRU for letting me use their Perkin Elmer fluorometer, Robbie for helping with FACS, Suzanne for the microscopy and CIDRI for the CD11b antibody.

I acknowledge the NRF, MRC and Marion Beatrice Waddel award for funding.

A special thanks to my mentor Prof. Mpiko Ntsekhe for allowing me his time and space, and sound advice. My sincere appreciation to Dr. Ndlovu and Prof. Hendricks for mediating and helping resolve the challenges I was facing. To Prof. Dandara for his encouraging words and listening.

Lastly, to my family and friends. Thank you for the love and support. To the God above, the one within and the ones who have passed on, without you I wouldn't have made it!

Abstract

Cavitation is a key facilitator in transmission of *Mycobacterium tuberculosis* (*M. tb*). Upregulation of matrix metalloproteases (MMPs) has been documented in patients with tuberculosis (TB), while their tissue inhibitor (TIMPs) levels remained the same. Animals which can develop cavities have well-conserved MMP-1 orthologs suggesting a pivotal role of MMP-1 in cavitation. The migration of immune cells to the site of infection and maturation of the granuloma is associated with MMP-9 expression. Our understanding of the phenotypic changes induced by *Mycobacterium smegmatis* (*M. smeg*) in THP-1 macrophages is central to understanding its avirulent nature especially its effects on MMPs. The aim of this study was to evaluate the role of MMP-1 and MMP-9, and their effectors in macrophages infected with *M. smeg*. Differentiated THP-1 monocytes were incubated in serum-free media with or without bacilli. Thereafter, the secretome and lysate were harvested at different time points. The activity of MMPs was analysed by zymography. The activity of MMP-1 and MMP-9 were specifically determined using an MMP-1 fluorogenic assay and a non-fluorogenic MMP-9 substrate monitored using the HPLC. Discovery proteomics was performed for the 18-hour time point with the use of mass spectrometry. The generated data was used to evaluate dysregulated proteins and those that act as upstream and downstream effectors of MMPs. The phenotypic changes induced by *M. smeg* were also analysed. In addition to that, the hosts' response to lipoarabinomannan H37Rv (LAM) treatment was assessed by discovery proteomics and zymography. There was an increase in gelatinase activity of secreted MMP-9 which was maintained between the 1 and 18-hour time points. The fold difference in activity between uninfected and infected declined at 24 hours, and at the 72-hour time point the uninfected was slightly higher versus the infected. The data also suggests a switch in the proteolytic repertoire of the macrophages between the 6- and 18-hour time points to one that potentially generates the same degradation products as the uninfected macrophages. The intracellular gelatinase activity of MMP-9 (82 kDa) was not significantly altered by the *M. smeg* infection, in fact the activity was slightly higher in the uninfected in the 18 and 24-hour time points.

In contrast to MMP-9, MMP-1 was secreted in the later time points and was significantly decreased by the infection. This supports the postulation that upregulation of MMP-1 is specific for *M. tb* infection. The proteomics data depict significant upregulation of MMP-9 in the lysate and secretome, while TIMP-1 was exclusively expressed and secreted by infected macrophages, validating the non-destructive ECM phenotype induced by *M. smeg*. The dysregulation of IL-1β and COX pathways were implicated in the overexpression of MMP-9, as well as tRNA aminoacylation in alternative splicing of MMPs. The GO enrichment of exosomes is postulated to play a role in the recycling of MMP-9. Intercellular communication is hypothesised to be delivered to neighbouring cells through exosomes carrying DNA, RNA, proteins and DNA/RNA binding proteins, and via signalling scaffolds formed by the 14-3-3 proteins amongst others. LAM treatment did not induce dysregulation in the activity of expressed and secreted MMP-9, however, TIMP-1 was upregulated explaining the lack of differential gelatinase activity between treated and non-treated macrophages. The C-type mannose receptor 2 (MRC2) and C-type lectin domain family 11 (CLEC11A) were only expressed by the LAM-treated macrophages and may partake in the recognition and uptake of *M. tb*. Interestingly, the data indicates the presence of chromatin in the secretome which may be responsible for the formation of extracellular traps (NETs) and facilitating the transport of LAM across the glomerular basal membrane (GBM) through exosomes. Inhibition of MMP activity by TIMPs could result in decreased aggregation of NETS (aggNETS) that trap the LAM from being transported by binding to the chromatin. This decreases the concentration of LAM in urine and means MMP inhibitors that chelate the active-site zinc could decrease the sensitivity of urine-LAM detection kits.

Table of Contents

List of Figures

List of Tables

Abbreviations

ACN	Acetonitrile
AIDS	Acquired immunodeficiency syndrome
APMA	4-aminophenylmercuric acetate
APOE	Apoliprotein E
BCA	Bicinchoninic assay
BSA	Bovine serum albumin
CD11b	Cluster of differentiation 11B
CD4	Cluster of differentiation 4
CENPA	H3-like centromeric protein A
CFP-10	10 kDa culture filtrate antigen
CID	Collision induced dissociation
COX II	Cyclooxygenase-II
CTGF	Connective tissue growth factor
DMSO	Dimethyl sulfoxide
DTT	Dithiothreitol
ECM	Extracellular matrix
EDT	Electron induced dissociation
EDTA	Ethylenediaminetetraacetic acid
ER	Endoplasmic reticulumn
ESAT-6	Early secretory antigenic target-6
ESI	Electron spray ionisation
FACS	Fluorescence-activated cell sorting
FASP	Filter aided sample preparation
FCS	Foetal calf serum
FDR	False discovery rate
FRET	Fluorescence resonance energy transfer
Gal-3	Galectin 3
GMC-SF	Granulocyte macrophage colony-stimulating factor
HCD	High-energy collision dissociation
Hemopexin	Hx
HIV	Human immune virus
HPLC	High performance liquid chromatography
iBAQ	Intensity based absolute quantitation
IFN-γ	Interferon-gamma
IL-10	Interleuken-10
IL-1β	Interleuken-1Beta
IL-4	Interleuken-4
IL-6	Interleuken-6
IL-8	Interleuken-8
LAM	Lipoarabinomannan
LC-MS/MS	Liquid chromatography-tandem mass spectrometry
LFQ	Label free quantitation
LPS	Lipopolysaccharide

LRP-1	Lipoprotein receptor-related protein-1
LRP-2	Lipoprotein receptor-related protein-2
LTA4H	Leukotriene A4 hydrolase
MALDI	Matrix-assisted laser desorption and ionisation
McolA	Murine collagenase-like A
MMPs	Matrix metalloproteases
MOI	Multiplicity of infection
MS	Mass spectrometry
Mycobacterium smegmatis	*M. smeg*
Mycobacterium tuberculosis	*M. tb*
NET	Neutrophil extracellular traps
NFκB	Nuclear factor kappa B
NGAL	Neutrophil gelatinase-associated lipocalin
OADC	Oleic albumin dextrose catalase
OD_{580}	Optical density at wavelength of 580 nm
PBS	Phosphate buffer saline
PDI	Protein disulphide isomerase
PGE_2	Prostaglandin-2
PMA	Phorbol-12-myristate-13-acetate
PTM	Post-translational modification
RD1	Region of difference 1
RIPA	Radioimmunoprecipitation assay
RPMI-media	Roswel park memorial institute media
S100A8	S100 calcium-binding protein A8
S100A9	S100 calcium-binding protein A9
SCX	Strong cation exchange
SDS	Sodium dodecyl sulfate
SDS-PAGE	Sodium dodecyl sulfate-polyacrylamide gel electrophoresis
SEM	Standard error of mean
STRING	Search tool for retrieval of interacting genes/proteins
TB	Tuberculosis
TFA	Trifluoroacetic acid
TGF-β	Transforming growth factor-Beta
Th1	Tcell helper-1
Th2	Tcell helper-2
TIC	Total ion chromatogram
TIMPs	Tissue inhibitors of matrix metalloproteases
TNF-α	Tumour necrosis factor alpha
TOF	Time-of-flight
VEGF	Vascular endothelial growth factor
WHO	World health organisation
α-CHCA	Alpha-cyano-4-hydroxyccinamic acid

Chapter 1

Introduction and literature review

1.1 Tuberculosis: Burden of disease and efficiency of transmission

Tuberculosis is one of the oldest diseases known to mankind dating as far back as the earliest migration and civilization of humans. Initially thought to be a hereditary disease, it was only in 1882 that Robert Koch demonstrated that in fact TB was caused by *Mycobacterium tuberculosis* (*M. tb*) (Ahidjo *et al.* 2016). TB is a highly infectious disease that propagates in humans through aerosol transmission. Only 10% of the infected individuals develop active TB and the remaining can contain or clear the infection (Kaplan *et al.* 2003;van Crevel *et al.* 2002). The burden of this disease has since risen due to co-infection with the immuno-compromising HIV/AIDS. The world health organisation predicts that there will be 1 billion new *M. tb* infections, 150 million new active TB cases and 37 million TB-related deaths by year 2020. Africa bares the most burden with South Africa recording an alarming 155 743 TB cases in 2014 (WHO, 2014).

Cavitation has been recognised as one of the key factors in transmission of TB. A single cavity is known to harbour 10^7 to 10^9 active bacilli and presents an ideal environment for rapid bacterial growth since they are isolated from the immune system (Nedeltchev *et al.* 2009). In turn, bacteria capitalise by mutating, forming strains that are immune and therapy resistant. This undermines the success of existing therapeutic drugs such as isoniazid and rifampicin influencing the emergence of drug resistant strains. Another factor posing a challenge is the rate of relapse, with cavitary lung disease being one of the key causes. The estimated relapse rate in patients with cavitary disease is between 21 to 25% and in some cases, this was observed after only 2 months of therapy (Nedeltchev *et al.* 2009). The mechanisms and mediators of cavity formation are yet to be fully described given the inherent complexity of the host and bacterial interactions. Studies toward understanding the host's response is novel and discovery of possible host targets is a critical area of research hence the interest of the current study.

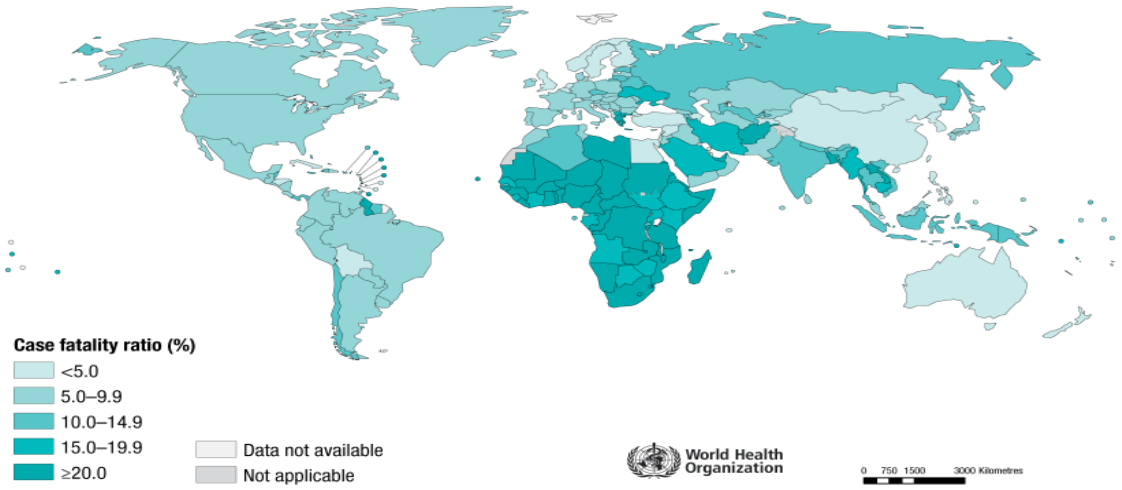

Figure 1-1: World map representing the rate of fatalities due to tuberculosis. Africa is mostly affected as indicated by darker areas. [Picture was adapted from WHO website, 2014].

1.2 Postulated mechanism (s) of cavity formation in TB

Although granuloma formation may be common in some diseases it is one of the pathological hallmarks that is best described in *M. tb* infection. Its function is to contain the infectious bacilli from spreading, however, the outcome of its formation is complex since it is also believed to be 'hi-jacked' by bacteria for replication and survival (Salgame 2011). The granuloma is well-structured (Figure 1-2) and is composed of monocytes, macrophages, dendritic cells (DC), T- and B- cells (small lymphocytes) and natural killer cells (large lymphocytes). Surrounding it, is a layer of fibroblasts that separate it from the lung tissue (Dartois 2014). The fibrotic layer surrounding the granuloma is meant to benefit the host by preventing active disease and dissemination of the bacteria but also inhibits vascularisation making the delivery of drugs to the bacteria which can still replicate under anaerobic conditions difficult.

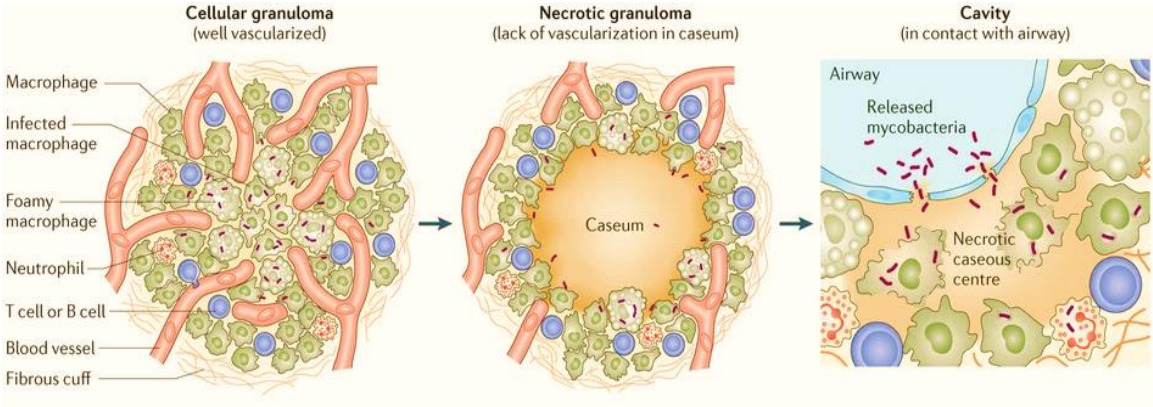

Figure 1-2: Schematic representation of different stages of the granuloma. Cells making up the granuloma are indicated along with their arrangement. [Adapted from (Dartois 2014)].

When a droplet of *M. tb*-containing nuclei is inhaled, a series of events are triggered upon reaching the lung. The initial encounter of the bacilli is with the residential alveolar macrophages where it is recognised by several receptor types. These include Toll-like receptors, Fc receptors, mannose receptors, scavenger receptors and complement receptors (Flannagan *et al.* 2009;Korb *et al.* 2016). Intriguingly, these receptors seem to confer different responses to macrophages stimulated with *M. tb*. For example *in vitro* studies investigating the ligation of Fc receptors to macrophages showed production of reactive oxygen intermediates and promotion of phagosome-lysosomal fusion, while complement receptor 3 prevented maturation of the phagosome (Sakamoto 2012). Recognition of the bacilli leads to phagocytosis by the macrophages which in turn causes the release of cytokines and chemokines. Cells of the immune system such as monocytes, macrophages, dendritic cells and neutrophils are then recruited to the site of infection where monocytes are differentiated to macrophages. Neutrophils and dendritic cells can engulf bacteria not phagocytosed by the alveolar macrophages. The adaptive immune system will be stimulated by the migration of activated alveolar macrophages and dendritic cells from the site of infection to the lung lymph nodes where they prime T-cells and recruit lymphocytes as components of the granuloma (Dheda *et al.* 2010). For these events to occur, namely the migration of cells, the basal membrane has to be broken down. As bacilli continue to replicate and grow within the granuloma, cells may undergo necrosis and in time form what is referred to as a 'caseous' necrosis centre owing to its cheese-like

appearance. If the caseous centre liquefies, it can spill into the airways leaving a cavity in the lungs. Aerosol transmission will occur once the infected individual coughs out the bacilli which will ultimately be inhaled by a susceptible individual. Another proposed mechanism of cavity formation is through sites of lipoid pneumonia, also requiring tissue remodelling (Elkington *et al.* 2011b;Korb *et al.* 2016). It is suggested that bacterial infection induces an imbalance in the efflux and influx of the hosts lipids culminating in the accumulation of lipids thereby transforming macrophages to foamy macrophages. These foamy macrophages, which can also form by engulfment of phagocytic cells, are a source of bacterial persistence that causes progression of disease to cavity formation. The architecture of the granuloma seems to aim for a balance of pro- and anti-inflammatory immune responses, where the caseous necrotic centre and cells that surround it express effectors that support the earlier and the latter, respectively (Marakalala *et al.* 2016). Interestingly in the same study the lipid-based inflammatory factor, LTA4H was expressed more abundantly in the necrotic caseum when compared to solid granulomas, where the necrotic centre was mostly composed of macrophages. What was also important to note was that the outermost cells of the granuloma in addition to increased expression of protein synthesis machinery (ribosomal and ER proteins) elicited a more reducing environment contrasting its necrotic centre. It is apparent that the mechanism of *M. tb* transmission is highly complex and efficient. This highlights the importance of attenuation of transmission in combating TB. What is also evident is that remodelling of the extracellular matrix is an integral component of cavity formation and dissemination from the lung interstitium into the airways for transmission. Studying host proteases such as MMP-1 that are involved and factors downstream and upstream of them is therefore essential (Elkington *et al.* 2011a).

1.2.1 Phagocytosis of bacilli and lysosomal fusion

The persistence of Mycobacteria owes to a large part its complex ability to inhabit the host environment by escaping killing and exploiting it for its survival (Case and Samuel 2016;Pieters and Gatfield 2002). It does this by a series of steps that uses the hosts proteins and lipids (including glycolipids) essential for phago-lysosomal fusion and/or using its own proteome to mimic that of the host for its survival. Phagocytosis is a process that cells, including the professional phagocytes such as macrophages, neutrophils and dendritic cells, employ to engulf extracellular material such as nutrients, bacteria, antigens and apoptotic cells which in this case is referred to as efferocytosis. It involves a series of steps such as, binding of the particle to a receptor, receptor clustering, cytoskeletal re-organisation which causes the extension of pseudopodia and membrane re-organisation, and finally entry of the ingested particle enclosed by the membrane leading to formation of the phagosome. This is followed by phagosomal maturation (Figure 1-3) entailing sequential interaction and fusion with endosomal compartments and cellular organelles causing the exchange of bactericidal and antigen processing molecules (Flannagan *et al.* 2009). The final and critical step is the fusion of the phagosome with the late endosomal/lysosomal compartments where majority of the bacterial killing occurs by hydrolases and bactericidal molecules. At this stage the phagosome has undergone intense acidification steps becoming more acidic with fusion to the lysosome. The pH has been documented to drop from 7.4 to 4.5 (Flannagan *et al.* 2009). This highlights the importance of pH in the spatial and temporal recruitment of different proteases such as matrix metalloproteases and cathepsins, which in general degrade the ECM optimally around pH 7 and 4.5, respectively. The drop in pH is largely influenced by recruitment of the proton pumping V-ATPases.

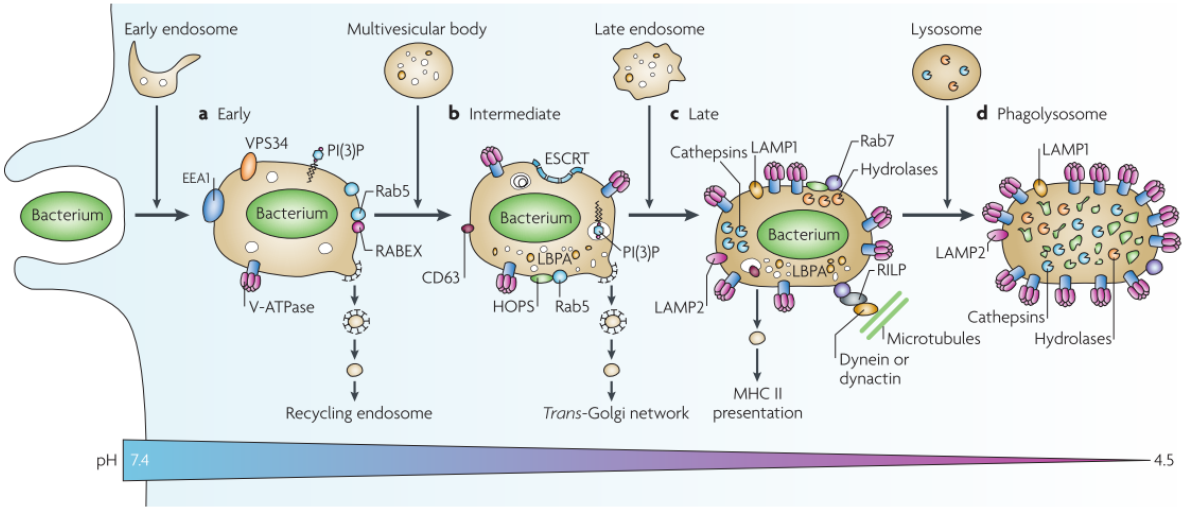

Figure 1-3: The maturation process of the phagosome. The series of steps leading to phagosome-lysosomal fusion and some of the essential markers acquired during this process have been indicated [Adapted from (Flannagan *et al.* 2009)].

Binding of bacilli is facilitated by recognition through pattern recognition receptors and by host factors such as opsonins (IgG and complement molecules) which bind to the Fcγ and complement receptor 3 (Flannagan *et al.* 2009;Sano *et al.* 2003). Galectin-3 (Gal-3) is a member of the lectin family of proteins that binds to β-galactoside. It functions both extracellularly in cell-cell adhesion, cell-ECM adhesion, cell activation and induction of cell migration such as neutrophils, monocytes and macrophages (Sano *et al.* 2003). Intracellularly it has been documented to be involved in inflammation, pre-mRNA splicing, cell cycle regulation and apoptosis. Gal-3 is also implicated in the opsonisation of apoptotic macrophages and their clearance. Accumulation of Gal-3 on the surfaces of phagosomal membranes that were generated from *Mycobacterium bovis* (BCG) infected macrophages (murine bone marrow-derived) was observed in macrophages that contained live rather than dead bacilli (Beatty *et al.* 2002). Some of the important proteins that are involved in the phagosomal maturation are summarised in Figure 1-3. The direct and specific participation of MMPs in these series of steps has not been exhaustively researched and documented, however MMPs can form direct/indirect interactions with some of the proteins involved such as v-ATPase, cathepsins, Gal-3 and the actin/microtubule family of proteins which are employed for cytoskeletal remodelling during phagocytosis (Bildyug 2016;Chen *et al.* 2014;Christensen and Shastri 2015;Feeley *et al.* 2017;Ochieng *et al.* 1994).

1.3 Components of the lung extracellular matrix

The lung is largely comprised of connective tissue which is intricately maintained by a balance between its components and proteases responsible for their turnover. The alveoli are mainly supported by fibrillar collagens and elastin providing the elastic and tensile strength to the lung with collagen I and III being the dominant components (Davidson 1990;Elkington *et al.* 2011a;Toshima *et al.* 2004). Additionally, the interaction of the extracellular matrix with cells is facilitated by adhesive molecules such as integrins, cadherins, fibronectin, laminin, thrombospondin, vitronectin and entactin. Under neutral pH physiological conditions, matrix metalloproteases are mainly responsible for the degradation of the ECM and its remodelling, hence their implicated role in disease pathologies when dysregulated.

1.3.1 Matrix metalloproteinases (MMPs): Structure and function

Matrix metalloproteinases (MMPs) are zinc-dependent endopeptidases belonging to the metzincin superfamily, which also includes the ADAMs (a disintegrin and metalloproteinases) (Jackson *et al*., 2006). The first MMP was discovered in metamorphosing tadpoles in 1962 (Gross and Lapiere 1962) by the ability of the respective tissue extracts to degrade fibrillar collagen at neutral pH (Gross and Lapiere 1962, this was then appropriately named MMP-1 or interstitial collagenase (Pardo and Selman 2005). To date, there are 28 membrane-bound and secreted vertebrate MMPs, 24 have been discovered in humans. Their substrate specificity (Figure 1-4), protein structure and localisation in the cell determines their classification (Klein and Bischoff 2011;Tokito and Jougasaki 2016) . Amongst the membrane-type MMPs, MMP-14 has collagenolytic activity and can degrade collagen I, II and III (Klein and Bischoff 2011). These membrane-type MMPs are anchored to the cell surface membrane through a transmembrane domain (type I) or a glycosyl-phosphatidylinosotol (GPI) anchor (Elkington *et al.* 2005b). In comparison, the *Drosophila melanogaster* expresses only two MMPs, *DmMMP-1* and *DmMMP-2 (LaFever et al. 2017)* which were initially thought to be soluble and GPI-anchored, respectively, however, both possess a GPI-anchoring domain. Interestingly, the mammalian antibodies cannot detect the *DmMMP-1* and *DmMMP-2* confirming that they are not orthologous. The full length recombinant proteins *DmMMP-1* and *DmMMP-2* specifically cleaved casein and

gelatin, respectively (LaFever *et al.* 2017). Despite their substrate specific classification there is overlapping ability to degrade certain substrates, for instance the gelatinases can degrade different types of collagens. MMP-1 can hydrolyse collagen I, II and III, but more preferentially collagen I and III (Davidson 1990;O'Connor and FitzGerald 1994). *In vitro*, the levels of collagen I and III had the most effect on the expression of MMP-1 compared to collagen IV (Kerkvliet *et al.* 2003). This was attributed to the spatial arrangement of fibroblasts with respect to the type of collagen. It was suggested that under normal conditions type IV collagen makes contact with fibroblasts whereas contact with type I or type III collagen is initiated during wound healing when increased cell proliferation is required (Kerkvliet *et al.* 2003). Thus, the spatiotemporal arrangement of the ECM and its molecules is essential in the progression of disease.

Fundamentally all MMPs contain a signal peptide, prodomain, catalytic domain and a hemopexin domain (except for MMP-7, MMP-23 and MMP-26) at the C-terminal region which partakes in catalysis either in substrate binding and/or recognition. The gelatinases, MMP-2 and MMP-9 contain fibronectin type II motifs while the MT-MMPs contain a transmembrane and cytoplasmic domain (Klein and Bischoff 2011). The zinc binding motif of the catalytic domain comprises three histidine residues (Figure 1-5), **HEXXHXXGXXH**, which coordinate the Zn in the active and inactive form. The role of the prodomain is to prevent accessibility of the zinc to a water molecule which is essential for catalysis. This is achieved through interaction of the zinc ion with the cysteine residue embedded in the prodomain's so called 'cysteine switch' motif, **PRCGXPD** (Klein and Bischoff 2011;Nagase *et al.* 2006;Ra and Parks 2007). This is represented by the ribbon structure in Figure 1-5. Additionally, there are 18 more cysteine residues within the structure including the two located in the signal peptide, seven pairs forming disulphide bonds, six located in the fibronectin repeats and two in the hemopexin domain, the other two are in hemopexin and in the loop region connecting the hemopexin and fibronectin repeat (Khan *et al.* 2012). During catalysis the glutamate residue in the catalytic domain and the Zn polarises the water molecule bound at the active site. The water acts as a nucleophile which in turn attacks the Scissile bond forming the Michaelis complex with the substrate (Ra and Parks 2007). There has been evidence that binding to gelatin or collagen IV induces activity of proMMP-9 via perturbation of its prodomain (Bannikov *et al.* 2002). In the same study the authors

highlight the lack of detection of active MMP-9 *in vivo* in both pathological and normal states, also the lack of proMMP-9 detection in tissues which had active MMP-9. In contrast to that, cancer cell lines express active forms of MMP-9 (Schröpfer *et al.* 2010). Others have suggested that in cancer cells, active MMP-9 is only present due to the presence of MMP-3 which activates it (Ramos-DeSimone *et al.* 1999). Thus, it is crucial to differentiate between active and non-active state of MMPs in different types of cells including the comparison between control and treated cells. This has implications on the phenotype of the MMP degradome. Targeting the proform of MMPs is one of the novel strategies that has been developed against proMMP-9 by Scannevin and colleagues (Scannevin *et al.* 2017).

MMPs are mainly recognised, as their name implies, for their ability to turn over and degrade the extracellular matrix. Also, of equal importance is their ability to process, amongst other substrates, the chemokines, cytokines, receptors and antimicrobial peptides (Ra and Parks 2007). Therefore, other vital processes they participate in, are immunity, apoptosis, cell migration, angiogenesis and wound healing (Zucchi *et al.* 2013). Their ability to localize to the cell surface is highly important with potential roles such as cell adherence and migration, invadopodia formation (Garamszegi *et al.* 2012;Van Doren *et al.* 2017;Watanabe *et al.* 2013) and cell-to-cell signal transduction which may be important in progression of diseases (Elkington *et al.* 2011b). It is hence not surprising that their expression and activity are tightly regulated under normal physiological conditions.

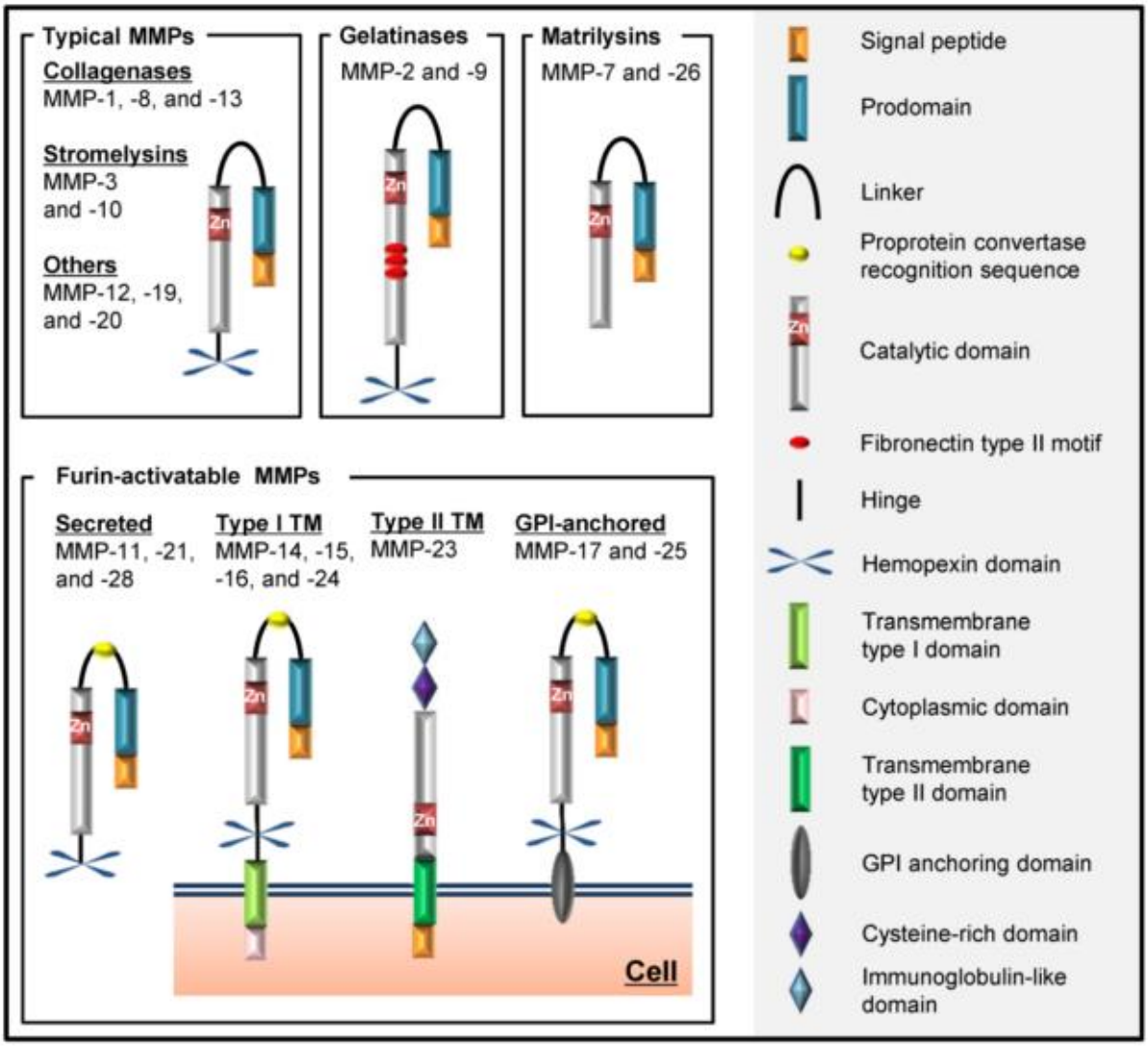

Figure 1-4 Basic structure and classification of MMPs. Structural components making up the different MMPs as per category (left-hand side) are depicted on the right-hand side [The picture was taken from (Tokito and Jougasaki 2016)].

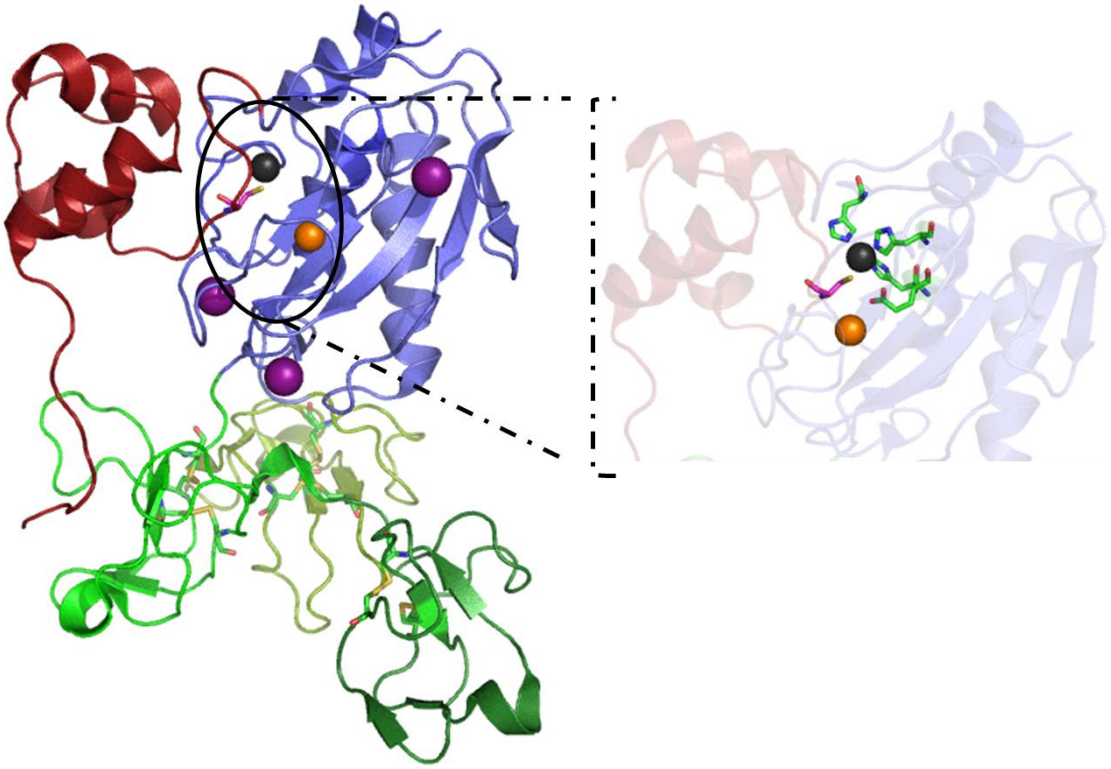

Figure 1-5 Cartoon representation of the structure of proMMP-9. The cysteine residue from the prodomain (red) is shown to interact with the N-domain's (blue) catalytic Zinc (black sphere). Fibronectin repeats (green) and the 12 cysteines forming disulphide bonds are indicated. The **HEXXHXXGXXH** motif that co-ordinates the Zinc is indicated on the right-hand side. Also included is the non-catalytic Zinc (orange sphere) and the calcium ions (purple spheres) [Generated using PyMOL v0.99 (DelaNo Scientific, 2006); PDB: 1L6J (Elkins *et al.* 2002)].

1.3.2 The expression, secretion and activation of matrix metalloproteases

Under homeostatic conditions, most of the MMPs are almost undetectable in tissues but are inducible in macrophages, fibroblasts, epithelial and endothelial cells (Pardo and Selman, 2005). They are differentially expressed during tissue remodelling and repair and also dysregulated in various diseased states including cancer, immune system disorders, diseases of the central nervous system (Fingleton 2008) and of course tuberculosis (Elkington *et al*., 2005). Their mode of action in these diseases is mostly through proteolysis of ECM components. Once MMPs are secreted, which is in their zymogenic form they are ultimately activated in the ECM where they also regulate cell-cell and cell-matrix signalling.

Their catalytic activity is regulated by control of gene expression, compartmentalisation, inhibition and by availability of substrate and affinity for the substrate (Ra and Parks 2007). MMPs are majorly and specifically inhibited through binding of endogenous tissue inhibitors of matrix metalloproteases (TIMPs). Other proteases able to inhibit their activity amongst others are α-macroglobulin, a general protease inhibitor and plasmin. As mentioned previously, breaking the Zn-cysteine interaction renders the MMP active by either allowing direct cleavage of the prodomain by other proteinases or autocatalysis, or reduction of the thiol group by oxidants. The prodomain of some MMPs, including MMP-11, MMP-28 and most of the membrane-anchored MMPs, MMP-14, MMP-15, MMP-16, MMP-17, MMP-23, MMP-24 and MMP-25 contain a furin-like proprotein convertase recognition site which allows proteolytic cleavage by furin or other proprotein convertases. This processing, which occurs intracellularly prior to secretion is relevant in about one third of MMPs containing the furin like protein sequence (Ra and Parks 2007). The furin itself is localised in the *trans*-Golgi network and has a secreted form referred to as shed furin (Cao *et al.* 2005). The rest of the MMPs, like MMP-1 and MMP-9, lack this recognition site suggesting they are secreted in their zymogenic form (Cao *et al.* 2005;Watanabe *et al.* 2001). Proteolytic cleavage of the prodomain can also be carried out by other proteins such as plasmin, kallikrein, other serine proteases such as trypsin and serine elastase, cathepsins or by other MMPs (MMP-2, MMP-3 and MMP-13) (Bouchet and Bauvois 2014;Christensen and Shastri 2015;Klein and Bischoff 2011;Saunders *et al.* 2005;Shamamian *et al.* 2001). The non-proteolytic activation of proMMPs can be artificially initiated by denaturants such as SDS during zymography or organomercuric compounds such as the widely used 4-aminophenylmercuric acetate (APMA). These cause allosteric perturbation of the Zn-cysteine interaction that primes autolytic and/or proteolytic cleavage of the MMP prodomain (Ra and Parks 2007). Activation of proMMPs with mercurial compounds such as APMA are only able to perturb the cysteine switch motif by direct interaction with the prodomain's cysteine residue but the MMP and TIMP complex is not perturbed. In addition to reacting to the prodomain's C75 residue, there is evidence of APMA interacting directly with the salt bridge forming residues R74 and D29 (Galazka *et al.* 1996). This was investigated using MMP-3. Production of reactive oxygen species can break the Zn-cysteine bond by reducing the thiol group of the cysteine residue.

Monocytes/macrophages secrete a 92 kDa proform of MMP-9 referred to as proMMP-9. The binding of TIMPs to MMPs is crucial and it can either be inhibitory or non-inhibitory. This is through direct binding of the TIMPs N-terminal domain to the active site and the latter by interaction of the C-terminal hemopexin domain and the TIMP C-terminal domain (Hamze *et al.* 2007;Roderfeld *et al.* 2007). The secretion and activity of MMP-9 in the extracellular matrix is controlled by TIMP-1. This was corroborated *in vitro* where MMP-9 was reported to co-localize with TIMP-1 in the Golgi apparatus and not the endoplasmic reticulum (Roderfeld *et al.* 2007) implying that the proMMP-9.TIMP-1 complex forms intracellularly prior to secretion. This is true for most cell types, with the exception of neutrophils which store and secrete MMP-9 from secondary granules not associated with TIMP-1. (Ogata *et al.* 1995;Roderfeld *et al.* 2007;Shapiro *et al.* 1995). Once in the ECM the proMMP-9.TIMP-1 can either be processed to yield the active form of MMP-9 or can remain in this form which may function to inhibit other MMPs by forming complexes with them (Figure 1-6). For example, the ternary complex that forms with MMP-3 abrogates the activity of MMP-3 (Figure 1-6), the same inhibitory mechanism occurs with MMP-1 (Ogata *et al.* 1995). Since MMP-3 can activate proMMP-9 in a stepwise manner (Ogata *et al.* 1992), the ternary complex formation may in turn act negatively in regulating the activation of proMMP-9.

The mechanism of activation also defines the subsequent forms of MMP-9 (Roderfeld *et al.* 2007). Cleavage of the propeptide accompanying APMA activation has been observed by circular dichroism to cause a decrease in the β-sheet content of MMP-2 (Crabbe *et al.* 1996) implying activation causes conformational perturbation. Activating the MMP-9.TIMP-1 complex with APMA yields the 'classic' active 82 kDa form while activation with MMP-3 yields the 82 kDa form which is further processed to the 50 kDa inactive form. Interestingly, incubating MMP-9 that is not in complex with TIMP-1 using APMA causes the conversion of the 92 kDa form to the 82 kDa followed by the 74 kDa intermediate within an hour of incubation. After four hours of incubation with APMA the 74 kDa intermediate is further converted to the 67 kDa active form lacking the C-terminal hemopexin domain. This suggests that the lack of further processing of MMP-9.TIMP-1 to the 67 kDa species is due to stabilisation of the C-terminal hemopexin by the TIMP-1. This 67 kDa form cannot be inhibited by TIMP-1 (Rossano *et al.* 2014). The C-terminal hemopexin domain does not show

any activity in zymography but its binding affinity to gelatin has been reported to be comparable to that of TIMP-1. Interestingly this domain has been reported to reduce the activity of MMP-9 (Roeb *et al.* 2002) This was demonstrated by use of gelatin zymography the activity of MMP-9 (1 ng and 0.2 ng) was inhibited by 61 and 71%, respectively. The inhibition was via its high affinity for gelatin rather than an antagonistic effect to MMP-9 (Ugarte-Berzal *et al.* 2016) since other substrates could be hydrolysed with the same efficiency despite the presence of the hemopexin domain.

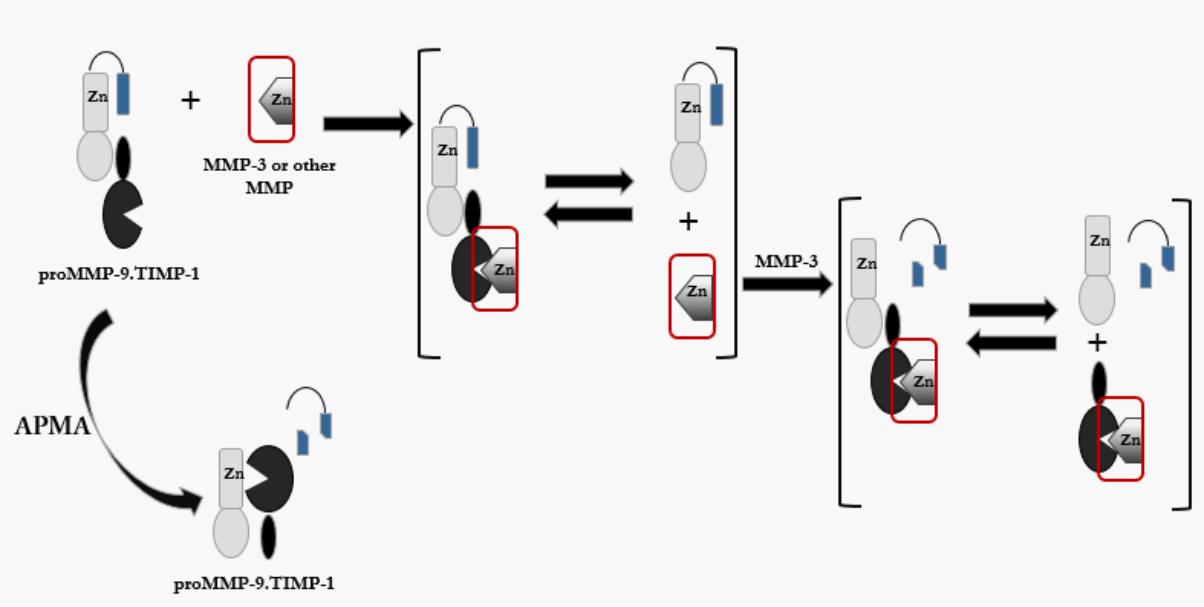

Figure 1-6 Activation of proMMP-9.TIMP-1 complex. Activation of the proMMP-1.TIMP-1 complex by MMP-3 (or other MMPs) and APMA/Trypsin. The proMMP-9.TIMP-1 complex inhibits MMP-3 (in other case MMP-1) with the MMP-9 catalytic site unbound [Picture is adapted from (Ogata *et al.* 1995)].

Under physiological conditions the C-terminal hemopexin domain of MMP-9 has been observed to inhibit not only angiogenesis an important factor that influences cavitation but also the migration of neutrophils and of colorectal cancer cells (Burg-Roderfeld *et al.* 2007;Spiller *et al.* 2011). MMPs form part of the major subgroup of the hemopexin superfamily. The hemopexin domain is associated with substrate recognition and binding, and has been reported to be responsible for the initial and local unwinding of the triple-helical collagen (Chung *et al.* 2004) which is followed by cleavage of the peptide bond at the unwound site.

Apparently, collagen binds at a pocket between the N- and C-domain and not directly to the hemopexins four-bladed propeller (Chen *et al.* 2011) which is affiliated with substrate recognition and binding.

Activation of proMMP-9 by trypsin cleavage of the propeptide has also been shown to be a stepwise process (Duncan *et al.* 1998), where complete cleavage to the 67 kDa form is observed after a 3-hour incubation with trypsin.

MMP-14 also referred to as membrane-type 1 matrix metalloprotease (MT-MMP-1) is a membrane bound collagenase that is also regulated by autolytic degradation, shedding, oligomerization and membrane trafficking (Wu *et al.* 2004). It is expressed as a 68 kDa zymogen containing a furin cleavage site which allows processing to the active 55 kDa form. Further cleavage at the linker region yields an inactive 34 kDa form (Wu *et al.* 2004). Only TIMP-2 and not TIMP-1 can inhibit MMP-14, and of importance is that the complex formation between TIMP-2 and MMP-14 catalyses the activation of proMMP-2. This ternary complex occurs via interaction of the TIMP-2 catalytic domain of MMP-14 and C-terminal hemopexin domain of proMMP-2.

1.3.3 Glycosylation of MMPs and effect in protein-protein interactions

Post-translational modification is a process that is exploited by cells for the modulation of proteins by specifically attaching chemical moieties to amino acids. This adds another layer of complexity and diversity to the functionality of proteins with respect to signal transduction, substrate (inhibitor) recognition/binding, metabolism, protein stability, folding and secretion. To date there are 200 types of PTMs that have been identified, these include glycosylation, phosphorylation, acetylation, ubiquitination, sumoylation, methylation and other forms (Kotra *et al.* 2002;Prabakaran *et al.* 2012).

Glycosylation involves the addition of oligosaccharides via N-glycosidic and O-glycosidic bonds. These modifications occur during translation and after folding in the Golgi and *trans*-Golgi, respectively (Boon *et al.* 2016). Glycans are important for the correct folding of proteins, protein-protein interactions and interaction of proteins with cell surface

molecules. Of all the MMPs, MMP-9 possesses the most glycosylation sites (Boon *et al.* 2016) with proMMP-9 having three N- and several O-glycosylation potential sites.

The O-glycosylation sites are mainly at the hinge region (Kotra *et al.* 2002) which comprises a proline rich stretch like α2(V) chain of collagen V. 14 potential sites are clustered in 50 amino acid region, thus MMP-9 is referred to being mucin-like in structure (Boon *et al.* 2016).

O-glycosylation has also been reported to influence the binding of its inhibitors including TIMP-1, LRP-2 (lipoprotein receptor-related protein-2) and LRP-1 (Duellman *et al.* 2015), the latter being essential for the re-internalisation of MMP-9. Also, this O-glycosylation site increases affinity for Gal-3 (Fry *et al.* 2006;Tandon and Sinha 2011). The N-glycosylation sites are at positions N38, N120 and N127 of the prodomain and the latter two at the catalytic domain, though the N127 site which is close to the gelatin binding domain is inaccessible to modification because of it being shielded from the solvent. (Kotra *et al.* 2002). However, the authors report that the N120 residue although being shown to be glycosylated does not partake in catalysis and substrate recognition suggesting another potential function for it. Interestingly desialyation has been reported to increase the activity of MMP-9 by perturbing its interaction with TIMP-1 (Boon *et al.* 2016;Wu *et al.* 2004).

Unlike MMP-9, MMP-14 (MT1MMP) contains only O-glycosylated sites, four in total, located in the linker region which is predicted to be important for catalysis. However, glycosylation is not important for collagenolysis but was found to be crucial for activation of proMMP-2. The authors suggest that a defect in MMP-14 glycosylation MMP-14 impairs the ability of TIMP-2 to facilitate its endocytosis hence affecting the activation of proMMP-2 (Wu *et al.* 2004). Differential glycoforms of MMP-14 were found in different cancer cell lines which suggests a role in pathology. Therefore, glycosylation may act as a regulatory mechanism that leads to differential MMP phenotypes repurposing their physiological functioning.

1.4 The role of matrix metalloproteinases (MMPs) in TB cavitation

The role of MMPs in *M. tb* granuloma and cavity formation has been emphasized (Elkington *et al.* 2011a;Elkington *et al.* 2007;Elkington *et al.* 2005a;Reece and Kaufmann 2012;Salgame 2011). Their role in TB cavitary pathogenesis is evolving, with particular interest in MMP-1 and MMP-9. Increased levels of MMPs, specifically MMP-9, were first identified in the bronchoalveolar fluid (BALF) of a TB patient (Chang *et al.* 1996). Severity of the disease as per extent of pulmonary lesion was later correlated with an increase in the levels of MMP-9 from the sera of TB patients (Elkington *et al.* 2007;Elkington *et al.* 2005a;Hrabec *et al.* 2002). Its function in granuloma cell recruitment and maturation, first reported in the zebra fish model is a well-documented phenomenon (Davis and Ramakrishnan 2009;Reece and Kaufmann 2012). This was also validated by use of MMP-9 knock-out mice which were shown to develop smaller granulomas with lesser macrophages recruited to the site of infection (Elkington *et al.* 2011a). Similarly, elevated levels of MMP-1, -2, -8 and -9 were detected in the pleural fluid of TB patients compared to those with heart failure (Elkington *et al.* 2011b) suggesting that *M. tb* is deliberately driving the upregulation MMPs.

Distribution of overexpressed MMPs varies within the cell types making up the granuloma. MMP-1 and MMP-7 were expressed in epithelioid and Langerhans cells, MMP-1 and MMP-9 in pulmonary epithelial cells and MMP-9 in epithelioid and multinucleated giant cells in tuberculosis of the lymph node (ref). Also, of note is that granulomas in an infected individual tend to vary in terms of their protein expression profile having an influence in the inflammation/immune response and ability to contain bacterial growth (Via *et al.* 2015). In granulomas of patients with tuberculosis of the central nervous system MMP-1, MMP-3 and MMP-9 were elevated (Elkington *et al.* 2011b). However, the levels of TIMPs in the above-mentioned studies were not elevated, again suggesting that *M. tb* infection induces this imbalance either as a host protective mechanism or for bacilli propagation. *Mycobacterial* factors that induce MMPs have not been investigated exhaustively. But, the *Mycobacterium* factor ESAT6 (early secretory antigenic target-6), is reported to stimulate MMP-9 expression in epithelial cells which in turn recruited new monocytes and macrophages to maintain granuloma formation and maturation (Davis and Ramakrishnan 2009;Volkman *et al.* 2010).

Animals have been used as models for TB studies, although they do not represent the complete repertoire of TB in humans (Converse *et al.* 1996;Elkington *et al.* 2011a;Nedeltchev *et al.* 2009). For instance, infected mice form cellular-like granulomas, but caseation and cavitation do not occur, similarly, guinea pigs form caseous necrosis without progression to cavitation. In rabbits though, necrotic granulomas do form with caseation, but only under certain conditions does liquefaction occur accompanied by cavitation (Nedeltchev *et al.* 2009). Of importance is that animals which do develop pulmonary cavities including humans, primates and rabbits have a conserved ortholog of MMP-1 (Elkington *et al.* 2011a). Also, mice do not express MMP-1 but its closest human ortholog McolA, is distantly related to it and shares only 58% amino acid identity (Pardo and Selman 2005). This strongly suggests that the lack of MMP-1 in mice is responsible for the lack in progression of disease to cavitation upon infection with *M. tb*. Even so, the mouse model has yielded key input in the probable role of MMP-1 in TB cavitation.

In wildtype mice infected with *M. tb*, McolA, MMP-8 and MMP-13 were not upregulated in the lungs, however McolA was expressed in the testis. *M. tb* infected MMP-1 transgenic mice depicted extensive damage of the lung tissue, but the architecture of the granuloma was unaffected, and the bacterial load was not increased. This led to the critical conclusion that ECM destruction and granuloma necrosis occur as separate events (Elkington *et al.* 2011a;Elkington *et al.* 2005a).

Granted that the mouse model has greatly facilitated the accumulated understanding of TB pathogenesis, it is even more crucial to note the importance of using the correct model since differences that maybe thought to be insignificant can in fact be fundamental in the pathophysiology of disease. The findings also give a strong indication that *M. tb* deliberately induces upregulation of MMP-1 and downregulation of TIMPs to yield an ECM degrading phenotype followed by cavity formation to promote dissemination. Children rarely form cavities upon *M. tb* infection. Interestingly, like adults, the MMPs are also upregulated, including MMP-1, MMP-7 and MMP-8 but in contrast the TIMPs (TIMP-1 and TIMP-3) are also elevated (Pavan Kumar *et al.* 2013).

Mycobacterial factors which drive these MMP upregulation have not been fully elucidated, however, *M. tb* strains which lack the region of difference 1 (RD1) gene, failed to cause MMP-1 upregulation, ECM damage and immunopathology (Elkington *et al.* 2011a;Elkington *et al.* 2011b). This RD1 gene which expresses the ESAT-6 and CFP-10 proteins, which are potent T-cell activators is absent in BCG, a strain which cannot cause cavities in humans (Dheda *et al.* 2010;Elkington *et al.* 2007). This suggests that the RD1 is a vital component in the pathogenesis of cavitation in humans.

In addition, *M. tb*-infected macrophages secrete detectable levels of MMP-1 compared to lipopolysaccharide (LPS) stimulated macrophages, whereas both LPS and *M. tb* increased MMP-7 secretion (Elkington *et al.* 2005a). Chang and colleagues have also indicated an upregulation of MMP-1 and MMP-9 mRNA when differentiated THP-1 macrophages were treated with lipoarabinomannan (LAM), one of the key components of the *M. tb* cell conferring virulence to the bacilli. An increase in MMP-9 activity correlated with increase in concentration of LAM treatment was also indicated by gelatin zymography (Chang *et al.* 1996). Since LAM is one of the breakdown products from the cell wall of *M. tb* it has been researched as a biomarker for TB (lung TB and TB pericarditis) diagnosis, however the mechanism by which it is processed and excreted in the kidney remains to be elucidated. Interestingly co-infection with HIV (with CD4 less than 100 cells/mm^3) enhanced the sensitivity of the urinary LAM diagnostic performance (Pandie *et al.* 2016).

It is also interesting to note that patients co-infected with HIV rarely present with cavitary TB (Munthali *et al.* 2014). In these patients and HIV negative controls MMP-1 was upregulated, however, the concentration of TMP-1 was lower in the latter (Elkington *et al.* 2011a). The ECM degrading phenotype characterised by elevation of MMPs is also depicted in sarcoidosis, a granulomatous pulmonary disease of unknown etiology. Like TB, bronchoalveolar fluid from sarcoidosis patients contained elevated levels of MMP-1, MMP-8, MMP-9 and MMP-13 with high collagenase activity. But cavitation is rarely reported in sarcoidoisis, which means additional/differential factors and pathways are required in TB cavitation that have not been fully understood.

1.5 Interaction of MMPs with other proteins

Protein-protein interactions are essential in regulating the function of proteins either as inhibitory or activating. Also, matrix metalloproteases have a broad spectrum of substrates aside from components of the ECM (Morrison *et al.* 2009) including CTGF, IL-8, APOE, Galectins, S100A8, S100A9, TNFα-pro and many others. They can also form complexes with other proteins, for example MMP-9 has been shown to form complexes via its C-terminal hemopexin domain suggesting a regulatory role with the respective proteins. These proteins include TIMPs, other MMPs, α2-macroglobulin, kallikrein, neutrophil gelatinase-associated lipocalin amongst others (Vemula *et al.* 2016). Neutrophil gelatinase-associated lipocalin and α2-macroglobulin have been shown to form disulphide bonds with the hemopexin domain. Since *Mycobacteria* is well-known for its ability to surpass the hosts immune and inflammatory system through the manipulation of its signalling pathways, better understanding of these pathways is thus important.

1.5.1 Pathways and intercellular networks involved in the regulation of MMPs

Two major pathways, p38 and extracellular signal-related pathway/mitogen activated protein kinase (ERK/MAPK) function in most cell types and they respond to direct *M. tb* infection and through cell-to-cell interactions. In macrophages, cyclooxygenase-II (COX II) and prostaglandin (PGE_2), which are downstream p38 have a predominant function. Treatment of TB by the COX targeting drug p-amino salicylic acid (PAS) has proven efficacious when administered with other TB drugs and it has been suggested to attenuate tissue distraction by inhibiting MMP-1 expression. At the transcriptional level, *M. tb*-induced MMPs are regulated by NFκB, activator protein-1 (AP-1) and signal transducer and activator of transcription 3 (STAT-3) signalling pathways.

The imbalance in the MMPs/TIMPs ratio in cavitary TB has been associated with the lack of promoter binding region of TIMP-1 (Elkington *et al.* 2011b) although other studies have discovered the presence of NFκB regulatory site about - 2.7 kb upstream of the TIMP-1 transcription site (Wilczynska *et al.* 2006). In addition to that, NFκB interacts with ESAT-6, this interaction might be essential in regulating the transcription of MMPs. Therefore,

different pathways may be switched on/off at different stages of infection to skew the ratio toward an increase in MMPs. Once these pathways are thoroughly understood then potential drug targets can be identified. These targets may have greater therapeutic potential over MMPs, which have diverse function in tissue homeostasis.

In TB pathology, intercellular networks are also integral in driving MMP expression. It has been shown that MMP-9 is upregulated by monocyte-monocyte networks; MMP-1 and MMP-9 are upregulated by monocyte-epithelial cell networks; and MMP-1 and MMP-3 are upregulated by monocyte-fibroblast networks whereby the latter is also able to activate MMP-1 (Elkington *et al.* 2005a;O'Kane *et al.* 2008). Through intercellular networks the upregulation of MMP-1 is not induced by a single cytokine but by a combination of two or more of the Th1 cytokines (Zhou *et al.* 2003). These cytokines include TNF-α, IL-1β, IFN-γ and GM-SCF. IFN-γ and GM-CSF stimulate the production of TNF-α resulting in the production of MMP-1 in macrophages (Zhou *et al.* 2003). Cytokine stimulation of MMP-1 is PGE_2-dependent, like LT4AH it is lipid-based inflammatory molecule. In contrast MMP-9 and TIMP-1 stimulation is PGE_2-independent in macrophages (Zhang *et al.* 1998b). Stimulation of MMP-9 by cytokines is higher compared to LPS which is PGE_2-dependent. In contrast macrophages stimulated with LPS released higher amounts of MMP-1 compared to cytokines. Also, MMP-9 and TIMP-1 could be induced by presence of the Th1 cytokines TNF-α, IL-1β or GM-CSF. MMP-1 was only detectable in the presence of GM-CSF with TNF-α or IL-1β or all three cytokines (Zhang *et al.* 1998b). This difference in the induction of MMP-1 and MMP-9 implies that they may be required at different stages of *M. tb* infection. The Th2 cytokines, IL-4 and IL-10 inhibited MMP and TIMP-1 expression via PGE_2.

Since cytokines are reported not to be upregulated in patients with TB, it means stimulation of MMP-1 *in vivo*, requires additional factors including *Mycobacterial* factors. A significant upregulation of MMP-1 and MMP-3 was observed when human fibroblasts were stimulated with a combination of cytokines, including TNF-α and oncostatin M (O'Kane *et al.* 2008;Wolf *et al.* 2011). Oncostatin M is a member of the IL-6 family and is said to be pro-angiogenic. It is expressed in monocytes and T-lymphocytes upon stimulation with LPS. MMP upregulation by OSM is PGE_2-dependent. In contrast, TIMP-1 and TIMP-2 were significantly downregulated.

1.5.2 Effects of MMPs on angiogenesis: Dissociation of the CTGF.VEGF$_{165}$ complex

Angiogenesis does not only play a major role in the pathology of TB and its progression but also in drug therapy. The early stages of granuloma formation are characterised by neovascularisation of the tubercle which has been attributed to a response in the VEGF signal (Korb *et al.* 2016). The increased blood vessels indicate that there is migration of dendritic cells, macrophages and lymphocytes to the infected area. When the serum levels of VEGF from patients with active and inactive pulmonary TB, and healthy controls were compared, levels were higher for active TB followed by inactive TB and healthy controls, respectively (Alatas *et al.* 2004).

Besides its collagenase activity MMP-1 has diverse functions in apoptosis, immunology and angiogenesis. In addition to collagen, MMP-1 can degrade other substrates including the connective tissue growth factor (CTGF), which is a downstream mediator of TGF-β. CTGF, also known as CCN2 belongs to the CCN family of extracellular matrix-associated heparin-binding proteins. Its functions include angiogenesis, ECM production, integrin expression and wound healing. Also, notably, it promotes granulation tissue formation (Hashimoto *et al.* 2002;Inoki *et al.* 2002). CTGF can complex with and inactivate the angiogenic factor VEGF$_{165}$. VEGF-A occurs in various isoforms that originate from alternative splicing of the same gene. The isoforms include VEGF$_{121}$, VEGF$_{145}$, VEGF$_{189}$, VEGF$_{206}$ and VEGF$_{165}$. VEGF$_{165}$ and VEGF$_{121}$, they are reported to have the greatest influence on angiogenesis and may account for about 98% of the expressed VEGF-A (Ozaki *et al.* 2002).

The most abundant isoform in the lungs is VEGF$_{165}$ (Marwick *et al.* 2006). VEGF$_{121}$, VEGF$_{165}$, and VEGF$_{189}$ are expressed in most tissue types, including human chondrocytes that form normal cartilage and to a larger extent in cartilage of osteoarthritis and rheumatoid arthritis. These tissues are known to be resistant to angiogenesis and the inhibition of VEGF by CTGF has been implicated in this phenomenon through the formation of the CTGF.VEGF$_{165}$ complex (Inoki *et al.* 2002). This complex has been localised to the extracellular matrix and CTGF has been said to anchor VEGF$_{165}$ to the extracellular matrix (Burgess *et al.* 2006).

Since both CTGF and VEGF are susceptible to degradation by proteolytic enzymes it would seem that the complex is a regulatory mechanism which can be disrupted by proteolysis (Hashimoto *et al.* 2002). MMP-1, MMP-2, MMP-3, MMP-13 and MMP-14 are able to degrade CTGF and not $VEGF_{165}$ which itself is degradable by plasmin, chymotrypsin and elastase. MMP-9 slowly degrades CTGF, while MMP-3 and MMP-13 degrade CTGF more efficiently than other MMPs including MMP-1. In the same study, it was found that the MMP cleavage sites are identical when incubation was with CTGF alone and with CTGF in complex with $VEGF_{165}$ given that the degradation fragments were identical. Some of these degradation fragments were detected in breast carcinoma (Hashimoto *et al.* 2002). Once $VEGF_{165}$ is released from the complex it is reactivated to induce angiogenesis. Therefore, it is important to investigate the influence of *M. tb* infection on the regulation of CTGF, $VEGF_{165}$ and CTGF.$VEGF_{165}$ complex formation in correlation to proteolysis by MMP-1 compared to MMP-9. This may give an indication of the possible roles of these MMPs in tissue remodelling at different time points of *M. tb* infection.

1.5.2.1 The role of angiogenesis in the pathology of tuberculosis

Extracellular membrane degradation can cause the release of the ECM/basement membrane-sequestered angiogenic factors such as VEGF, TGF-β and bFGF (Benjamin and Khalil 2012). Angiogenic factors can induce the expression of MMPs, and in turn the MMPs can increase their bioavailability. This induction of MMPs has been demonstrated in endothelial and stromal cells. The positive feedback loop may be another possible explanation for the upregulated MMP-1 and -9 in cavitary TB. Upregulation of VEGF has been reported in sarcoidosis and active pulmonary TB (Zucchi *et al.* 2013). Abe and colleagues investigated the relationship of VEGF with cavity formation in active pulmonary TB (Abe *et al.* 2001). Their study compared the serum levels of VEGF and cytokines (TNF-α and IL-8) between patients with cavities and those without cavities. VEGF was higher in the non-cavity group and the cytokine levels were not significantly different between the two groups. They concluded that overexpression of VEGF causes increased generation of blood vessels and oxygen supply, which hinders the formation of cavities in TB (Abe *et al.* 2001).

In another study which highlighted the role of angiogenesis in TB, Zielonka and colleagues examined the number of microvessels formed in mice post injection with lymphocytes or mononuclear cells (MNC) pre-treated with sera from TB patients or healthy donors (Zielonka *et al.* 2011). There was a significant decrease in the number of microvessels when mice were treated with lymphocytes pre-treated with TB sera compared to the MNC treated with same sera. In contrast, lymphocytes treated with sera from healthy donors caused a significant increase in number of microvessels compared to injection with MNC treated with same sera (Zielonka *et al.* 2011). The authors then concluded that *M. tb* infected monocytes develop a matrix-degrading phenotype which initiates angiogenesis. The anti-angiogenic role of CTGF has not been investigated in the pathogenesis of TB cavitation but it may be acquired for resistance to VEGF-induced angiogenesis leading to cavitation. In systemic sclerosis (SSc) fibroblasts, CTGF silencing with specific siRNA caused increase in MMP-1 and decreased TIMP-1 and collagen type I after stimulation with TGF-β (Ishibuchi *et al.* 2010). In contrast, the fibroblasts of normal subjects showed decreased collagen type I after stimulation with TGF-β and no increase in MMP-1. Therefore, there may be some overlap in the pathways that regulate the expression of MMP-1 and CTFGs

Both CTGF and VEGF have been implicated in the pathophysiology of cancer, including MMPs which have influence on tumour metastasis and invasion. In non-small cell lung cancer (NSCLC), administration of Bevacizumab, a monoclonal antibody targeting VEGF-A, although beneficial caused cavitation in the pulmonary lesions (Nishino *et al.* 2012). Cavitation occurred in 14% of patients treated with Bevacizumab and in another study where VEGF inhibitor was used, 24% of those patients developed cavities (Nishino *et al.* 2012). Some of these patients also showed interstitial abnormalities. Its thus not surprising that recent evidence suggests that *Mycobacteria* exploits angiogenesis for its own growth and dissemination (Oehlers *et al.* 2015;Polena *et al.* 2016). Therefore, it is critical to investigate the role of angiogenic factors in TB cavitation.

1.6 Infection of THP-1 macrophages with *Mycobacterium smegmatis* as an *in situ* model

The illustration of what manifests *in situ* during disease states by using systems *in vitro* poses various limitations one being choosing models that would closely resemble the system being studied. Phenotypic differences in macrophages are associated with their origin (e. g cell line, primary, human, mouse) accounting for the differences in their properties and interaction with *Mycobacteria* hence having the possibility of eliciting responses that differ slightly or majorly to the state *in situ*. Ultimately, downstream conclusions should be taken with careful consideration. Although the use of monocyte-derived macrophages (MDM) over cell line macrophages would be ideal for mimicking alveolar macrophages, there are advantages to using cell line macrophages further elaborated below. The THP-1 cell line was first established in the 1980s by Tsuchiya and colleagues (Tsuchiya *et al.* 1980), and it was derived from a male patient with acute monocytic leukaemia. They are morphologically alike primary monocytic cells. Post-differentiation with phorbol-12-myristate-13-acetate (PMA) these cells acquire the repertoire of monocyte-derived macrophages including a flat spindle-shaped like morphology that is adherent to the culture plate, with a low rate of proliferation and a higher rate of phagocytosis than do monocytic cells.

In addition to that, the THP-1 macrophages overexpress markers such as CD11b, acquire free ribosomes in abundance, and have well-developed Golgi apparatuses and rough endoplasmic reticula (Qin 2012). This makes them ideal and still relevant to date in mimicking *in vivo* conditions since they resemble primary and monocyte-derived macrophages. There are advantages to using these cells over monocyte-derived macrophages including longer periods of survival (in both liquid nitrogen storage and in culture), no donor variability and purification steps making them good for experimental reproducibility. Other studies have demonstrated successfully the exploitation of THP-1 macrophages as models of alveolar macrophages e.g. in *M. tb*-induced apoptosis (Riendeau and Kornfeld 2003), several studies have used the THP-1 macrophages as host response models mimicking *Mycobacterium* infections as it occurs *in vivo* (Kaewseekhao *et al.* 2015;Stokes and Doxsee 1999;Theus *et al.* 2004;Wong *et al.* 2018). Direct comparison

between differentiated THP-1 macrophages and monocyte-derived macrophages indicated that the percentage of macrophages that interacted with *M. tb* did not differ between the two, however the percentage of MDM's with bound zymosan were higher when compared to the THP-1 macrophages (Stokes and Doxsee 1999). The authors implied this being attributed to low expression levels of glucan and mannan receptors by the latter. Killing of the intracellular bacteria by isoniazid was similarly efficient between the cell types. Therefore, the similarity or contrasts of the elicited response depends on what is being investigated.

Mycobacterium smegmatis (*M*. *smeg*) which acquired its name in 1885 after isolation from human smegma (Reyrat and Kahn 2001) has been widely used as a model for the virulent *M. tuberculosis* because of its fast-growing, less laboriously intensity and ease of genetic manipulation nature. It has contributed immensely in understanding the pathogenesis of tuberculosis and drug development albeit its inability to disseminate in humans. Thus far, it has been established/estimated that its genome is approximately twice as large as that of *M. tb* and about 69.8% of 4034 of proteins encoded in *M. tb* (H37Ra) have orthologues in *M. smeg* (Altaf *et al.* 2010). In the same study, it was found that 48 to 58% of a library of inhibitors that were active against *M. tb* were effective in deterring the growth of *M. smeg*. Even so the discovery of the clinically used therapeutic drug diarylquinolines was discovered by using *M. smeg*. The dormancy of *M. tb* has been successfully modelled using *M. smeg* owing to the shared similarity of the responding genes from both strains to host conditions that trigger this phenomenon (Shiloh and Champion 2010). Therefore, the data extrapolation from infection model systems can serve as hypotheses of what occurs *in situ* and guide the process of drug discovery.

1.7 Aims and objectives

It is hypothesized that proteases, such as MMP-1 and MMP-9, including their effectors are involved in the macrophage response to *Mycobacterial* infection. Thus, the aim of the study was to evaluate the role of MMP-1 and MMP-9 including their effectors during a time course infection with *Mycobaterium smegmatis*.

This was achieved by:

1. Harvesting at different time points the lysate and media from differentiated THP-1 monocytes that are uninfected and infected with *M. smeg*.
2. Comparing the extracellular and intracellular activity of MMP-1 and MMP-9 between uninfected and infected, also between the different harvest time points.
3. Identifying upstream and downstream effectors of MMPs that may be influencing their activity and expression through generating proteomic data by mass spectrometry. This will be accomplished by:
    - Quantifying (label free) differentially expressed proteins (uninfected versus infected proteome, and between different time points).
    - Characterise the differentially expressed and secreted proteins and those that are exclusively expressed/secreted using gene ontology terms. STRING will then be used to assess if any of these proteins interact with MMP-1 or MMP-9 directly/indirectly and pathways that may influence their dysregulation will be mapped out.

Chapter 2
Materials and methods

2.1 Tissue culture

2.1.1 Maintenance of the THP-1 human monocytic cell line in culture

The THP-1 cells, first described by Tsuchiya and colleagues (Tsuchiya *et al.* 1980) were proliferated and cultured in suspension using RPMI-1640 media containing 10% FCS, 100 U/ml penicillin and 100 µg/ml streptomycin and incubated at 37 °C in a humidified atmosphere of 5% CO_2. Media change was done every second day. To ensure their viability, the cell density was kept between 2 x 10^5 and 2 x 10^6 cells/ml. If the cell density is above or below this density, clumping occurs, and cells grow very slowly or stop dividing. When the cells reached ~ 1 x 10^6 cells/ml, they were split, this was usually between 48 and 72 hours.

2.1.2 Proliferation of THP-1 cells from frozen ampoules and preparation of stocks

To proliferate cells from frozen ampoules, the vial containing cells was thawed and the contents were immediately dispensed into a falcon tube containing 10 ml of pre-warmed RPMI-1640 media. Centrifugation was carried out at 200 g for 3 minutes. After decanting the supernatant, the pellet was re-suspended to homogeneity in 5 ml of warm media by gently aspirating up-and-down with a pipette. This step was done to wash off the dimethyl sulfoxide (DMSO) used as an antifreeze agent. It has been documented that DMSO can induce monocyte differentiation and lysis by upregulating TNF (Depraetere *et al.* 1995).

The cell suspension was then transferred into a T25 flask and incubated overnight in a humidified 37 ^oC incubator with 5% CO_2. After 24 hours, the media was changed by centrifuging at 200 g for 3 minutes and the re-suspended cells were left to proliferate to a cell density of 1 x 10^6 cells/ml. These were then split accordingly.

Preparation of freezer stocks entailed growing cells until a cell density of ~ 1 x 10^6 cells/ml in a T150 flask with media volume of 20 ml. Cells were spun down at 200 g for 3 minutes and the pellet was re-suspended in 4.75 ml of ice-cold 100% FCS. The falcon tube containing the cell suspension was kept on ice while gently aspirating the contents to ensure homogeneity. To preserve the cells from the harsh freezing conditions, 250 µl of DMSO was added in a drop wise manner to the cell suspension before dispensing 1 ml aliquots into five cryotubes. The ampoules were frozen slowly using a freezing container or "Mr Frosty" (NalGeneTM, Cryo 1 °C freezing container, Catalogue No: 5100-0001) and stored at – 80 °C for 48 hours before transferring to a liquid nitrogen tank. The ampoules were reconstituted to check for viability and mycoplasma infection before transferring to a liquid nitrogen tank.

2.1.3 Differentiation of human THP-1 monocytes to macrophages using PMA and preparation for infection

Macrophages are more potent MMP secretors than monocytes (Elkington *et al.* 2005a). To differentiate the cells, phorbol 12-myristate-13-acetate (PMA also known as TPA), which is a widely used differentiation agent was used throughout the experiments (Tominaga *et al.* 1998). Once the macrophages are treated with PMA they stop growing and adhere to the culture plate. The cells were counted four times using a Neubauer haemocytometer before seeding at 2 x 10^6 cells/ml in a 10 cm dish. Cells were re-suspended in media containing 20 nM PMA and left to differentiate for 72 hours. The cells were rested and starved with FCS-free RPMI-1640 media for 6 hours prior infection or treatment.

2.1.3.1 Evaluation of optimum PMA concentration on CD11b expression using fluorescence-activated cell sorting (FACS)

The differentiation of monocytes to macrophages is accompanied by the expression of cell surface markers such as CD11b which is expressed at very low levels in monocytes. Therefore, THP-1 monocytes were treated with different concentrations of PMA and plated on six-well plates at 1 x 10^6 cells per well. The concentrations used included 0, 10, 20 and 100 nM PMA where incubation was allowed for 72 hours. The PMA-containing media was

then discarded, and the cells were rested in RPMI media. Pre-warmed lidocaine (600 µl per well) was used to lift the adherent cells (a sterile syringe was used to scrape the cells off the plate as most of them were still adherent even after 5 minutes of incubation at 37 °C). Lidocaine is preferred over trypsin-EDTA for this experiment because it is thought that the CD11b receptor may be solubilised with trypsin-EDTA treatment. The cells were pelleted by centrifuging at 350 g for 5 minutes at 10 °C and re-suspended in FACS blocking buffer (5% BSA in PBS). These were incubated for an hour on ice. Following that, the cells were pelleted and re-suspended in FACS blocking buffer (100 µl per well), either containing CD11b (PE-Cy7 conjugated) antibody (10 µl) or no antibody, for each PMA treatment. Since the fluorophore is light sensitive, the cell-antibody (or no antibody) suspension was incubated in the dark and on ice for an hour. Again, the cells were centrifuged and re-suspended in FACS wash buffer (0.5% BSA in PBS), this was done three times. Finally, the cells were re-suspended in FACS fix buffer (300 µl of 1% (v/v) formaldehyde in FACS WASH) and analysed using FACS Aria cell sorter. The BD FACSDIVA software, version 6.1.3 was used.

To further ascertain the effects of PMA, the morphological changes were captured using phase contrast microscopy. THP-1 monocytes were plated in 35 mm dishes at 1 x 10^6 cells per well and incubated with 20 nM PMA or without PMA.

2.2 Proliferation of Mycobacterial smegmatis (*M. smeg*)

The non-pathogenic and fast growing, *Mycobacterium smegmatis* is a widely used model of *Mycobacterium tuberculosis* and was thus employed in this study.

2.2.1 Proliferation of *Mycobacterium smegmatis* from freezer stocks

To grow *M. smeg*, 7H9 media containing OADC and 0.05% Tween-80 was inoculated with *M. smeg* freezer stocks at a 1:100 ratio. The culture was incubated at 37 °C with shaking at 225 rpm until OD_{580} between 0.6 and 1. It took between 22 and 30 hours to reach the respective OD_{580} reading

2.2.2 Glycerol stock preparation

Glycerol stocks were prepared by growing *M. smeg* until OD_{580} between 0.6 and 1 in 7H9 media. The culture was mixed 1:1 with 50% glycerol to make up 1 ml stocks and these were kept at -80 °C freezer.

2.2.3 Infection of THP-1 macrophages with *Mycobacterium smegmatis*

The infection of differentiated THP-1 macrophages was done at an MOI (multiplicity of infection) of 1:10 (i.e. macrophage: bacilli). The macrophage monolayer (1 x 10^6 cells) was prepared as explained in section 2.1.3 before adding the bacterial suspension. When the optical density of the growing bacteria reached between 0.6 and 1, 5 ml was pipetted into a falcon tube and centrifuged for 10 minutes at 4000 rpm. Two washes with PBS buffer containing 0.05% Tween-80 was performed, followed by another wash with FCS-free RPMI media. Ultimately, the macrophages were incubated in media containing bacilli (1 x 10^7 cells) at 37 °C for an hour to allow phagocytosis. At this point the harvested media and lysate were referred to as the 1-hour time point. For the remainder of the non-harvested wells, the bacilli containing media was removed and extracellular bacteria was removed by washing three times with warmed FCS-free RPMI. Thereafter, the uninfected and infected cells and media were collected at different time points. Two biological replicates were carried out. The media was filter sterilised using a 0.2-µm syringe filters. The cells were lysed on ice using 500 µl of 1 X RIPA lysis buffer also containing a cocktail of protease inhibitors and DNase [3X RIPA lysis buffer recipe: 150 mM NaCl, 100 mM Tris HCl, 0.5% Sodium deoxycholate, 1% SDS, pH 7.6]. Lysis was facilitated by pipetting up and down until the lysate was less viscous. To remove cell debris, the lysate was spun down at 10 000 rpm for 20 minutes, the supernatant was then collected and kept at – 20 °C until further analysis.

2.2.4 Treatment of macrophages with lipoarabinomannan (LAM)

Differentiated THP-1 macrophages (1 x 10^6 cells) were serum starved for 6 hours before incubation in RPMI (FCS-free) containing 1 µg/ml LAM. For this experiment, the cell monolayer was rinsed once with warmed RPMI prior incubation with LAM containing media.

The cells and media were collected after 24 hours. Lysis was carried out as previously (section 2.2.3) and the media was not processed any further.

2.3 Evaluating the activity of MMPs

2.3.1 Activity of MMP-9 using a non-fluorogenic peptide substrate: Analysis by High Performance Liquid Chromatography (HPLC)

HPLC was used to monitor substrate hydrolysis of the non-fluorogenic peptide with the sequence (GCREKGPRQITERCG) (Figure 2-1) (Bracher *et al.* 2013;Kridel *et al.* 2001). At the suggested scissile bond Q9/I10, the sequences and masses of the expected products are depicted in Figure 2-1, however, it is possible that cleavage can be at other sites (Kridel *et al.* 2001). The media and buffers were filtered before use. Thereafter the secreted MMP-9 was either activated or non-activated using APMA by incubation at 37 ˚C for 16 hours prior incubation with the substrate at 37 ˚C. The recombinant MMP-9 (recMMP-9) was included as a positive control to aid in identifying and confirming the cleavage products with analysis by mass spectrometry (MS). Incubation with substrate was performed at different periods for analytical reasons that will be stated. Samples were analysed with a Poroshell 120 EC-C18 column on the Agilent 1260 infinity Hplc system and injected at volume of 10 µl unless stated differently. The peptides were eluted using 0 - 100% B (95% ACN, 0.1% TFA) over 12 min; at a flow rate of 0.5 mL/min and monitored at wavelengths 214 nm; 280 nm and 260 nm.

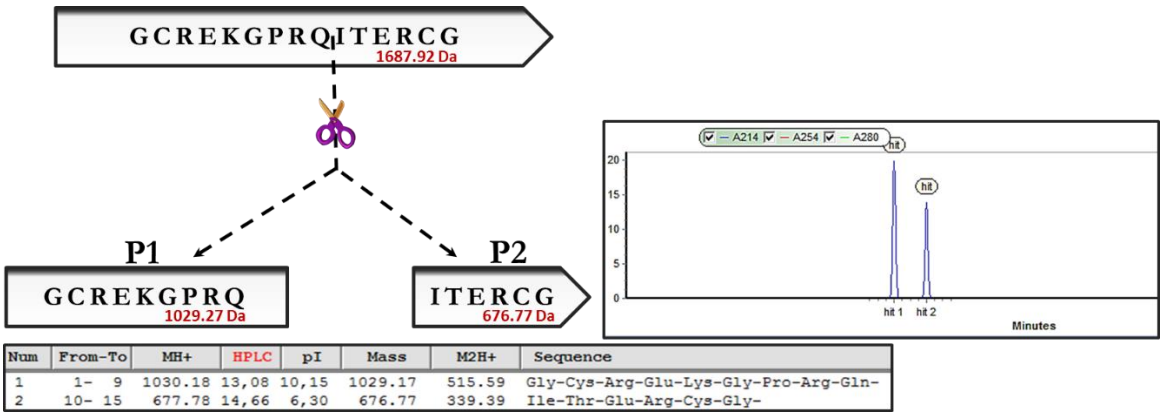

Figure 2-1: Schematic of non-fluorogenic substrate and expected MMP-9 cleavage site. The non-fluorogenic peptide is cleaved by MMP-9 at the indicated site. GPMAW was used to predict the HPLC elution profile and the masses of the cleavage products. The cleavage site has been previously described (Kridel *et al.* 2001).

2.3.2 Evaluation of the cleavage products using mass spectrometry

Analysis with MALDI-TOF

The substrate was incubated at 37 °C either with recombinant proMMP-9, APMA-activated recombinant proMMP-9 or with APMA for four hours before analysis with the HPLC and MALDI-TOF. Each peptide mixture was analysed using the HPLC with the method described in section 2.3.1 prior MALDI analysis. For the MALDI, the peptides were prepared by using the desalting method described in section. Thereafter, the samples were mixed with the matrix α-Cyano-4-hydroxyccinamic acid (α-CHCA) to a final concentration of 1 µg/µl. The sample spots were prepared by loading 1 µl of the sample-matrix mixtures on the stainless steel MALDI plate and left to dry for 15 minutes. This step was repeated twice by overlaying the sample spot with 1 µL of the same sample-matrix mixture. Thus, a final concentration of 3 µg of peptide was loaded for each sample. For each experiment, three MALDI spots were evaluated. BSA and matrix were included in the analysis as controls. The peptide digests were analysed using MALDI laser desorption at a fixed laser frequency of 5107 Hz. The MS spectra was monitored between m/z 500 and m/z 2000, with a total of 400 laser shots per spectra.

Analysis using Q-Exactive and TSQ analysis

The substrate was incubated at 37 °C with APMA-activated recombinant proMMP-9 for 1, 2 and 24 hours. Only the 2-hour experiment was analysed by mass spectrometry. Briefly, the 30 µl of 2-hour sample was injected into the HPLC column and peptides were collected in glass vials as individual peaks eluting from the column. The HPLC conditions described in section 2.3.1 were applied for this experiment. For the Q-Exactive and TSQ mass spectrometry, the collected peptide solutions were concentrated using a vacuum concentrator and desalted using the method described in section.

The samples were injected on a monolithic HPLC column with a 6 to 36-minute gradient. The peptides were eluted initially using a 31-minute constant flow rate of 100 µl/min as follows: 3 to 8% solution B (95% acetonitrile, 0.1 formic acid) from 0 to 5 minutes, 8 to 60% solution B from 5 to 20 minutes, 60 to 80% solution B from 20 to 21 minutes and then 80% solution B from 21 to 31 minutes. Thereafter, the gradient was returned to 3% solution B at a flow rate of 200 µl/min for 5 minutes. Re-equilibration of the column was performed for 20 minutes at 3% solution B. Analysis was performed using TSQ Vantage with Accela 600 pump set for MS1 scan only at a range of 300 to 1500 m/z. Peptides collected from peak C and E (please see peak designation in Figure 3-4) were injected and analysed separately. Following that, peptide samples collected from peak A, B, C, D and E were mixed and analysed with the TSQ.

Only peptides collected from peak A were evaluated using the Q-Exactive Quadrupole-Orbitrap mass spectrometry (Thermo Scientific) which was coupled to the Dionex Ultimate 3500 RSLC nano_LC system (Thermo Scientific). The sample injection volume was 10 µl. The sample was loaded on a 40 cm C18 analytical column (packed in- house with Aeris peptide 3.6 µM beads, Phenomenex), thereafter elution was carried out using a linear gradient of 6 – 35% solvent B (95% acetonitrile, 0.1 formic acid), at a constant flow rate of 300 nl/min. The acquisition of data was carried out using Xcalibur software (Thermo scientific, v2.2) in positive ion mode. MS1 scans were acquired with a resolution of 70 000, an automatic gain control of 3×10^6 and an ion injection time of 250 ms. The MS/MS scans were acquired at a resolution of 17 500, AGC target of 2×10^5, ion injection of 120 ms. The peptide matching was set to 'preferred', isotopic exclusion and a dynamic exclusion of 30 s.

2.3.3 Investigation of MMP-1 and MMP-9 activity using gelatin, casein and collagen zymography

Zymography is an electrophoretic technique that was developed in the 1980s (Heussen and Dowdle 1980) and it is still used to date for detecting protease activity especially of MMPs. This technique is based on their ability to hydrolyse substrate that has been incorporated by co-polymerisation with the separating gel. Discrimination between enzymes relies on migration and formation of clear bands indicative of hydrolysis of the substrate at the respective molecular weight of the enzymes. This technique has been widely used for analysis of the MMP's active and zymogenic forms. The zymogenic form can be identified on the zymogram since the SDS perturbs the cysteine switch motif formed between the catalytic zinc and the prodomain's cysteine residue while the prodomain itself remains uncleaved. In addition to that, both the covalent and non-covalent interactions between the MMP and TIMP is broken by SDS, these bonds can reform following refolding by exchange of the SDS with Triton X-100.

The experiments were carried out as described by Gogly and colleagues (1998), with sample preparation under non-reducing conditions (Gogly *et al.* 1998). Briefly, total protein concentration was determined by the BCA method thereafter samples were adjusted so that equivalent total protein concentrations are loaded on the gels. The 1X nonreducing sample buffer was used for loading the samples. Electrophoresis was carried out using ice-cold running buffer at a current of 15 mA until the sample front had reached the separating gel and then constantly at 35 mA. Following that, the denaturant i.e. SDS was washed by a two-step exchange with 2.5% Triton X-100 for 30 minutes each to allow renaturation of the proteins. For subsequent substrate hydrolysis, gels were placed in incubation buffer for 16 - 20 hours at 37 ^{o}C. Staining was carried out in 0.25% Coomassie Brilliant blue for about an hour and destained until clear bands indicating proteolytic activity were observed. Since zymograms differ, 10 ng of the positive control (recombinant MMP-9) was loaded on the gels. Bands were scanned in triplicate and for normalisation the scan units of the positive control were divided by each sample band, thereafter the quotients of uninfected or infected were plotted as bar graphs.

2.3.4 Assessing the activity of secreted MMP-1 using a fluorogenic substrate

The activity of secreted MMP-1 was assessed by means of a fluorogenic Sensolyte® Plus 520 MMP-1 assay kit according to the manufacturer's instruction. These methods of assessing the activity of MMPs has been developed over the years and described (Menges *et al.* 1997). Briefly, the secretome was incubated for 2 hours with the MMP-1 antibody (coated on the microplates) for selective binding to occur. This was done at room temperature with constant shaking of the microplate. After a series of washes to remove unbound molecules, the bound MMP-1 was either activated with APMA (ultimately measuring the active form and activated proMMP-1) for 4 hours or not activated to measure the endogenously secreted active form alone. Thereafter, substrate hydrolysis was monitored for 2 hours at a fluorescence excitation/emission wavelength of 490/520 nm dependent on the 5-FAM/QXL^{TM}520 FRET substrate. The Perkin Elmer fluorimeter (EnSpire) was used.

2.4 Investigation of MMP-1 and MMP-9 expression by western blotting

To assess alterations in the expression of MMP-1 and MMP-9 that may have been induced by infection of THP-1 macrophages, western blotting was used. SDS-PAGE was carried out with accordance to Laemmli's conditions (see Appendix 1), this was followed by an hour of protein transfer (see Appendix 1). Membrane blocking was done for an hour in blocking buffer. After that, the membrane was probed with an anti-MMP1 or anti-MMP-9 primary antibody diluted 1:1000 in blocking buffer. The membrane was then incubated at 4 °C overnight with gentle shaking. Prior probing with secondary antibody, the membrane was rinsed six times with blocking buffer and then placed in blocking buffer containing anti-mouse secondary antibody diluted a 1000-fold. Binding of secondary antibody was allowed to occur at room temperature for two hours. A series of rinsing steps were done, three times briefly with blocking buffer and three times with TBS-T buffer 15 minutes each time. To visualise the bound antibodies, BioRad Immuno-Star Western C kit which exploits the horseradish peroxidase (HRP) conjugated to the secondary antibody was used.

Chapter 3

Matrix metalloprotease activity

The function of MMP's is pivotal in remodelling of the ECM and anomaly in their activity is implicated in pathology of diseases such as cancer and tuberculosis. In TB, the expression of MMP-9 is associated with granuloma formation and maturation, whilst the degradation of collagen is correlated with increased MMP-1 activity. These events have been documented to cause cavitation and dissemination which culminate in transmission (Elkington *et al.* 2005a;Elkington *et al.* 2005b;Hrabec *et al.* 2002;Kubler *et al.* 2015;Salgame 2011). Inhibiting MMP's is thus ideal but the similarities in the active site pocket poses a challenge in designing specific inhibitors and substrates for assaying them. Different methods of assessing their activity have been used including zymography, labelled and nonlabelled peptides.

Therefore, the objectives of the study on analysing the effect of *M. smeg* infected macrophages on the activity of MMPs were as follows:

1. Assessing the proliferation and differentiation of THP-1 macrophages.
2. Harvesting at different time points the lysate and media from differentiated THP-1 monocytes that are uninfected and infected with *M. smeg*.

Comparing the extracellular and intracellular activity of MMP-1 and MMP-9 between uninfected and infected, also between the different harvest time points.

3.1 Evaluation of THP-1 proliferation and differentiation

Since macrophages are more potent secretors of MMPs than monocytes, the THP-1 cells were differentiated prior to infection. This also allows adherence of the cells to the plate and inhibits further growth of the cells. The optimum concentration of PMA that is required to induce differentiation without being toxic to the cells was assessed using FACS and the accompanying morphology was evaluated using phase contrast microscopy. Within 18 hours of incubation with PMA, the monocytes had adhered and were adopting a macrophage-like appearance that is more flattened, elongated and spindle-like shaped (Figure 3-1). This is a typical morphological transition also observed in other studies (Mehta and Lopez-Berestein 1986;Tsuchiya *et al.* 1980). Another important marker of differentiation is CD11b which is almost exclusively expressed by differentiated macrophages.

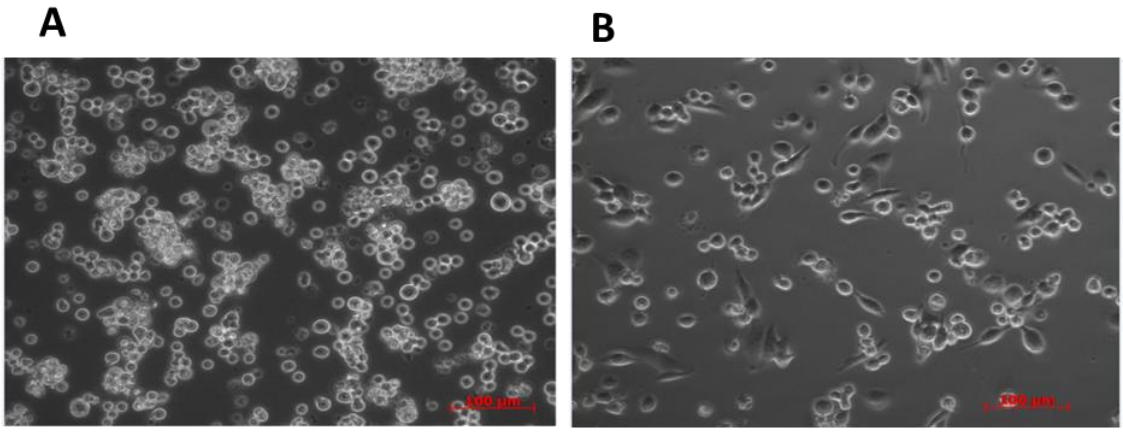

Figure 3-1: Morphology of undifferentiated and PMA-differentiated THP-1 cells. Phase contrast microscopy was used to visualise and compare (**A**) undifferentiated and (**B**) differentiated THP-1 monocytes treated with 20 nM PMA. Because the font for scale bar is so small, maybe you can indicate. The scale bar corresponds to 100 µm

In cells treated with 20 nM PMA, 93% of the cells which were CD11b positive (Figure 3-2), this was comparable to other PMA concentrations used. The heterogeneity in the population is comparable to other studies (Mehta and Lopez-Berestein 1986;Qin 2012;Tominaga *et al.* 1998). Since 20 nM of PMA was sufficient to induce differentiated and more adherent monocytes than the 10 nM, it was used for all experiments.

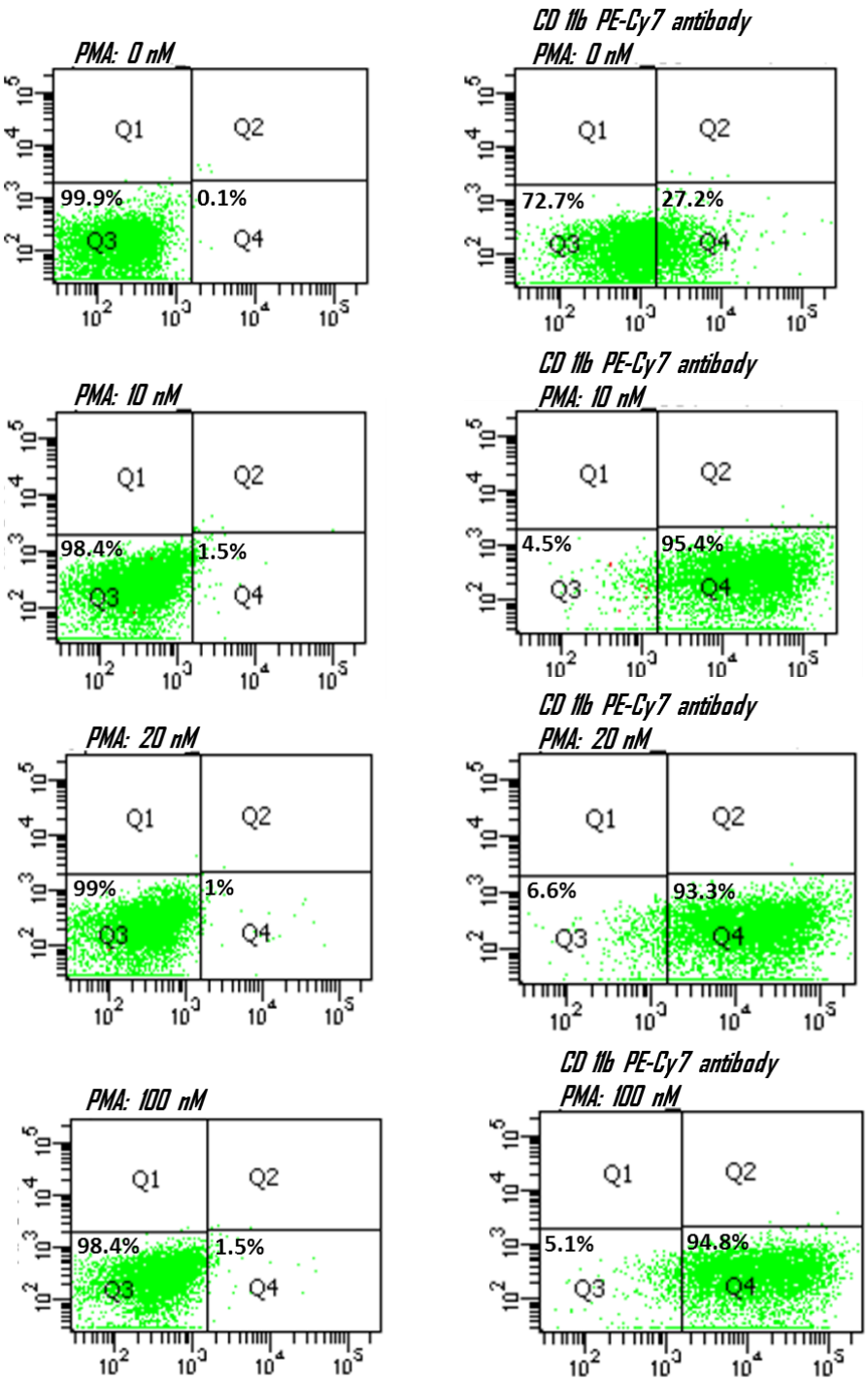

Figure 3-2: Assessing CD11b expression levels using different concentrations of PMA. FACS was used to analyse the expression of CD11b. Undifferentiated (without PMA) and differentiated THP-1 cells were either incubated with or without the CD11b antibody which is conjugated to the PE-Cy7 fluorescent dye. BD FACSDIVA version 1.6.3 was used to analyse the data.

3.2. MMP activity of *Mycobacterium smegmatis* infected THP-1 macrophages

3.2.1 Assessing MMP-9 activity using a non-fluorogenic substrate and HPLC

MMPs are similar in molecular weight and can act upon a large number of overlapping substrates due to the similar architecture of their active sites. Specifically, the catlytic site of MMP9 is closely related to other MMPs emphasising the need for specific and quantitative assay for assessing its enzymatic activity. Thus, a synthetic peptide substrate that has a very high k_{cat}/K_m for MMP9 (Kridel *et al.* 2001) was used to quantify and compare the activity between the uninfected and infected secretome.

3.2.1.1 Characterising the specificity of recombinant MMP9 using HPLC and mass spectrometry

Briefly, the substrate GCREKGPRQITERCG was incubated with recombinant proMMP-9 with and without APMA activation. To characterise the cleavage products and the effect of APMA on the substrate, HPLC followed by MALDI-TOF mass spectrometry using the matrix α-cyano-4-hydroxyccinamic acid (α-CHCA) was carried out (Figure 3-3). Incubation of the non-activated recMMP-9 with substrate yielded a single peak that overlays with the substrate peak with lower peak area indicating partial substrate hydrolysis (Figure 3-3A). The products resulting from cleavage at the Q9/I10 bond were identified. Specifically peaks at m/z of 678.39 and 1030.60 were observed and these were in close agreement with the peptides ITERCG (677.77) and GCREKGPRQ (1030.54) (Table 3-1). It is important to note that the aforementioned products were not observed in the control where substrate was incubated with APMA (Figure 3-3C). Other cleavage sites that were identified included I10/T11 and E4/K5. Since the products could not be conclusively matched to the HPLC chromatograph peaks, further analysis of individually collected peaks was performed using the Q-Exactive and TSQ mass spectrometry (Described in Chapter 2, Section 2.3.2).

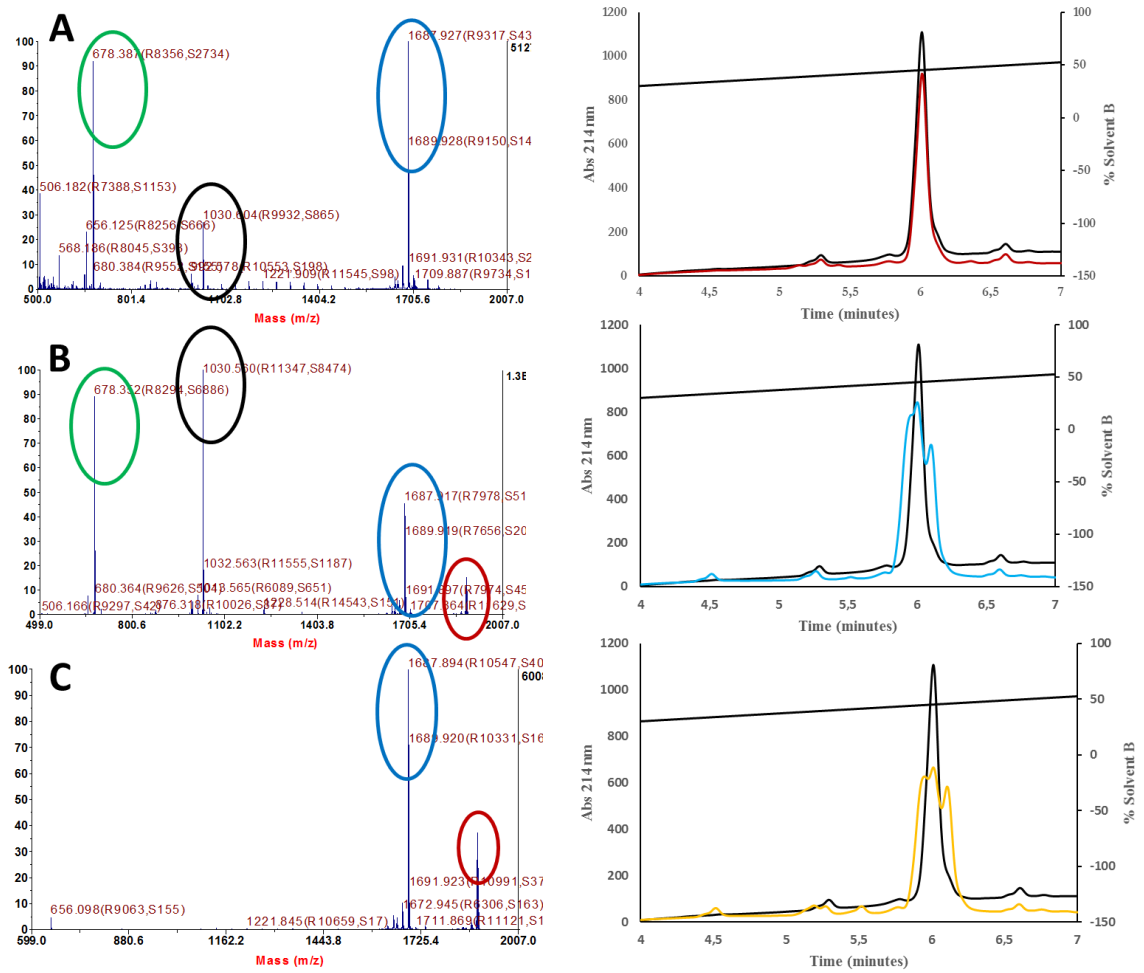

Figure 3-3: Analysis of MMP-9 cleavage products using MALDI. The MALDI spectra (left panel) and representative HPLC chromatograms (right) are depicted. (**A**) Recombinant MMP-9 non-activated (red chromatogram), (**B**) activated with APMA (blue chromatogram), and (**C**) APMA without MMP-9 (yellow chromatogram) were incubated with substrate at 37 ˚C for 4 hours. The MALDI identified the substrate 1687.9 (blue circle), and product peptides 678.39 (green circle) and 1030.60 (black circle). The 1889.84 peptide (red circle) was only identified in the presence of APMA.

Table 3-1. Summary of the MALDI-TOF analysis of the MMP-9 substrate cleavage products

Non-activated Rec_MMP-9 +	Activated Rec_MMP-9 + substrate	APMA + substrate	Fragment sequence	Theoretical mass (Da)	Cleavage site
m/z	*m/z*	*m/z*			
**678.39	678.35	N/a	ITERCG	677.70	Q9/I10
680.38	680.36	N/a	KGPRQI	680.42	E4/K5 & I10/T11
**1030.60	1030.50	N/a	GCREKGPRQ	1030.54	Q9/I10
1687.92	1687.91	1687.89	GCREKGPRQITERCG	1687.92	Intact substrate
1689.92	1689.91	1689.92	GCREKGPRQITERCG	1689.94	Intact substrate

***Q9/I10 cleavage products**.

APMA-activated recMMP-9 was incubated with substrate for 1, 2 or 24 hours and peptides resolved by HPLC. The peaks from the 2-hour incubation were collected and MS analysis was carried out. The chromatogram (absorbance at 214 nm) shows that after an hour, there is some substrate hydrolysis with partial resolution of some peptides indicated by peaks with 'shoulders' (Figure 3-4A). The recombinant MMP-9 elutes at 6.64 minutes (chromatogram not shown) which is after the elution of substrate and peak E3. Peak E1 disappears after 24 hours whereas there is little change in E2 and E3 compared to the 2-hour incubation. The area under these peaks was computed as a single peak since they are not fully resolved. There was a 2-fold increase in products A, C and D after 24 hours (compared to after 2 hours) and a decrease in B and E (Figure 3-4B). This suggests that there is sequential hydrolysis of the substrate. Assessment of the peaks by MS (Q-Exactive and TSQ) confirmed the co-elution and the sequential cleavage of the substrate, the data is summarised in Table 3-2. Peaks at m/z of 677.95 and 695.85 observed and these were in agreement with the calculated masses of the peptides 677.78 and 696.37. These peptides correspond to cleavage at the Q9/I10 bond, and R3/E4 and Q9/I10 cleavage bonds, respectively. Other cleavage sites that were identified include G6/P7, R3/E4, E12/R13 and I10/T11. Although there were some cleavage products identified in peak A and E, the dominant molecules were APMA and substrate, respectively.

Substrate hydrolysis was also evident when the substrate was incubated with APMA-activated MMP-1 and chymotrypsin which yielded similarities in the peak pattern to hydrolysis by MMP-9 (Figure 3-5).

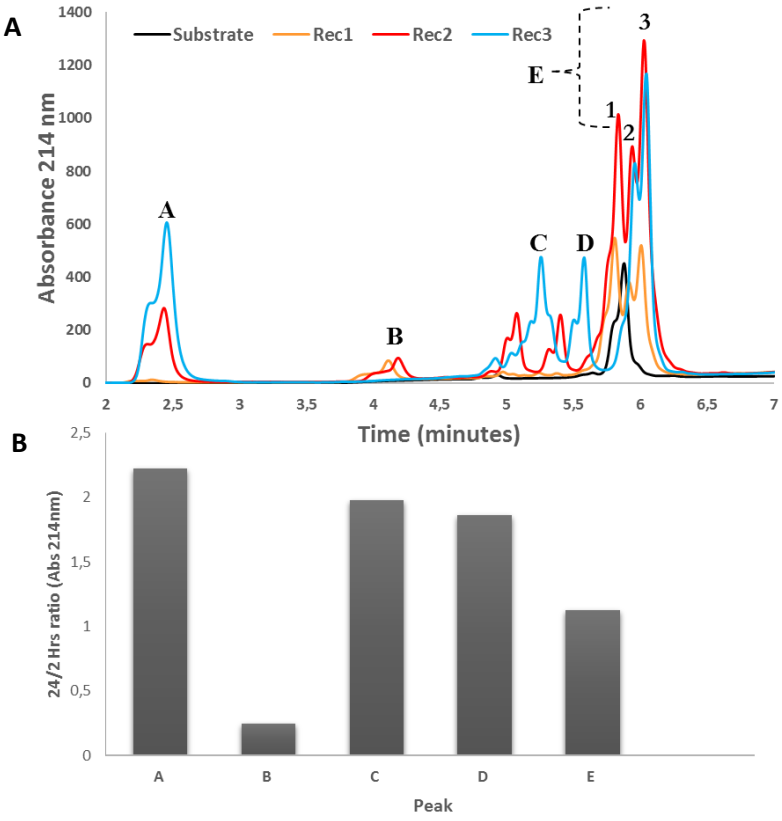

Figure 3-4: Determination of the product peaks by time course analysis. (**A**) The chromatogram of the substrate incubated with activated recombinant MMP-9 for 1 hour (Rec1), 2 hours (Rec2) and 24 hours (Rec3). The elution peaks are also indicated (A to E). (**B**) Bar graph representing peak ratios calculated from the area of the 24 to 2-hour period of hydrolysis.

Table 3-2: Mass spectrometry analysis of cleavage products of MMP-9 substrate with APMA activated recombinant MMP-9.

The peaks were collected after 2 hours of incubation with substrate and were assigned according the HPLC chromatogram in Figure 3-15.

Peak	m/z	Charge state	Instrument	Fragment sequence	Theoretical mass (Da)	Cleavage site
A	333.28	MH+	QE (MS2)	GCR/RCG	334.14	R3/E4 OR E12/R13
	648.51	MH+		GCREKG	648.74	G6/P7
C	677.95	MH+	TSQ (MS1)	ITERCG	677.78	Q9/I10
D	695.85	MH+	TSQ (MS1)	EKGPRQ	696.37	R3/E4 & Q9/I10

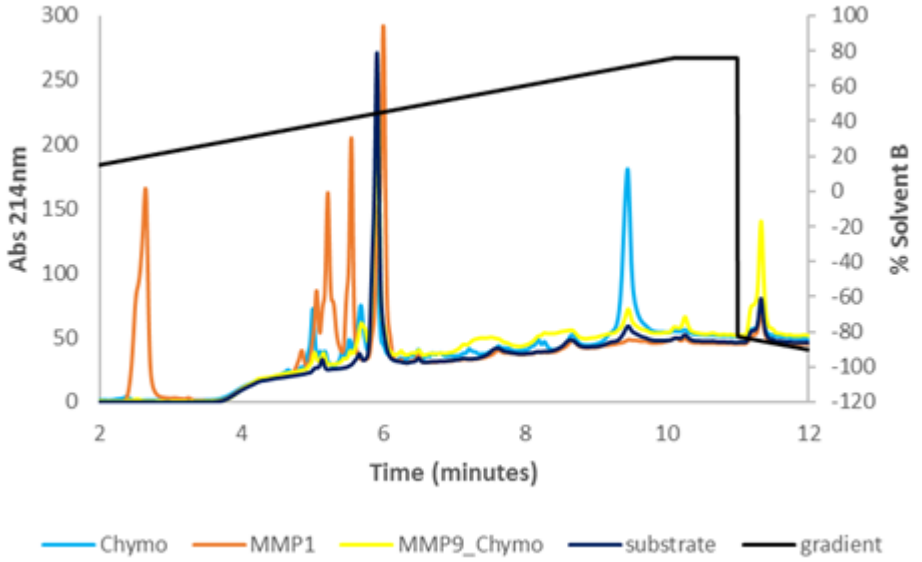

Figure 3-5: HPLC chromatogram of MMP-9 substrate hydrolysis by other enzymes. The substrate was incubated with chymotrypsin, activated MMP-1 or chymotrypsin and MMP-9. The cleavage products were monitored by HPLC at a wavelength of 214 nm.

3.2.1.2 Evaluating the substrate hydrolysis pattern of uninfected and infected secreted proteins

The hydrolysis of the MMP9 substrate by the uninfected and infected secretome was assessed with and without APMA-activation. A representative chromatogram of the peaks generated with the APMA-activated secretome (Figure 3-6) corresponds to the peaks assigned in Figure 3-4. Differences between uninfected and infected secretome were analysed by computing the ratio of the individual peaks to the substrate (Figure 3-7 to Figure 3-13). Only peak C and D were compared since peak A and E mainly represent APMA and substrate peaks, respectively. B was ignored since the product concentrations from the secretome hydrolysis were too low.

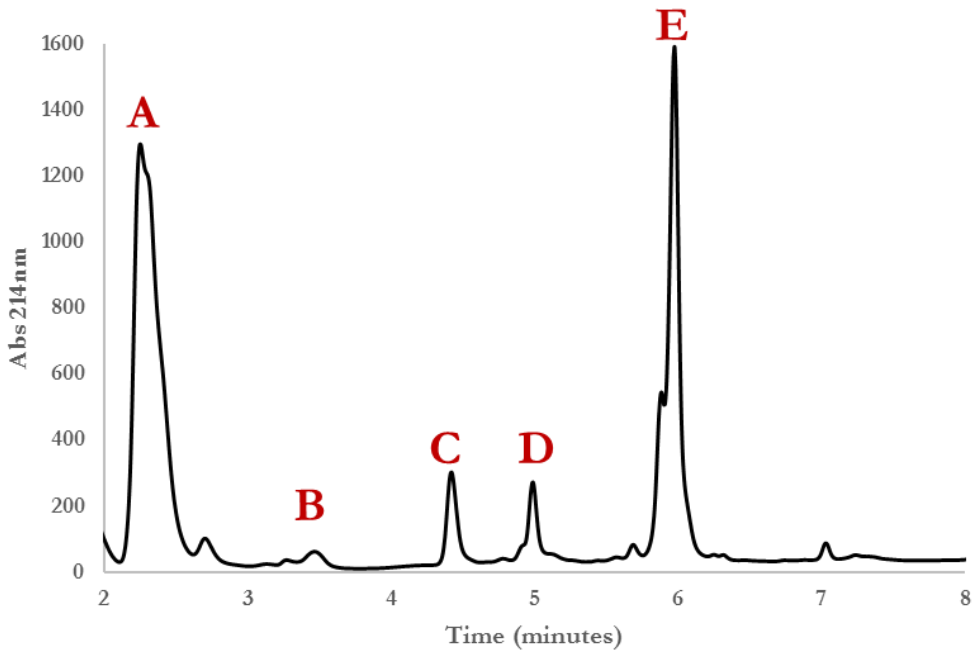

Figure 3-6: Representative chromatogram of the secretome hydrolysis of the MMP9 substrate. The peaks depicted are from incubation of the substrate and APMA-activated secretome and are assigned A to E similar to the hydrolysis pattern resulting from APMA-activated recombinant MMP-9.

For the 1-hour time point, there was no significant difference in products C and D between the infected and uninfected in both the 1-hour and 6-hour incubations (Figure 3-7). Similarly, following APMA-activation of the secretome there were no differences observed between uninfected and infected (Figure 3-8).

For the 3-hour time point the area of the product peaks was only slightly higher in the uninfected (Figure 3-9). In contrast, APMA activation masked these differences between infected and uninfected (Figure 3-10).

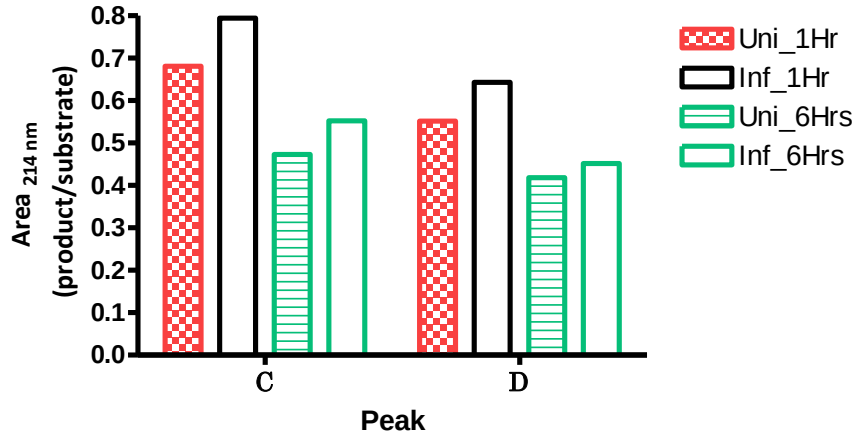

Figure 3-7: Hydrolysis of substrate by the 1-hour time point media. The substrate was incubated with the uninfected (Uni) and infected (Inf) media for 1 hour (Uni_1Hr and Inf_1Hr) or 6 hours (Uni_6Hrs and Inf_6Hrs).

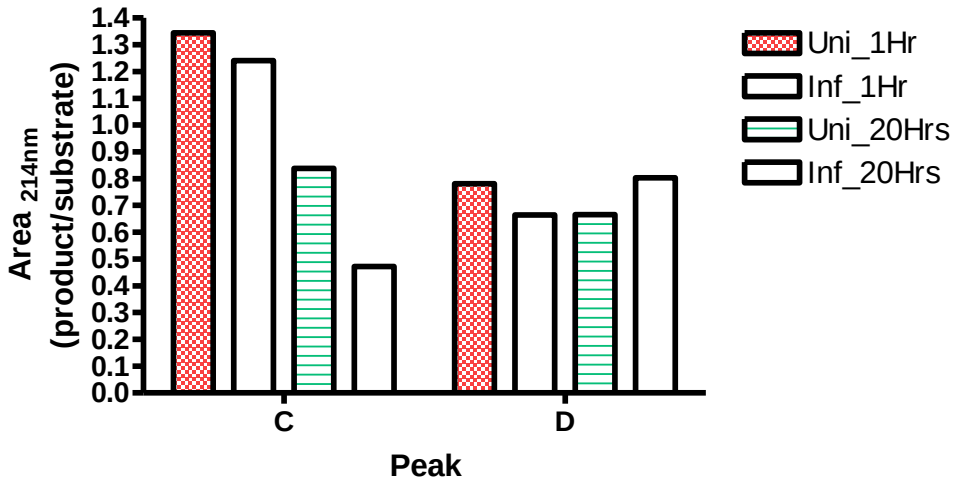

Figure 3-8: Effect of APMA on substrate hydrolysis of the 1-hour time point. Prior to hydrolysis the media was incubated with APMA for 16 hours. Thereafter the substrate was incubated with the uninfected (Uni) and infected (Inf) media for 1 hour (Uni_1Hr and Inf_1Hr) or 20 hours (Uni_20Hrs and Inf_20Hrs).

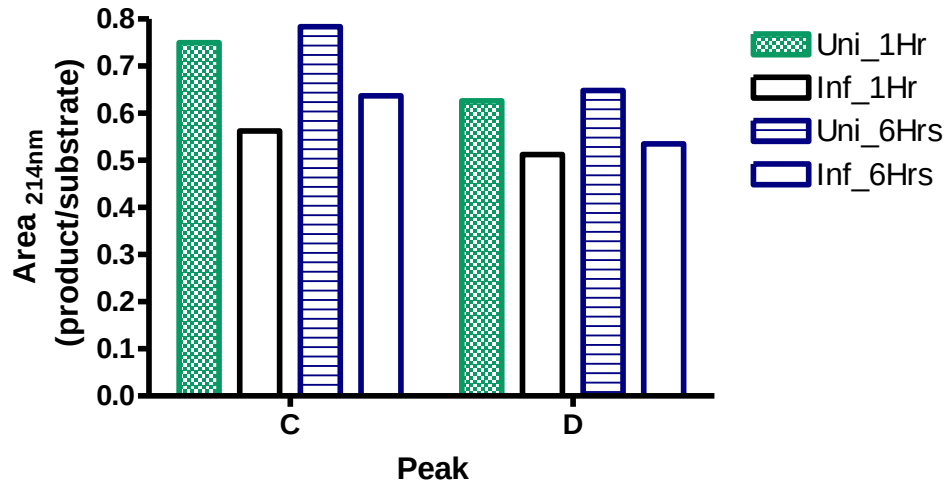

Figure 3-9: Substrate hydrolysis with the 3-hour time point. The substrate was incubated with the uninfected (Uni) and infected (Inf) media for 1 hour (Uni_1Hr and Inf_1Hr) or 6 hours (Uni_6Hrs and Inf_6Hrs).

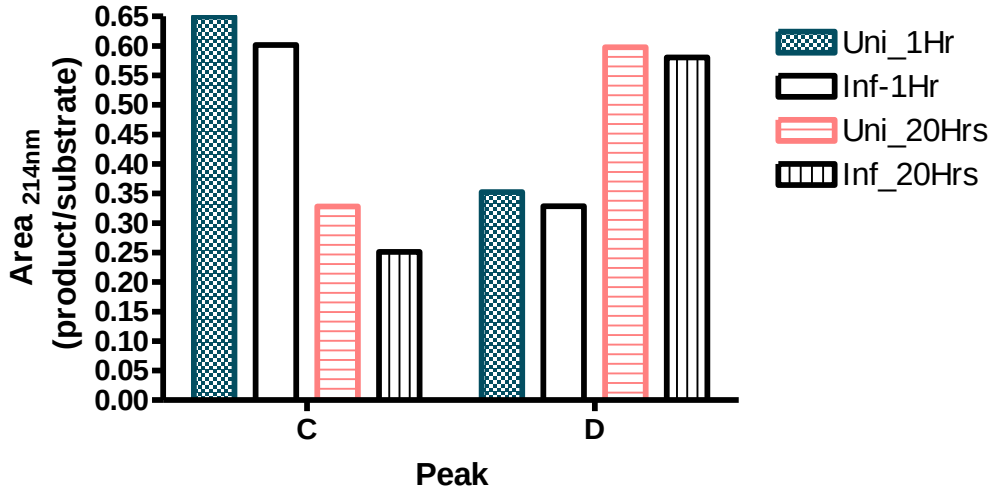

Figure 3-10: Substrate hydrolysis with the APMA-treated 3-hour time point. Prior to hydrolysis the media was incubated with APMA for 16 hours. Thereafter the substrate was incubated with the uninfected (Uni) and infected (Inf) media for 1 hour (Uni-1Hr and Inf_1Hr) or 20 hours (Uni_20Hrs and Inf_20Hrs).

At the 6-hour time point, there is a 2-fold increase in D in the infected media after 1 hour of incubation with the substrate. However, incubating the media with the substrate for 6 hours abolished this difference (Figure 3-11). For the 18-hour time point, there were no significant differences between the uninfected and infected after 1 and 6 hours of incubation with substrate (Figure 3-13). Overall, there were no significant differences observed induced by the *M. smeg* infection and the results were not conclusive.

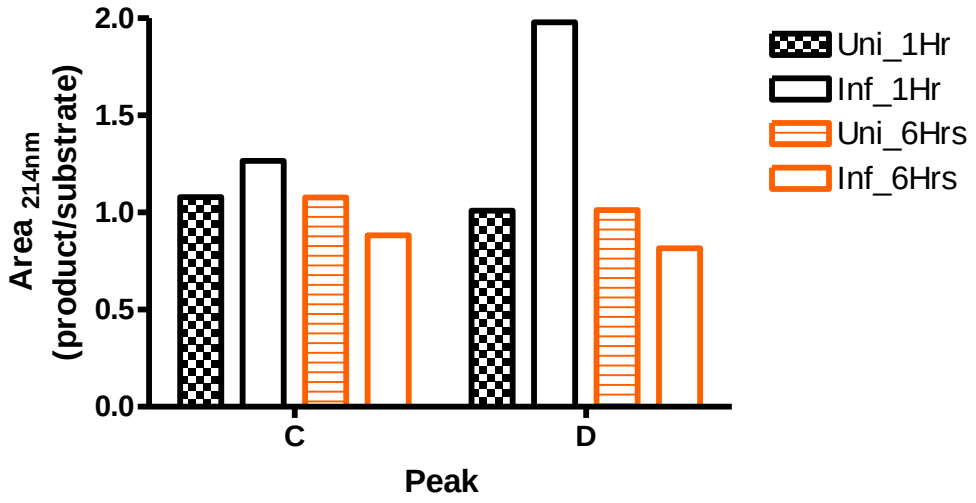

Figure 3-11: Product formation from the 6-hour time point substrate digestion. The substrate was incubated with the uninfected (Uni) and infected (Inf) media for 1 hour (Uni_1Hr) or 6 hours (6_Hrs).

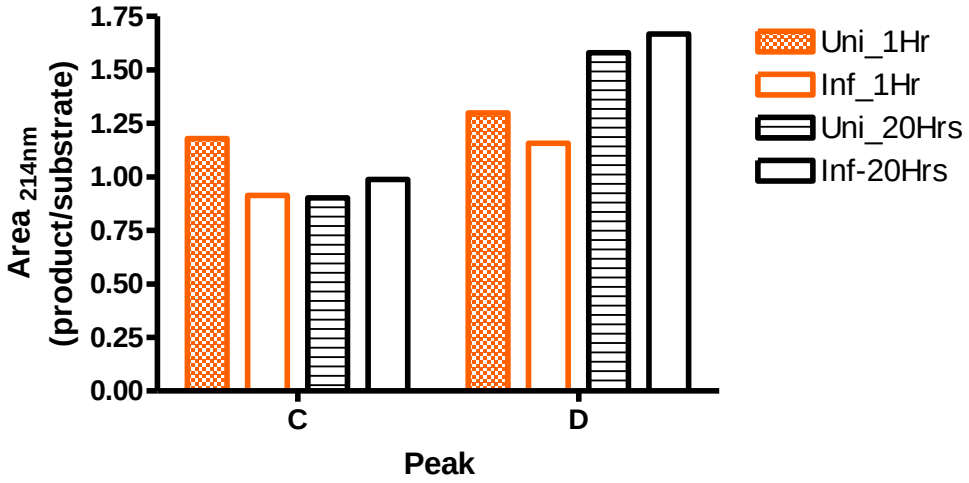

Figure 3-12: Product elution profile from APMA-treated 6-hour time point substrate digestion. Prior hydrolysis the media was incubated with APMA for 16 hours. Thereafter the substrate was incubated with the uninfected (Uni) and infected (Inf) media for 1 hour (Uni_1Hr and Inf_1Hr) or 6 hours (Uni_20Hrs and Inf_20Hrs).

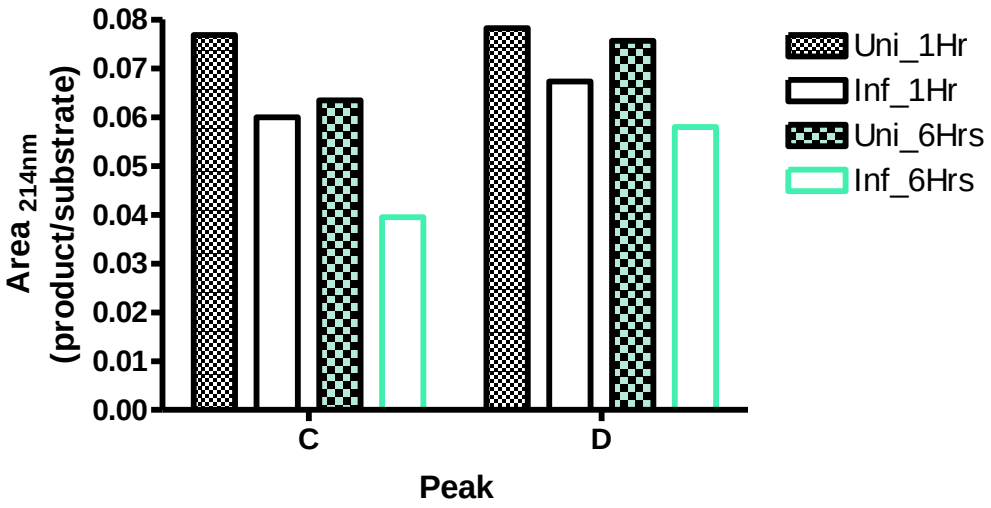

Figure 3-13: Evaluation of substrate hydrolysis with the 18-hour time point in the absence of APMA. The substrate was incubated with the uninfected (Uni) and infected (Inf) media for 1 hour (Uni_1Hr and Inf_1Hr) or 6 hours (Uni_6Hrs and Inf_6Hrs).

3.2.2 Evaluation of MMP-9 and MMP-1 activity using zymography

Owing to the challenges associated with the HPLC-based enzyme assay, zymography was employed to assess the effect of *M. smeg* infection on the activity of secreted and intracellular MMPs. Substrates including gelatin, casein and collagen were used to evaluate any differential hydrolysis due to the infection or type of substrate. The activation of proMMP-9 and proMMP-1 are stepwise processes summarised below (Figure 3-14) and in more detail in Section 1.3.2.

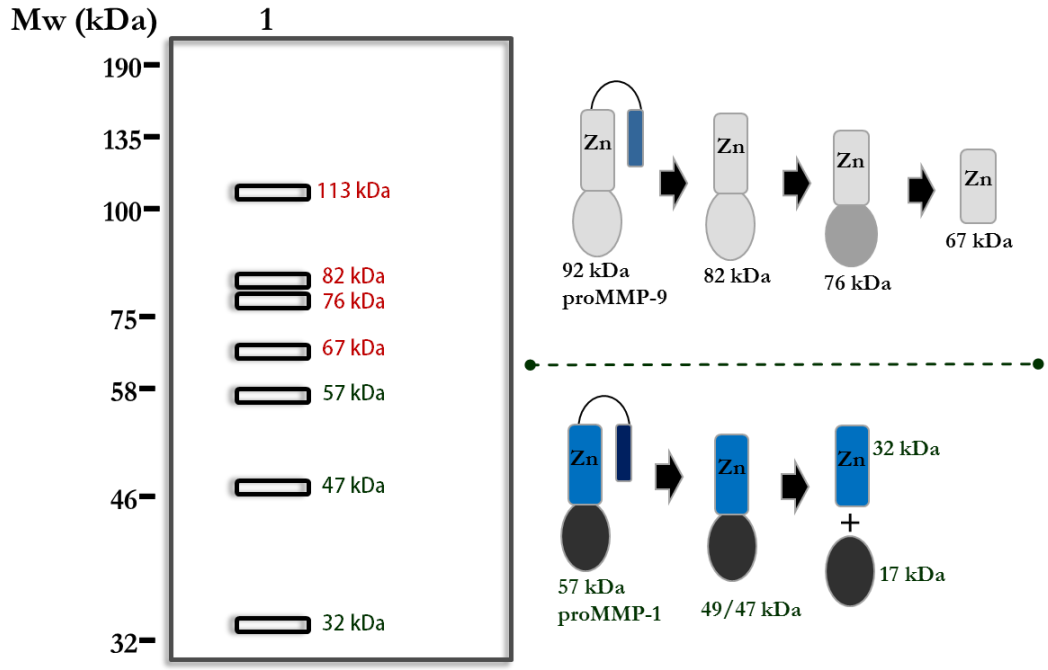

Figure 3-14 Schematic migration pattern of different MMP-9 and MMP-1 forms on zymograms. In lane 1 are the expected bands with respect to the molecular weight marker (Mw). Also illustrated are the steps involved in conversion of the proMMP-9 and proMMP-1 to their different forms.

In the secretome, the difference in enzymatic activity of MMP9 between infected and uninfected macrophages was most pronounced at 6 and 18-hour time points as indicated by the zone of clearing at 82-kDa (Figure 3-15A and B). This was clearly indicated by densitometric analysis (Figure 3-15D). There was an approximate 5- and 11-fold increase in MMP activity at 6 and 18 hours, respectively. Thereafter the fold difference in activity between uninfected and infected declined at 24 hours, and at the 72-hour time point the uninfected was slightly higher versus the infected. Interestingly, in the 72-hour infected macrophages the 82 kDa band migrates more slowly than that observed in the uninfected (Figure 3-15B). In addition, the infected secretome had a larger molecular weight band (113 kDa) that was absent in the uninfected. This band was also present in the 6-hour time point of the infected secretome. This may represent proMMP-9 or the formation of multimeric complexes. This will be discussed later in Chapter 4. The band observed at 57 kDa in the 24- and 72-hour time points in the uninfected secretome corresponds to proMMP-1 hydrolysis (Figure 3-15C).

Additionally, at higher protein concentrations the uninfected secretome at 72 hours showed a 47 kDa band that is likely the active form of MMP-1 (Appendix Figure 6-1). This suggests that at higher protein concentrations proMMP-1 undergoes autolysis. In summary, there is an overall increase in the gelatinase activity of secreted MMP-9 in the secretome of infected macrophages. In contrast, secreted proMMP-1/MMP-1 activity was observed only in the 24 and 72-hour uninfected harvests.

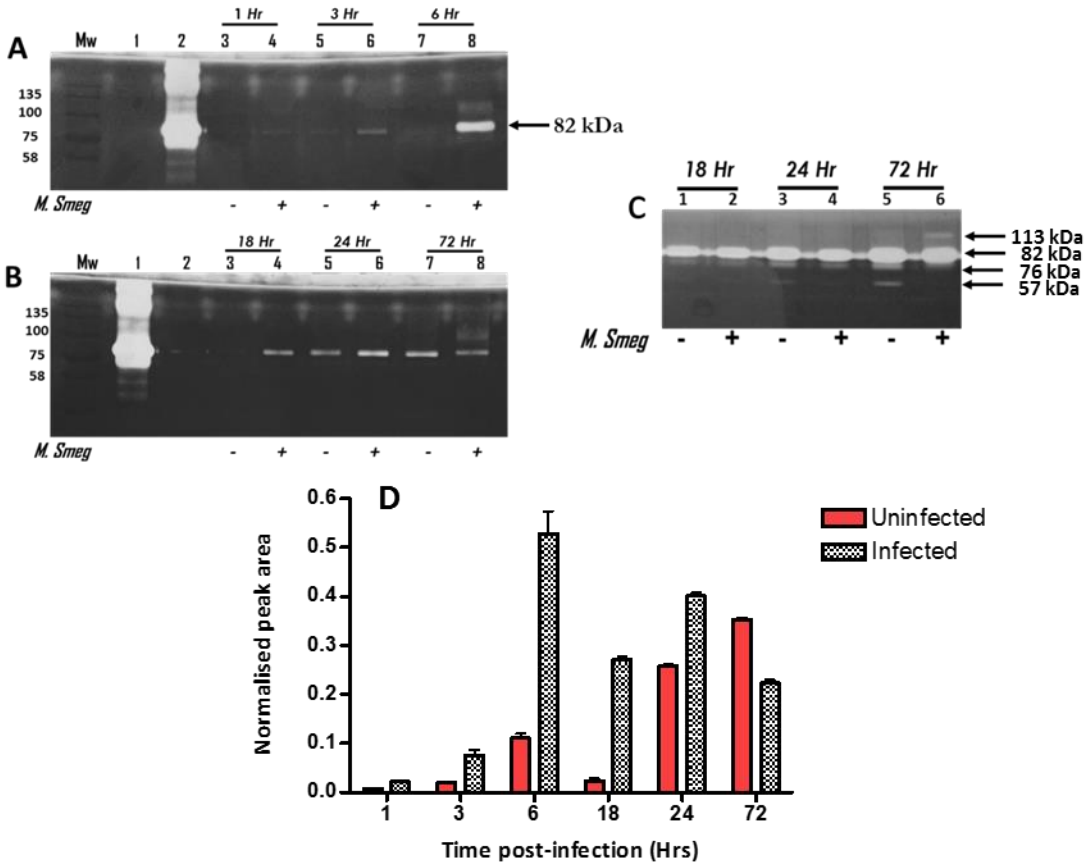

Figure 3-15: Gelatinase activity of the secretome from M. smeg infected versus uninfected macrophages. The different harvest time points post infection are indicated. The uninfected and infected samples are depicted as (-) and (+), respectively. As a control, recombinant proMMP-9 was loaded in lanes 2 and 1, in gel (**A)** and (**B)**, respectively. (**C**) Loading higher concentrations of the same samples results in appearance of other bands as indicated by the arrows. (**D**) Bands were scanned in triplicate and quantified using ImageJ, and data was represented as mean ± SEM.

Collagen hydrolysis by the 82 kDa form was higher for the infected secretome compared to the uninfected between the 1 and 18-hours (Figure 3-16A and C). In contrast to the other time points the activity for the uninfected secretome at 6 hours was almost undetectable. It

is important to note that the highest differential activity observed between the time points was substrate dependent, where collagenase activity is about 13-fold higher for the infected at the 6-hour time point versus 11-fold higher at the 18-hour time point. In the later time points, i.e. 24 and 72 hours, collagen hydrolysis was similar for both infected and uninfected, and slightly higher for the uninfected at 24 hours post-infection (Figure 3-16B). The band corresponding to the 76 kDa form of MMP-9 had collagenolytic activity that was higher in the infected versus uninfected especially at the 18-hour time point, and in contrast the uninfected was 2.5-fold higher at 72 hours. Intriguingly, this band was absent in the 6-hour time point.

Elastin which is a primary substrate for MMP-12 was also used. No enzymatic activity was detected for both infected and uninfected macrophages, implying that MMP-12 might not be expressed and secreted by the THP-1 macrophages (results not shown).

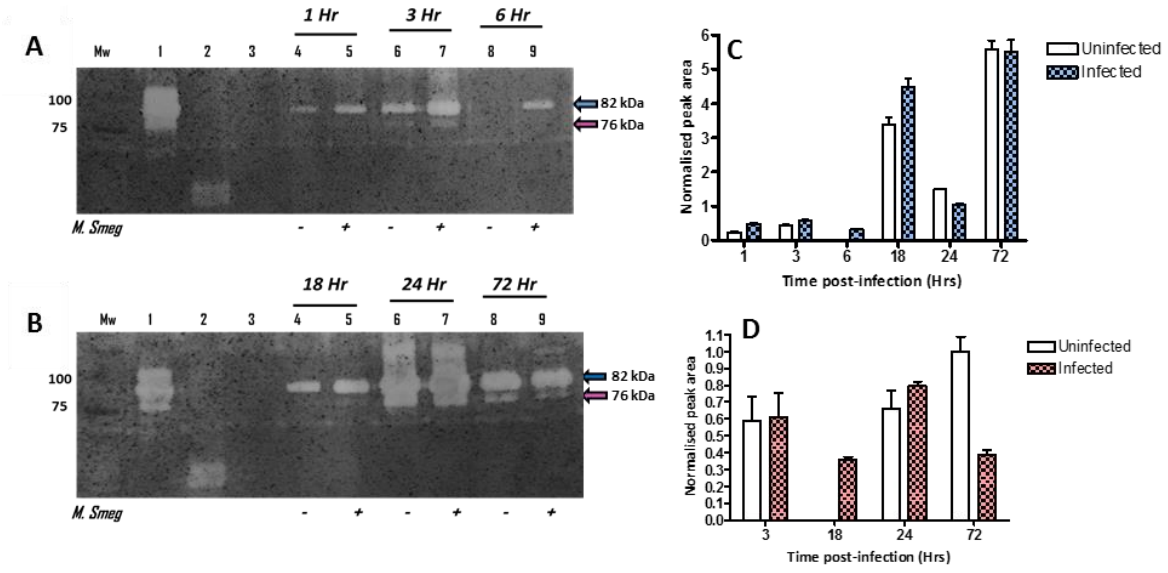

Figure 3-16: Analysis of collagen I hydrolysis by M. smeg infected and uninfected secretome. The secretome collected for the (**A**) earlier and (**B**) later time points were loaded as defined. Lanes 1 and 2 represent recombinant proMMP-9 and proMMP-1, respectively, in both gels. The bands corresponding to the (**C**) 82 kDa and (**D**) 76 kDa bands, and recombinant proMMP-9 (lane 1) were quantified using ImageJ. Bands were scanned in triplicate and data represented as mean ± SEM.

When casein was used as a substrate, the secretome from the earlier time points (1 to 6-hours) showed no enzyme activity for both uninfected and infected cells (Figure 3-17A) in

contrast to the later time points (Figure 3-17B). This trend, and the discrepancy in the highest differential activity observed between time points when gelatin and collagen were used, suggests that there is a switch in substrate specificity of MMP-9 between the 6- and 18-hour time points. This will be discussed further in Chapter 4. At 24 hours the casein hydrolysis was slightly higher in the uninfected compared to the infected secretome; however, at 72 hours the uninfected shows 2.2-fold increase in activity (Figure 3-17B and C). Casein is typically used to determine the activity of MMP-3 and MMP-1, which have similar molecular weights; however, zymography did not show any bands at the corresponding lower molecular weights that correspond to these enzymes (Figure 3-17A and B).

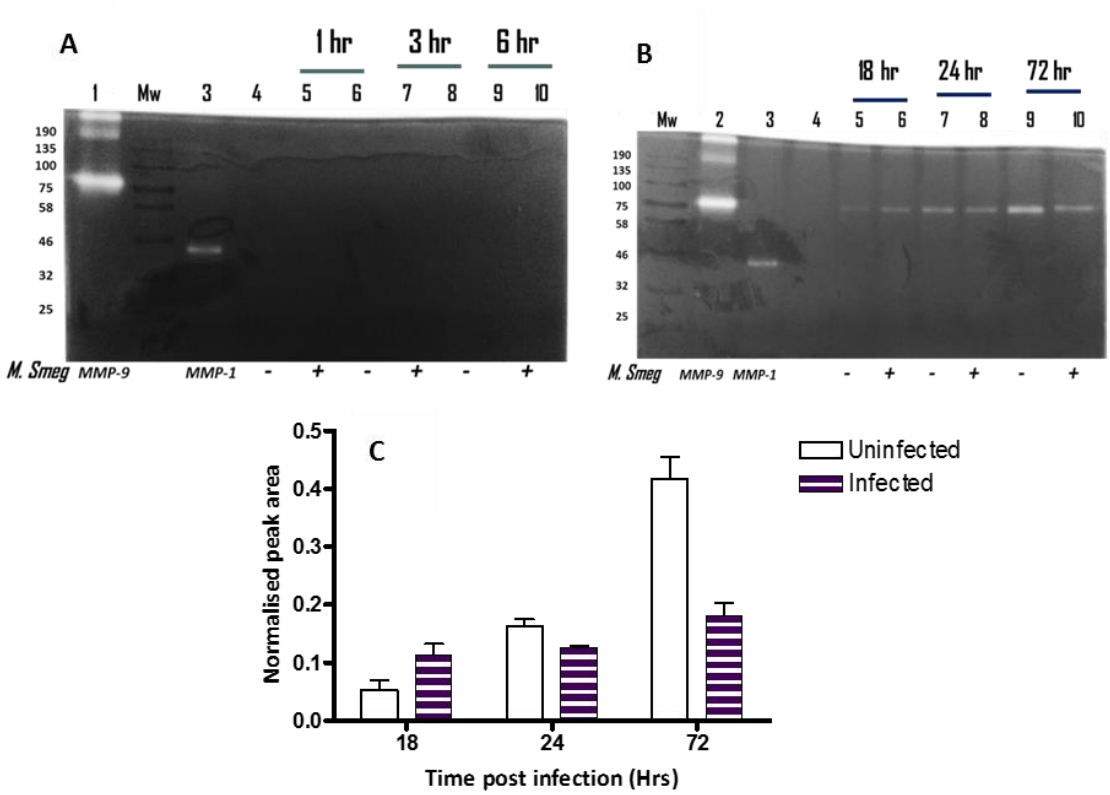

Figure 3-17: Caseinolytic activity of the uninfected and infected secretome. Casein was used as a substrate to evaluate MMP activity of harvested media. (**A**) The recombinant proMMP-9 (lane 1) and proMMP-1 (lane 3) were also loaded as controls. (**B**) Positive controls proMMP-9 and proMMP-1 were loaded in lanes 2 and 3, respectively. (**C**) The bands corresponding to the 82 kDa band and recombinant proMMP-9 were scanned and quantified using ImageJ. Bands were scanned in triplicate and data represented as mean ± SEM.

At the intracellular level, the activity for the 82 kDa form of MMP-9 was comparable between the infected and uninfected samples at all the time points (Figure 3-18 (A and C). The gelatinolytic banding pattern of the 72-hour time point (Figure 3-18B) was similar to that of its secretome where the presumed MMP-9 band (82 kDa) in the uninfected migrated more rapidly. In addition, a 57kDa-band corresponding to proMMP-1 was observed in the uninfected but was absent in the infected lysate. The band corresponding to the active form of MMP-1 (47 kDa) migrated more slowly in the infected samples of the 18 and 24-hour time points and was not observed in the infected cells at 72 hours (Figure 3-18B). Like the secretome, this highlights the contrasting effects that the *M. smeg* has on the expression and activity of MMP-1 versus MMP-9 in the THP-1 macrophages. The gelatinase activity corresponding to MMP-9 (67 kDa band) was higher in the uninfected lysates for the earlier time points (1 to 6 hours) as well as 72 hours (Figure 3-18 B and D). The proMMP-1 (57kDa) which was only observed in the 72-hour time point migrated slightly more quickly in the uninfected and showed higher activity than in the infected (Figure 3-18D). Unlike the secretome, the intracellular samples did not hydrolyse casein (Figure 3-19A and B).

proMMP-9 contains 19 cysteine residues, some of which have been shown to be important for its secretion and/or activity. Therefore, gelatin zymography was used to assess the activity of secreted and lysate MMP-9 when exposed to the reducing agent β-mercaptoethanol (Figure 3-20). The recombinant MMP-9 loaded as a control was also reduced using β- mercaptoethanol. Under these conditions the activity of secreted MMP-9 was abrogated in the 3 and 6-hour time points, and greatly decreased for the later time points when compared to non-reducing conditions (Figure 3-15). The bands showing hydrolytic activity including the control migrated more slowly (closer to 100 kDa), compared to non-reducing conditions.

Similarly, the activity of intracellular MMP-9 was abolished in the presence of β-mercaptoethanol (Figure 3-21) in all the time points except for the 24-hour cells which had some residual bands of activity (Figure 3-21). This contrasts with the lysates under non-reducing conditions (Figure 3-18). The band corresponding to the proMMP-1 at 47 kDa maintained activity under reducing conditions.

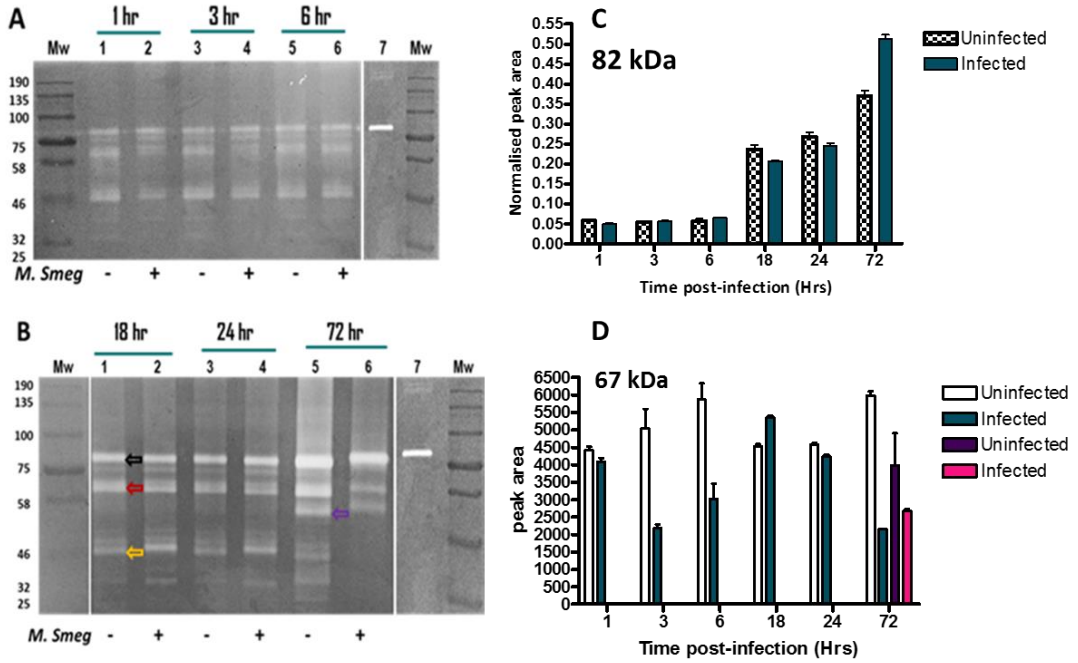

Figure 3-18: Effect of M. smeg infection on gelatin hydrolysis by the lysate. (**A** and **B**) Lysate harvests from uninfected and infected cells were loaded on the respective lanes. The recombinant proMMP-9 (lane 7) was loaded as a positive control. (**C** & **D**) The bands corresponding to the MMP-9 82 kDa (black arrow) and 67 kDa (red arrow) were scanned and quantified using ImageJ. Also, quantified in the 72-hour time point is the proMMP-1 band (purple arrow) represented by the purple and pink bars (**D**). The active form of MMP-1 is also indicated (yellow arrow). The bands were scanned in triplicate and data represented as mean ± SEM.

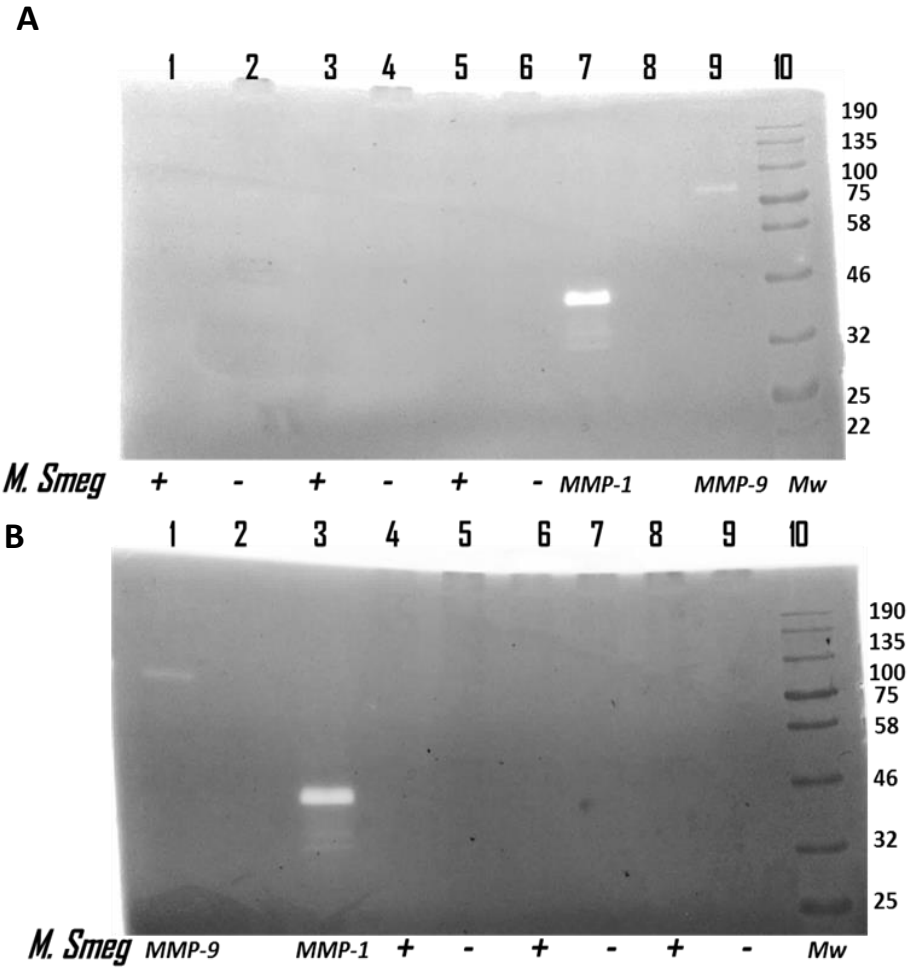

Figure 3-19: Hydrolysis of casein by uninfected and infected intracellular proteome. The harvested lysate **(A)** from hour 1, 3 and 6 hours post-infection are represented by lanes 1-2, 3-4 and 5-6, respectively and **(B)** lanes 4-5, lanes 6-7 and lanes 8-9 represent the later time point harvests 18, 24 and 72 hours, respectively.

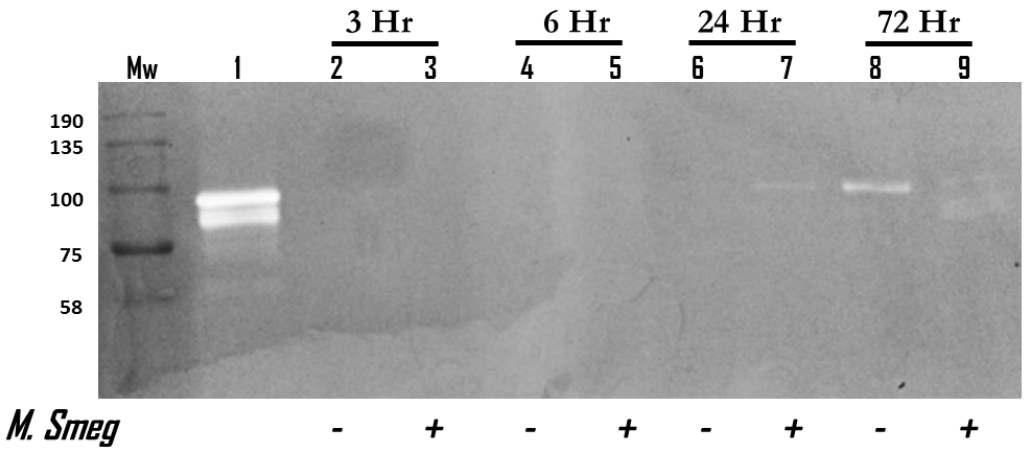

Figure 3-20: Analysis of gelatinase activity of the secretome under reducing conditions. The media samples from the indicated time points were prepared with sample buffer containing 10% β-mercaptoethanol prior electrophoresis. Recombinant proMMP-9 was also prepared under reducing conditions and loaded (lane 1) as a control.

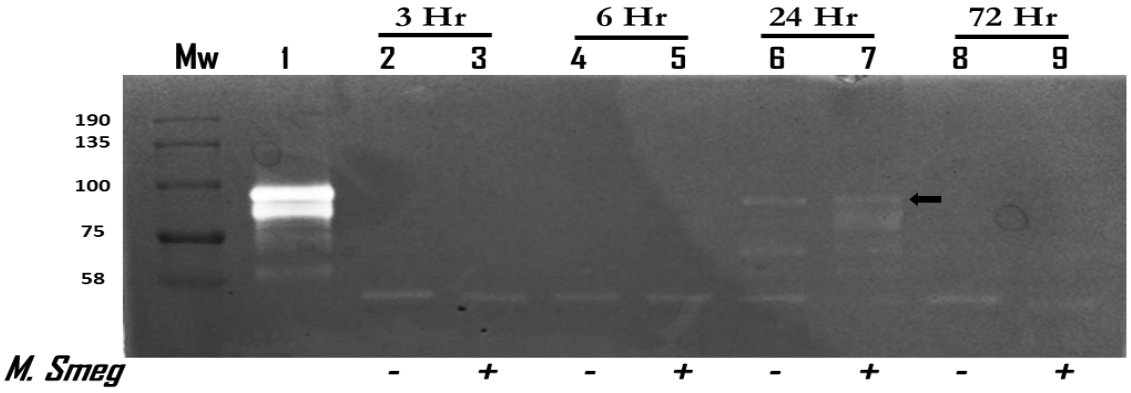

Figure 3-21: Effect of reducing conditions on the gelatinase activity of the lysate. The lysate samples were prepared using buffer containing 10% β-mercaptoethanol including recombinant proMMP-9 loaded (lane 1) as a control. Representative samples from the earlier and later time points are indicated.

3.3 Evaluation of APMA activated media using gelatin zymography

The presence of the prodomain inhibits MMP activity by co-ordination of its cysteine residue with the active site catalytic zinc thus preventing the acquisition of the water molecule essential for catalysis. Non-proteolytic activation of MMPs can be carried out using APMA which interacts directly with the prodomain cysteine inducing a conformational

change that allows for hydrolysis but still retaining the prodomain. This form corresponds to a molecular weight of 92 kDa as observed by zymography and SDS-PAGE (Shapiro *et al.* 1995). Cleavage of the prodomain yields an 82 kDa active form of MMP-9 apparently via autoproteolysis or hydrolysis by other proteases.

Zymography was used to assess the effects of APMA-activation of the secretome on gelatin hydrolysis. The uninfected and infected secretomes from the 6 and 72-hour time points were incubated at 37 ˚C for 16 hours with or without APMA. In the zymogram there is a distinct difference in the banding pattern between the APMA activated and non-activated secretome (Figure 3-22A). Activation with APMA results in the disappearance of the band at 120 kDa (Figure 3-22A) and the conversion of the 82 kDa MMP-9 to its 67 kDa form which occurs more slowly with non-activated. This 67 kDa active form of MMP-9 lacking the C-terminal hemopexin domain is more prominent in the APMA activated samples. At 6 hours, APMA activation results in faster conversion to the 67 kDa form in the uninfected compared to the infected media. In the absence of APMA, this time point harvest depicts a hydrolytic band at 57 kDa corresponding to proMMP-1 and the 120 kDa form in both infected and uninfected that is absent with the APMA activation. The 120 kDa band is higher in intensity in the uninfected secretome. Interestingly, in the absence of APMA the 72-hour uninfected secretome shows increased activity of the 67 kDa fragment including bands of activity for proMMP-1 (57 kDa), active MMP-1 (47 kDa) and the 32 kDa MMP-1 autocatalytic fragment which were not visualised in the infected secretome (Figure 3-22A). In contrast, the infected secretome shows almost no activity at 67 kDa but elicits comparable activity at 82 kDa and 120 kDa to the uninfected. Overall, treatment with APMA results in a more rapid conversion from the 82 kDa to the 67 kDa form of MMP-9 with the absence of proMMP-1/MMP-1 and 120 kDa multimer activity.

When the 6-hour time point media was incubated for 2 hours with and without APMA at 37 ˚C, there was no difference between APMA and non-activated (Figure 3-22B). For instance, the uninfected depicted equal activity for the 82 and 67 kDa form. In contrast, the corresponding infected secretome samples showed much lower activity for the 67 kDa versus the 82 kDa form and increased activity of the 120 kDa multimer.

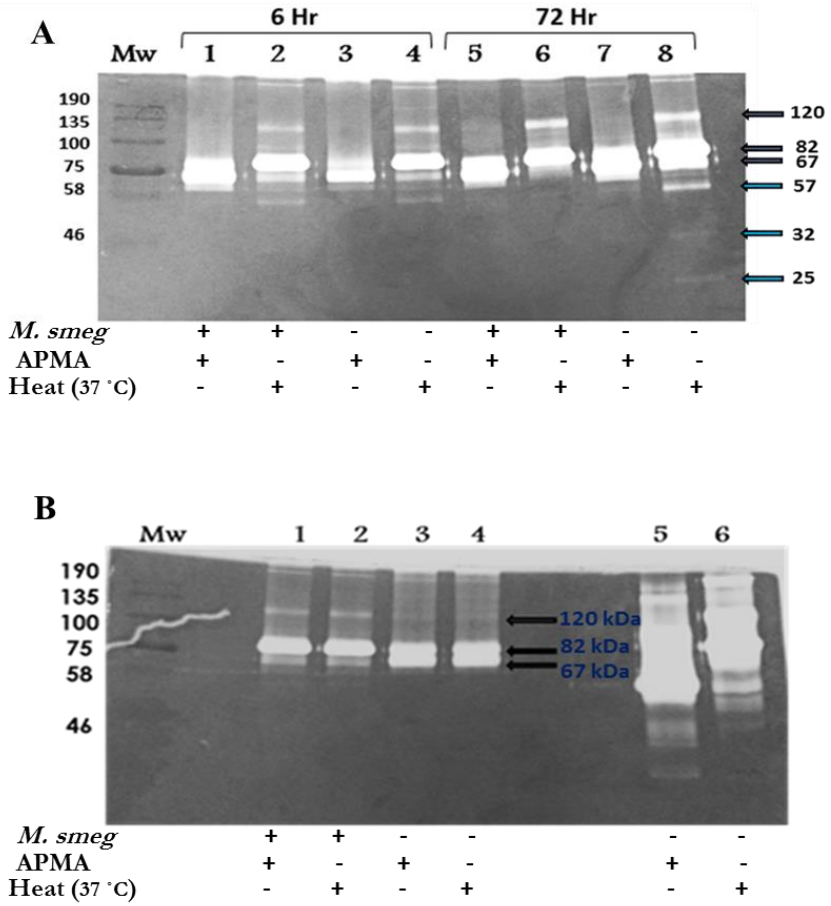

Figure 3-22: The effect of APMA-activation and heat-activation on the gelatinase activity of infected and uninfected secretome. (**A**) The secretome harvested from the 6 and 72-hour time points were incubated with (+) or without (-) APMA for 16 hours at 37 ˚C. (**B**) The 6-hour time point secretome (Lanes 1 to 4) and recombinant proMMP-9 (Lanes 5 and 6) were incubated for 2 hours with (+) or without (-) APMA at 37 ˚C.

3.4 The effect of *Mycobacterium smegmatis* infection on the specific activity of secreted MMP-1

Due to the limited sensitivity and specificity of the zymography assay for MMP-1, an assay where a specific anti-MMP-1 monoclonal antibody is used in combination with an MMP fluorogenic substrate was used for further comparative analysis. Analysing the secreted MMP-1 without prior activation with APMA resulted in no measurable activity (data not shown). Therefore, APMA was used to activate MMP-1, meaning the endogenously active and pro-forms were measured. The enzyme activity was only detectable at the 24 and 72-hour time points suggesting that MMP-1 is secreted after 24 hours incubation with the macrophages. This delayed secretion when compared to that of MMP-9 was also observed in other studies where THP-1 monocytic cells were used (Friedland *et al.* 2002). The activity was higher in the uninfected versus infected, especially after 72 hours where there was a 4.9-fold increase in activity (p <0,008) (Figure 3-23). This agrees with the gelatin zymography of the secretome from *M. smeg* infected versus uninfected macrophages (Figure 3-15C).

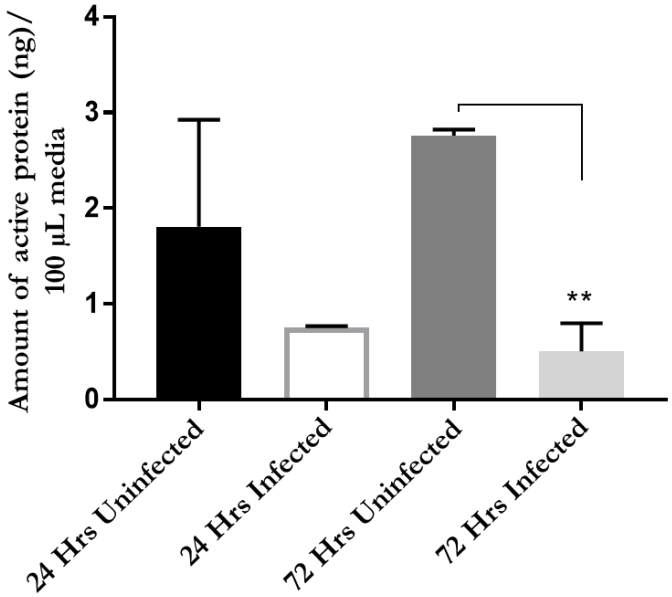

Figure 3-23: Effect of M. smeg infection on activity of secreted MMP-1. The activity of secreted MMP-1 post-treatment with APMA (proMMP-1 and MMP-1) was compared between uninfected and infected for harvested time points at 24 and 72 hours post-infection. The experiments were done in triplicate for each of the two biological replicates. No significant difference was observed after 24 hours (p = 0,381), the only significant difference (p = 0,008) was observed for the 72-hour time point.

3.5 Comparing the expression pattern of MMP-1 and MMP-9 in infected and uninfected THP-1 macrophages

To investigate whether there is any correlation between the expression and activity of MMP-1 and MMP-9, western blotting was carried out with a polyclonal anti proMMP-1 antibody (Figure 3-24). Under non-reducing conditions the active form of MMP-1 (47 kDa) was visible only in the uninfected 72-hour harvest, again supporting the zymography data (Figure 3-15C). Under reducing conditions, the pro-form (57 kDa) was present in both uninfected and infected; however, there was more of the active form (47 kDa) in the infected lysate. Other bands were also detected at 25 and 32 kDa in the uninfected and infected samples, respectively. These may be active degradation products generated by other proteases or autolysis products of MMP-1.

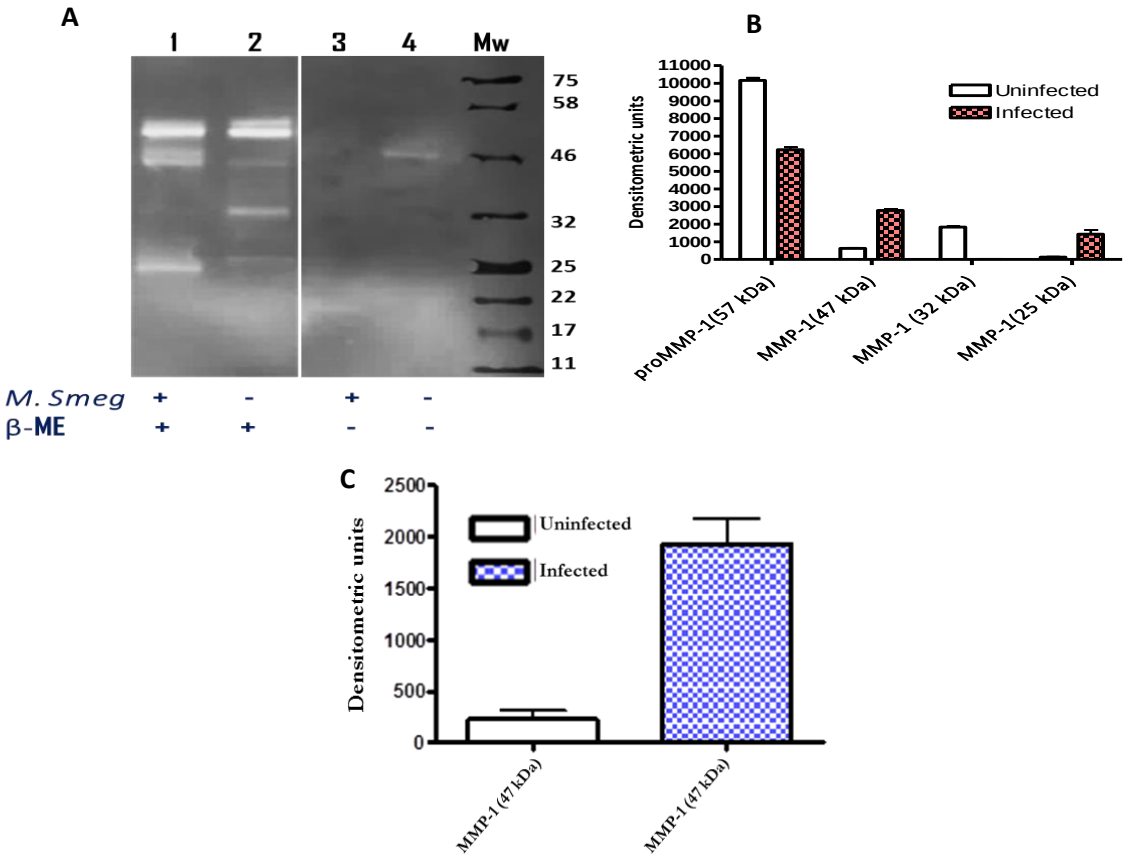

Figure 3-24: The migration pattern of expressed MMP-1 under reducing and non-reducing conditions. (**A**) Lysate harvested from uninfected and infected THP-1 macrophages after 72 hours post infection was prepared with or without β-mecarptoethanol before electrophoresis. The MMP-1 antibody was used to probe and compare the expression pattern. (**B**) The reduced MMP-1 bands in lanes 1 and 2 were scanned in triplicate and represented as mean ± SEM. (**C**) The non-reduced bands in lanes 3 and 4 were scanned in triplicate and represented as mean ± SEM.

The monoclonal proMMP-9 antibody did not detect any proMMP-9 in the lysate (both reducing and non-reducing sample buffer), which implies that the THP-1 macrophages express the active form of the enzyme. This corroborates the zymography results (Figure 3-15) where the 82 kDa active form is detected.

Discussion

Implication of MMP-1 and MMP-9 in the macrophage response against *M. smeg* infection

Mycobacterium smegmatis is used to model its virulent counterpart *Mycobacterium tuberculosis* because of its fast-growing and less laborious nature. Both MMP-1 and MMP-9 have been documented to be upregulated in patients with tuberculosis and in primary monocytes infected with *M. tb* (Elkington *et al.* 2007;Elkington *et al.* 2005a;Elkington *et al.* 2005b;Ordonez *et al.* 2016). In all the cases there was no counterbalance by the TIMPs. This led to the conclusion that *M. tb* deliberately drives this tissue degrading phenotype that causes cavitation culminating in transmission (Elkington *et al.* 2007;Elkington *et al.* 2005a;Elkington *et al.* 2005b;Ordonez *et al.* 2016). Analysing the expression and activity of MMPs in response to *M. smeg* infection is an important comparative study.

3.6 Hydrolysis of the MMP-9 synthetic substrate

The overlap in substrates cleaved by MMPs poses a challenge in designing drugs that are specific for different MMPs. Novel ways of inhibiting or regulating MMPs have been described including targeting their activation (Scannevin *et al.* 2017). Variability in the sequences of their Hx domain (Piccard *et al.* 2007) makes it another potential target for rational drug design. The selectivity of MMP-9 to the synthetic substrate has been mainly attributed to Arg at P2 and Ser/Thr at the P2´ site of the substrate (Kridel *et al.* 2001). However, the substrate has a consensus sequence (SGKGPPRQITA) that can be cleaved by MMP-7 and MMP-13 at a catalytic efficiency about 10-fold lower than that of MMP-9. MMP-7 is a matrilysin that lacks the C-terminal Hx domain and like MMP-1, MMP-13 is a collagenase. The derivation of the MMP-9 substrate was mainly based on collagen and gelatin cleavage sites (Kridel *et al.* 2001). In the current study the expected Q9/I10 cleavage site described by Kridel and colleagues was confirmed with the identified proteolytic products (GCREKGPRQ) with the molecular weight 1030.54 Da (Table 3-1) and ITERCG with a molecular weight of 677.78 Da (peak C) (Table 3-1 and Table 3-2) by mass spectrometry.

Unbound APMA reacts with the substrate at the cysteine and possibly arginine residues (Galazka *et al.* 1996), resulting in the deamination of APMA or of the substrates amino acid residues. Thus, the shoulder peaks eluting with substrate in presence of APMA suggests some interaction between APMA and substrate. Other cleavage sites that were identified include the I10/T11, E4/K5, R3/E4, G6/P7 and E12/R13. The findings of the current study suggest that MMP-9 cleaves the substrate at multiple sites mainly via gelatinolytic, collagenolytic and serine protease activity. The postulated serine protease activity has not been investigated exhaustively in the current study, but since MMPs can activate each other and/or undergo autolysis, thus they could be mimicking the serine proteases; plasmin and trypsin which are well-known MMP-activating proteases (Duncan *et al.* 1998). The simulated cleavage sites for the serine proteinases trypsin and proteinase K that overlap with the postulated cleavage sites by MMP-9 are R3/K4; and E4/K5, I10/T11 and E12/R13, respectively. To further support the postulated serine protease activity of MMP-9, the crystallised structure of proMMP-1 illustrates intermolecular interactions between the Hx domain and the prodomain (Piccard *et al.* 2007) advocating for the auto-activation of MMPs occurring via the serine protease cleavage of their Hx domain. Besides its role in sequestering heme, other functions have been described for hemopexin namely its serine protease activity and suppression of lymphocyte necrosis amongst others (Mauk *et al.* 2011). Although it lacks the typical catalytic triad ascribed to serine proteinases, there is enough evidence to suggest that it has serine protease activity, for example it is inhibited by serine protease inhibitors (Mauk *et al.* 2011). A study by Mecham and colleagues showed that glycine and alanine were more preferred at the P1 site of elastin over leucine and isoleucine by MMP-9 (Mecham *et al.* 1997). This supports the G6/P7 cleavage site that was identified in the current study.

The difference in the hydrolysis of the synthetic substrate between infected and uninfected macrophages was insignificant for all the time points. There are some limiting factors in the activity assays. The presence of MMP inhibitors and other proteinases in the media with the potential of cleaving the substrate add a layer of complexity in analysis. The use of the synthetic substrate cannot discern whether the lack or reduced activity is due to inhibition by TIMPs or secretion of proMMPs.

The study confirmed the Q9/I10 cleavage site described by Kridel and colleagues (Kridel *et al.* 2001) and identified other cleavage sites, but additional supporting data is required. Identification of the scissile amino acids by mass spectrometry could have benefitted from labelling, for example, with Edmans reagent (Lombard *et al.* 2005). This would also enhance the signal of low abundant product peptides. The limitations of using the non-labelled synthetic substrate was identifying the product peaks on the HPLC with confidence making quantitation inconclusive. Identification and quantitation of the peptides could have been done by mass spectrometry given its high-resolution power and sensitivity over the HPLC but due to limited availability of the instrument the activity experiments were carried out using the HPLC. In future, optimisation of the gradient could be performed for example using a longer gradient for separating the product peaks further and enhancing the quantitation.

3.7 Analysis of MMP-1 and MMP-9 activity by zymography

Activity of secreted MMP-9 and MMP-1

Zymography was used for further of the activity and has the advantage of discerning the activity of different forms of MMPs including their pro-forms. *M. smeg* induced an increase in MMP-9 activity which was maintained until 18 hours. Thereafter, a decline in the differential activity is observed in the 24-hour time point. Although the 18-hour time point shows the highest difference in activity (11-fold higher in the infected) there is an observed drop in gelatinolysis for both uninfected and infected compared to the 6-hour time point. This is important to note as it is indicative of a switch in the proteolytic phenotype, specifically, in the MMP repertoire of the macrophages between the 6 and 18-hour time point. It is well-documented that MMP-9 is responsible for recruiting macrophages to the site of infection and for granuloma maturation, therefore its enhanced activity is not surprising as it is imperative for degradation of the basal membrane and migration of cells to the site of infection.

The secreted 113 kDa gelatinolytic band observed in the 6 and 72-hour infected harvests could represent heterodimerisation of the 82 kDa form of MMP-9 for regulating its activity and/or that of its interacting partner. There is a plethora of plausible interacting proteins

(discussed in the Proteomics Chapter 5) including sideroflexin and the 32 kDa form of MMP-1. Absence of the 32 kDa MMP-1 form in the infected lysate compared to the uninfected (Western blotting) supports the heterodimerisation of the 82 kDa MMP-9 and 32 kDa MMP-1 in the infected secretome. Other studies have reported that dimerization of the proMMP-9 (TIMP free) and MMP-1 yields an active complex that functions synergistically in the hydrolysis of gelatin and collagen (Goldberg *et al.* 1992). It is therefore possible that MMP-1 and MMP-9 interact to regulate their ECM degrading function. The presence of the 57 kDa gelatinolytic band presumed to be proMMP-1 in the uninfected secretome and its absence in the infected at 72 hours could be evidence of the postulated proMMP-9.TIMP-1 dimer forming a ternary complex with proMMP-1 and inhibiting its activity in the infected secretome (Ogata *et al.* 1995). Neutrophil gelatinase-associated lipocalin is a 25 KDa protein that can form disulphide bonds with the C-terminal hemopexin domain of proMMP-9 (Bouchet and Bauvois 2014). This complex has been detected in urine, blood, tissue and brain tumours and has been documented to indicate severity of disease in cancer (Bouchet and Bauvois 2014;Yan *et al.* 2001). In addition to neutrophils, NGAL is also expressed by other cells either than neutrophils, including macrophages, kidney cells (Jung *et al.* 2016;Miharada *et al.* 2008) and adipocytes (Zhao *et al.* 2014). In the case of *M. smeg* infection the presence of NGAL in the infected and not the uninfected secretome may be to regulate the activity of MMP-9 with the aim of controlling substrate binding and recognition via the C-terminal hemopexin domain. Its binding to MMP-9 has also been reported to prevent its own degradation (Yan *et al.* 2001). Another important and relevant function of NGAL is its ability to scavenge bacterial siderophores and prevent egress of intracellular iron to the extracellular matrix starving bacteria thereby preventing their growth (Flo *et al.* 2004;Zughaier *et al.* 2014). Thus, this interaction implies a dual role, that is a balance in the antimicrobial activity of NGAL and the tissue degrading activity of MMP-9. There was no evidence of the expression of proMMP-9 when the lysate and media (results not shown) were probed with the proMMP-9 monoclonal antibody (Appendix 2, Figure 6-11) suggesting that 82 kDa form of MMP-9 and not proMMP-9 is expressed and secreted by the THP-1 macrophages. However, zymography is a more sensitive technique than western blotting thus the 113 kDa band could represent proMMP-9. Other possibilities include post-translational modifications such as glycosylation and disulfide modification (Khan *et al.*

2012). In a previous study the upper band has been attributed to activity of proMMP-9 or the fully glycosylated form (Ashley *et al.* 2017).

When comparing the hydrolysis pattern between gelatin and collagen, collagenolysis between uninfected and infected is not significantly different, except in the 6-hour time point where collagen hydrolysis is significantly higher in the infected versus uninfected. Similar results were evident when the second biological replicate was analysed (Appendix 2, Figure 6-3). Even so, the fact that the infected at 6 hours still shows similar hydrolytic activity to the uninfected at 3 hours validates the postulated substrate switch at the 6-hour time point with the objective of minimising the breakdown of gelatin and especially collagen type I. Thus, infection with *M. smeg*, results in the host restricting extracellular degradation especially of the lung collagen given its primary role in providing tensile strength to the lung possibly by balancing the pro- and anti-inflammatory responses. This is indicated by the regulation of MMPs which are also secreted as a response to inflammation. Additionally, collagen degradation has been associated with dissemination of *M. tb*, this rationalizes the tight regulation of collagen hydrolysis observed with zymography. Also, the 24 and 72-hour uninfected time point harvests show activity of proMMP-1 but not its active form even under serum starvation. The absence of proMMP-1 activity when either casein or collagen were used as substrates indicates that it is secreted at levels lower than the detection minima of the respective zymograms or largely in its pro-form to regulate its activity. Due to its narrower collagen binding site and the steric hindrance conferred by the propeptide (Nagase *et al.* 2006), cleavage of collagen in its native triple helical state and detection of proMMP-1 by collagen zymography is difficult.

Elastin is a primary substrate for elastases such as MMP-12 but can also be cleaved by MMP-9 (Mecham *et al.* 1997;Senior *et al.* 1991) which was loaded as a positive control in elastin zymography. There was no enzymatic activity when elastin was used as a substrate, this could be attributed to the insolubility of the elastin (Mecham *et al.* 1997) making it difficult for cross-linking and polymerisation with acrylamide. This would hinder the retention of the Coomasie-blue background by the gel rendering the clear zones of hydrolysis undefined and invisible.

Another possibility is that the elastases were either not secreted by the macrophages or were secreted at concentrations lower than the detection limit of elastin zymography.

To contain *M. tb* infection, well-formed granulomas and recruiting macrophages to the site of infection is important and is associated with the upregulation of MMP-9. The pronounced increase in the gelatinase activity of MMP-9 which declined in the later time points suggests that factors that are expressed and secreted as the macrophage response system (including resident macrophages) are sufficient in killing *M. smeg*. Thus, an alternate mechanism is employed by the host in sterilizing *M. smeg* without causing irreparable tissue damage. In this case by switching the substrate specificity of secreted MMP-9 as was evident in the later time points having caseinolytic activity in contrast to the earlier time points. The switch is postulated to occur between the 6 and 18-hour time point. The mutation of the propeptide cysteine residues in proMMP-3 to serine or histidine (C75S and C57H) resulted in proteins that were only able to hydrolyse casein when activated with APMA (Galazka *et al.* 1996) and that the R74/D79 salt bridge of the propeptide are important for APMA activation suggesting direct interaction with these residues. The R74 (R106 in proMMP-9) has also been shown to be important for the small inhibitor JNJ0966 binding and inhibiting activation of MMP-9 from the 86 kDa to the fully active 82 kDa form. Since both the uninfected and infected secretome had caseinolytic activity only in the later time points and none in the lysate, this indicates that to generate the fully activated form of MMP-9 (82 kDa) requires that it be secreted together with other factors that destabilise the propeptide such as temperature, oxidation and other proteins that accompany prolonged incubation. It is possible that the earlier time points secrete the 86 kDa form while the later ones secrete the 82 kDa form, which would be indistinguishable by zymography given the small difference in molecular weight. Another explanation is that these differences reflect the effects of alternative splicing or posttranslational modifications of proMMP-9 that are ultimately processed differently in the ECM. These may be strategies employed by the host in preventing chronic gelatinase activity resulting in severe tissue damage and repurposing the function of MMP-9 toward regulation of processes such as angiogenesis and wound healing amongst others.

Activity of intracellular MMP-9 and MMP-1

The intracellular gelatinase activity of MMP-9 (82 kDa) was not significantly altered by the *M. smeg* infection, in fact the activity was only slightly higher in the uninfected in the 18 and 24-hour time points (Figure 3-18), suggesting that the activity of secreted MMP-9 is controlled in the ECM. The gelatinolytic band corresponding to the 67 kDa molecular weight shows higher activity in the uninfected during the 3, 6 and 72-hour time points suggesting that its presence in the infected is suppressed by minimising activation of the 82 kDa form. There is appearance of the band corresponding to proMMP-1 at 72 hours which had higher activity in the uninfected versus infected, a pattern observed in the secretome and expression levels as evident from the western blotting. This contrasts with *M. tb* infection which is characterised by an increase in the expression and activity of MMP-1 (Elkington *et al.* 2011a;Elkington *et al.* 2005a). The absence of caseinolysis in the cell lysates, despite eliciting gelatinase activity and with the later time points of the secretome showing caseinolysis, indicates that the proteolytic phenotype does not favour casein as a substrate. Substrate preference could be dictated by the presence of other proteins or by posttranslational modifications which ultimately conferred caseinolytic activity to the secreted MMP-9 at the later time points. It is also important to note that the structure of casein is more complex than that of gelatin with O-glycan linked sites, disulfides and phosphorylation sites (Ecroyd *et al.* 2010;Lasa *et al.* 1997). Processes such as invadopodia formation, phagocytosis, exo- and endocytosis require cytoskeletal remodelling and consume energy (Kolonko *et al.* 2014;Ressad *et al.* 1999;Thomas *et al.* 2006), therefore intracellular energy could be reserved for these processes and diverged from breakdown of complex substrates hence the absence of casein hydrolysis by intracellular proteases. Maintenance of the microtubular structure has also been reported to be highly important for the secretion of MMP-9 and facilitating endocytosis (Chintala *et al.* 1998;Hanania *et al.* 2012). Regulation via modification of cysteine residues could also alter the secretion and substrate specificity of MMP-9 given the location of these cysteines as alluded to earlier. Protein disulphide isomerase (PDI) is one of the enzymes that has been shown to regulate the activity of MMP-9, not only does it increase the secretion of MMP-9 but was also able to reactivate and renature reduced and denatured MMP-9 (Ali Khan and Mutus 2014;Khan *et al.* 2012).

In the uninfected lysate, MMP-9 migrated more slowly than in the infected lysate at 18 and 24-hour time points, unlike the 72-hour time point. This could be attributed to a difference in posttranslational modification and/or alternative splicing of MMP-9. These modifications may be impacting the secretion and activity of MMP-9. For example, the activity of the 82 kDa form of MMP-9 was higher in the infected secretome at 18 and 24 hours unlike in the 72-hour time point where activity of the infected is lower than the uninfected secretome. The differential migration pattern may be influenced by two important factors, that is, glycosylation and redox modification of the disulfide bonds possibly located at the cysteine switch, fibronectin and/or Hx domain. Khan and colleagues have demonstrated that the cysteine to serine mutations in the cysteine switch, fibronectin repeats and to a lesser extent the Hx domain resulted in underglycosylated forms. Interestingly, these mutations abrogated the secretion of MMP-9 while the ones located in the Hx domain only decreased its secretion (Khan *et al.* 2012). With regards to redox control, the reduction of MMP-9 resulted in slower migration and significant decrease in activity (Figure 3-20 and 3-21). In the current study the faster migration of MMP-9 in the infected at the 18 and 24-hour time points is indicative of a drop in pH and an oxidative burst that accompany phagolysosomal fusion and bacterial killing an environment that could have resulted in modification of the cysteines redox state. These alterations would in turn lead to underglycosylation in the infected cells, a strategy employed to decrease its secretion and activation in the ECM where the differential activity declines in the 24 and 72-hour time points. The drop in pH is associated with the acidification steps during phagolysosomal fusion facilitated by vATPase which has been shown to decrease and increase the activity of MMP-9 and MMP-2, respectively, when inhibited with concanamycin in pancreatic cancer cells (Chung *et al.* 2010;Chung *et al.* 2011). Although PDI has been shown to rescue denatured and reduced MMP-9 its role during the acidification steps is ambiguous and may be acquired to minimise its secretion and activation. In contrast to the 18 and 24-hour time points, the faster migration of MMP-9 in the uninfected at the 72-hour time point is intriguing and may depict the ability of the macrophages to restore homeostatic conditions as indicated by the higher activity of secreted MMP-9 in the uninfected versus the infected.

The migration of MMP-1 is contrary to that of MMP-9. The active 47 kDa form of MMP-1 migrates more quickly in the infected lysate versus uninfected in the 18 and 24-hour

harvests. Whereas in the 72-hour lysate, like the secretome, this band disappears in the presence of *M. smeg*. Western blotting of reduced MMP-1 migrates more slowly than non-reduced (Appendix 2, Figure 6-10) implying that discrepancies in the redox conditions may be responsible for different migration patterns. Reduction of the lysate with β-mercaptoethanol abrogated gelatinolysis of MMP-9 while the MMP-1 was resistant with the band of activity migrating more slowly for all the time points. Thus, it is possible that the 113 kDa band in the ECM is indeed a heterodimer of MMP-9 and MMP-1 that is induced by changes in their redox and glycosylation states, a synergy that serves to control degradation of the ECM. In relation to TB cavitary granulomas, a study reported that the outermost environment of the necrotic centre is reducing (Marakalala *et al.* 2016) this suggests that at this site the activity of MMP-9 is abrogated allowing the release of MMP-1 from the heterodimer to degrade collagen causing severe tissue damage and dissemination of *M*. *tb*.

Although zymography is an inexpensive and sensitive technique, quantitation by densitometry can be limited by the overlap in molecular weight making the discernibility of the bands a challenge. The difficulty in solubilizing substrates such as collagen can affect the sensitivity of the technique hence a positive control was also loaded with the gels. Working with unknown concentrations of MMPs makes it difficult to load concentrations that are within linear detection limit. The use of a purified MMP control curbs this problem as normalisation methods can be used during densitometric analysis like in the current study. Loading equal amounts of total protein for the uninfected and infected also minimises biases. These methods are widely applied in zymography (Gogly *et al.* 1998;Ren *et al.* 2017;Scannevin *et al.* 2017).

3.8 Hydrolysis of the MMP-1 fluorogenic substrate

The higher level of MMP-1 activity secreted by uninfected macrophages compared to infected in the 24-hour time point and with significance in the 72-hour time point supports the zymography data. As mentioned earlier MMPs are regulated at different levels, this is important to note since they perform various other functions besides ECM degradation. The MMP-1 fluorescence activity assays suggest that the activity of secreted MMP-1 is regulated at different levels in the uninfected and infected macrophages. For the uninfected the regulation is implied at the level of activation where cleavage of the propeptide is either

inhibited or occurring at a very slow rate post-secretion. This is also indicated by gelatin zymography where the observed hydrolysis band corresponds to the proMMP-1 rather than its active form. Loading higher protein concentrations resulted in 47 kDa active form also observed only in the uninfected (Appendix 2, Figure 6-1), suggesting that at higher concentrations proMMP-1 autoproteolysis and activation occurs. Interestingly, in the infected cells the significantly lower levels of activity at 72 hours implied that the secretion of proMMP-1 is tightly regulated compared to the uninfected (also depicted by absence of secreted proMMP-1 band of activity in Figure 3-15C) and/or the expression levels are lower compared to the infected. Further investigation was carried using western blotting and discussed in section 3.9.

Although, this high-throughput method is expensive it is specific as it involves capturing MMP-1 with a specific antibody coated on the plate prior assaying the activity. This minimises substrate hydrolysis by other MMPs, a well-known challenge when using synthetic MMP substrate (Bracher *et al.* 2013;Kridel *et al.* 2001). Although quantitation was carried out with the use of a standard curve the nonlinear relationship between substrate concentration and fluorescence changes because of 'inner filter effects' which is common with use of fluorogenic substrates (Lombard *et al.* 2005) should be considered. Unlike zymography the concentration of proMMP-1 could not be quantified as the change in fluorescence was very minute hence APMA activation of the secretome was done prior assaying the activity.

3.9 Expression levels of MMP-1

When examining the expression pattern of MMP-1 from lysate samples prepared under non-reducing versus reducing conditions, only a faint band of active form of MMP-1 (46 kDa) was detected in the uninfected 72-hour time point under non-reducing conditions (Figure 3-24). Under reducing conditions multiple bands of the pro- and active forms were detected. The amount of proMMP-1 detected in the uninfected was elevated by about 1.6-fold compared to the infected lysate. This implies that the infected cells also expressed proMMP-1 but at a slightly slower rate, thus regulating MMP-1 activity in the ECM by mainly controlling its secretion, whereas in the uninfected cells the activity is regulated by controlling its activation in the ECM. The 32 and 25 kDa bands that were detected in the

uninfected and infected, respectively, could potentially be due to autolysis and degradation, respectively. This is substantiated by the absence of the intracellular 32 kDa gelatinolytic band for the infected versus uninfected in the lysate of the 72-hour time point. Autolysis is concentration dependent again suggesting that the expression of MMP-1 may be slightly higher in the uninfected. The MMP-1 catalytic domain (32 kDa) alone has been shown to be capable of hydrolysing non-collagenous substrates only, such as gelatin (Chung *et al.* 2004). Truncation of the MMP-1 C-terminal hemopexin domain caused inhibition of collagen hydrolysis by compromising its binding and unwinding ability to the collagen triple helical structure (Chung *et al.* 2004). Therefore, *M. smeg* alters the pathways which govern the secretion and/or expression of MMP-1. These pathways/mechanisms are also implied to be different from those induced by stress conditions. This is because the differential activity induced by *M. smeg* was not markedly masked by the potential stress that might have been caused by the serum-free conditions in which the macrophages were cultured.

3.10 Effect of APMA- and heat-activation on gelatin hydrolysis

The differences in the gelatinolytic pattern between heat-activated and APMA-activated secretome suggests that the concentration of the 67, 82 and 120 kDa forms, in the physiological context may result in different hydrolysis products of the same biological substrates. The Hx domain contributes to substrate binding and selectivity (Chung *et al.* 2004;Eckhard *et al.* 2014;Overall 2002;Piccard *et al.* 2007) thus it is possible that the 82 kDa and 67 kDa forms have different substrate cleavage sites. The Hx domain is also responsible for the interaction of MMPs with other proteins and multimerization to higher molecular weight proteins which exhibit gelatinolysis such as the 120 kDa form. The findings also highlighted the importance in the period of activation since the 2-hour and 16-hour activation generated different concentrations of the MMP-9 forms. Therefore, under physiological conditions during infection with *M. tb*, the activation of MMPs may either be beneficial or detrimental to the host as a result from masked differences in MMPs secreted by uninfected and infected macrophages. In turn, factors such as inflammation and ECM destruction would be perpetuated. This also highlights the importance of TIMP-1 in minimising the activation and conversion of MMP-9 through binding and stabilising the Hx domain.

Summary

In the current study, *M. smeg*-induced an increase and decrease in the activity of MMP-9 and MMP-1 respectively in macrophages in contrast to *M. tb* infection. This supports the postulation that upregulation of MMP-1 is specific for *M. tb* infection (Elkington *et al.* 2005a). The ability of macrophages to clear the *M. smeg* infection without causing irreparable tissue damage is by inducing a switch in the proteolytic repertoire of the macrophages to one that generates the same degradation products as the uninfected macrophages. This switch is induced between the 6-hour and 18-hour time point and could be facilitated and regulated by oxidoreductases and isomerases. These enzymes may alter the specificity of the MMPs by acting on the substrate and/or the MMPs. Therefore, the challenge in designing specific MMP inhibitors is also due to their activation which is accompanied by dissociation of the Hx domain resulting in loss of substrate specificity.

Chapter 4

Proteomics: Introduction and literature review

Since homeostasis is essential for normal functioning of the body, studying physiological processes at the protein level provides a broader scope of knowledge in context of their molecular function. Proteomics, particularly mass spectrometry-based proteomics, allows for monitoring of the dynamic function of proteins in complex systems such as tissue samples, whole cell lysates, the secretome and blood/plasma samples. It is a powerful tool employed in deciphering protein networks in context to their spatial and temporal expression, including their dysregulation in diseased compared to non-diseased states, hence its significance in the discovery of biomarkers, diagnostics and drug discovery.

4.1.1 Bottom-up proteomics: A simplified work flow

In principle, gel-based techniques such as western blotting and 2D-PAGE are aimed at analysing intact proteins, with the latter profiling larger numbers of proteins as opposed to a single protein. Although generating greater information content than western blotting, 2D-PAGE still falls short in terms of high-throughput screening, which has evolved and advanced the field of science. Comparing data between different samples by 2D-PAGE can be complex requiring expertise in pattern-matching thus limiting the number of samples and data output that could be analysed (Aebersold and Mann 2003). The other limitation of the technique is that only highly abundant proteins are profiled and the limited dynamic range (Aebersold and Mann 2003). However, with 2D-PAGE isoforms can be clearly separated and identified on the gels, which is difficult with mass spectrometry where cleavage of proteins causes loss of the isoform defining features. Bottom-up proteomics involves the analysis of peptides, ultimately matching them to their respective proteins, whereas top-down proteomics deals foremost with intact proteins (Aebersold and Mann 2016). Mass spectrometers are instruments exploited largely for bottom-up proteomics and utilise the ionisation of peptides to generate spectra of mass to charge ratio (m/z) versus intensity. This is termed the total ion chromatogram (TIC) produced by the first mass analyser (MS1)

and correlates with the relative abundance of peptides. The second mass analyser (MS2), which is relevant in the case of tandem mass spectrometry (MS/MS) used in this study, deconvolutes the peptide sequence, allowing for matching to the respective proteins (Aebersold and Mann 2003;Aebersold and Mann 2016). Briefly, a typical work flow (Figure 4-1) commences with tryptic digest of the proteins followed by in-line chromatographic separation of the tryptic digest by reverse phase HPLC. The peptides are then ionised by either matrix assisted laser desorption and ionisation (MALDI) or electrospray ionisation (ESI) and enter the mass spectrometer where they are sequentially subjected to MS1, fragmentation, and MS2 scans. The acquired spectra are then matched to theoretical spectra, which are produced *in silico* from predicting tryptic fragments of the database protein sequences (Aebersold and Mann 2003;Aebersold and Mann 2016).

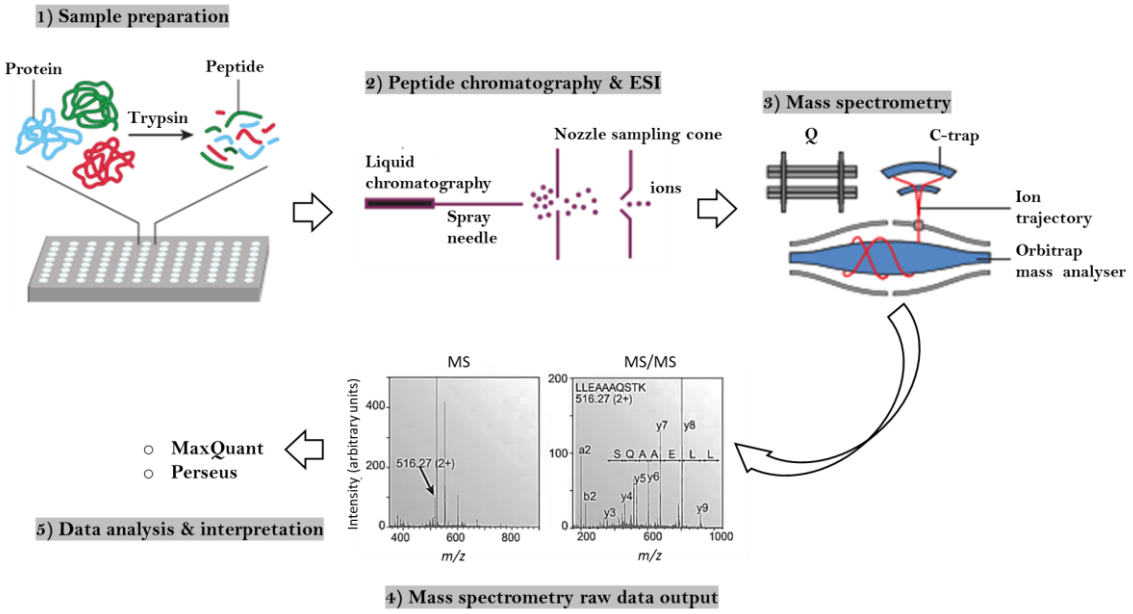

Figure 4-1: illustration of a typical proteomics experiment workflow. [adapted from (Aebersold and Mann 2003;Aebersold and Mann 2016)]

4.1.2 Tandem mass spectrometry (LC-MS/MS)

Given that this technique relies mainly on the measurement of the mass of molecules residing in complex systems, accuracy, reproducibility, resolution and sensitivity are inherently important to a mass analyser. There are four mass analysers currently in use for proteomics which includes the time-of-flight (TOF), Fourier transform ion cyclotron (FT-MS/FT-ICR), linear quadrupole ion trap (LIT) and the orbitrap mass analyser. These mass

analysers have been further developed in combination/hybrid with respect to their individual capabilities to produce high-performing instruments (Aebersold and Mann 2003;Eliuk and Makarov 2015).

In the current study, discovery proteomics was performed by employing a Q-Exactive instrument which has a built in Orbitrap mass analyser (Michalski *et al.* 2011) (Figure 4-2). This type of mass analyser exploits the electrostatic field generated axially by the inner spindle-like electrode forcing the axial acceleration of the ions upon injection, which are then trapped in orbital motion by the outer-barrel electrode. Detection of the current produced by the oscillating ions is through the differential amplifier situated in the outer-barrel electrode of the orbitrap. The spectrum of the m/z charge ratio is extrapolated from the image current by using Fourier transformation (Eliuk and Makarov 2015).

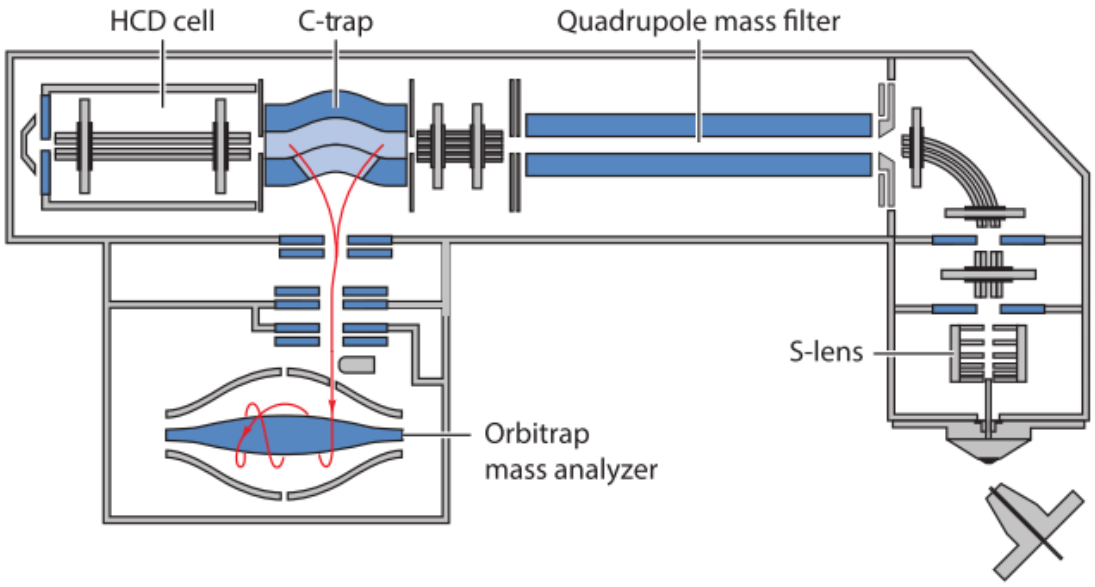

Figure 4-2: Schematic diagram of the Q-Exactive instrument.
[adapted from (Eliuk and Makarov 2015)]

4.1.3 Mass spectrometry as a tool for proteomic studies

There are several factors that contribute to a successful proteomics experiment, including sample preparation, the ion source, mass analyser, and for data output and analysis, the software and algorithms used. The MALDI and ESI are commonly used for ionizing peptides and/or intact proteins for the earlier. The electron spray ionisation (ESI) is employed for

analysis of more complex material since it is easily coupled to ion traps or triple quadrupole analysers which allow further fractionation by either collision induced dissociation (Quesada *et al.* 1997) and/or electron induced dissociation (ETD) of pre-selected ions (Aebersold and Mann 2003). In the current study high-energy collision dissociation (HCD), a type of CID, was coupled to ESI.

Fragmentation by ETD generates the c and z ion fragments by cleaving the bond between the R-group primary carbon and the N-terminal side of the amide bond. ETD induces fragmentation only by transfer of electrons to this bond hence preserving post-translational modifications such as sulfonation, phosphorylation and glycosylation (Figure 4-3). Regarding fragmentation by CID, once ions are in the gaseous phase they are allowed to collide with neutral molecules such as helium, cleaving the peptide bond thus producing b and y ions (Mikesh *et al.* 2006).

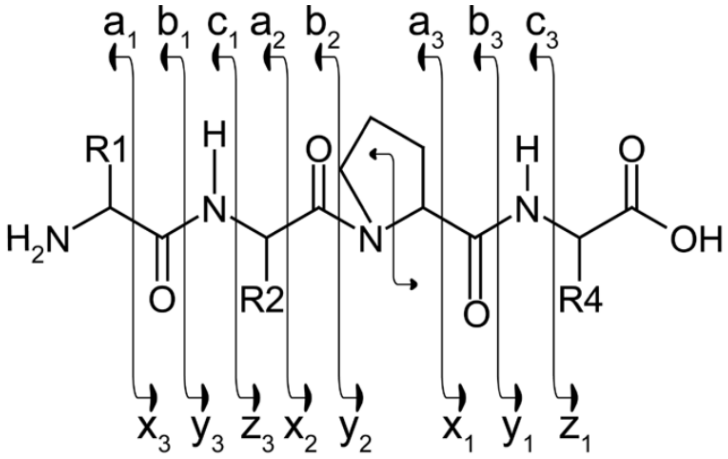

Figure 4-3: Illustration of the nomenclature of fragmented ions.
[adapted from (Mikesh *et al.* 2006)

Since ESI requires the sample to be in liquid form, it is often coupled to liquid chromatography (LC). Once the sample is ionised it is ultimately introduced into the first mass analyser (MS1) where the generated m/z versus intensity spectra of the measured peptide is relatively correlated to its abundance (Aebersold and Mann 2003). To acquire MS2 data and sequence coverage, a round of fragmentation is performed by preselection of ions for further fragmentation, usually the 'top 10' ions with the highest intensity in a given window are selected for fragmentation. Here, the intensity of the peptide is dependent on

the experimental preparation, hence referred to as data-dependent acquisition. Bias in identification of high abundant peptides over less abundant peptides is minimised by setting the dynamic exclusion. Dynamic exclusion refers to the exclusion of peptides with the use of precursor masses of peptides to be excluded within a set period during MS/MS analyses (Domon and Aebersold 2010;Hodge *et al.* 2013;Zhang *et al.* 2016). This eliminates selecting the same peptides, usually high abundant proteins thereby broadening the peptide sequences covered.

4.1.3.1 Methods of quantitative data analysis

The methods used for quantifying peptides are mostly relative however absolute quantitation can be applied by spiking a peptide sample with a labelled peptide as a reference standard with a known absolute value. This would allow for extrapolation using a standard curve. With relative quantitation both labelled, or label-free approaches can be used. Addition of tags/labels can be achieved through metabolic, chemical or enzymatic methods yielding isotopes that can be differentiated by mass shifts. These include SILAC, iCAT, iTRAQ amongst others, however these methods are more expensive, and can therefore be limiting in terms of the number of comparative samples that can be analysed (Cox *et al.* 2014;Tate *et al.* 2013). For the purposes of this study a label-free approach was used.

Label-free quantitation

The use of high-resolution mass analysers allows label-free quantitation (LFQ) at the MS1 level where the m/z elution profile of a peptide is quantified as a function of the LC retention time. This is different from other methods that utilise spectral counting and extraction ion chromatograms (Cox *et al.* 2014;Tate *et al.* 2013). Since the Orbitrap meets the high mass resolution requisite, label-free quantitation was used in the current study. MaxQuant has two built-in algorithms that can be used for label-free quantitation namely LFQ and iBAQ. Given that the LFQ depends on the m/z elution profile of a peptide, compared across samples, this poses limitations since a protein group can be reported as unidentified based on the reproducibility of the selected peptide across samples especially

for low abundant proteins (Cox *et al.* 2014). To compound this, the MaxLFQ algorithm uses stringent normalisation formulas for a peptide to be reported quantifiable thus undermining the biological significance that can be learned from the proteomics data. In contrast, iBAQ uses the inferred total intensity of the protein divided by the number of observed tryptic peptides with a length between 6 to 30 amino acids (Krey *et al.* 2014). The recently developing data independent acquisition method (DIA), SWATH (Sequential Window Acquisition of ALL Theoretical Fragment Ion Spectra) is performed on fast scanning hybrid MS usually a quadrupole mass analyser in conjunction with a TOF or Orbitrap (Ludwig *et al.* 2018). It entails the recording of a single precursor ion (MS1) followed by a series of MS2 scans over a defined wide precursor isolation windows. Thus, information is generated from extracting ion chromatographs at the MS1 and MS2 level (Ludwig *et al.* 2018). Peptide-centric scoring can be used to analyse SWATH-MS generated data.

4.2.1 Filter aided sample preparation (FASP)

FASP was first described by Wisniewski and colleagues (Wisniewski *et al.* 2009) and was used to prepare all the samples for discovery proteomics. 30 kDa MWCO filters (Merck) were used, and both the 18-hour time-point media (also referred to as the secretome) and lysate samples were centrifuged at 15 000 rpm until the dead volume is reached. Thereafter, protein denaturation was performed using 200 µl of UA solution [8 M Urea; 0.1 M Tris; pH 8.5] which was added to the filters and spun at 15 000 rpm for 15 minutes. This step was repeated twice for the lysate samples. Sample reduction was carried out by incubation with 0.1 M DTT in 50 mM NH_4CO_3 buffer for 30 minutes. To prevent disulphide bond re-formation, 0.05 M of iodoacetamide (prepared in 50 mM NH_4CO_3) was incubated with protein samples for 20 minutes in the dark. After the flow-through was discarded the samples were washed twice with urea solution and three times with 50 mM NH_4CO_3 buffer containing 20 mM calcium chloride ($CaCl_2$), with pH 8 (optimum trypsin activity). Digestion with trypsin, which was prepared in 50 mM NH_4CO_3 buffer containing 20 mM $CaCl_2$ was carried out at a ratio of 1:100 with respect to protein concentration. Finally, the samples were incubated at 37 °C for 16 hours in a humidified chamber. To prevent further digestion, formic acid was added to a final concentration of 0.1% to the peptide solution. About 80 µl of the peptide digest was eluted from the filter into new collection tubes by centrifuging at 15 000 rpm for 10 minutes. To elute the peptides further, the filter was washed with 40 µl with ammonium bicarbonate buffer.

The eluent was desalted using an in-house packed C18 stage tip. Prior to loading the sample on the C18 stage tip, the C18 was activated by washing three times, first with solution B (80% Acetonitrile; 0.1% Trifluoroacetic acid), then with solution A (2% Acetonitrile; 0.1% Trifluoroacetic acid). The acidified tryptic peptides were loaded onto the stage tip, followed by washing three times with solution A. Peptides were eluted using 50 µl of solvent C (60% Acetonitrile; 0.1% Trifluoroacetic acid) and collected in glass vials. A vacuum concentrator was used to evaporate solution C by centrifuging the samples for 30 minutes at 30 °C. Once

the peptide pellet had dried, it was re-suspended in 50 µl of solution A for mass spectrometry analysis.

4.2.2 Liquid chromatography mass spectrometry (LC-MS/MS) analysis parameters

All the discovery proteomics experiments were performed on a Q-Exactive Quadrupole-Orbitrap mass spectrometry (Thermo Scientific) which was coupled to the Dionex Ultimate 3500 RSLC nano_LC system (Thermo Scientific). It should be noted that three technical replicates (i.e. three injections per experiment) were analysed for both lysate and media. The sample injection volume was optimised to give comparable MS intensity levels between the samples, with a minimum intensity of 3E9. Peptide samples were loaded on a 40 cm C18 analytical column (packed in- house with Aeris peptide 3.6 µM beads, Phenomenex), thereafter elution was carried out using a linear gradient of 6 – 35% solvent B (95% acetonitrile, 0.1 formic acid), at a constant flow rate of 300 nl/min. The gradient was 45 mins and 120 mins long for the secretome and lysate, respectively. The acquisition of data was carried out using Xcalibur software (Thermo scientific, v2.2) in positive ion mode. MS1 scans were acquired with a resolution of 70 000, an automatic gain control of 3×10^6 and an ion injection time of 250 ms. The MS/MS scans were acquired at a resolution of 17 500, AGC target of 2×10^5, ion injection of 120 ms and the normalised collision energy (NCE) of 25. The peptide matching was set to 'preferred', isotopic exclusion and a dynamic exclusion of 30 s.

4.3 Raw data analysis and processing

Analysis of the raw data files was performed by MaxQuant (version 1.5.3.12) using Andromeda search engine in the Blackburn Lab, searching against the Human Uniprot database (2018) and *Mycobacterium smegmatis* EC122 database (2018) to generate protein quantification and identification data. The raw files were run simultaneously, and each technical replicate was set as a separate experiment on MaxQuant. The majority of the MaxQuant settings used were default, with the false discovery rate (FDR) set at 1% against a reverse decoy of the database, with variable modifications of oxidation (M), and Acetyl

(Protein N-term), and a fixed modification of carbamidomethyl (C). A maximum of two missed cleavages was allowed. To quantify proteins, only unique peptides were used to increase the confidence of identified protein groups and iBAQ was selected and used downstream for further analysis. Thereafter the generated quantitative data were further analysed with Perseus (version 1.6.1.3).

The peptides that were identified as contaminants, reverse/decoy, or identified only by site were excluded. To compare between uninfected and infected samples, peptides that were identified in at least two of the replicates were used in the two-sample t-test (p-value < 0.05) to identify differentially expressed proteins. A p-value < 0.05 was used as a cut-off and any proteins that had a p-value less 0.05 were considered significantly differentially regulated. Since the p-value considers the variances between samples this also justifies using these proteins for downstream analysis and biological interpretation. Additionally, interference from false positives is less likely since the FDR was set at 1% in MaxQuant to exclude them. The gene/protein IDs that were found to be significantly different were assessed for biological relevance and function using FunRich 3.1.3 tool and STRING for analysing protein-protein interactions. The same assessment tools were used for proteins that were found to be uniquely expressed in either uninfected or infected samples (for both lysate and media). For a protein group to be considered as exclusively identified, a minimum of 2 peptides were required to be identified in the uninfected and 0 in the infected, or visce versa. This builds stronger evidence for differences induced by the infection.

The GO terms that had p-values < 0.05 were considered significantly enriched, and for STRING analyses the level of confidence was set at high confidence and medium confidence for the lysate and secretome, respectively. This reason being that the secretome had a smaller data set compared to the lysate. The thicker the line between the proteins the stronger the confidence of interaction between the proteins. Non-interacting proteins were removed.

Results

Modification of the THP-1 macrophage proteome and secretome by infection with *M. smeg*

The inherent function and tight regulation of matrix metalloproteinases (MMPs) for tissue homeostasis and remodelling has already been emphasised, including their dysregulation in diseased states. It is thus important to understand the factors that regulate them upstream and downstream. This is essential because the overlap in the substrates they degrade and close similarity in their catalytic and substrate binding sites still poses challenges in developing specific inhibitors, therefore, targeting factors that regulate MMPs and their regulatory/binding sites is an option still to be explored. Briefly, THP-1 macrophages were infected with *M. smeg*, followed by harvesting of the media and lysate at different time points. The 18-hour time point was prepared using the FASP protocol and analysed by the Q-Exactive.

There was a clear difference in chromatographs of the secretome (Figure 4-4), where the uninfected samples had peptides eluting between 16 and 26 minutes that were not visible in the infected samples. The chromatographs from the lysate showed no obvious differences (Figure 4-5) and the TIC intensities were comparable. The trypsin digestion was efficient, with 89.6% of identified peptides containing no missed cleavages (Figure 4-6). Between the media and lysate samples, 2878 protein groups were identified, with 24 and 29 identified as contaminants and decoy hits, respectively.

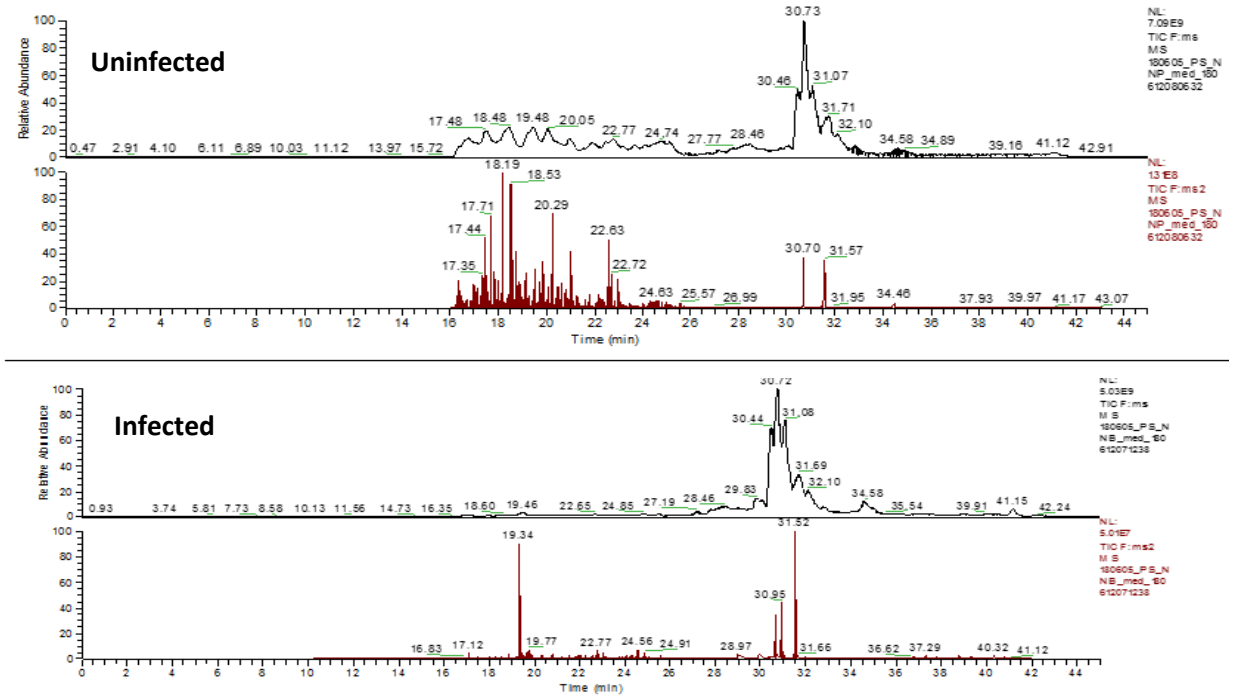

Figure 4-4. Representative chromatograph of the uninfected and infected secretome.

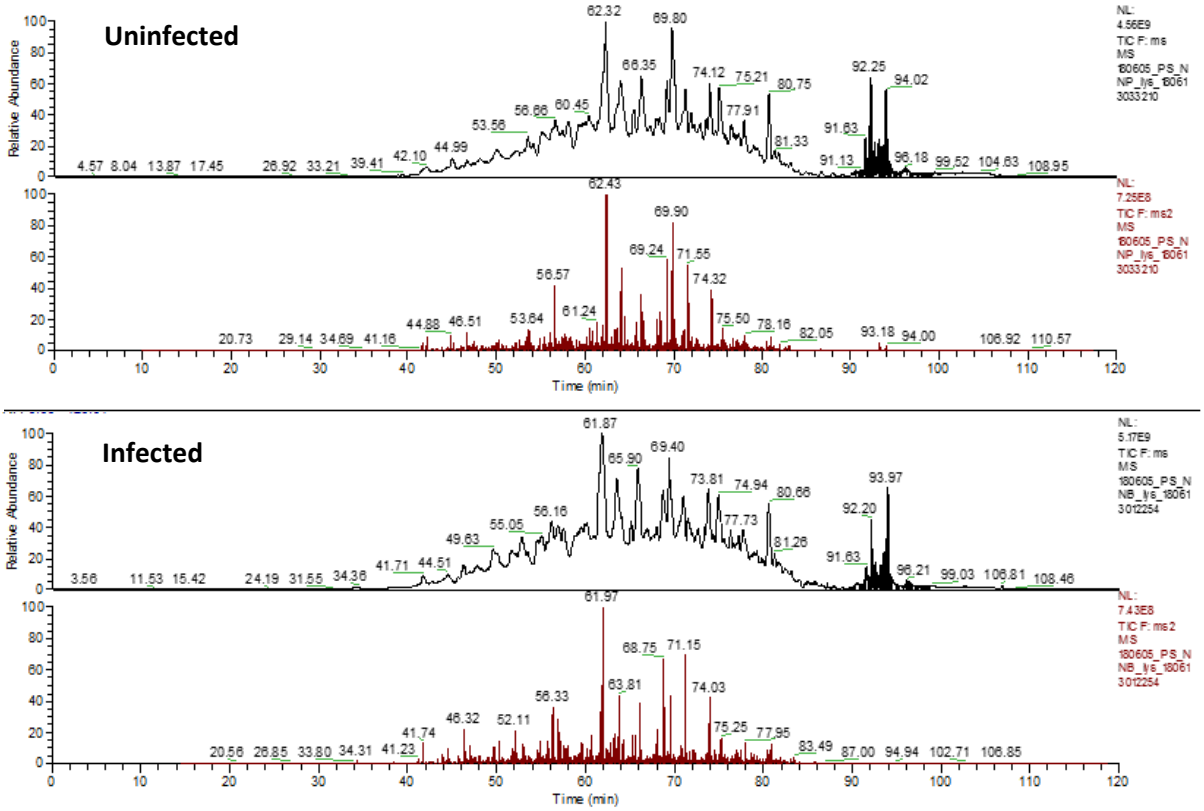

Figure 4-5: Representative chromatograph of the uninfected and infected lysate.

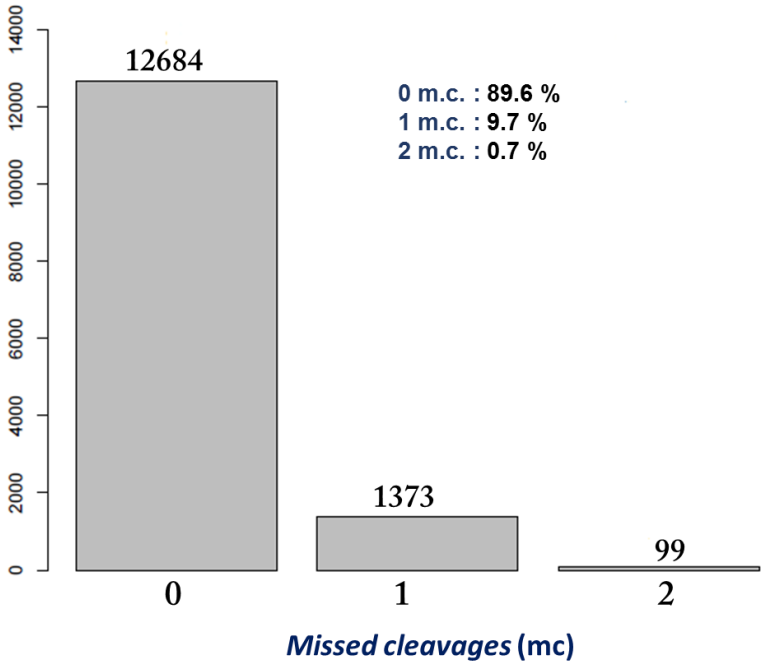

Figure 4-6: Efficiency of trypsin digestion. All The identified peptides are presented according to the number of missed trypsin cleavage.

All the 238 protein groups that were identified in the secretome overlapped with the 2107 protein groups in the lysate. Out of the 202048 spectra submitted, 36.98% were identified. The ion injection times and percentage of MS/MS identified (Figure 4-7) are similar between the triplicates, except for the infected secretome. This is corroborated by the multi-scatterplots, which show good correlation coefficients, between 0.763 and 0.929, for the lysate samples, while the secretome had correlation coefficients of 0.101 and 0.951 (Figure 4-8). This may be due to the low abundance of secreted proteins, and the high sample-sample variation observed in the secretome samples in this dataset. The loss of proteins during FASP preparation could also explain the variability since a dilute sample concentration, that is, media can lead to low abundance during the concentration steps.

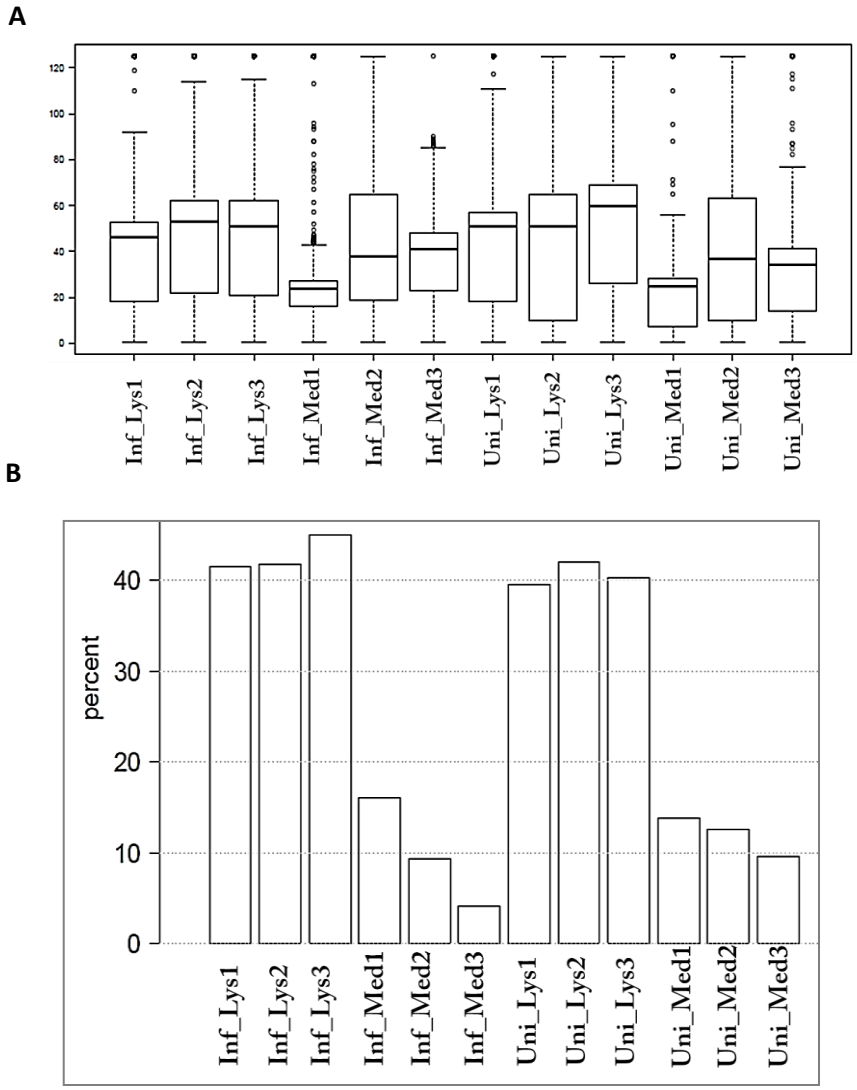

Figure 4-7: Reproducibility of data from technical injection replicates. (**A**) The ion injection times and (**B**) percentage of MS/MS identifications were used to analyse differences between the three technical replicates. Inf_Lys1 and Inf_Med1 represent infected lysate and media, respectively, followed by the number of the technical replicate. Similarly, Uni_Lys1 and Med_Lys1 represent uninfected lysate and media, respectively, followed by the number of the technical replicate.

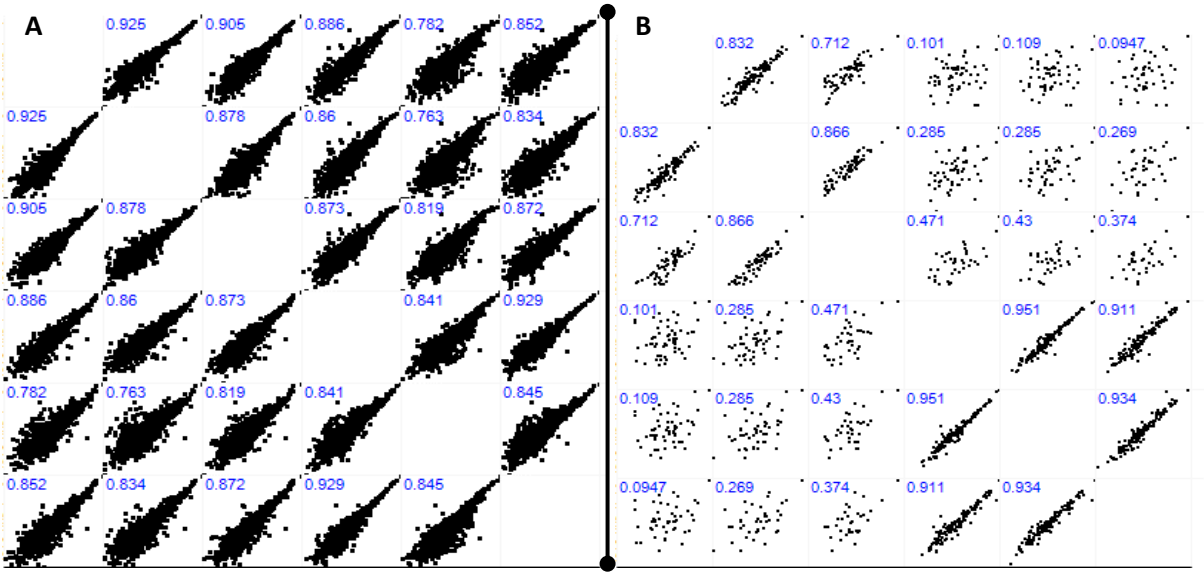

Figure 4-8: Scatterplot of the technical replicates. (**A**) The lysate and (**B**) secretome injection replicates were compared using the correlation co-efficient (R^2). The R^2 values are indicated (blue). Three technical replicates were analysed for each experiment.

4.4 Characterisation of differentially expressed and secreted proteins

As mentioned earlier, iBAQ was used for quantification and for qualitative analysis of the data. The three technical triplicates of the secretome and lysate each clustered together as well as the infected and uninfected (Figure 4-9). Differential expression of proteins is depicted in the heat map. There are 295 (Appendix 3, Table 6-4) and 18 (Appendix 3, Table 6-5) significantly differentially regulated protein groups between *M. smeg* infected and uninfected lysate and secretome samples, respectively. Interestingly, out of these, there were only two overlapping proteins between the secretome and lysate (Figure 4-10), and these were MMP-9 and Beta-hexosaminidase subunit beta (HEXB) (Accession IDs: P14780 and P07686, respectively). Differential expression of the protein groups was visualised by volcano plots (Figure 4-10B and C) which indicate fewer protein groups (Appendix 3, Table 6-6) are significantly differentially regulated than indicated by two-sample t test as expected since volcano plots are FDR corrected. The significantly different proteins groups calculated by the two-sample t test were used for downstream analysis and for biological interpretation. This is because p-values take into account variation between samples, peptides that were identified in at least two of the replicates were used in the two-sample t-test, FDR of 1% was used to filter false positives in MaxQuant and most of the false

positives would be outliers and excluded in STRING and GO analysis. Thus, the volcano plots were used to validate the highly significantly differentially expressed and secreted proteins.

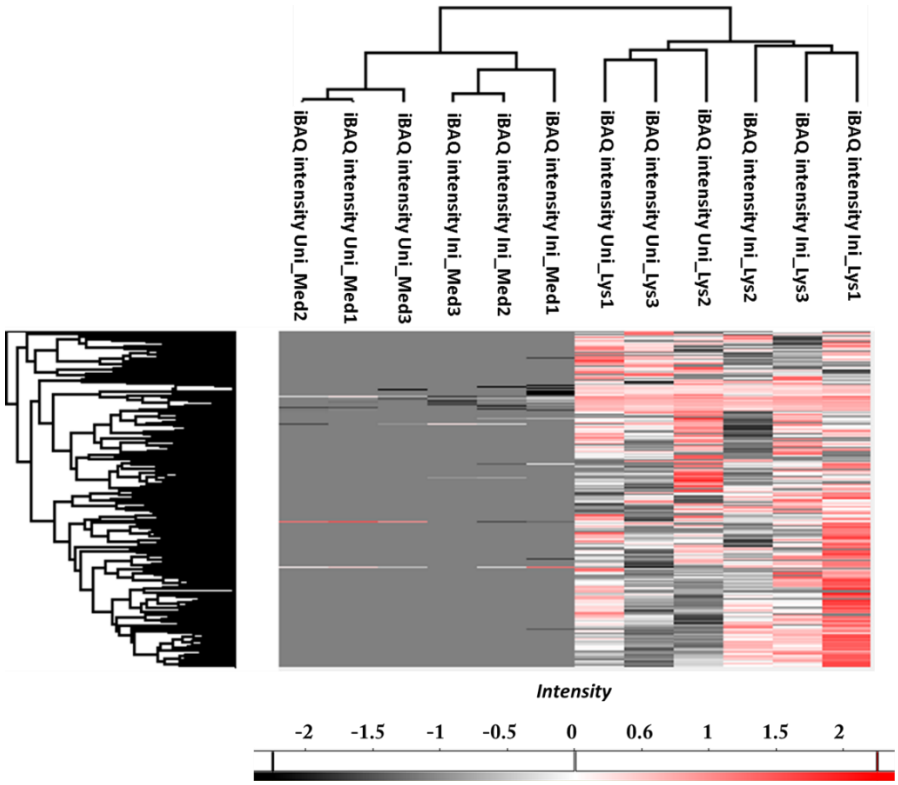

Figure 4-9: Hierarchal cluster analysis of intracellular and secreted proteins. The iBAQ intensity was used and k-means were selected for data analysis and processing of the three technical replicates of each experiment.

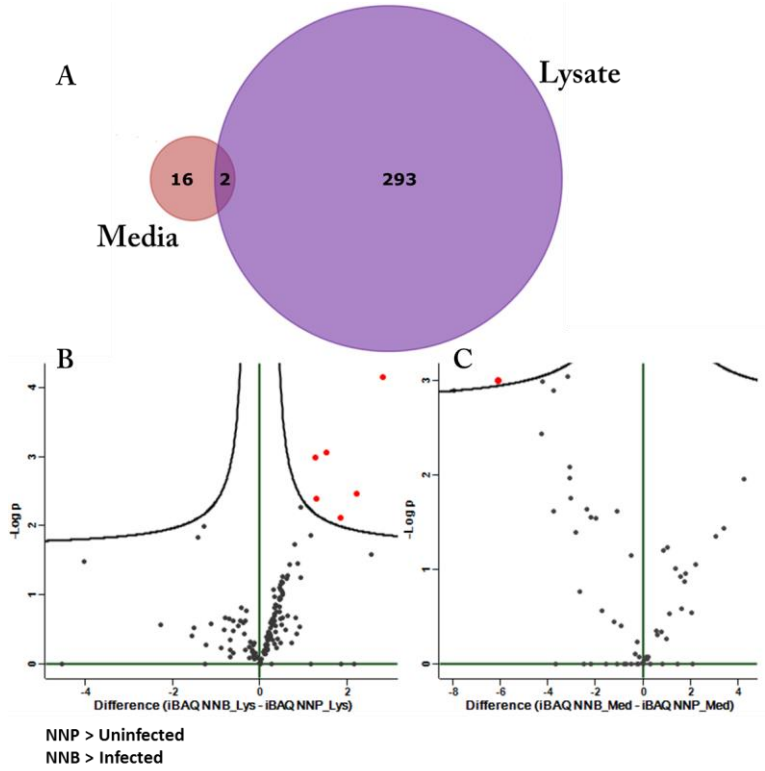

Figure 4-10: Representation of the computed dysregulated proteins. (**A**) The Venn diagram represents and compares the significantly different protein groups between infected versus uninfected in the media and the lysate as calculated by the two-sample test. (**B**) Volcano plots of the lysate and (**C**) media indicated the upregulated and downregulated protein groups. The significantly different ones are depicted by red dots.

The iBAQ intensities of MMP-1, MMP-3, MMP-14 and tissue inhibitors TIMP-1 and TIMP-3 were compared between infected and uninfected samples prior to normalisation using bar graphs (Figure 4-11). MMP-1 was only identified in the secretome and was only 2-fold higher in the infected samples, while MMP-9 was upregulated in both the lysate and secretome. The expression of MMP-14 in the secretome was comparable between uninfected and infected. While TIMP-1 was only identified in the infected lysate and secretome, TIMP-3 was only identified in the uninfected secretome. These were identified in the three replicates excluding the possibility of an artefact.

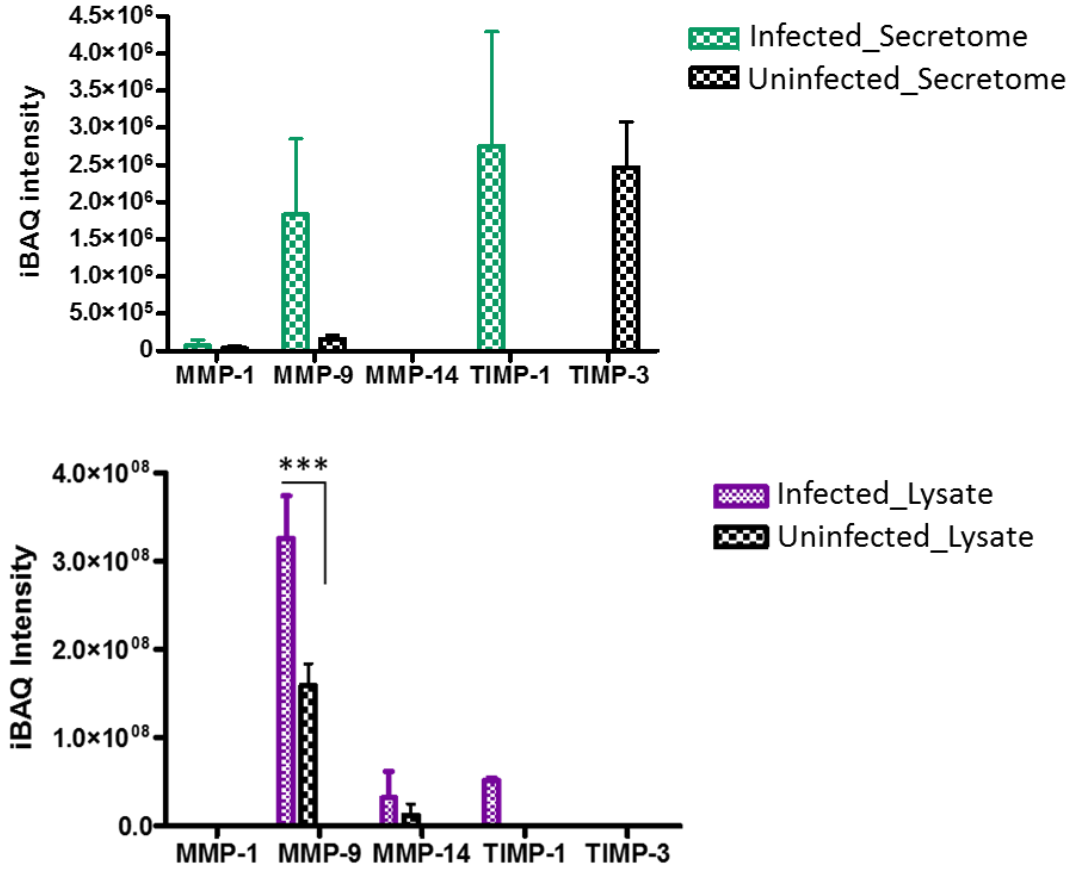

Figure 4-11: iBAQ intensity of identified MMPs in infected versus uninfected in the lysate and secretome. MMP-9 was significantly dysregulated with a p-value < 0.0001.

Functional annotation: Dysregulated lysate proteome

GO enrichment terms that were considered significantly enriched were those with p-values ≤ 0.05. The differentially expressed proteins in the lysate proteome indicate enrichment of GO terms for exosomes, lysosomes, mitochondrion, centrosomes and cytoplasm. The disregulated proteins are also associated with GO terms that indicate enzyme activity from different classes of enzymes (including ligases, GTPases, oxidoreductases) (Figure 4-12). The infection enriched biological processes in energy pathways and metabolism (Figure 4-13). With respect to RNA binding, the tRNA aminoacylation was the biological pathway that was mostly represented. Purine nucleotide *de novo* biosynthesis II which conincides with the ligase activity that is increased in the molecular function classification was another

biological pathway present (Figure 4-12). Another valuable classification was the site of expression which yielded the ascites cancer cells and monocyte in the top two (Figure 4-13).

Protein-protein interactions of MMP-9 and dysregulated lysate proteome

The significantly dysregulated proteins were analysed for protein-protein interaction by STRING database (STRING-DB) (Figure 4-14). MMP-9 has direct interactions with ILB-1 (Interleukein-1β), ICAM (Intercellular adhesion molecule 1), IL-1RN (Interleukin-1 receptor antagonist protein), PYCARD (Apoptosis-associated speck-like protein containing a CARD) and indirectly with PSAP (Prosaposin), PLAUR (Urokinase plasminogen activator surface receptor), MYLK (Myosin light chain kinase, smooth muscle), VCP (Transitional endoplasmic reticulum ATPase), DARS (Aspartate--tRNA ligase, cytoplasmic) and FSCN1 (Fascin). MMP-9 together with IL-1RN, ICAM-1, PLAUR and PSAP were also found to be significantly dysregulated when volcano plots were used. The Rab-related proteins also form an important part of this network.

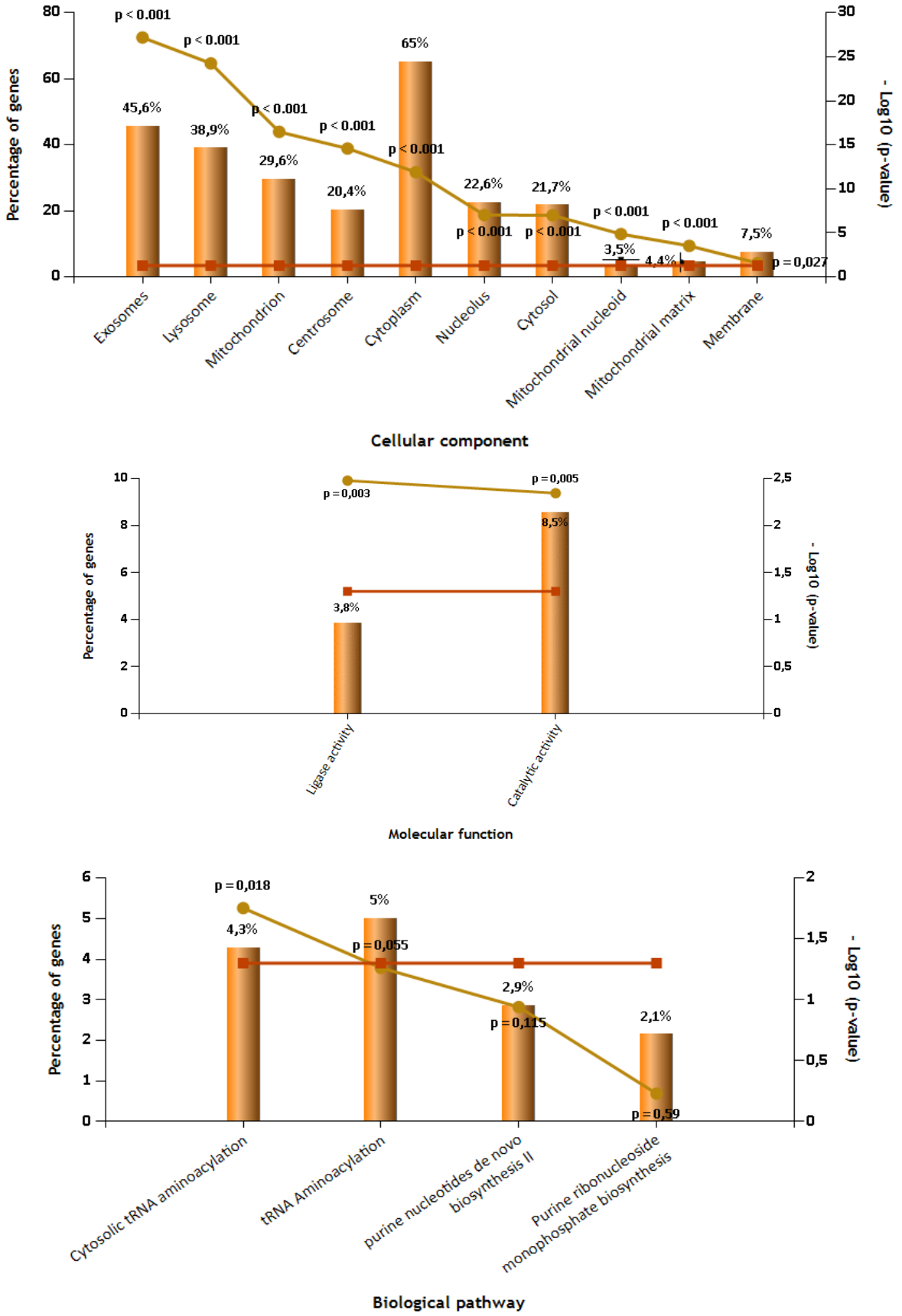

Figure 4-12: Functional annotation of dysregulated proteins from the lysate harvest.

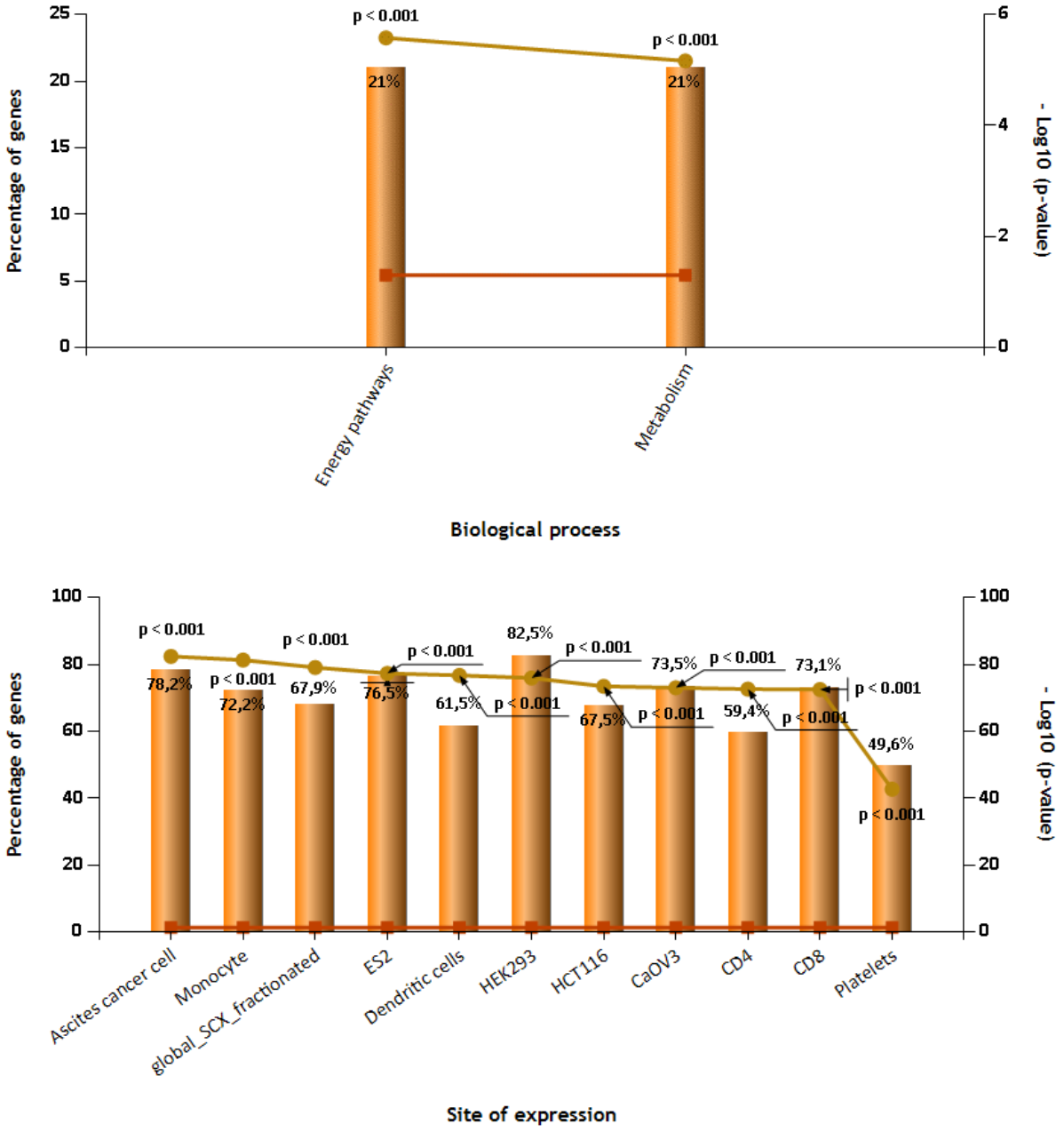

Figure 4-13: Further classification of dysregulated proteins harvested from the lysate.

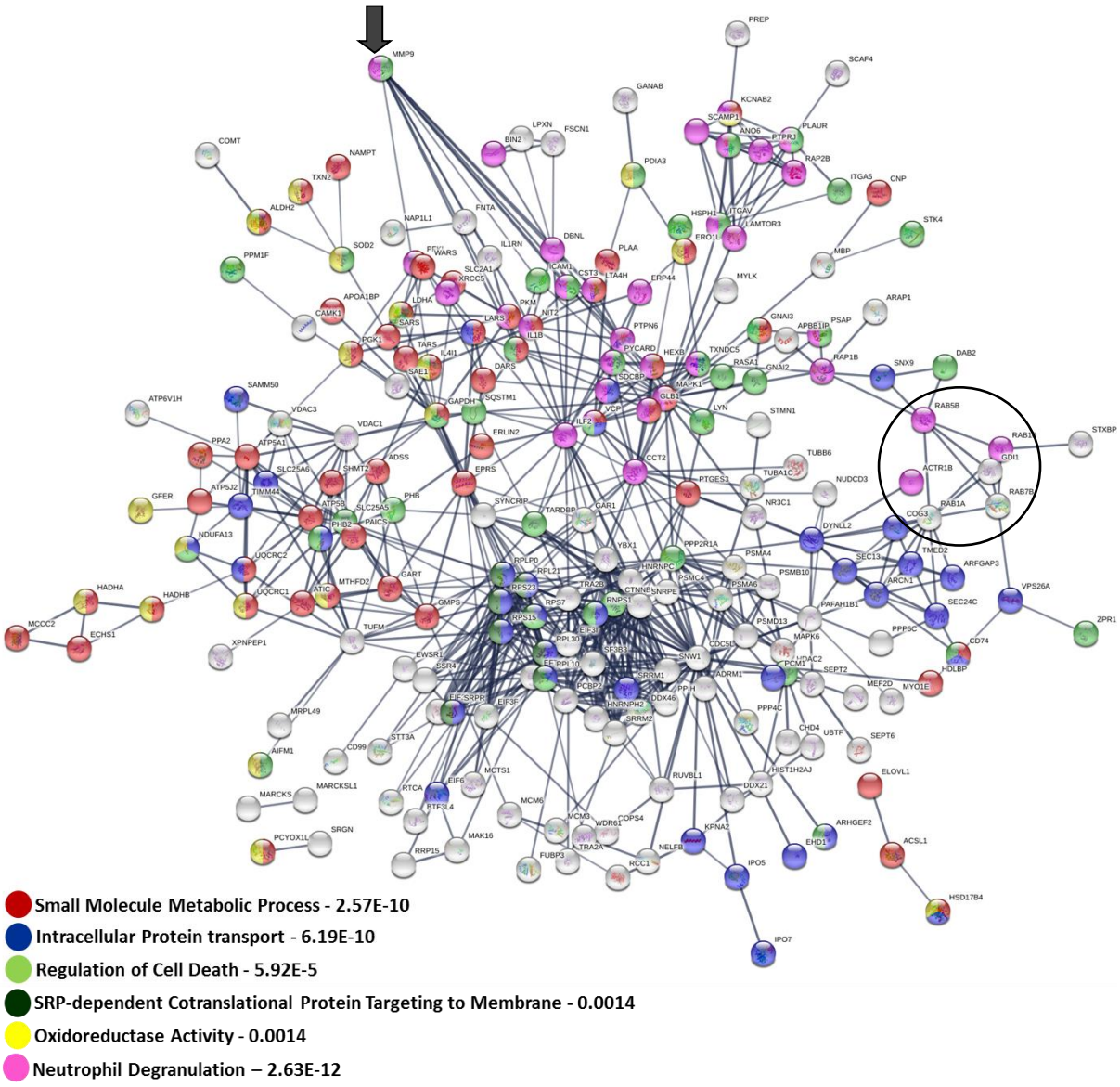

Figure 4-14: MMP-9 protein-protein interactions with other dysregulated intracellular proteins. MMP-9 (arrow) and its interacting proteins are illustrated. Rab-related proteins are also depicted (black circle). The proteins are colour coded according to their biological function (colour key) and FDR values are indicated as predicted by STRING.

Functional annotation: Dysregulated proteins in the secretome

The 18 protein groups that were differentially regulated were mostly associated with the nucleosome, centrosome, nucleoplasm, exosomes and nucleolus, with the p-value for enrichment less than 0.001 (Figure 4-15). It is interesting to note that proteins that are part of the nuclear component are more enhanced in the secretome compared to the lysate. Therefore, it is not surprising that the major molecular function and biological process signatures were DNA binding and regulation of nucleobase, nucleoside, nucleotide and

nucleic acid metabolism, respectively (Results not shown). The H4 (histone H4) domain (p-value < 0.001) was the enriched protein domains (Results not shown). This is interesting since H4 was shown to be dysregulated by volcano plots and two sample t-test and indicates the presence of chromatin in the secretome. It is also possible that some cell lysis could have occurred during sample harvest or preparation. However, this will be discussed further with respect to extracellular traps. The biological pathways that are depicted were mainly focused on packaging of telomere ends, RNA polymerase I promoter opening, deposition of New CENPA-containing nucleosomes at the centromere, nucleosome assembly, meiotic recombination and meiotic synapsis (Figure 4-15). These findings are captivating and make for interesting discussions and hypothesis generation.

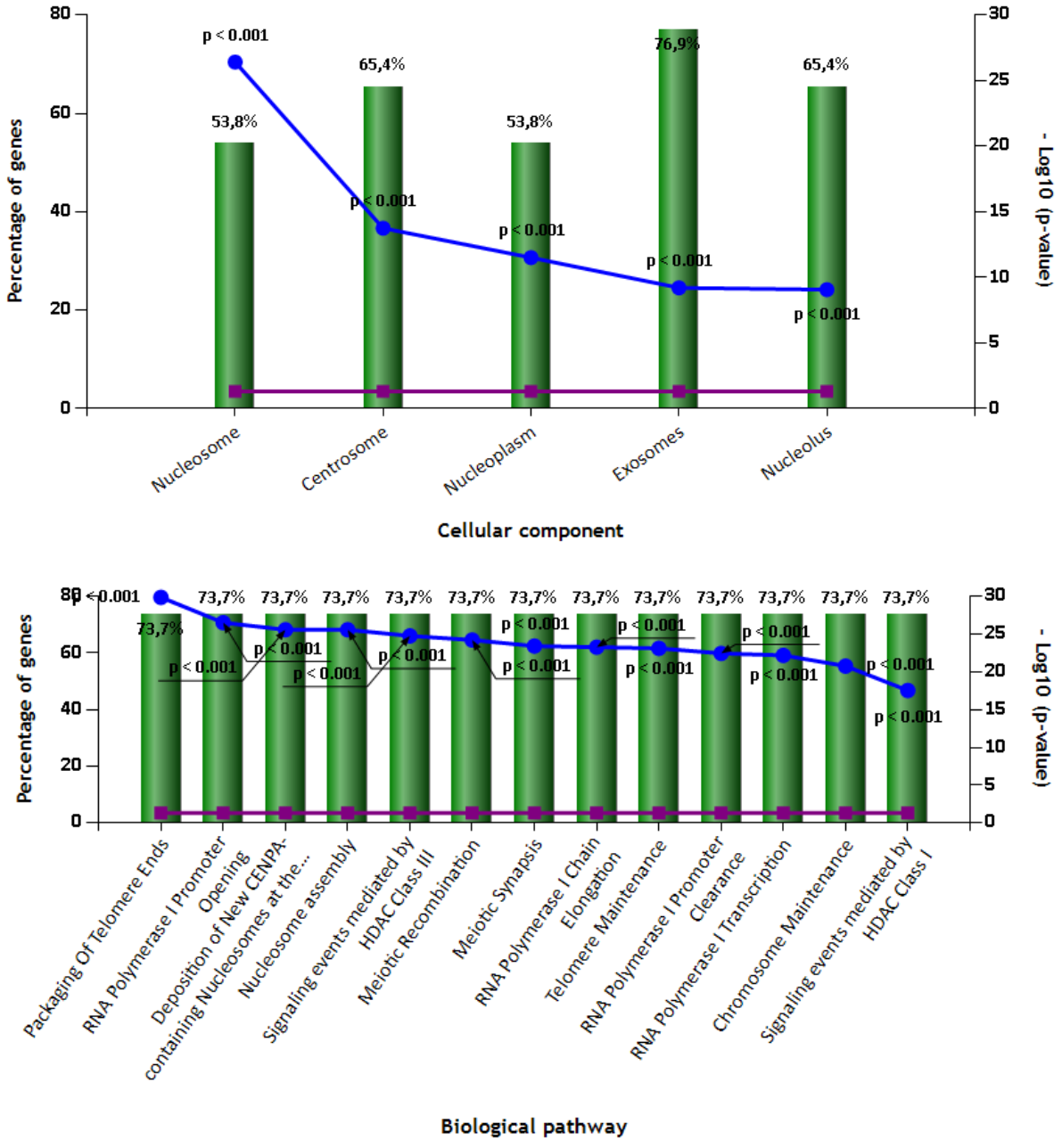

Figure 4-15: Analysis of the functional representation of the secretome.

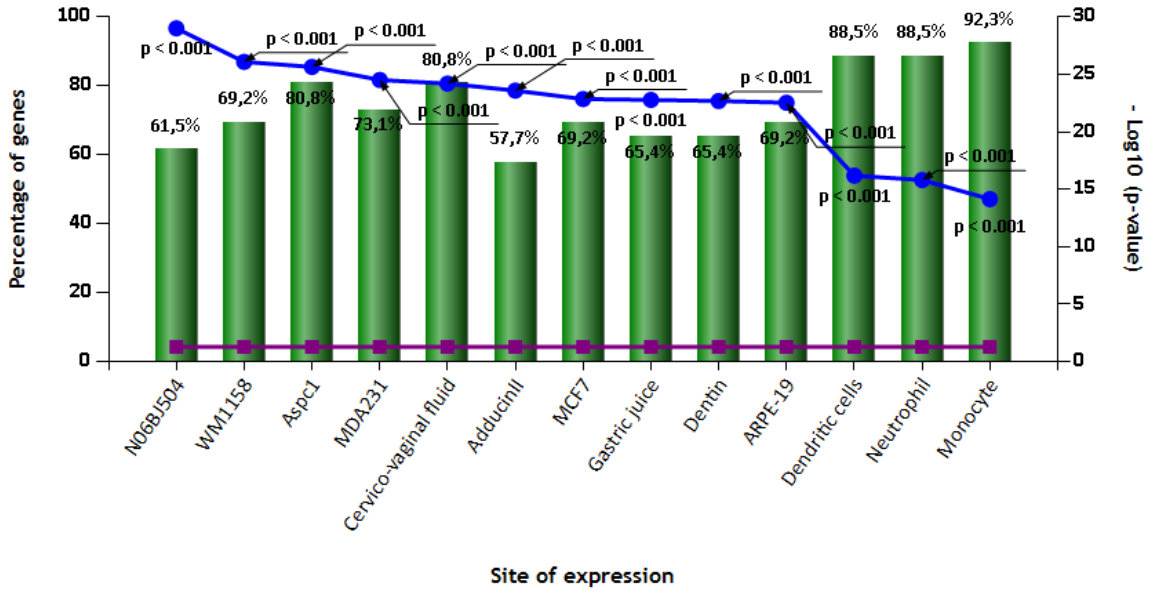

Figure 4-16: Functional representation of the secretome.

Protein-protein interactions of MMP-9 and other dysregulated proteins of the secretome

The protein-protein interactions that were formed by the dysregulated proteins were analysed using STRING-DB as before, and are portrayed in Figure 4-17. MMP-9 formed direct interactions with PPIA (Peptidyl-prolyl cis-trans isomerase A), A2M (α-2-macroglobulin), VIM (vimentin), COL6A1 (Collagen alpha-1(VI)), ANXA2 (Annexin A2) and CHI3L1 (Chitinase-3-like protein 1). STRING analysis also suggested that glycosaminoglycan degradation, extracellular matrix organization and chondroitin sufate metabolic process were enhanced in the secretome. Given that MMP-9 is the most glycosylated MMP and that glycosylation has a role in protein-protein interactions (section 1.3.3) this is an important discovery that also validates its earlier mention in the zymography discussion (Chapter 3).

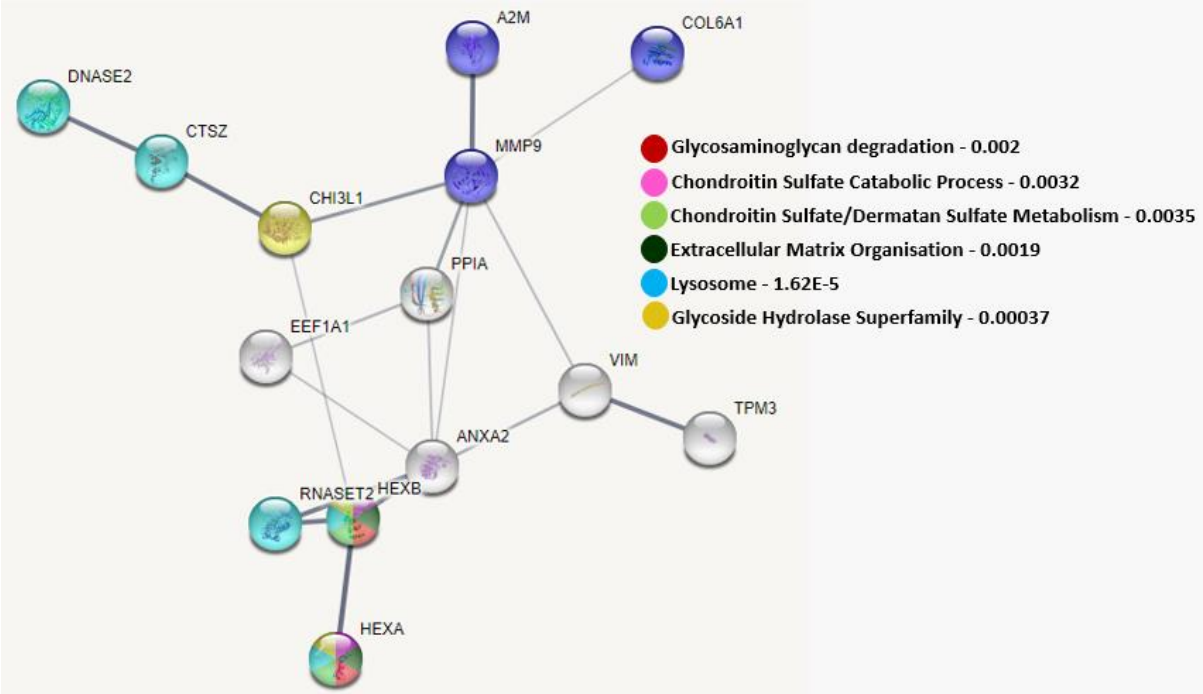

Figure 4-17: MMP-9 interacting protein with other significantly different proteins in the secretome. The proteins are colour coded according to their functions as computed by STRING. The FDR values are also given.

4.5 Description of uninfected and infected phenotypes using exclusively expressed and secreted proteins

Understanding the phenotypic changes induced by *M. smeg* is central to better our knowledge of its avirulent nature to the host in comparisons to *M. tb*. Thus, protein groups that were exclusively identified in the unifected and not in the infected lysate and secretome were analysed. A minimum of 2 peptides were required to be identified in the uninfected and 0 in the infected (and vise versa) to be considered exclusively identified for that protein group. Three technical replicates were considered for each experiment. This builds stronger evidence for phenotypic differences induced by the infection. The overlapping proteins between the infected lysate and secretome were insulin-like growth factor binding protein 3 isoform b (IGFBP3) and between uninfected lysate and secretome was apolipoprotein C-I (APOC1), while ADAM DEC1 was expressed in the infected lysate and uninfected media (Figure 4-18).

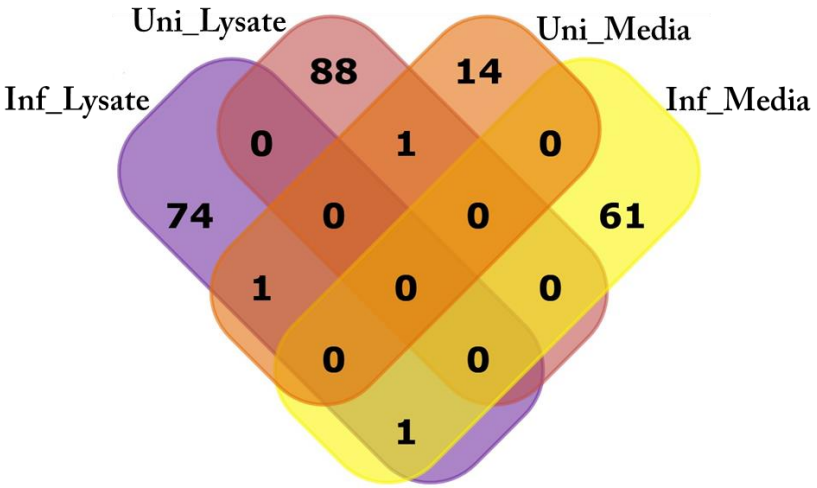

Figure 4-18: Overlap pattern of exclusively intracellular and secreted proteins. The overlapping protein groups in the uninfected (Uni) and Infected (Inf) were compared between the media and lysate.

Functional annotation of the exclusively expressed protein groups: Lysate

The protein groups that were exclusively expressed in the infected and uninfected lysate did not show any significantly enriched GO terms at least as analysed using FunRich (Results not shown).

Analysis of protein-protein interactions: Uninfected versus infected lysate

The interactions that were observed in the infected lysate was the clustering of the nuclear factors NF-kappa-B subunits NFKB1 and NFKB2 forming direct interactions with interleukin-8 (CXCL8) which in turn interacts with prostaglandin G/H synthase 2 (PTGS2) (Figure 4-19). The latter also forms interactions with STAT6 (Signal transducer and activator of transcription 6). These predicted contacts are important and relevant in *Mycobacterial* infections. On the other hand, the protein groups in the uninfected formed fewer interactions (Appendix 3, Figure 6-12).

Functional annotation of the exclusively expressed protein groups:

Secretome

Both the uninfected and infected secretome depicted GO enrichment in exosomes and lysosomes which had comparable number of genes. In contrast the enriched mitochondrion and cytoplasmic proteins had a higher percentage of representative genes in the infected than the uninfected (Figure 4-20). The signature biological pathways that were enriched and only observed in the infected media were aspartate degradation II, FOxO family signalling, insulin-mediated glucose transport and p38 signalling mediated by MAPKAP kinases (Figure 4-21). Also interesting was the conserved 14-3-3 protein domain enrichment in the infected whereas the uninfected was enriched with the calcium binding domains ANX (Figure 4-21). This implies that signal transduction pathways are modified by the infection from being dominantly calcium-dependent to phosphorylation-dependent ones.

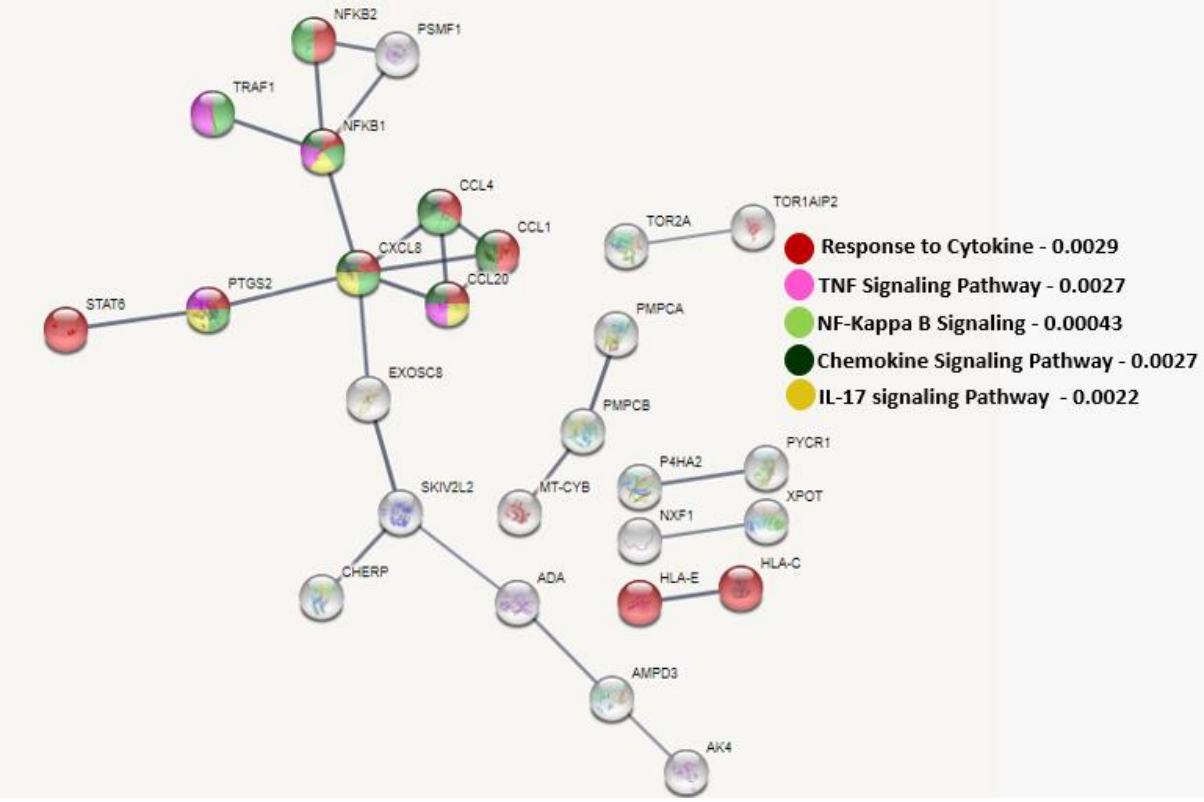

Figure 4-19: Protein-protein interaction of NFkB1 in infected lysate. The KEGG pathways are indicated by the colour keys and FDR values are also included.

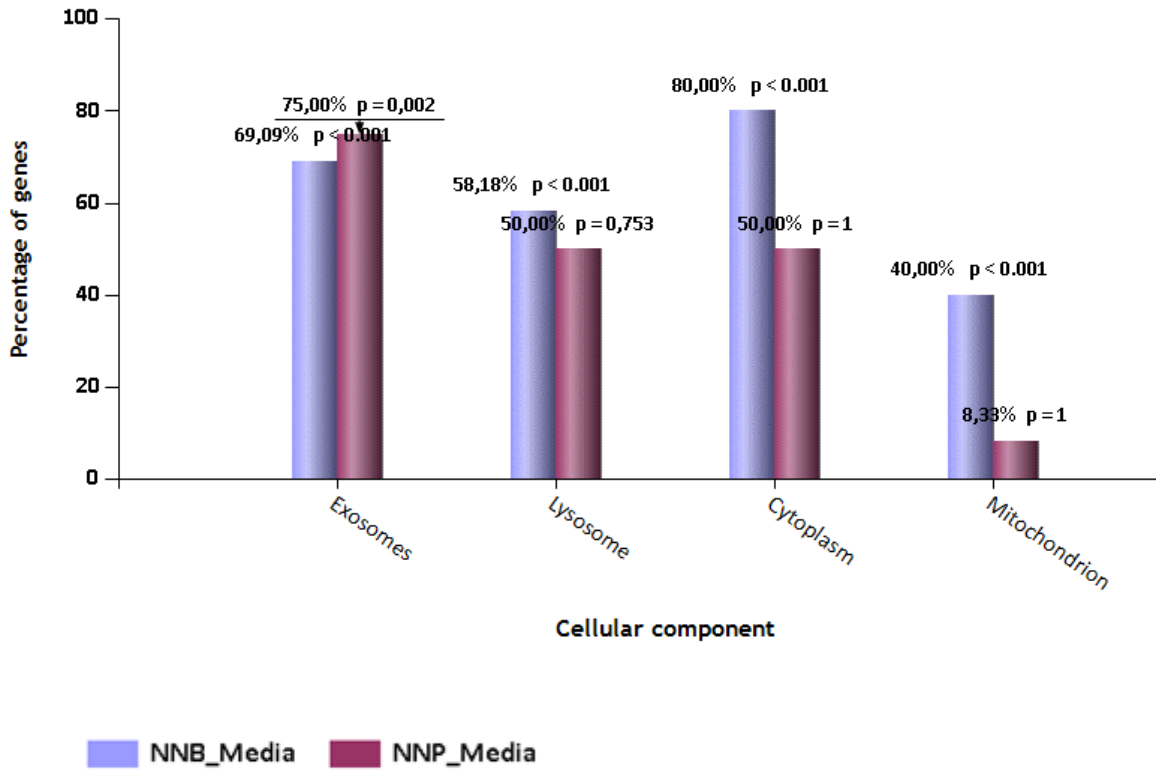

Figure 4-20: Illustration of the GO enrichment of the secretome.

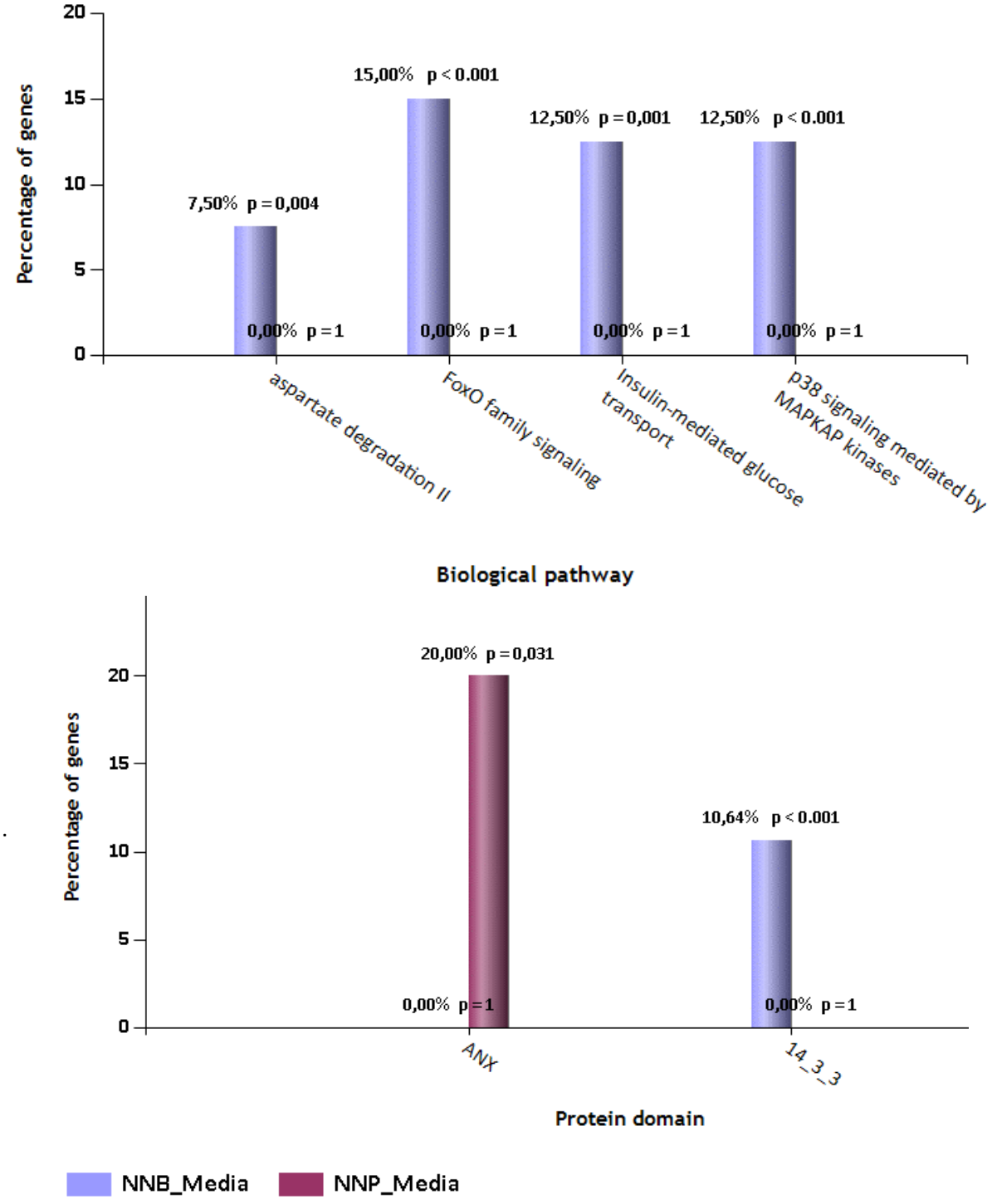

Figure 4-21: Illustration of the biological pathways and protein domain enrichment of the secretome.

Analysis of protein-protein interactions: Uninfected versus infected secretome

The STRING-DB predicted protein network of the infected secretome displayed interactions with TIMP-1 which is relevant in the study of MMPs (Figure 4-22). This MMP inhibitor interacted directly with Amyloid-like protein 2 (APLP2), Nucleobindin-1 (NUCB1), Calumenin (CALU), Glucosidase 2 subunit beta (PRKCSH), insulin-like growth factor binding protein 3 isoform b (IGFBP3). It forms indirect contact with cation-independent mannose-6-phosphate receptor (IGF2R), intercellular adhesion molecule 1 (ICAM1), urokinase plasminogen activator surface receptor (PLAUR) and alpha-actinin-4 (ACTN4). The IGF2R makes contact with the actin-related proteins 2 (ACTR2) and 3 (ACTR3). Another exciting discovery within this network was the 14-3-3 proteins which are conserved in eukaryotic cells and regulate signalling molecules. These make direct interactions with Tubulin beta-4B chain (TUBB4B).

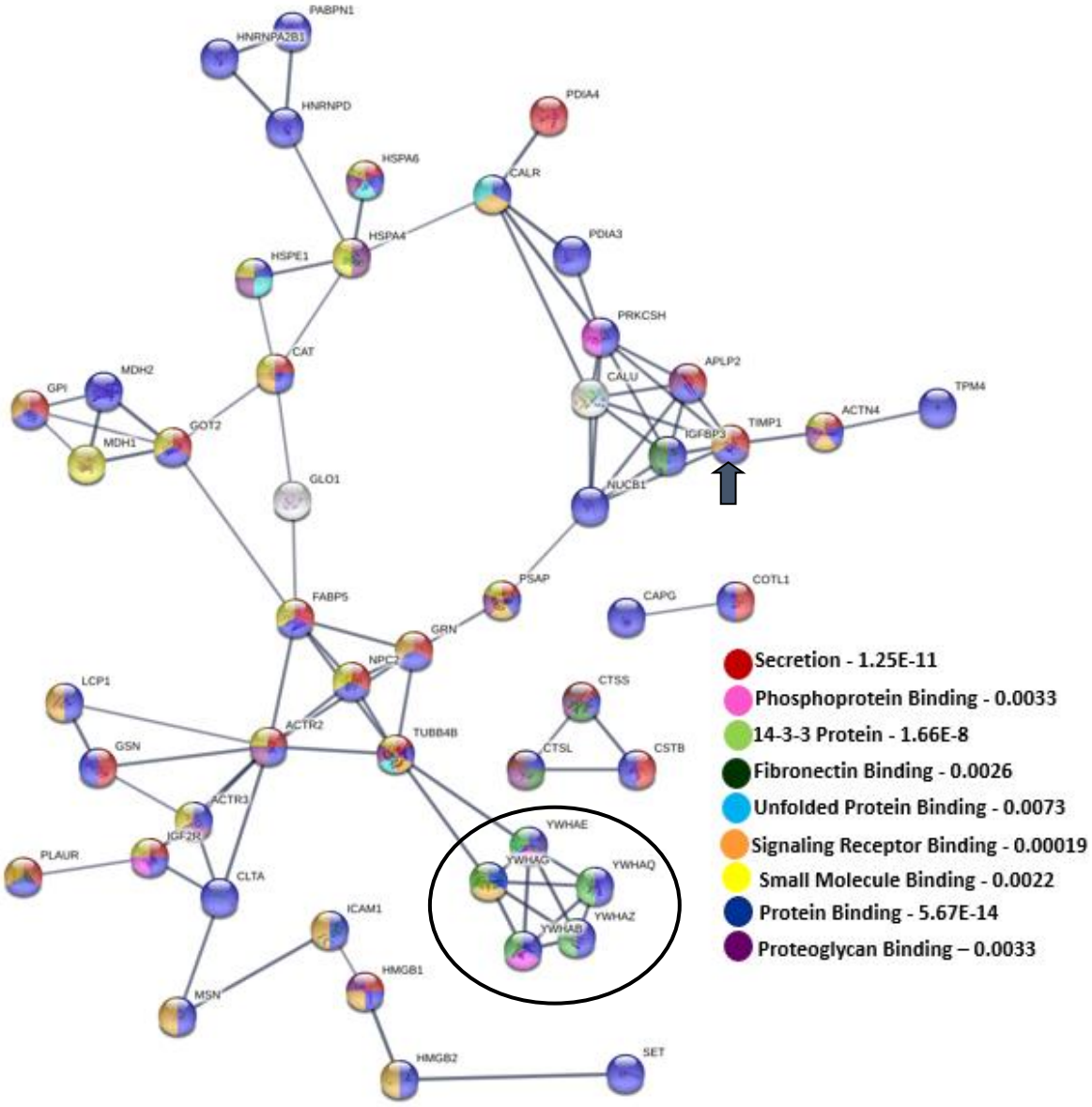

Figure 4-22: Protein-protein interactions of TIMP-1 in the infected <u>secretome</u>. TIMP-1 is indicated with an arrow (black) and the 14-3-3 conserved proteins are depicted (black circle).

4.6.1 The upstream and downstream regulation of MMPs

The tight regulation of MMPs is inherent to the homeostasis of the ECM and regulation of other cellular processes such as angiogenesis, cell proliferation and immune system amongst others. Understanding pathways that are responsible for their dysregulation in disease pathologies is essential for strategic therapeutic development. These include pathways that control their expression, secretion and activation. The current study postulates that the significant expression of MMP-9 induced by *M. smeg* infection is cytokine driven. With respect to exclusively expressed protein groups the pro-form of IL-16 and the IFN-γ receptor were present in the uninfected lysate in contrast to IL-8 and IL-27B in the infected lysate. IL-1β was the second most upregulated protein intracellularly. It is a potent inducer of MMP-9 which only induces the overexpression of MMP-1 when in combination with GM-CSF and TNF-α (Elkington *et al.* 2011b;Zhang *et al.* 1998b). The effects of IL1-β may in turn be regulated upstream via phosphorylation/dephosphorylation by interaction with LYN (Tyrosine-protein kinase Lyn), a non-receptor tyrosine kinase and negatively by the interleukin-1 receptor antagonist protein (IL1RN) which were both also significantly dysregulated. The pathways that were enriched in the lysate were mostly concerned with RNA processing and metabolism.

The COX reaction pathways were also enriched, with prostaglandin E synthase 3 (PTGES3) being significantly different and prostaglandin G/H synthase 2 (PGH2) only identified in the infected lysate. Thus, the cytokines may be driving the expression of MMP-9 in response to *M. smeg* and due to inflammation. The inflammation could also be caused by serum-starvation however the comparison with the uninfected validates that it did not mask the differences induced by the infection.

The significant dysregulation of intracellular and secreted MMP-9 was accompanied by the presence of TIMP-1 which was only identified in the infected secretome. This suggests that TIMP-1 is deliberately secreted to inhibit the activity of MMP-9 and/or control its secretion, given its documented role of complexing with MMP-9 prior to secretion (Roderfeld *et al.*

2007;Shapiro *et al.* 1995). Thus, the study validates the non-destructive ECM phenotype induced by *M. smeg* contrasting that of *M. tb*. Coinciding with this was the observed decrease in MMP-1 activity observed by zymography and MMP-1 activity assays.

MMP-9 was upregulated intracellularly and in the secretome, while β-hexosaminidase subunit beta (HEXB) was upregulated intracellularly but downregulated in the secretome. This indicates another regulatory mechanism of MMP-9 via recycling, possibly via exosomes in turn preventing chronic inflammation and degradation of the ECM. This exosome compartmentalisation could be a strategy to control its secretion, and to prevent its degradation and denaturation from the acidic environment induced by serum-starvation and acidification steps during phagosomal processing.

Since tRNA aminoacylation was induced by the infection, it is possible that the multiple bands observed by zymography are splice variants of MMP-9 possibly arising from the WHE-TRS protein domain that was enriched by dysregulated intracellular proteome. It is a helix-turn-helix domain which is found abundantly in glutamyl-prolyl tRNA synthetase (EPRS). It is essential for the interaction of protein-protein interaction of synthetases and has also been observed in alternative splicing of proteins such as the angiogenic factor VEGFA (Halawani *et al.* 2018;Mthembu *et al.* 2017;Ray and Fox 2014). Interestingly MMP-9 has glutamic acid-proline repeats (EPEP) repeats at the C-terminal domain implying that tRNA glutamyl-prolyl tRNA synthetase may be binding to it and generating alternative splicing. Since most of the RNA binding proteins were also exosome proteins, it is possible that MMP-9 interacts with WHE-TRS and glutamyl-prolyl tRNA synthetase and aspartate--tRNA ligase which has been shown to interact with MMP-9 by STRING, supporting its transportation through exosomes.

Therefore, the expression of MMP-9 may be regulated by IL-1β in a COX-prostaglandin synthase-dependent manner, and also via alternative splicing. To compare, the THP-1 and primary monocytes that were infected with *M. tb* upregulated the expression of MMP-1 and MMP-9 which was protein kinase C (PKC), PKA and protein tyrosine kinase (PTK) dependent which was not the case for TIMP-1 (Friedland *et al.* 2002). This implies that the secretion of MMP-9 is not TIMP-1-dependent as is the case with *M. smeg* infections. Thus, the upstream

regulatory mechanisms exploited by *M. smeg* and *M. tb* in controlling MMPs/TIMPs are distinct.

proMMP-9 is composed of 19 cysteine residues and is sensitive to changes in redox conditions which in this case could be induced by the acidification processing of the phagosome. Thus, the host might respond by preserving and counteracting these effects to control the expression, secretion and activation of MMP-9 including other redox sensitive proteins required for clearing the infection. Protein disulfide-isomerase (PDI) has been shown not only to be able to rescue and restore the gelatinase activity of denatured and reduced MMP-9 but also control its secretion (Ali Khan and Mutus 2014). Another study observed that inhibiting the gelatinase activity of MMP-9 (and MMP-2) caused an increase in the cell-surface of PDIA3 with a decrease in its secreted form (Rosewell *et al.* 2011). PDIA3 was significantly dysregulated in the lysate and was also identified together with its isoform PDIA4 only in the infected secretome suggesting a regulatory loop mechanism between it and MMP-9, also highlighting the relevance of PDI secretion due to infection. Like MMPs, the function of the high mobility group protein-1 (HMGB1) is redox controlled for instance when its fully reduced it acts as a chemoattractant for proinflammatory cells, acts as a cytokine when its partially reduced/oxidised and finally in its oxidised form it has neither activities (Antoine *et al.* 2014). HGMB1 and HMGB2 were identified in the infected secretome while HMGA1 (high mobility group protein HMG-I/HMG-Y) was significantly dysregulated in the lysate. Ribonuclease T2 (RNASET2) which was dysregulated in the secretome has optimum activity under acidic conditions and may degrade the lysosomal ribosomal RNA (Luhtala and Parker 2010). Therefore, its dysregulation is not coincidental but together with the RNA binding proteins, PDIs and HMGBs amongst other proteins may be employed during *M. smeg* infection to localise, maintain some expression and activity of MMPs and other matrix degrading proteins such as cathepsins.

Cathepsins L1 and S (CTSL and CTSS) which are lysosomal cysteine proteases able to activate MMPs were identified in the infected lysate while cathepsin Z (CTSZ) was downregulated in the media. This implies that secreted proMMP-9 may be activated by cathepsins (Christensen and Shastri 2015;Shamamian *et al.* 2001). The generation of reactive oxygen species (ROS) is not only essential for antimicrobial activity and apoptosis but also for

activation of MMPs (Fu *et al.* 2001;Gu *et al.* 2002). The upregulation of superoxide dismutase (SOD (Mn)) in the lysate may be to control the activity of MMPs via its ability to convert oxygen to hydrogen peroxide ultimately forming hypochlorous acid (HOCl) that activates proMMPs (Fu *et al.* 2001).

The overrepresentation of the purine nucleotide de novo biosynthesis II pathway (infected intracellular proteome), purine ribonucleoside degradation to ribose-1-phosphate (dysregulated intracellular proteome) and nucleotide metabolic (dysregulated secretome) pathways could be essential for generating NADPH which retains the reduced state of glutathione (GSH) for scavenging ROS and also for generating NADP required for scavenging superoxides which would lead to further activation of the MMPs (Banki *et al.* 1996;Flannagan *et al.* 2009). Purine catabolism is essential in that the enzyme adenosine deaminase has been widely used as a marker for TB diagnosis (Atta *et al.* 2015;Baba *et al.* 2008) even in pleural fluid of patients co-infected with HIV having a CD4 count less than 50 cells/µL however this is not the case in TB pericarditis fluid (Baba *et al.* 2008). Adenosine deaminase catalyses the deamination of adenosine to inosine and it is also a marker of monocyte differentiation to macrophages (Atta *et al.* 2015;Baba *et al.* 2008). It was only in the infected lysate that this enzyme was expressed, and it depicts further differentiation of the macrophages with an active immune response. Interestingly the uninfected secretome was enriched with the transaminase molecular function highlighting the importance of deamination in *Mycobacterial* infection. The presence of calcium-binding and calcium channel proteins annexin A1 and A4, in the uninfected secretome suggests that in the absence of infection the calcium-dependent MMP-9 activity is regulated by controlling extracellular levels of calcium.

Another way of controlling the activity of MMPs besides through activation is by regulating their secretion. As mentioned earlier TIMP-1 is reported to do this by complexing to proMMP-9 and controlling its secretion. The secretion of MMP-9 has also been shown to rely on the maintenance of actin polymerisation and intact microtubules (Bildyug 2016;Hanania *et al.* 2012) which could explain the intracellular upregulation of the cytoskeletal structural proteins such as tubulin β-chain (TUBB), tubulin β6 chain (TUBB6), tubulin α-1 chain (TUBA1C) and tubulin-8 (TUBB8), adenylyl cyclase-associated protein 1

(CAP1) in the infected lysate. To corroborate this, CAP-1 which is involved in the recycling of G-actin monomers from ADF/cofilins was expressed in the infected lysate. The identified alpha-actinin-4 (ACTN4), actin-related proteins 2 and 3 (ARP2 and ARP3) in the infected secretome could also facilitate the secretion and or re-internalisation of MMP-9 (Chintala *et al.* 1998). In a review by Bildyug, one of the insightful conclusions was that the polymerisation of actin was more likely to upregulate MMP-9 and downregulate MMP-2 (Bildyug 2016), suggesting that the gelatinase activity of MMP-9 is only one of the reasons for its upregulation in *Mycobacterial* infections which will be discussed below. Alterations in redox and glycosylation state, together with alternate splicing would also modify the TIMP-1 binding to MMP-9 advocating for other functions of MMP-9 and TIMP-1 either than ECM remodelling.

4.6.2 The function of MMPs in the internalisation of *M. smeg* and phagosome maturation

The role of MMPs in cancer metastasis and invasion has been widely documented and is still an exciting area of research. Remodelling of the cytoskeleton is a dynamic event entailing the assembling, disassembling and recycling of actin and microtubule filaments. This phenomenon is true not only in tumour progression but also in phagocytosis of microbes and in subsequent events of phagosomal processing. The localisation of MMPs to cell membranes and lipid rafts is essential for invadopodia formation (Jacob and Prekeris 2015;Poincloux *et al.* 2009;Watanabe *et al.* 2013;Yamaguchi *et al.* 2009). Analysis of protein-protein interactions with STRING showed MMP-9 forming direct interactions with ILB-1 (Interleukein-1β), ICAM (Intercellular adhesion molecule 1), IL-1RN (Interleukin-1 receptor antagonist protein), PYCARD (Apoptosis-associated speck-like protein containing a CARD) and indirectly with PSAP (Prosaposin), PLAUR also uPAR (Urokinase plasminogen activator surface receptor), MYLK (Myosin light chain kinase, smooth muscle), VCP (Transitional endoplasmic reticulum ATPase), DARS (Aspartate--tRNA ligase, cytoplasmic) and FSCN1 (Fascin).

Fascin is an actin binding protein, like MMPs it can localise to filopodia and invadopodia (Li *et al.* 2010). MYLK is involved in muscle contraction through the phosphorylation of myosin light chain (Gao *et al.* 2013). The interaction network between MMP-9 with fascin, MYLK, ICAM1 and uPAR taken together with its ability to colocalise to cell membranes and lipid rafts suggests that it may be important in the uptake of *M. smeg*. The urokinase plasminogen family of proteins are not only able to activate MMPs, specifically plasmin has been shown to have a direct interaction but also plays a direct role in collagen turnover. Urokinase plasminogen activator receptor-associated protein (uPARAP) also known as ENDO180 is a 180 kDa protein and a homolog of the C-type mannose receptor protein that can recognise and bind various types of carbohydrates making it relevant in the current study. It is well-known for its ability to bind and internalise collagen or gelatin localising it to the lysosomal compartment where it is degraded (Melander *et al.* 2015;Paracuellos *et al.* 2015). It comprises the fibronectin repeats which are collagen-binding domains similar to that of MMP-9 and MMP-2. This protein is stable at low pH and low calcium concentrations, which do not affect collagen binding or release (Paracuellos *et al.* 2015). Thus, it is possible that uPARAP (although not identified in our data), uPAR and MMP-9 may be interacting on the cell surface facilitating *M. smeg* recognition, binding and internalisation. Since MMP-9 can form multimers, it is also possible that it localises to the cell membrane via uPAR.

The presence of extracellular actin, enrichment of glycosaminoglycans (GAGs) and plasminogen have been reported to be essential receptors for *Mycoplasma hyopneumoniae* (Raymond *et al.* 2018). Similarly, and as mentioned earlier the actin related proteins (ARP-2, ARP-3 and ACTN4) and uPAR identified in infected secretome, and enrichment of the glycosaminoglycan catabolic processes displayed by the dysregulated secretome suggests that these proteins together with MMP-9 may be forming a protein scaffold that is important in recognition and internalisation of *M. smeg*. Since MMP-9 has the most glycosylation sites amongst all the MMPs, it is possible that binding and internalisation of *M. smeg* is facilitated by the interaction of the mannose sugars on its cell wall with the glycosylated MMP-9. In addition, CD44 is a hyaluronan binding protein that was identified to be significantly dysregulated and to form direct interactions with MMP-9 when label free quantification (LFQ) was used. It is expressed in most cells and its interaction with F-actin is mediated by ezrin/radixin/moesin and/or akyrin. CD44 has been shown to dock MMP-9 into

the cell membrane (Zhang *et al.* 1998a) as well as bind the hemopexin domain of MMP-14 localising it to lamellipodia (Mori *et al.* 2002). Moesin was one of the proteins identified to be exclusively identified in infected media when both LFQ and iBAQ are used. Also, the cytoskeletal proteins moesin, actin and tubulin are part of proteins making up exosomes (Atay and Godwin 2014) and could play a role in the morphological changes required by the cell during phagocytosis. The interaction of MMP-9 with the precursor protein prosaposin supports its role in *M. smeg* phagocytosis. Prosaposin is processed to saposins A-D which localise and function in the lysosomal compartments (Morimoto *et al.* 1990). It is also fascinating that genetic mutations found in prosaposin are associated with Tay Sachs a lysosomal storage disease which is associated with resistance of TB through deficiency of α-hexosaminidase (Withrock *et al.* 2015). There was significant downregulation β-hexosaminidase, both alpha (HEXA) and beta (HEXB) subunits in the secretome, whereas HEXB was significantly dysregulated in the intracellular. This means that its peptidoglycan hydrolase activity is not relevant in the ECM but rather the internalisation and localisation of *M. smeg* to the lysosome is required for exerting its hydrolase function.

Another plausible internalisation mechanism could be via the already mentioned PDIs. Phagocytosis of the *Leishmania chagasi* promastigotes have been reported to be enhanced in the presence of PDI which colocalised with macrophage NADPH oxidase (Santos *et al.* 2009). The role of PDI and redox conditions has also been documented to regulate positively the uptake of other bacteria such as *Chlamydia* (Abromaitis and Stephens 2009). Very interesting is its role in reducing the thiol groups of HIV gp120 preceding its uptake by lymphocytes (Santos *et al.* 2009). Like MMP-9, peptidyl-prolyl cis-trans isomerase A (PPIA) was also upregulated in the secretome by *M. smeg* infection and formed direct interactions with MMP-9 suggesting that it could also be important for phagocytosis. The binding and entry of HIV has been reported to be PPIA dependent (Gallina *et al.* 2002). To corroborate this further, PPIA is an MMP-14 substrate (Rodríguez *et al.* 2010) which was not identified in the secretome and was not dysregulated in the lysate. Therefore, the enrichment of PPIA, PDI and other proteins involved in oxidoreductase activity could alter the *M. smeg* phenotype directly and possibly facilitating its phagocytosis. Further investigation into the function and/or interaction of MMPs at the cell membrane and their possible role in facilitating phagocytosis and endosomolysis, a process whereby bacteria is released into the

cytoplasm may endorse the design of specific MMP inhibitors. Although there was no correlation between bacterial burden and upregulation of MMP-1 in *M. tb*-infected MMP-1 transgenic mice (Elkington *et al.* 2011a), it is still possible that other MMPs such as MMP-14 that are internalised via clathrin-dependent and caveolae mediated pathways (Remacle *et al.* 2003) are associated with the release and/or phagocytosis of *M. tb* into the cytoplasm.

4.6.3 Clearance and bacteriostatic effects on *M. smeg* by THP-1 macrophages

Mycobacterium smegmatis infections are cleared efficiently in non-immunocompromised individuals and its inability to progress to cavitary disease is relevant in this study since MMPs have been linked to progression of disease. In the current study, we postulate mechanisms by which bacterial growth may be slowed or halted, namely scavenging of ions like iron to prevent growth, phagosome and lysosome fusion, extracellular trapping of bacilli and finally apoptosis as a way of preventing excessive inflammation and necrosis.

The role of β-hexosaminidase in controlling bacterial growth has been described in macrophage infections with *Mycobacterium marinum* (*M. marinum*). It was found to be active on the cell membrane surface during uptake suggesting that it is the first line of defence against the bacteria making direct interactions and modifying the bacterial cell wall (Koo *et al.* 2008). Its upregulation in the intracellular implies that it could be eliciting its bacteriostatic effects by localising the bacilli to the lysosome synergistically with MMP-9. Controlling bacterial growth by preventing the availability of ions such as Fe^{2+}, Mn^{2+} and Zn^{2+} is a strategy also employed by the host (Flannagan *et al.* 2009). The intracellular survival of *M. tb* has been attributed to its ability to sequester the host iron for its own growth. Sideroflexin-1 (also known as tricarboxylate carrier protein) is essential in differentiation of erythrocytes and for iron ion homeostasis and transport across the mitochondria. Induction of its expression by *M. smeg* suggests that, like NGAL, it may function to scavenge iron resulting in a bacteriostatic effect. Amusingly, SOD (Zhou *et al.*) was one of the top five of the significantly upregulated proteins in the lysate. Since Mn^{2+} is required by pathogenic SOD as a protective enzyme (Flannagan *et al.* 2009) it is plausible that the SOD is expressed deliberately by macrophages to outcompete the bacterial SOD for Mn^{2+} thus eliciting its bacteriostatic effects. The current study has demonstrated that incubation of the secretome

with and without APMA at 37 ˚C results in conversion of MMP-9 (82 kDa) to its 67 kDa form which lacks the hemopexin domain (Hx), also showing that the conversion was faster when APMA was included (Section 3.3). Thus, the postulation that MMP-9 could be transported between the cytoplasm and the ECM through exosomes could be a strategy for preventing the degradation of its Hx domain possibly to iron, biliverdin and carbon monoxide by heme oxygenases (Vinchi *et al.* 2016). However other studies have shown a protective effect of the Hx domain by preventing iron toxicity (Kapojos *et al.* 2003). TIMP-1 in the infected secretome could be binding directly to the Hx and stabilising it, thus preventing its release. This is an important finding that suggests that the low levels of TIMP-1 in *M. tb* infected macrophages and TB patients could be an inherent factor in cavity formation and dissemination, hence TB-patients co-infected with HIV and children with TB rarely progress to cavity formation because of the upregulation of MMPs that is accompanied by TIMP-1 increase.

Another interesting function of the Hx domain is its ability to inhibit neutrophil infiltration, something that is also observed in the overexpression of tyrosine-protein kinase Lyn in OVA-induced airway inflammation (Wang *et al.* 2017). The presence of iron has also been shown to polarise macrophages toward the M1 proinflammatory phenotype and the administration of the human hemopexin (Hx) to sickle mice rescued and attenuated this iron driven M1 phenotype (Vinchi *et al.* 2016). Therefore, attaining iron homeostasis by preventing the conversion of Hx might not only be essential for preventing the availability of iron for bacterial growth but for avoiding chronic inflammation which is vital for the process of wound healing, an inherent factor for efficient clearance of infection which may be time-dependent. Again, this highlights the importance of TIMP-1 in preventing chronic inflammation by stabilising the MMP-9. Another mechanism that is employed to attenuate inflammation is apoptosis. It plays a crucial role in eradicating damaged or dead cells without eliciting an immune response thus preventing chronic tissue damage by proteases especially MMPs. An important function of HMGB-1 (identified in infected the secretome) is its role in attenuating the engulfment of apoptotic neutrophils by macrophages (Friggeri *et al.* 2010;Velegraki *et al.* 2013). So, the exclusive identification of HMGB-1 and HMGB-2 in the infected secretome suggests that they have a role in regulating inflammation through engulfment of apoptotic cells. Both apoptotic and autophagic cells are reported to secrete

HMGB-1. The upregulation of isomerases which are essential in minimising protein aggregation could indicate that the cells are undergoing autophagy which facilitates clearance of protein aggregates and intracellular pathogens (Zeng and Carlin 2013).

A study by Zeng and colleagues investigated the role of autophagy in adenovirus infected airway epithelial cells and suggested that autophagosomes can intercept endosomal processing by also preventing the exchange of Rab5a and Rab7 associated with early and late endosomes, respectively. This led to the conclusion that the host was unable to control the intracellular release and replication of adenovirus (Zeng and Carlin 2013). In the current study Rab7B and Rab10 were upregulated intracellularly meaning there is phagosomal processing of *M. smeg*. Cathepsins are involved in direct killing of *Mycobacteria* and antigen presentation, and also in apoptosis (Pires *et al.* 2016). The upregulation of these lysosomal proteins, cathepsin B and D, and ribonuclease T2 in the secretome is an indication that there is phagolysosomal fusion, also plausible programmed cell death via the cathepsins.

A very exciting discovery in our study was evidence of secreted histones, DNA, RNA, granulins and actin-like proteins induced by the infection. Extracellular traps have been described for neutrophils, namely neutrophil extracellular traps (NETs) and have been documented to immobilise and kill extracellular microbes (Schauer *et al.* 2014). NETs are characterised by secretion of chromatin, bactericidal protein and other proteins such as fibrils that trap bacilli. They are known to be induced by ROS and apoptosis, and depending on the cell density of neutrophils, it has been demonstrated that a high cell density induces formation of aggregates that can sequester and degrade proinflammatory molecules (Khan *et al.* 2017;Schauer *et al.* 2014). These NETs are referred to as aggNETS (this will also be referred to in Chapter 5). Schauer and colleagues also showed that inhibiting proteinase 3, elastase and serine proteinases abolished the ability of these aggregates to degrade the inflammatory molecules. In contrast, EDTA or inhibitors of tissue transglutaminases did not prevent the degradation of inflammatory molecules but prevented formation of these aggregates. This suggests that zinc-dependent metalloproteases like MMP-9 may not be beneficial for mediating the degradation of these inflammatory molecules but for the formation of aggregates that release factors that sequester the pro-inflammatory cytokines. Although the cytokines were expressed, none of them were found in the secretome samples

implying that the extracellular traps are employed for degrading them. Given that MMPs have cytokines and chemokines as substrates (Morrison *et al.* 2009) for example MMP-9 can degrade the neutrophil attractant IL-8 (Rodríguez *et al.* 2010), MMP-9 could also be important for their intracellular degradation and regulation.

IL-8 was identified in the infected lysate, while IL-1β was upregulated in the lysate in contrast only interleukin-1 receptor antagonist protein (ILRA) was identified in the infected secretome suggesting that other proteases could be degrading cytokines if they are secreted. Proteins such as PDIs, PPIA and HGMBs which regulate aggregation illustrate the presence of extracellular aggregates, the latter through inducing autophagy which clears toxic protein aggregates and the others by facilitating protein folding and renaturation. Thus, the host elicits multiple mechanisms that may be working collectively to clear bacteria.

4.6.4 Role of extracellular exosomes, poly(A)RNA binding and 14-3-3 proteins in cell-to-cell communication

The transmission of intercellular signalling is as vital as the cellular response to direct interaction with bacterial molecules. Analysis of the data lead to the hypothesis that cellular communication is delivered to neighbouring cells through exosomes carrying DNA, RNA, proteins and DNA/RNA binding proteins, and via signalling scaffolds formed by the 14-3-3 proteins amongst others. In the secretome, the 'deposition of new CENPA containing nucleosome at the centromere' pathway was enhanced, in addition to that downregulation of deoxyribonuclease-2-alpha and ribonuclease T2 which has optimum activity under acidic conditions suggests that the DNA/RNA molecules are deliberately secreted and are protected from degradation.

RNA binding proteins play a crucial role in the regulation of gene expression especially in splicing and capping (Chennathukuzhi *et al.* 2001). Poly(A) RNA binding proteins (Pabs) bind to polyadenosile RNA (poly (A) RNA) and function to stabilize, localise and enhance translation of the poly(A) RNA. Since most of the Pabs were also exosome proteins this implies that they could be protected from degradation by ECM proteases thus allowing their delivery to neighbouring cells. The transporting of genetic and/or epigenetic material as a

means of crosstalk between cells is interesting in infectious disease as a strategy in acquiring adaptive immunity and/or resistance against pathogens. RNA contained in vesicles can act as protein carriers that could alter the epigenetic of neighbouring cells by acting on chromatin structures thus modifying gene expression (Di Liegro *et al.* 2017). The multiple bands that were observed by western blotting of MMP-1 (Figure 3-24) and MMP-9 by zymography (Figure 3-18) and western blotting of MMP-9 (Appendix 2, Figure 6-11) may be splice variants resulting from tRNA/RNA binding proteins delivered to nearby cells through exosomes. As alluded to earlier, the splice variants may be inactive forms of the MMPs that could be performing other functions.

CENPA is an H3-like centromeric protein A that is responsible for kinetochore assembling ensuring proper chromosome segregation (Carroll and Straight 2007;Niikura *et al.* 2016). Centromeric DNA is not well-conserved, however CENPA is required and conserved in centromeric nucleosomes thus being accepted as an epigenetic mark of centromere function (Carroll and Straight 2007;Niikura *et al.* 2016). The 14-3-3 proteins which were identified in the infected secretome are highly conserved acidic proteins in eukaryotes and are involved in signal transduction, apoptosis, cell proliferation, adhesion, differentiation and survival (Mhawech 2005). Very interesting is that they are mostly phosphoserine-binding proteins and could be acting to relay intercellular signalling. These 14-3-3 proteins form a network of interactions with clathrin light chain A (CLTA) which is anchored to the IGF2R (Cation-independent mannose-6-phosphate receptor) a receptor that binds and transports phosphomannosyl substrates from the cell-surface and Golgi apparatus to the lysosome. Therefore, the above implies that the phenotypic changes that are acquired during *M. smeg* infection are not induced by mutations in DNA sequences but rather through modification of gene expression in neighbouring cells by delivery of genetic material and proteins via exosomes. On the other hand, the protein groups uniquely expressed in the uninfected formed fewer interactions where the main cluster comprised of interactions between PP4R2 (Serine/threonine-protein phosphatase 4 regulatory subunit 2) and PPP1CC (Serine/threonine-protein phosphatase PP1-gamma catalytic subunit) which are anchored to the cleavage and polyadenylation specific factor 3, 73kDa, isoform CRA_b (CPSF3) and Nuclear pore complex protein Nup205 (NUP205). These suggest that phosphatases in particular GTPases may be regulating proteins involved in the translocation

of macromolecules between the nucleus and cytoplasm, facilitating the processing and maturation of mRNA.

Chapter 5

Proteomics of THP-1 macrophages in response to treatment with lipoarabinomannan (H37Rv)

Lipoarabinomannan (LAM) upregulates the expression of MMP-1 and MMP-9 genes in THP-1 macrophages. Also, MMP-9 depicted an increase in gelatinase activity with increasing LAM concentrations (Chang *et al.* 1996). Since the composition of the glycolipids in the cell wall of *M. tb* differ from that of *M. smeg*, these discrepancies could result in major differences in the macrophage response. Thus, the exposure of the THP-1 macrophages to LAM (H37Rv) for a 24-hour incubation period was assessed for differences in the expression and secretion of proteins. Although there was no increase in the gelatinase activity of intracellular and secreted MMP-9 (Section 5.4), the resultant phenotypic changes studied by discovery proteomics will give an insight into the effects of this virulent factor in isolation on the host's response.

5.1 Raw data analysis and processing

Three technical (injections) replicates were analysed. The processing of the raw data files was performed using MaxQuant (1.5.3.12) and the human Uniprot database to generate protein quantification and identification data. The raw files were run simultaneously, and each technical replicate was set as a separate experiment on MaxQuant. The analytic parameters used were as described in Chapter 4.

The representative ion chromatograph of the media (Figure 5-1) and lysate (Figure 5-2) were from infected and uninfected samples had comparable intensities. The efficiency of trypsin digestion was 89% (Figure 5-3). The media and lysate samples generated a combined total of 2646 protein groups, with 38 and 26 identified as contaminants and decoy hits, respectively. Out of the 198613 spectra submitted, 41.7% were identified. The ion injection times and percentage of MS/MS identified (Figure 5-4) were similar between triplicate

repeats. Further analysis using histograms showed that the data were normally distributed (Figure 5-5), except for the LAM-treated media sample (L_Med3). This was confirmed by the scatterplots (Figure 5-6) which gave a correlation co-efficient (R^2) between 0.771 and 0.915 for the lysate and 0.796 and 0.933 for the secretome.

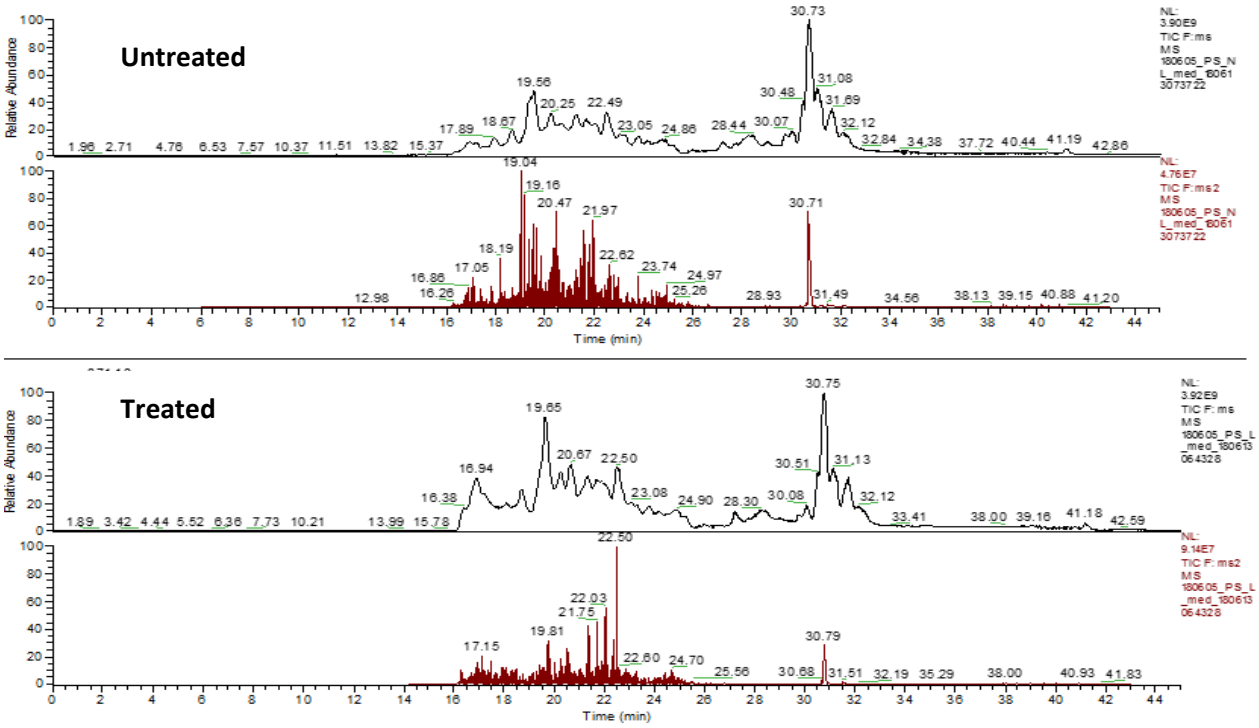

Figure 5-1. Representative chromatogram of the secretome from untreated and LAM-treated macrophages.

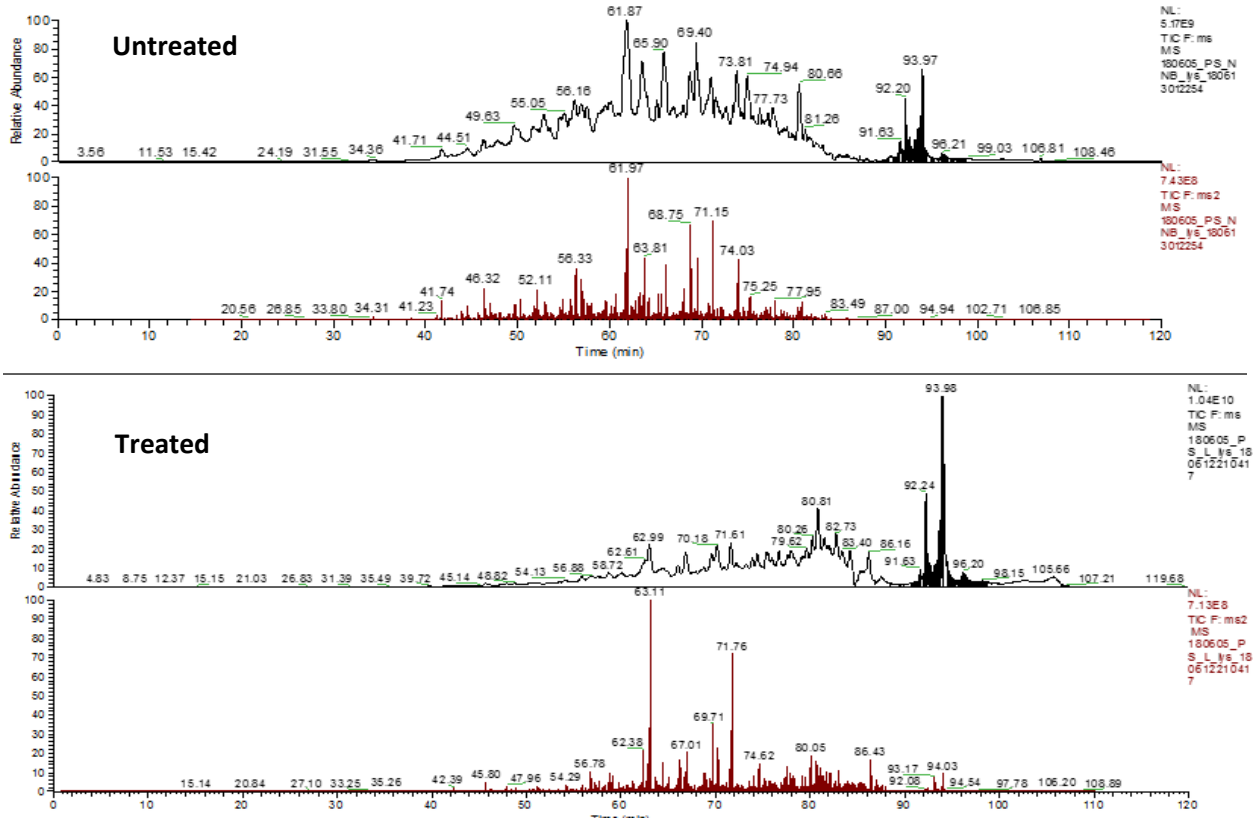

Figure 5-2. Representative chromatogram of the lysate from untreated and LAM-treated macrophages

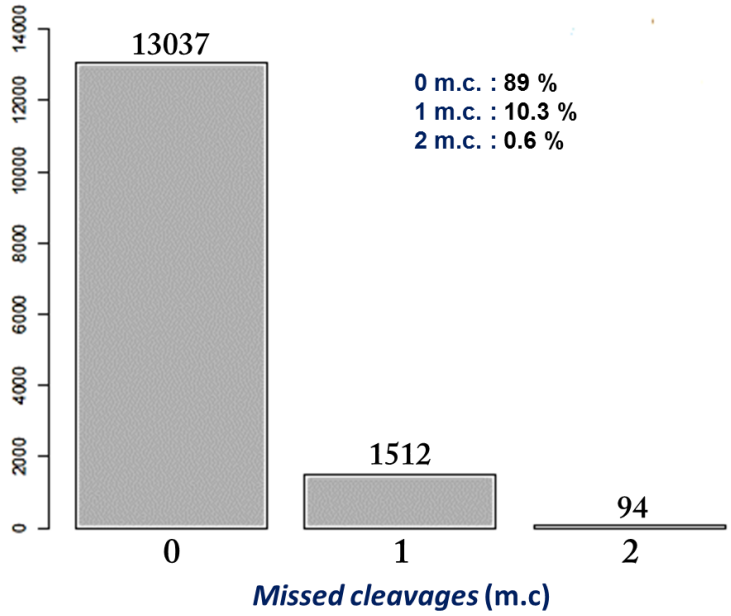

Figure 5-3: Number of missed cleavages. The number of peptides generated are depicted by the bar graphs as a function of missed cleavages by trypsin.

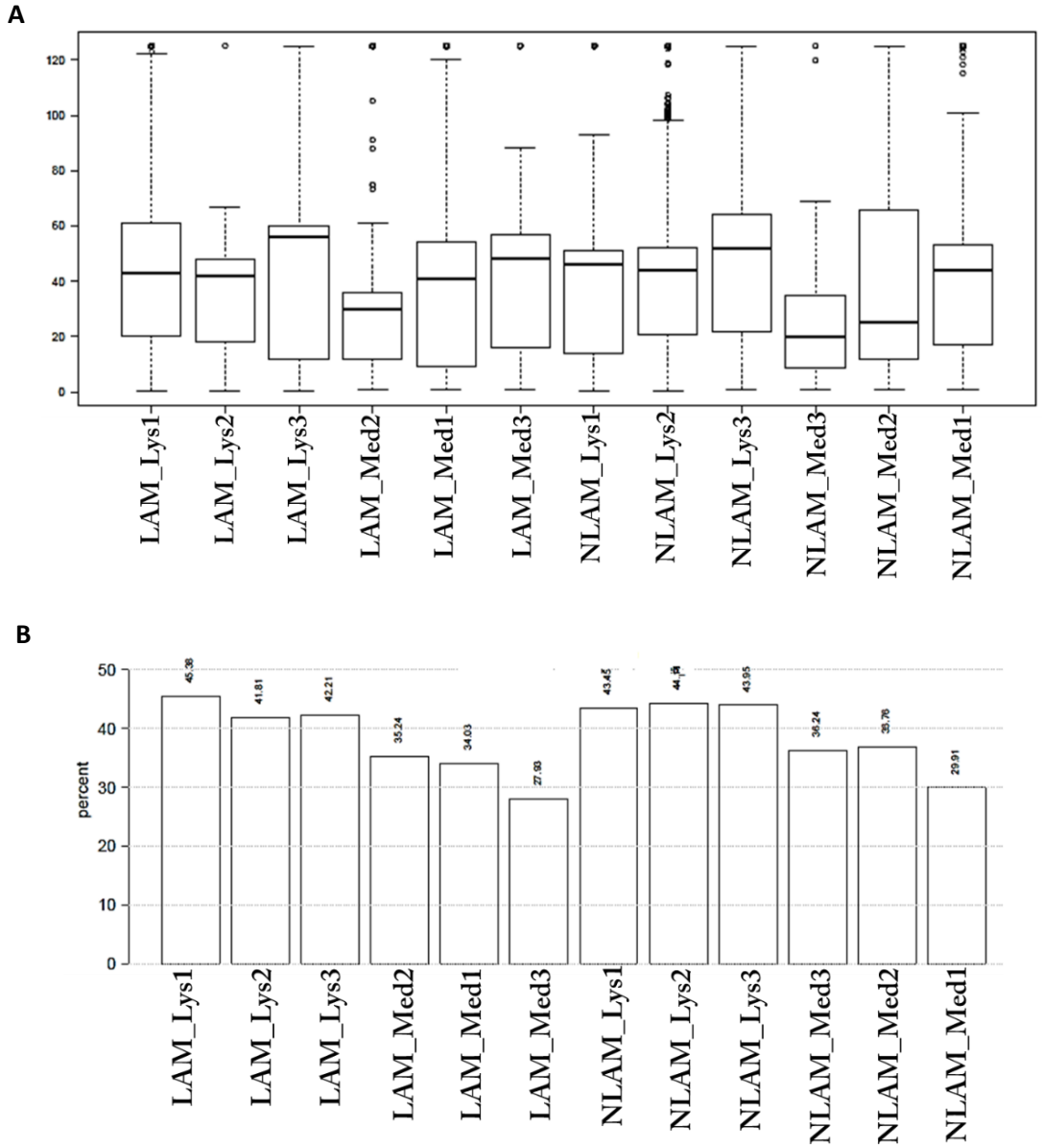

Figure 5-4: Analysis of the injection replicates. The injection times (A) and the (B) Ms/Ms percentage for each of the three technical replicates. LAM_Lys1 and LAM_Med1 represent lysate and media samples from LAM-treated macrophages, followed by the number of the technical replicate. Similarly, NLAM_Lys1 and NLAM_Med1 represent lysate and media samples from macrophages not treated with LAM, followed by the number of the technical replicate.

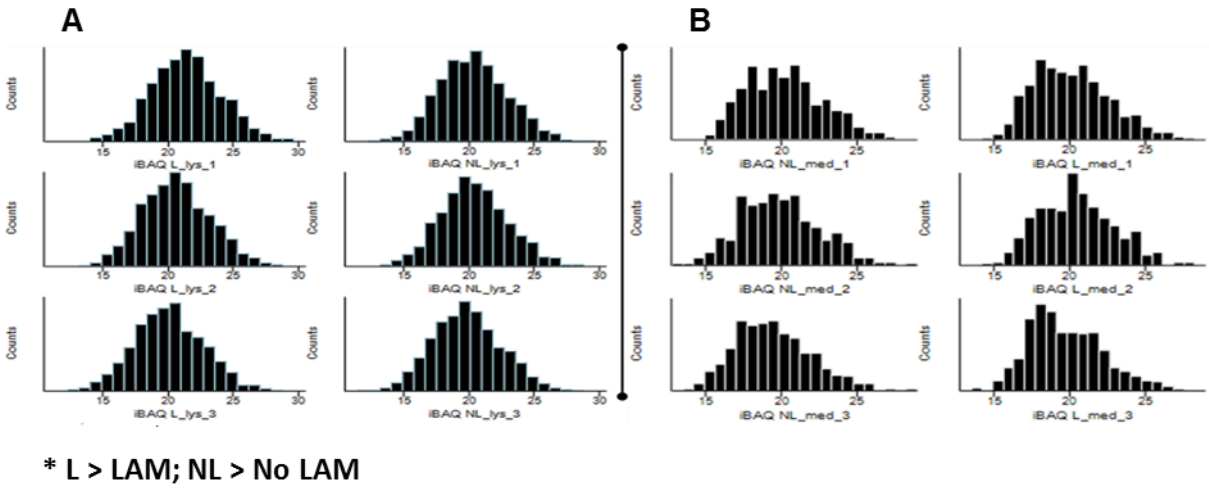

Figure 5-5: Description of the data distribution by histograms. (**A**) The lysate and (**B**) media were plotted using the counts as a function of the iBAQ intensities. Three technical replicates were analysed.

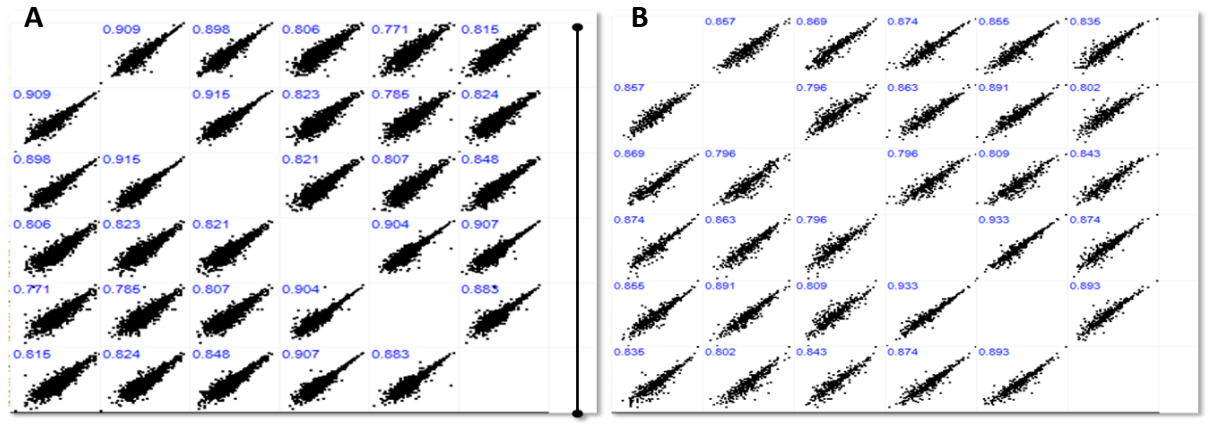

Figure 5-6: Assessment of data reproducibility of the technical replicates. The scatter plots represent the computed correlation co-efficient (R^2) between the three technical replicates of the lysate (**A**) and media (**B**).

5.2 Quantitative and qualitative data analysis of the LAM (*H37Rv*) treated macrophages

The same data processing and analysis that was used for the *M. smeg* infected and uninfected macrophages was carried out for the LAM stimulated and non-stimulated macrophages. All the quantifiable protein groups found in the media were also found in the lysate (Figure 5-7). A set of 264 of the lysate protein groups (Appendix 3, Table 6-7) were significantly different between uninfected and infected, and the secretome had 28 significantly different protein groups (Appendix 3, Table 6-8) between uninfected and infected of which none were overlapping with the lysate (Figure 5-7). These were computed using the two-sample t-test without multiple hypothesis testing. According to volcano plots, six and three protein groups (Appendix 3, Table 6-9) were significantly dysregulated in the lysate and secretome, respectively (Figure 5-8). For biological analyses and interpretation, the differentially regulated proteins computed using the two-sample t-test was used. To compare between uninfected and infected samples, peptides that were identified in at least two of the replicates were used in the two-sample t-test (p-value < 0.05) to identify differentially expressed proteins. A p-value < 0.05 was used as a cut-off and any proteins that had a p-value less 0.05 were considered significantly differentially regulated. Since the p-value considers the variances between samples this also justifies using these proteins for downstream analysis and biological interpretation. Additionally, interference from false positives is less likely since the FDR was set at 1% in MaxQuant to exclude them. None of the MMPs were differentially regulated following LAM stimulation except TIMP-1, which was significantly dysregulated in the intracellular proteome and secretome (Figure 5-9). This coincides with the zymography results and explains the lack of a difference in the gelatinase activity between LAM treated and untreated samples (Section 5.5).

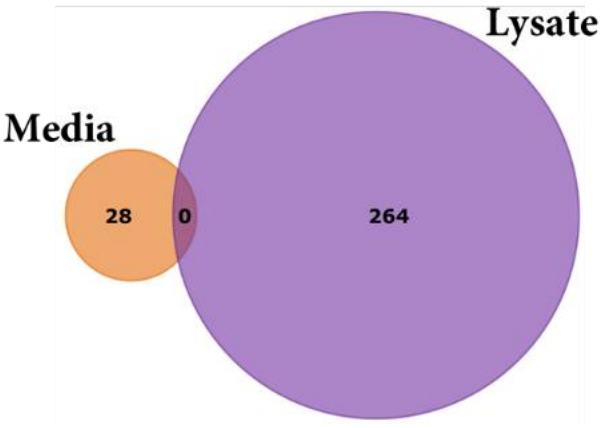

Figure 5-7: Visualisation of overlapping protein groups between the lysate and secretome. The protein groups calculated to be significantly different in the lysate and secretome did not overlap.

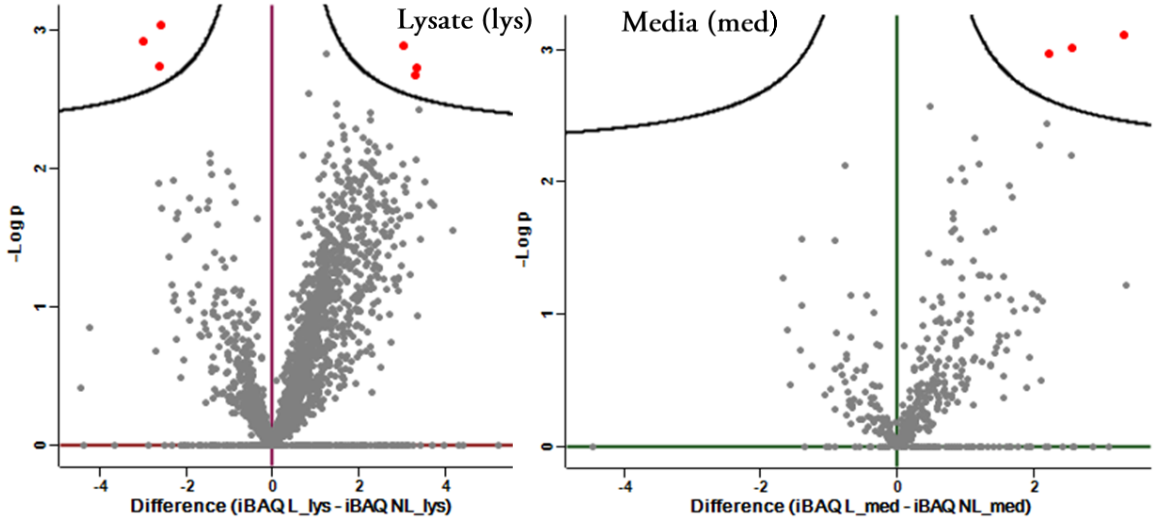

Figure 5-8: Visualisation of computed differentially regulated protein groups induced by LAM treatment. Volcano plots from Perseus 1.6.1.3 were used to compare the differences in iBAQ intensity between treated (L_) and untreated (NL_) samples as well as the significantly different protein groups (red spheres).

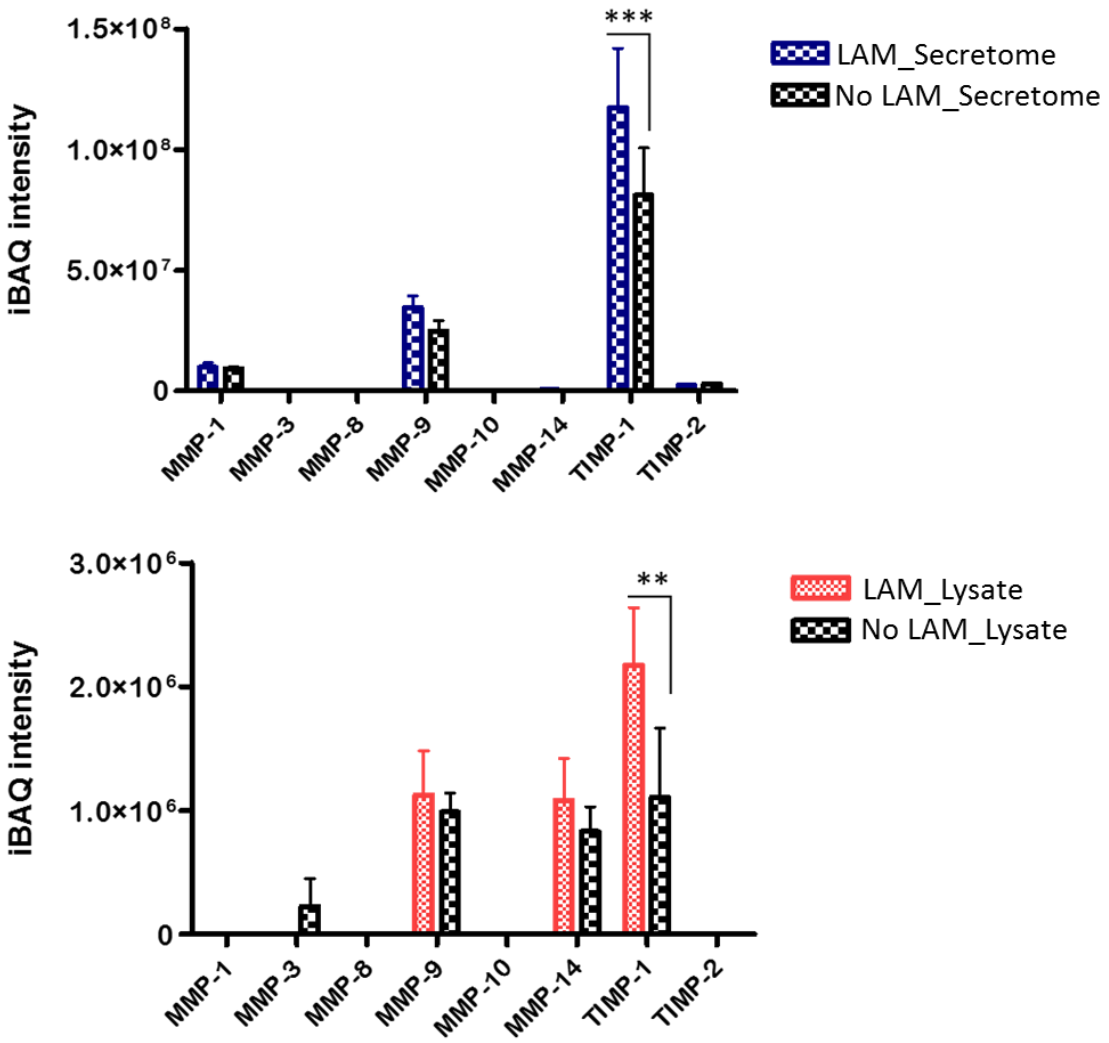

Figure 5-9: iBAQ intensity of identified MMPs in LAM-treated and untreated in the lysate and secretome. Only TIMP-1 in the secretome was found to be significantly upregulated with a p-value <0.001.

Biological function and classification of dysregulated protein groups: Lysate

LAM treatment caused dysregulation of proteins of the lysosome, exosome, cytoplasm, cytosol and centrosome cellular components which were observed with a GO enrichment p-values less than 0.001 (Figure 5-10). The expressed molecular function signatures with a p-value less than 0.05 are ubiquitin-specific protease activity and cytoskeletal protein binding (Results not shown). Protein metabolism was the most enriched biological process, and to a

lesser extent energy pathways and protein modification were also represented (Results not shown).

The H4, coiled coil region, RAB, 14-3-3 and ANX were amongst the enriched protein domains (Figure 5-10). The main pathways depicted were mRNA/RNA metabolism, p38 signalling mediated by MAPKAP kinases, Trk receptor signalling mediated by PI3K and PLC-γ and host interactions of HIV factors (Figure 5-11). The site of expression classification indicated global-SCX-fractionated, CaOV3 (ovarian cancer cells) and dendritic cells in the top three (Figure 5-11). The former is a strong ion exchange (SCX) chromatographic method used to enrich phosphopeptides suggesting that the lysate is highly charged with phosphopeptides. None of the clinical phenotypes were observed with good confidence.

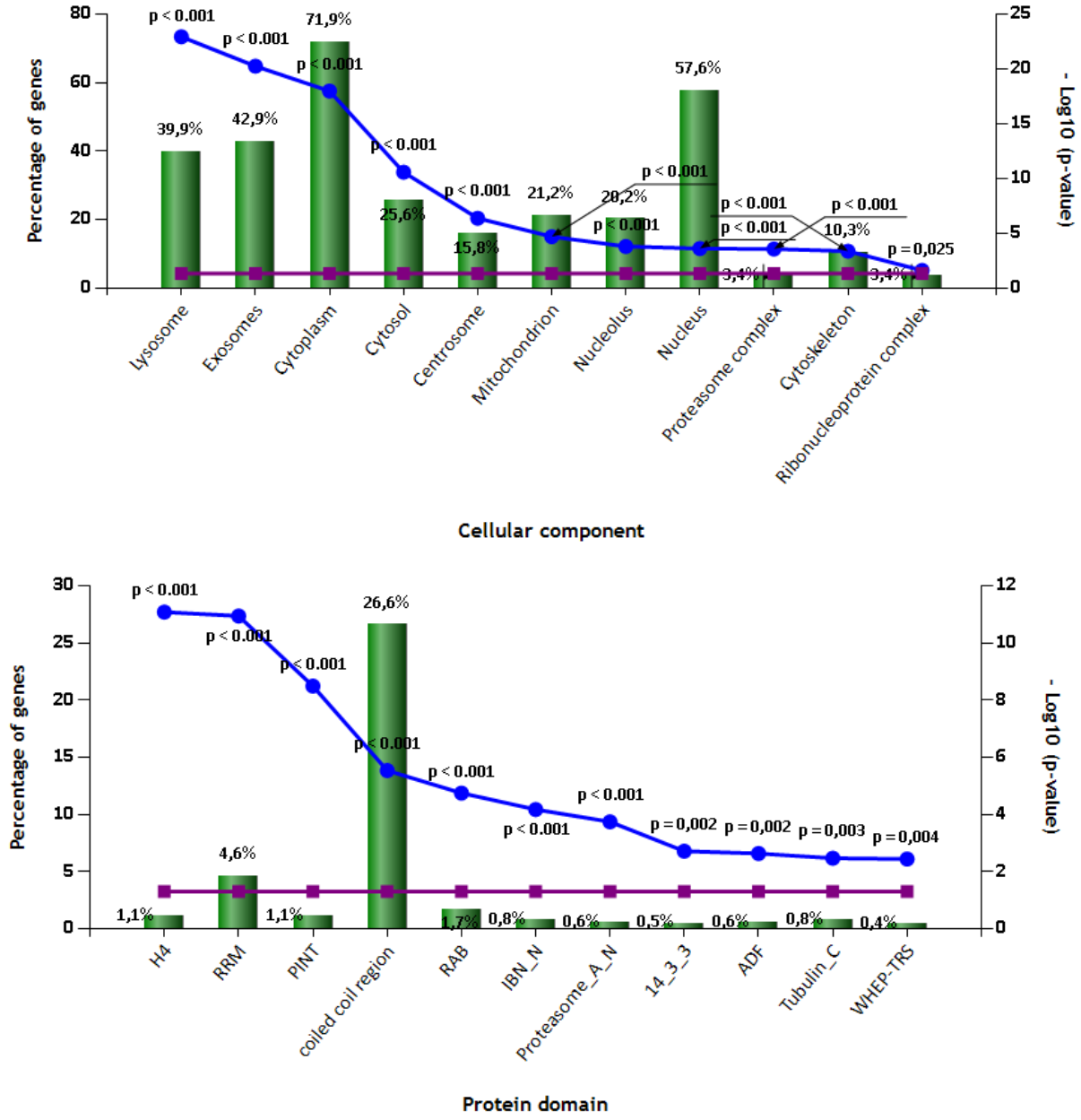

Figure 5-10: Biological function classification of dysregulated protein groups in the lysate.

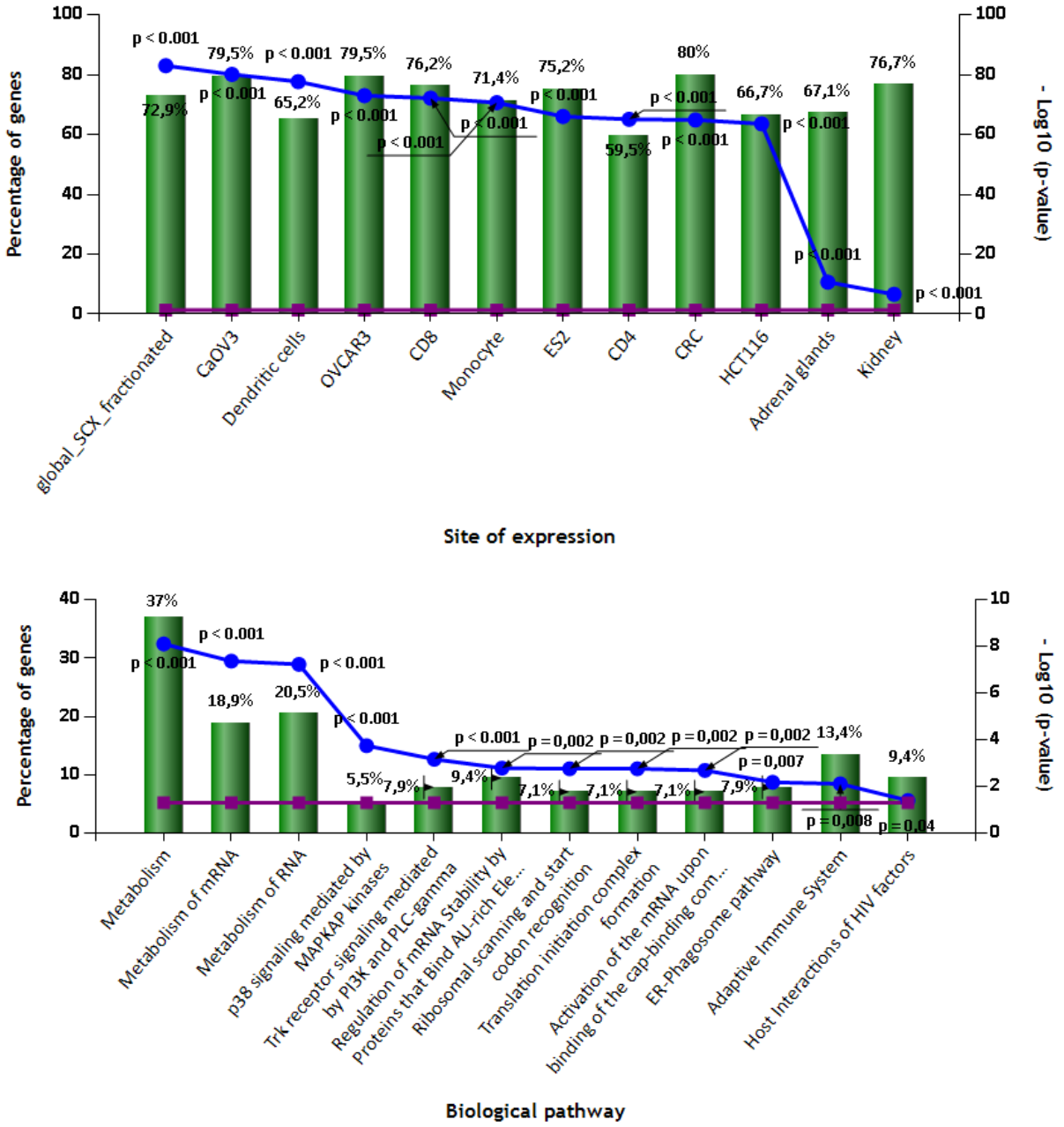

Figure 5-11: Annotation of the biological function of dysregulated protein groups in the lysate.

Protein-protein interactions: Dysregulated intracellular proteome

Most of the dysregulated protein groups are known to form protein-protein interactions displaying clusters including ones associated with the 14-3-3 proteins and the calcium binding proteins (Figure 5-12). Most of the proteins were protein binding proteins and involved in intracellular transport. Also, of note was the clustering of proteins involved in 'symbiosis encompassing mutualism through parasitism' which were mostly the proteasome subunit proteins and the Rab/Rap proteins.

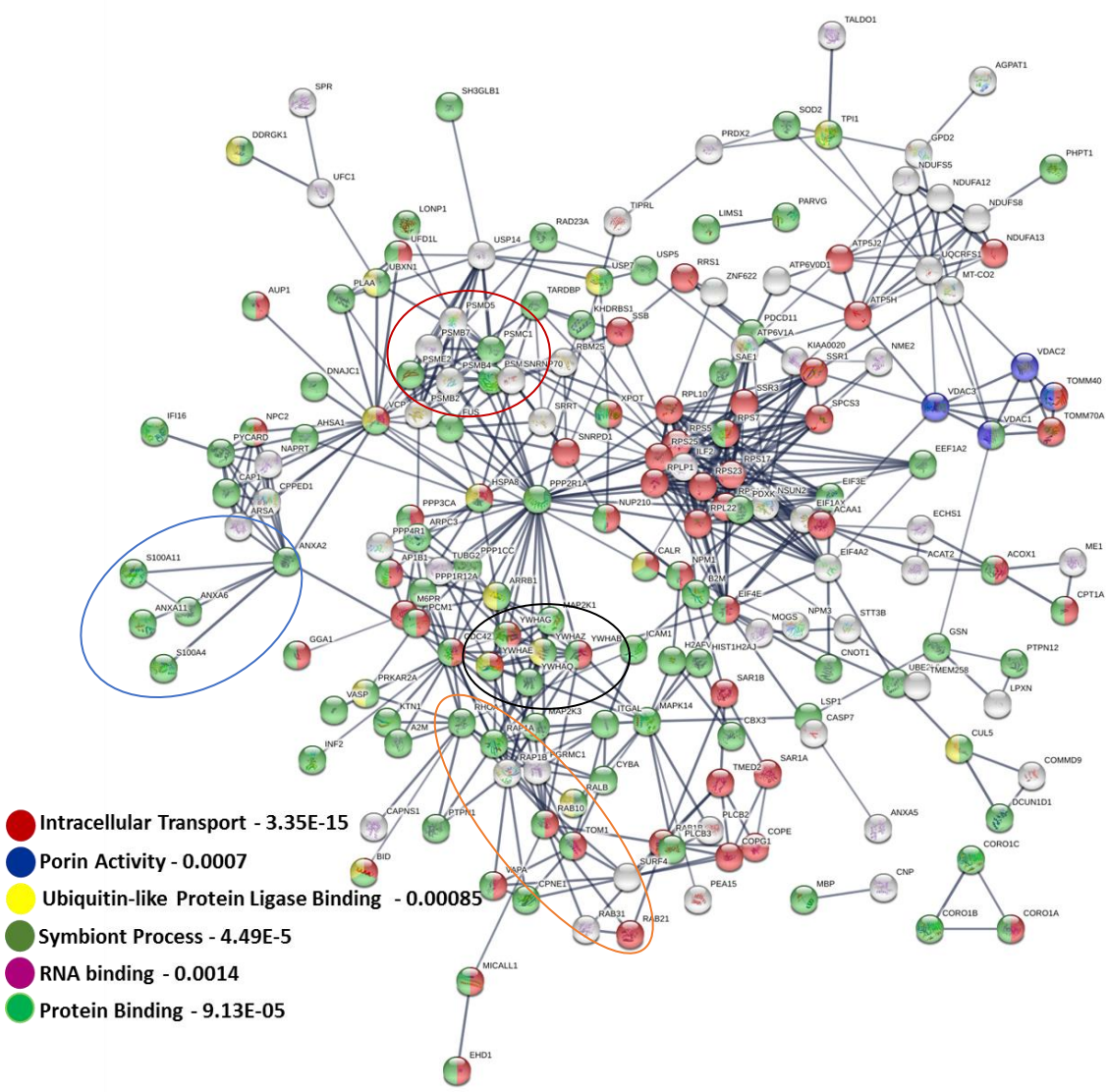

Figure 5-12: Protein interactions of dysregulated intracellular proteome induced by LAM. The 14-3-3 conserved proteins (black circle), calcium binding proteins (blue circle), Rab related proteins (orange) and proteasome subunits (red circle) are indicated. The GO protein classification terms (biological process and molecular function) were also determined by STRING and are colour coded (colour key). The FDR values are indicated.

Biological function of dysregulated protein groups: Secretome

The secretome had differentially regulated proteins with GO classification in the nucleosome, nucleus, centrosome, exosome and ribonucleoprotein complex (Figure 5-13). Proteins that form part of the nucleic acid metabolic processes were mainly DNA binding (results not shown). Coinciding with that was H4 as the main protein domain enrichment and the GO metabolic process representing regulation of nucleoside, nucleotide and nucleic acid, suggesting the presence of chromatin in the secretome. The overrepresented GO biological processes were packaging of telomere ends, RNA polymerase I promoter opening, deposition of new CENPA containing nucleosome at the centromere, signalling events mediated by HDAC class III and meiotic recombination and synapsis (Figure 5-13).

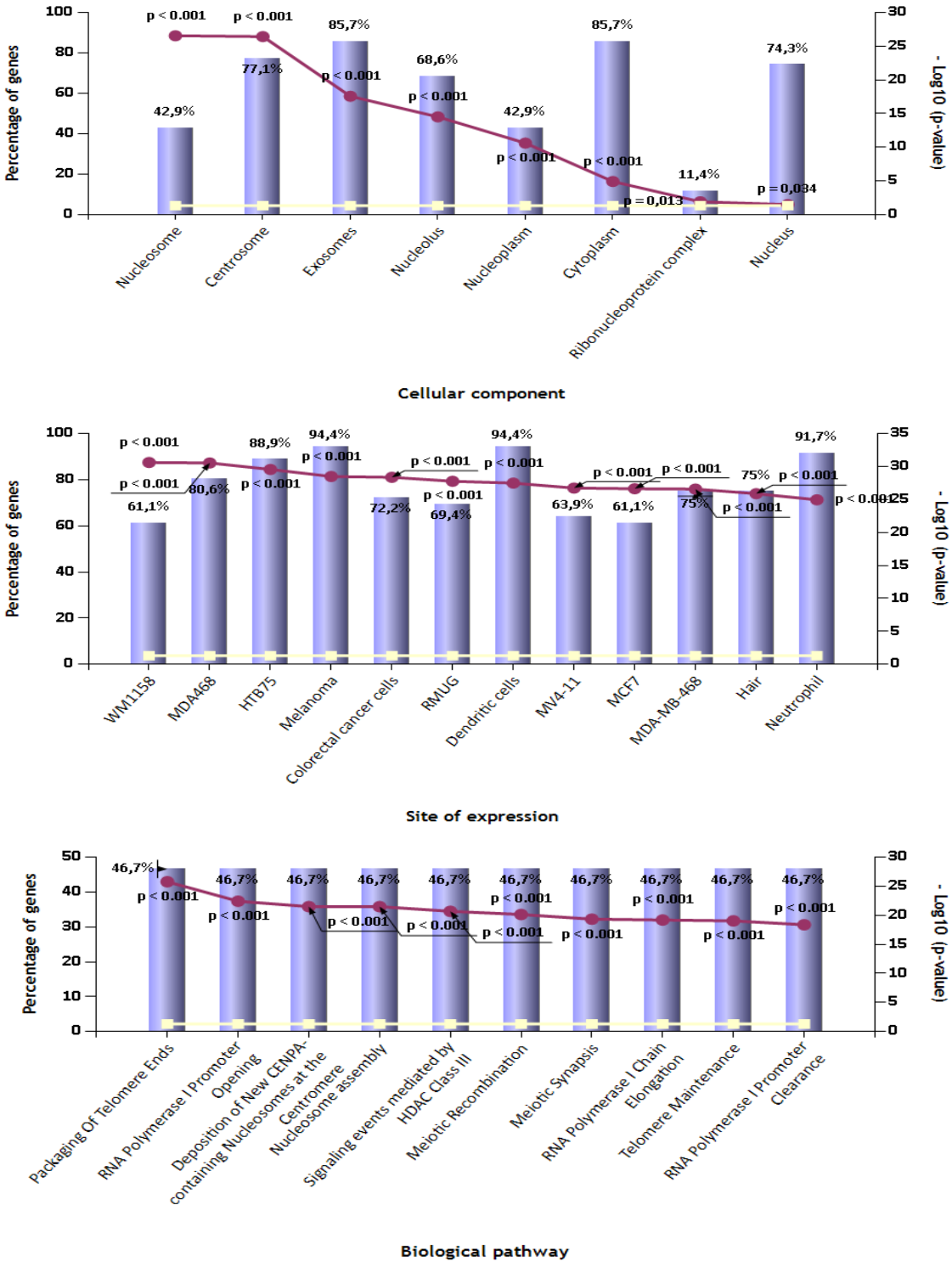

Figure 5-13: Dysregulated protein groups of the <u>secretome</u> were classified with accordance to GO terms.

Protein-protein interactions: Dysregulated proteins in the secretome

Following analysis using STRING-DB, all but one of the dysregulated proteins in the secretome formed an interaction network (Figure 5-14).

Most of these proteins were classified as protein-containing complexes. The presence of kinase binding proteins implies possible effects on intercellular signalling. The integrins ITGB2 and ITGB5 formed interactions with fibronectin (FN1) and myosin regulatory light chain 12A (MYL12A). The actin-related protein 3 (ACTR3), actin-related protein 2/3 complex subunit 5 (ARPC5), clathrin heavy chain 1 (CLTC) and GAPDH (Glyceraldehyde-3-phosphate dehydrogenase) network anchor to the FN1 via ILF3 (Interleukin enhancer-binding factor 3). This is important to note because ARPC5, ACTR3 and ITGB2 are involved in phagocytosis (Figure 5-14) and ARPC5, CLTC and FN1 were classified as 'bacterial invasion of epithelial cells' (Results not shown). These are relevant in postulating the transportation of LAM or intact *M. tb* across the glomerular epithelial layer and ultimately secreted in urine.

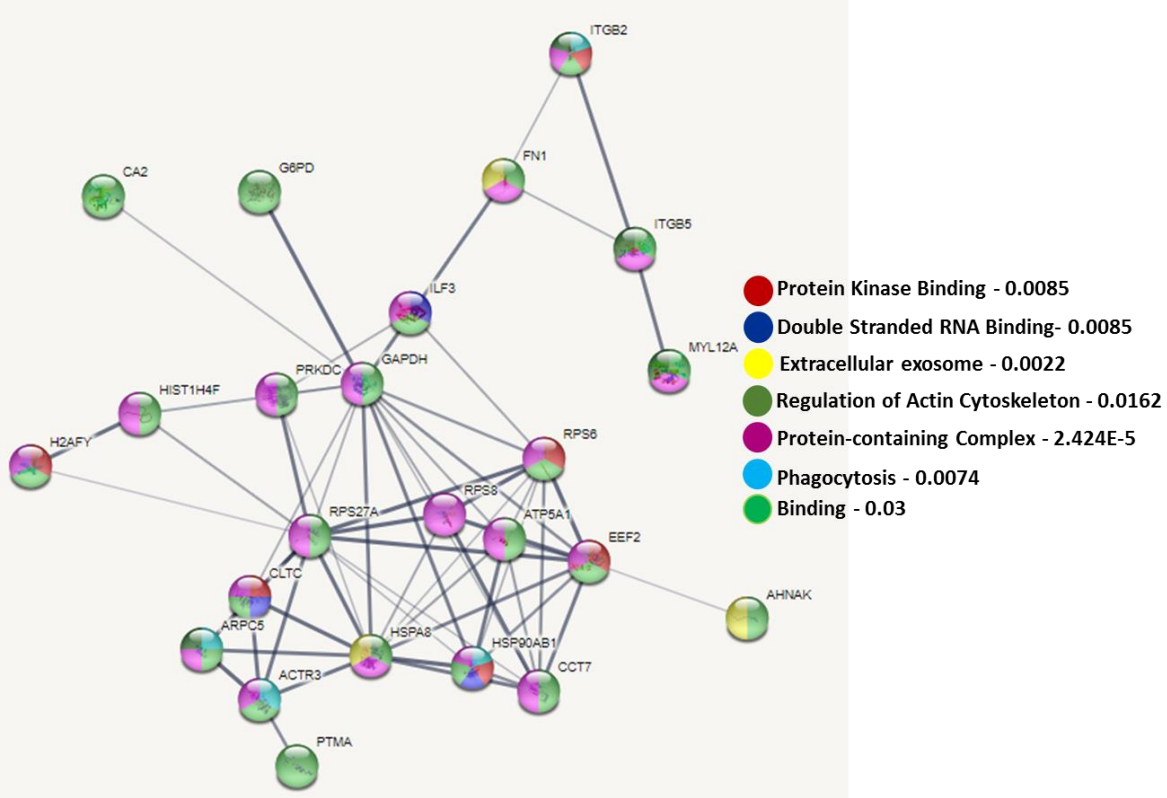

Figure 5-14: Visualisation of dysregulated proteins in the <u>secretome</u>. The GO terms were also represented by the different colour coding with their computed FDR values.

5.3 Evaluation of LAM treatment on the THP-1 macrophage phenotype using exclusively expressed and secreted proteins

The protein groups that were exclusively identified in the unifected and not in the infected lysate and secretome were analysed. A minimum of 2 peptides was required to be identified in the uninfected and 0 in the infected (and vice versa) to be considered exclusively identified for that protein group. This would in turn build stronger evidence for differences induced by the LAM-treatment. The number of proteins for each category are illustrated with a Venn diagram (Figure 5-15), including the overlapping proteins between the LAM-treated media and lysate, untreated media and lysate, finally between LAM-treated lysate and untreated media. These proteins were density-regulated protein (DENR), v-type proton ATPase subunit G 1 (VATG1) and copper transport protein ATOX1 (ATOX1), respectively.

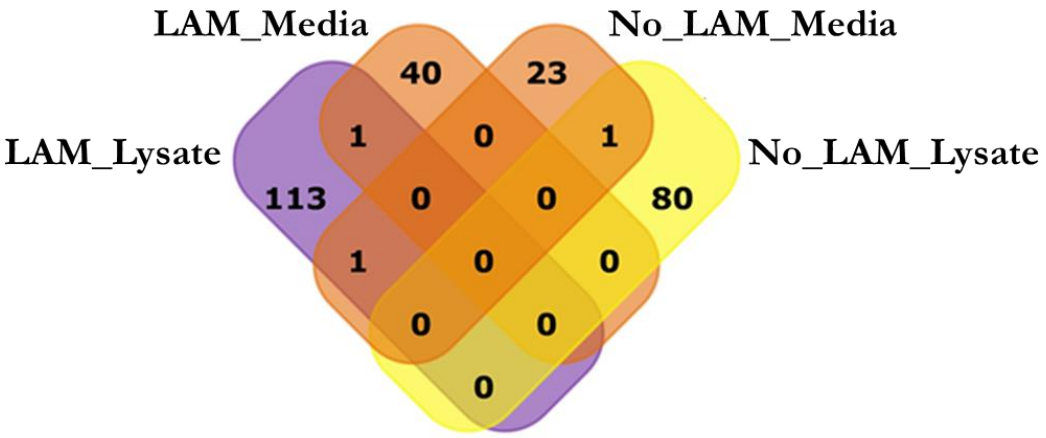

Figure 5-15: Visualisation of the exclusively expressed proteins.

Biological function of the LAM treated versus untreated THP-1 macrophages

The protein groups exclusively expressed by the LAM treated and untreated lysate depicted enrichment in the GO classification of the lysosome. The percentage gene representation of the lysosome was higher in the untreated macrophages (Figure 5-16).

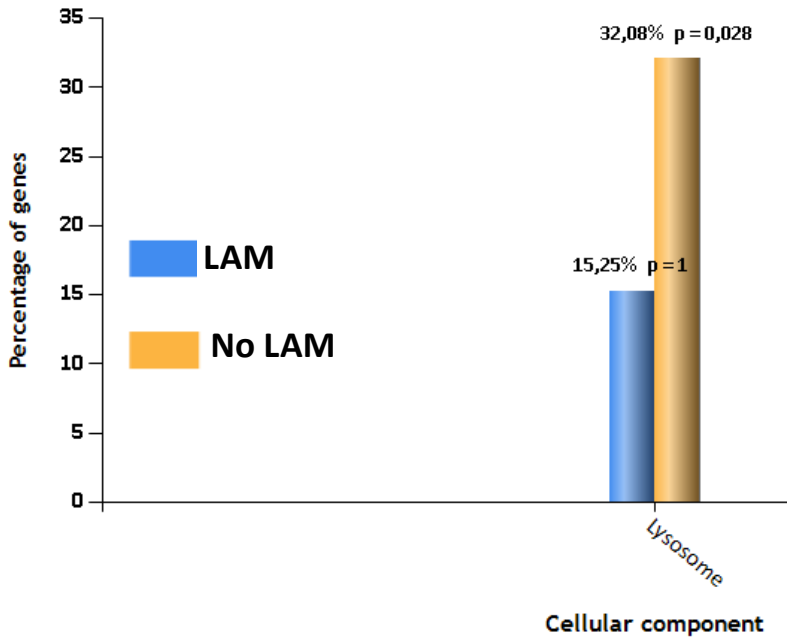

Figure 5-16: Classification of LAM-treated versus untreated lysate proteome.

Protein-protein interactions of intracellular proteome: LAM-treated versus untreated macrophages

In the LAM-treated proteome (Figure 5-17) the ribosome biogenesis protein (WDR12) was predicted by STRING database to form a cluster of networks directly with the WD repeat-containing protein 3 (WDR3), Protein AATF (AATF), tetratricopeptide repeat protein 27 (TTC27) and U3 small nucleolar RNA-associated protein 14 homolog A (UTP14C) which are mostly proteins associated with the ribonucleoprotein complexes. The cluster of the mitochondrial ribosomal proteins (MRPLs) with the pentatricopeptide repeat domain-containing protein 3 (PTCD3) is also depicted (Figure 5-17). Most of the protein genes represent proteins involved in acetylation.

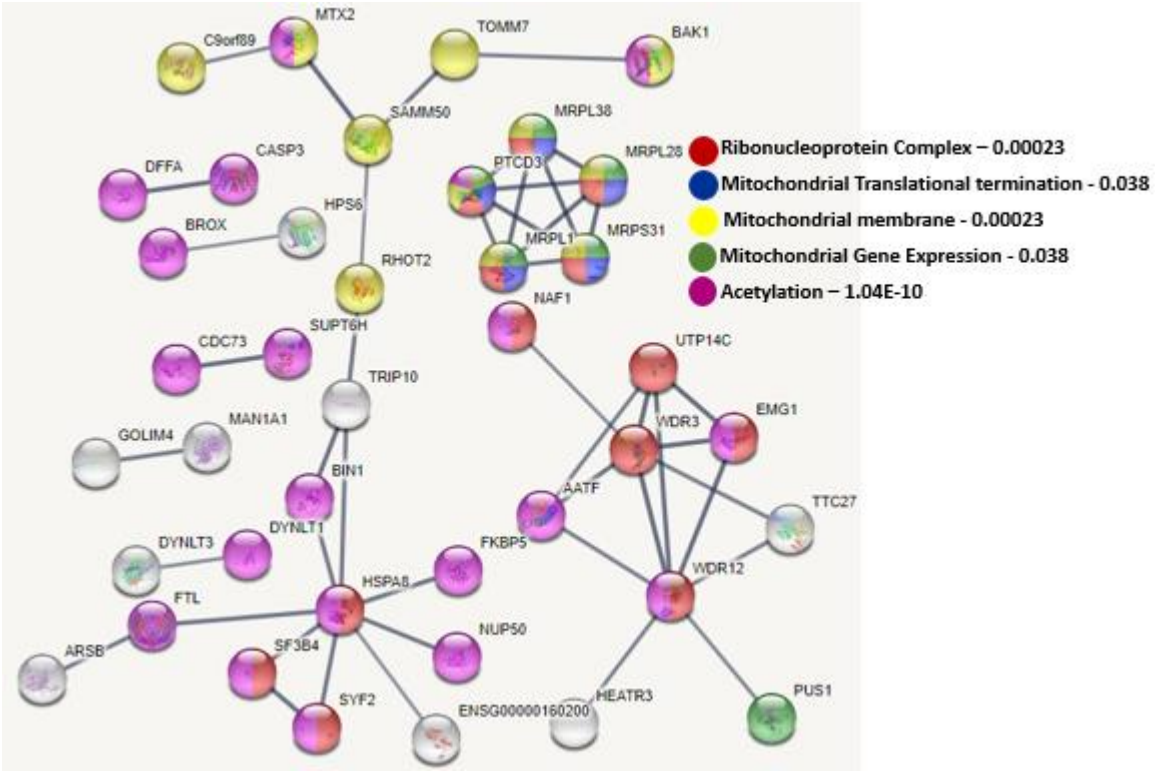

Figure 5-17: Interactions between proteins exclusively expressed in LAM treated macrophages. Also represented were the GO classification terms of the proteins (colour coding) and their FDR values.

In the uninfected intracellular proteome, Deoxyribonuclease-2-alpha (DNASE2) forms a triad with CTSZ (Cathepsin Z) and HSPA8 (Heat shock cognate 71 kDa protein) which forms part of the lysosome vesicle biogenesis together with CLTA (Clathrin light chain A). Another network was between Sec61 subunit alpha isoform 1 (SEC61A1) and the ribosomal proteins that form intracellular organelle part cellular compartments and function in macromolecule catabolic process (Figure 5-18).

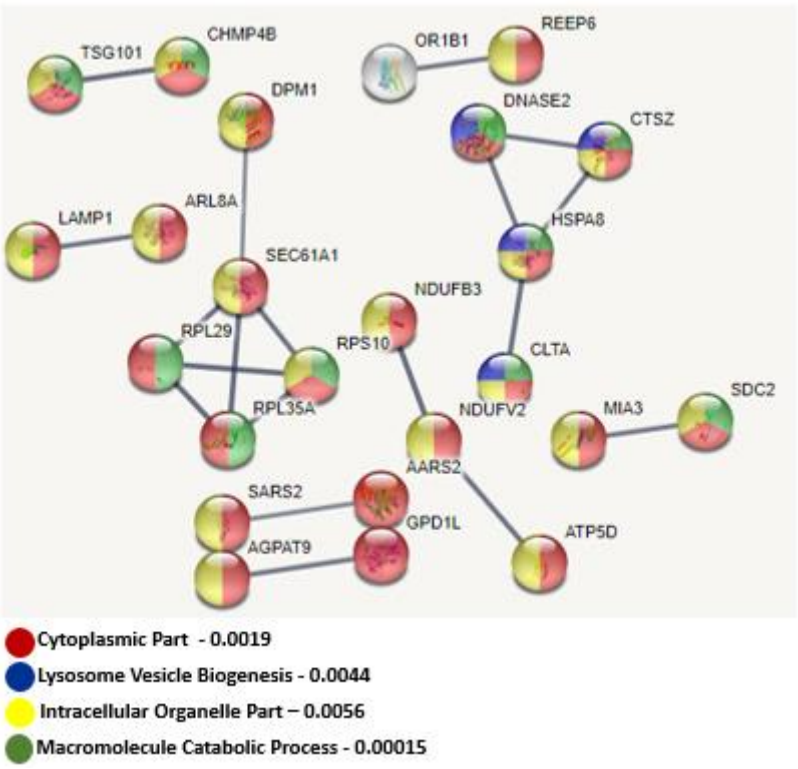

Figure 5-18: depiction of protein-protein interactions expressed by untreated macrophages.
Also represented were the GO classification terms (colour coding) and the FDR values are given.

Biological function of LAM-treated versus untreated secretome

The GO cellular component terms that had the highest percentage genes in the LAM-treated secretome versus untreated were the mitochondrion, centrosome, and mitochondrial nucleoid. The GO molecular function depicted higher percentage of genes representing the ribonucleoprotein and catalytic activity for the untreated and treated secretome, respectively (Figure 5-19).

Protein-protein interactions in the secretome: LAM-treated versus untreated macrophages

The LAM-treated macrophages specifically induced secretion of proteins that were predicted using STRING-DB to form protein-protein interactions around clustering of the ribosomal proteins (RPLS) which interacted with the early transcription factor, EIF2A and the

elongation factor 1-alpha 1 (EEF1A1). This network is anchored to the GTPase enzyme RAB7A and RHOG (Figure 5-20). This suggests that the GTPases may also be transporting these factors across cells via exosomes as a means of cell-cell communication.

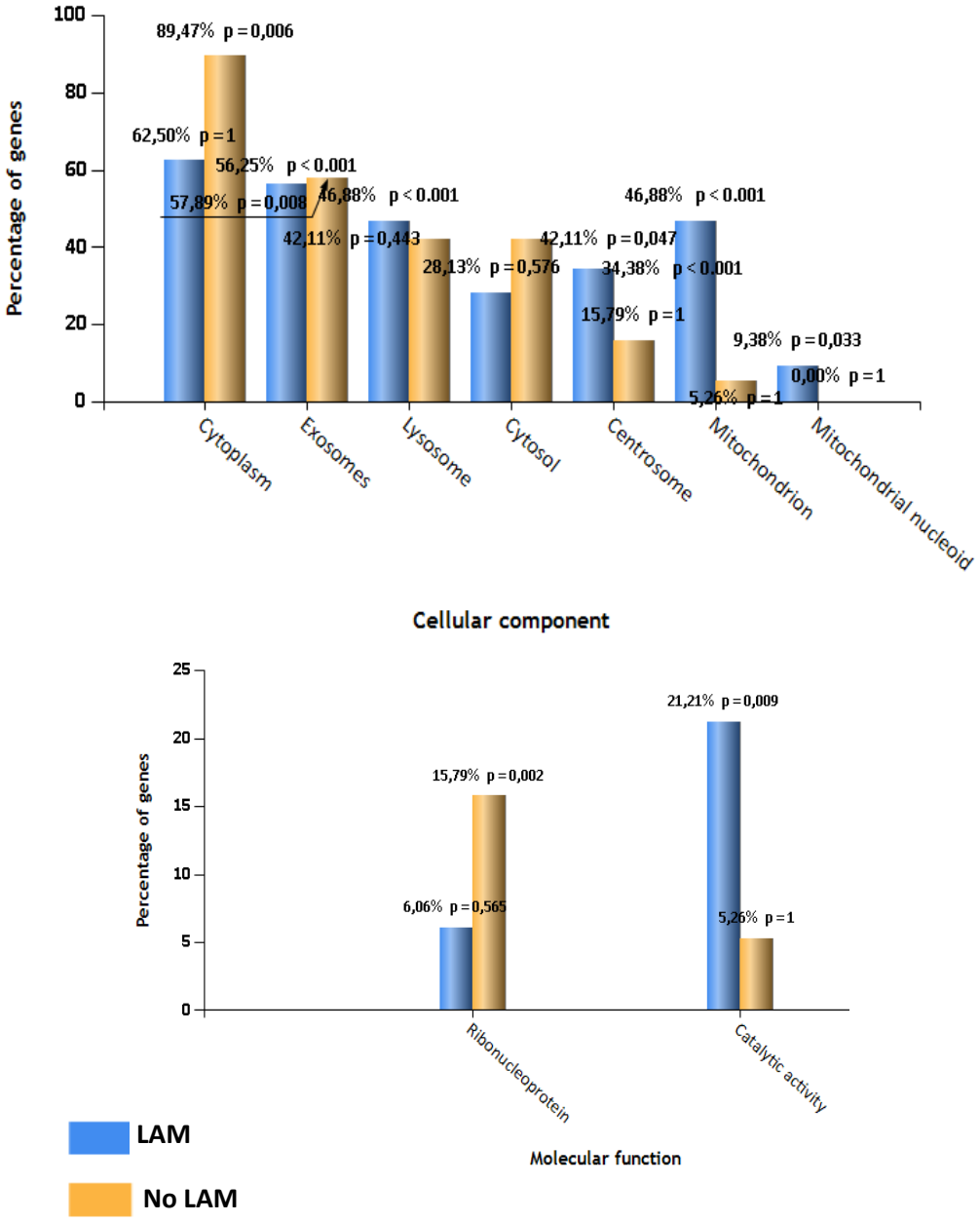

Figure 5-19: Cellular component, molecular function and biological process annotation of LAM-treated and untreated secretome.

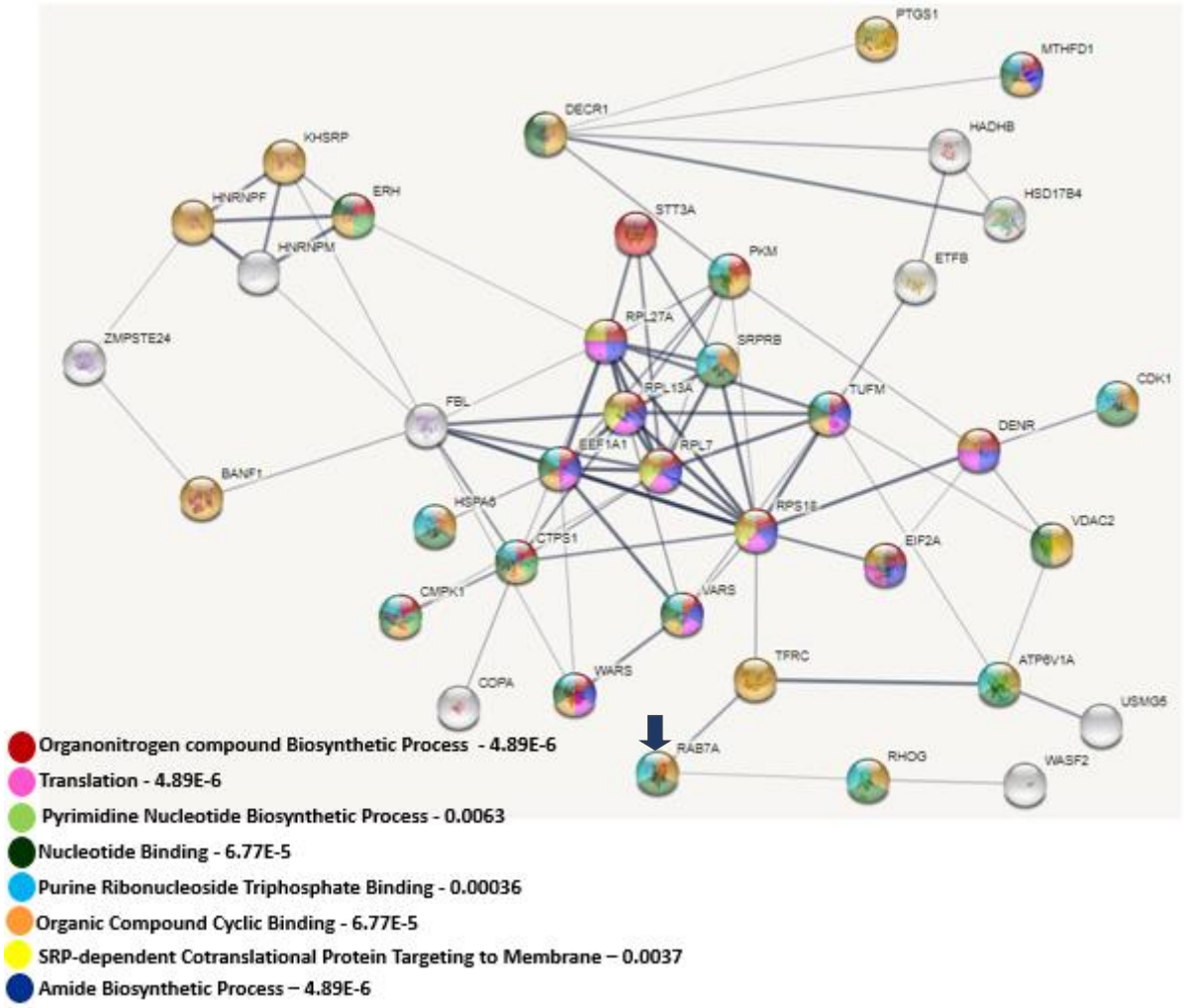

Figure 5-20: Protein-protein interactions of proteins <u>secreted</u> from the LAM-treated macrophages. Also represented were the GO classification terms (colour coded) and FDR values are shown. Rab7a is indicate with an arrow.

The uninfected secretome displayed protein interactions predicted by STRING-DB to form part of the spliceosome, and GRB2 (Growth factor receptor-bound protein 2), CRKL (Crk-like protein) and HNRNPK (Heterogeneous nuclear ribonucleoprotein K) are part of microRNAs in cancer. This suggests that gene silencing between cells is carried through exosomes and binding to the GTPase, RAB11B (Figure 5-21).

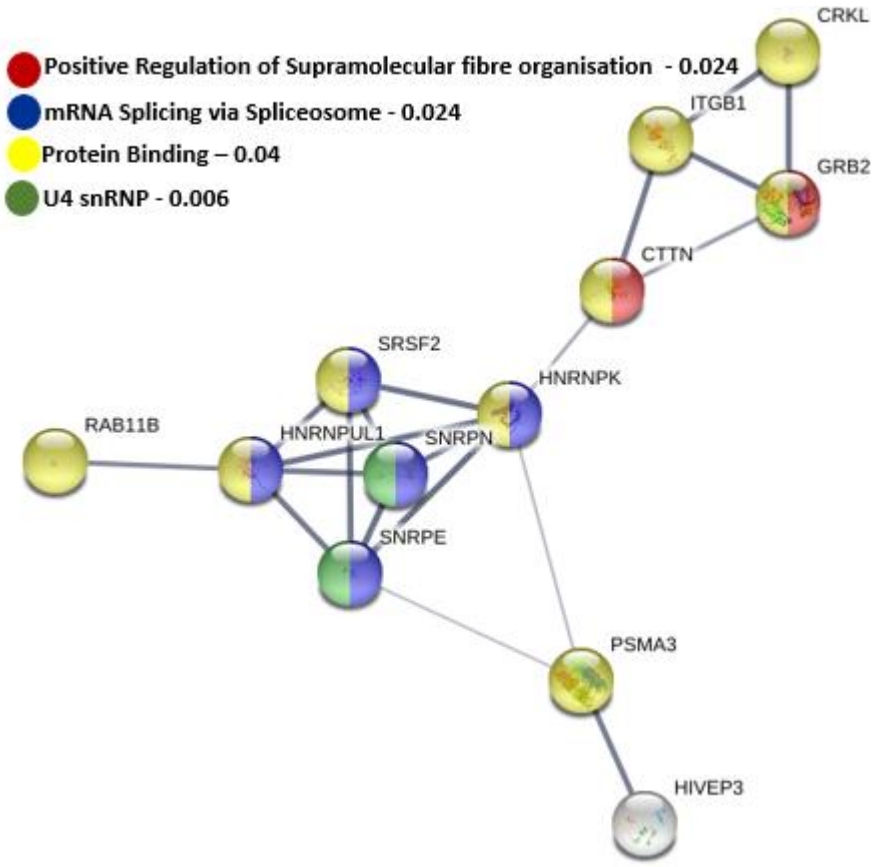

Figure 5-21: Interaction of the <u>secreted</u> proteins from untreated macrophages. Also represented are the GO classification terms (colour coding) and FDR values are shown.

5.4 Effect of LAM on the gelatinase activity of secreted and expressed proteins in from THP-1 macrophages

The lysate and media harvests from the 4 and 24-hour incubation with LAM were analysed by gelatin zymography for MMP activity (Figure 5-22). There was no significant difference in activity between stimulated and non-stimulated lysate and media, even after 24 hours in serum-free media.

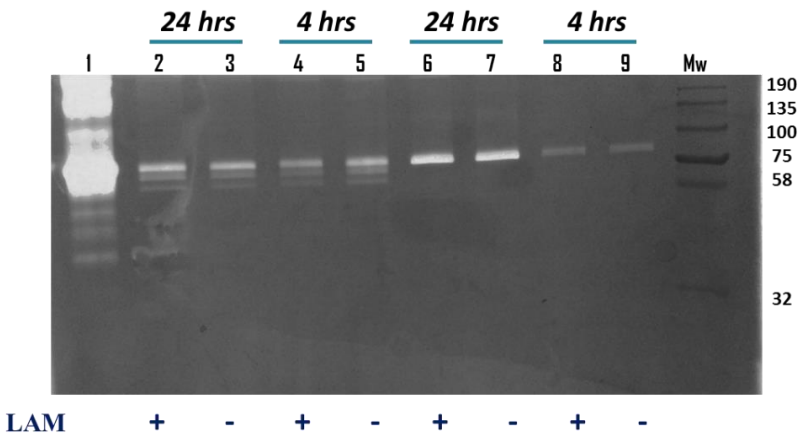

Figure 5-22: Hydrolysis of gelatin by LAM stimulated and unstimulated macrophages. The lysate (lanes 1 to 5) and media (lanes 6 to 9) harvested from macrophages that were stimulated for 4 or 24 hours were run on gelatin zymography. The recombinant MMP-9 was loaded as a control (lane 1).

5.5.1 Implications of MMP-9 dysregulation and LAM (H37Rv) recognition

Both the expression and secretion of MMP-9 were not significantly dysregulated, whilst its gelatinase activity was also not altered by the presence of LAM, implying that other factors, most probably *Mycobacterial* factors are required. However, significant upregulation of TIMP-1 in the media and lysate was observed. This also explains the lack of a difference in the gelatinase activity between the treated and untreated macrophages. The LAM component of *M. smeg* and *M. tb* are distinguished by the capping subunits where the latter comprises mono, di-, or tri- α(1→ 2) man units (man-LAM) whereas *M. smeg* contains phosphoinositol (PI-LAM) caps (Appelmelk *et al.* 2008;Fukuda *et al.* 2013). These differences in capping may result in some differences in the recognition pattern prerequisite and response from the host, thus eliciting unique proteomic phenotypes.

The C-type mannose receptor 2 (MRC2) and C-type lectin domain family 11 (CLEC11A) were only expressed by the LAM-treated macrophages. The C-type lectin superfamily of proteins are part of the LAM recognition pattern expressed on the host cell membrane and are important sero-biomarkers associated with innate immunity (Alagarasu *et al.* 2007). This suggests that expression of these proteins is LAM-induced. As discussed with the *M. smeg* infections, the MRC2 and its homolog ENDO-180 (urokinase plasminogen activator receptor-associated protein or uPARAP) act as the main route for the non-phagocytic uptake of collagen in cells for degradation in lysosomal compartments (Paracuellos *et al.* 2015). Like MMP-2 and -9, they contain the fibronectin-II repeats that bind collagen and gelatin. The overexpression of MRC2 or ENDO-180 caused the internalisation of labelled collagen, which was at a slower rate to that of gelatin. The authors also concluded that the collagen binding and release from this complex is neither pH- or calcium-dependent. Although others have reported that LAM induces an increase in MMP-1 and -9 genes and MMP-9 activity (Chang *et al*., 1996), however the induced expression of MRC2 observed in our study offers an alternate mechanism of gelatin and/or collagen degradation.

Although MMP-9 is important for recruiting immune cells to the granuloma and for its maturation, MMP-9 knock-out mice infected with *M. tb* still resulted in albeit smaller

granulomas and less macrophages to the site of infection (Elkington *et al.* 2011a). Therefore, remodelling of the basal membrane and migration of immune cells may not be triggered by and solely dependent on MMP-9. This also suggests that the extracellular degradome of MMPs especially from collagen or gelatin may influence the phenotype that causes progression of disease to dissemination or cavitation. The LAM-treated macrophages depict a phenotype that implies preservation of collagen and/or gelatin breakdown hence the cathepsins which can breakdown ECM components were also not dysregulated. This further suggests that cathepsins regulate MMPs by activating them as discussed for the *M. smeg* infection (section 4.6.1).

The immune response displayed by the treated macrophages supports that the contact between the bacterial cell-wall and host cell membrane triggers the initial immune response. In addition to that, LAM caused GO protein enrichment of the lysosome cellular compartment in dysregulated proteins of the lysate and the secretion of GTPases/RAB system including the late RAB7A that are crucial for phagolysosomal fusion and maturation. Thus, the aforementioned suggests that an increase in the levels and activity of MMP-9 may not be fundamental to granuloma formation and maturation, and phagolysosomal fusion. This endorses developing specific MMP-9 inhibitors as potential therapeutic drugs to alleviate chronic ECM degradation associated with cavity formation.

5.5.2 LAM filtration in urine and its induction of proteinuria

The detection of LAM in the urine of TB patients has been documented with research focused on development of diagnostic tools; however, the mechanism by which it is processed and excreted in the kidney remains to be elucidated. The presence of *M. tb* DNA in half of LAM-positive patients co-infected with HIV has been reported (Wood *et al.* 2015). Although there are several mechanisms that have been postulated which Cox and colleagues (Cox *et al.* 2015) have reviewed none has been fully investigated and accepted. These include 1) direct entry of intact *M. tb* through the glomerular basal membrane (GBM) from the bloodstream but was considered unlikely because of its size; 2) entry of LAM on its own or in an immune-complexed form but the latter would also be too large to cross the membrane; 3) finally the authors concluded that whilst GBM leakage and proteinuria would

allow passage of large molecules, their data demonstrated glomerulopathy in only 2 of the 5 patients that were LAM-positive without renal TB, and 1 in 3 of LAM-negative in TB patients, whilst another study found only a weak correlation between LAM-positivity and proteinuria (Cox *et al.* 2015). Thus, the likelihood of circulating LAM crossing the membrane is a possibility that remains to be explored. Importantly, co-infection with HIV (with CD4 less than 100 cells/mm^3) enhanced the sensitivity of the urinary LAM diagnostic performance (Lawn and Gupta-Wright 2016;Pandie *et al.* 2016). Also, urine LAM detection in children has also been unsuccessful and according to Lawn and Gupta-Wright this is due to the paucibacillary nature of *M. tb* and inability to disseminate (Lawn and Gupta-Wright 2016).

It is vital to note that patients co-infected with HIV rarely present with cavitary TB (Munthali *et al.* 2014) and the reduced tissue damage is associated with decreased concentrations of MMPs (Walker *et al.* 2012). In these patients and HIV negative controls MMP-1 was upregulated, however the concentration of TIMP-1 was lower in the latter (Elkington *et al.* 2005a;Walker *et al.* 2012). Children rarely form cavities upon *M. tb* infection. Interestingly, like the HIV-positive adults co-infected with TB, the MMPs are upregulated, including MMP-1, MMP-7 and MMP-8 but the TIMPs (TIMP-1 and TIMP-3) are also elevated (Pavan Kumar *et al.* 2013). As previously mentioned, dissemination and cavitation are associated with an upregulation and increased activity of MMP-1.

The current study postulates that 1) LAM recognition and binding is through the interaction with MRC2 in conjunction with MMP-9, and/or uPA related receptors. 2) Thus, the number of macrophages and expression of MRC2 on the surface affects the concentration of LAM binding and circulating in the plasma. 3) The formation of extracellular traps causes ejection of chromatin into the secretome (plasma) facilitating the transport of LAM across the GBM through exosomes. 4) The inhibition of MMPs by binding to the catalytic Zn-binding site reduces the formation of aggNETS which may trap the LAM preventing its transportation across the GBM. Therefore, in patients who are HIV +ve and have lower CD4 cell counts, reduced MRC2 cell-surface expression may result in lower concentrations of bound LAM. The LAM still circulating in the blood may then be delivered and transported across the GBM through binding to chromatin via electrostatic interactions. This complex is then transported across the GBM via exosomes through fusion to the GTPases. Since formation of aggNETS was abolished by treatment with EDTA but not serine protease inhibitors (Schauer *et al.*

2014), inhibition of MMP activity by TIMPs could result in decreased aggregation that traps the LAM from being transported via the chromatin. Thus, patients who are HIV +ve and have high cell density may have lower urine concentrations of LAM because of aggNETs trapping the LAM and/or higher concentrations of MRC2-bound LAM. The paucibacillary phenotype in children could be due to the extracellular traps and aggNETS causing less transportation of bacteria and LAM across the GBM.

The glomerular filtration barrier is made up of three layers including the endothelial cells, podocytes and the glomerular basal membrane (GBM). They are important in conferring selectivity to permeability of the membrane. The GBM is the ECM component that lies between the endothelial cells and podocytes and is initially synthesised by the endothelial cells and podocytes. The plasma that flows through the capillaries reaches the GBM through the highly fenestrated endothelial layer (Miner 2011;Miner 2012). The absence of increased MMP activity suggests that proteinuria may not be due to breakdown of the GBM, thus another mechanism may be more relevant.

As mentioned earlier the significant overexpression and secretion of TIMP-1 is essential given its role in binding and stabilising the Hx domain. The intrarenal infusion of Hx domain into rats causes glomerular damage and proteinuria, which are both abolished by serine protease inhibitors rather than collagenase inhibitors (Bakker *et al.* 2005). That study suggested that this was partly due to the loss of glomerular ectoapyrase and sialoglycoproteins. Transgenic mice overexpressing heparanase resulted in decreased concentrations of heparan sulfate and presented minimal albuminuria which was however significantly different to the controls (van den Hoven *et al.* 2008). Removing the GBM glycosaminoglycans with bacterial glycosaminoglycan degrading enzymes has been associated with the presence of albumin and ferritin in urine (Kanwar *et al.* 1980). The dysregulated secretome from our *M. smeg* infections depicted enrichment of glycosaminoglycans, chondroitin sufate metabolic process and chondroitin sulfate proteoglycan metabolic process. Additionally, protein groups overexpressed by LAM-stimulated macrophages depicted phosphatase activity and GO enrichment in global-SCX-fraction. These imply that LAM alone, that is, without other *Mycobacterial* factors, might cause proteinuria and renal damage through the loss of negative charge derived from

phosphates. It is also plausible that during infection with *M. tb*, increased body temperatures cause the destabilisation of the MMP-9 leading to accumulation of the Hx domain in the plasma. This in turn could cause proteinuria when in direct contact with the kidney glomeruli through the loss of glomeruli glycoaminoglycans. This suggests that MMP substrate recognition and cleavage depends on the form of MMP. The specific targeting of their potential serine protease activity through inhibitors targeting the Hx domain rather than their collagenase or gelatinase activity could minimise proteinuria and the GBM filtration of LAM.

5.5.3 Pathways enriched by LAM stimulation

The LAM induced the GO enrichment in ubiquitin-specific protease activity molecular functions which is an essential post-translational modification (PTM) that regulates various biological processes including pathways that are involved in pathogenesis of *Mycobacterial* infections. Ubiquitination has been shown to be a vital regulatory PTM in the lysosomal localisation and macrophage apoptosis of *Mycobacteria*. Alonso and colleagues show that peptides derived from ubiquitin localise to the lysosome and are microbicidal against *Mycobaterium tuberculosis* and *smegmatis*. Transportation of these peptides to the lysosome was via multivesicular bodies (MVBs) and exert their effect by forming pores that cause permeability of the *Mycobacterial* cell wall and vulnerability to other antimicrobial molecules. This effect is enhanced by autophagy and is essential in early infection (Alonso *et al.* 2007). The implication of the antimicrobial properties of these peptides was attributed to histones and the ribosomal proteins L30, S30 and S19. Our data show GO enrichment of the lysosome cellular compartment and the dysregulation of the ribosomal proteins including RPL27A, RPL7, RPS8 amongst others in both secretome and intracellular protein. Interestingly these ribosomal proteins are predicted to form an interaction network with porin proteins (see Figure 5-12) in dysregulated intracellular proteins. It is possible that LAM alone causes ubiquitination generating ubiquitin-derived peptides that allow survival of the macrophage and bacteria.

Most of these dysregulated proteins were predicted to form protein-protein interactions, in addition to being classified under the GO biological process ‘symbiosis process’. This

suggests that LAM induces phagolysosomal fusion but generates ubiquitin-derived peptides that culminates in escape and survival of the bacteria within the macrophages. The uniquely identified apoptosis regulating proteins BAK-1 and caspase-3 in the LAM-treated intracellular proteome are essential and in the same sample caspase-3 and DNA fragmentation factor subunit alpha (DFFA) were predicted to form protein-protein interactions. Caspase-3 causes the activation of DNA fragmentation factor (DFF) inducing the fragmentation of DNA during apoptosis by acting on DFFA (Wolf *et al.* 1999). The activation of ubiquitin-specific protease activity and 14-3-3 protein domain in the LAM treated macrophages suggests that the balance between pro-apoptosis and anti-apoptosis is mediated by ubiquitination and phosphorylation by kinases. Thus, the host may be protecting itself from the detrimental effects of necrosis by inducing a Bak and caspase-3 dependent cell death.

The Trk receptor signalling pathway is important to note and offers another mechanism by which the host is exploited for survival of the bacteria. Tropomyosin-related kinase (Trk) receptor tyrosine kinase are transmembrane glycoproteins with an extracellular domain containing multiple glycosylation sites, more specifically sialylation sites. *Trypanosoma cruzi* (*T. cruzi*) the causative agent of Chagasi disease is well-documented for its ability to exploit and evade the host system by transfer of the hosts sialic acid to the parasites mucin-like molecules of its cell surface and between the hosts glycoconjugates (Freire-de-Lima *et al.* 2016;Freire-de-Lima *et al.* 2015). This is executed by the *trans*-sialidase (also known as parasite-derived neurotrophic factor) on the cell surface of *T. cruzi*. This enzyme interacts and activates TrkA and TrkC utilising TrkC for entry into the host (Weinkauf *et al.* 2011). This suggests that during *M. tb* infection LAM may be modified through interaction of Trk receptors and *Mycobacterial* factors that modify the cell-wall sugars resulting in the intracellular survival of *M. tb*. Methylthio-D-xylose (MTX) is a motif that's been identified on the mannoside caps of LAM and is substituted via α-(1→4)-linkage (Angala *et al.* 2017). It is postulated to have a role in the host-*Mycobacteria* interaction and in conferring the antioxidative properties of LAM. Therefore, LAM can be modified to facilitate its survival in the host by redox- and glycosylation-dependent mechanisms.

5.6 Conclusions

MMPs have been implicated in the pathophysiology of TB cavitation by causing irreparable tissue damage. The expression of MMP-9 is associated with granuloma formation and maturation, whilst the degradation of collagen is correlated with increased MMP-1 activity. These events have been documented to cause cavitation and dissemination which culminate in transmission (Elkington *et al.* 2005a;Elkington *et al.* 2005b;Hrabec *et al.* 2002;Kubler *et al.* 2015;Salgame 2011). Thus, MMPs are possible drug targets in combating tissue damage associated with cavitation but the major challenges include the similarity in their active site pockets, they perform important functions besides ECM degradation and remodelling, and their role as protective or detrimental agents has not been conclusively defined. Studying their upstream and downstream effectors in conjunction with their activity is essential and is the basis of this study. The avirulent *M. smegmatis* was used as the *Mycobacterial* model for monitoring the THP-1 macrophage response upon infection. An indirect but valuable comparison was carried out with the virulent H37Rv cell wall component LAM.

The major findings of the activity assays were that *M. smeg* caused a general increase in the activity of MMP-9 and a decrease in MMP-1 activity. LAM did not cause any increase in the expression and activity of MMPs. This validates that MMP-1 activity is deliberately and specifically increased by *M. tb* (Elkington *et al.* 2005a;Elkington *et al.* 2005b;Hrabec *et al.* 2002;Kubler *et al.* 2015;Salgame 2011). In addition to LAM, other *Mycobacterial* virulent factors are responsible for inducing the upregulation and increase in the activity of MMP-1 and MMP-9. Similarly, *M. smeg* and LAM on its own, were able to activate an immune response. The C-type lectin superfamily of proteins are part of the LAM recognition pattern expressed on the host cell membrane and are important sero-biomarkers associated with innate immunity (Alagarasu *et al.* 2007). Interestingly, C-type mannose receptor 2 (MRC2) and C-type lectin domain family 11 (CLEC11A) were only expressed by the LAM-treated macrophages. It is possible that CLEC11A and MRC2 are specifically expressed for recognition of the *M. tb* cell wall rather than *M. smeg* however the signal does not induce dysregulation of MMPs. MRC2 and its homolog ENDO-180 (urokinase plasminogen activator receptor-associated protein or uPARAP) act as the main route for the non-phagocytic uptake of collagen in cells for degradation in lysosomal compartments (Paracuellos *et al.* 2015).

Thus, MRC2 offers an alternate mechanism of gelatin and/or collagen degradation suggesting that this may be an initial response that facilitates migration of immune cells to the site of infection.

Survival of *M. tb* inside macrophages may be facilitated by two other mechanisms namely, ubiquitination and through interaction of Trk receptors and *Mycobacterial* factors. Trk receptors could be interacting with LAM, modifying the sugars of the *M. tb* cell-wall component such as the methylthio-D-xylose (MTX) motif that has been identified on the mannoside caps of LAM to be substituted via α-(1→4)-linkage (Angala *et al.* 2017). This substitution is postulated to have a role in the host-*Mycobacteria* interaction and in conferring the antioxidative properties of LAM. Therefore, LAM can be modified to facilitate *M. tb* survival in the host by redox- and glycosylation-dependent mechanisms.

Ubiquitin-derived peptides localise to the lysosome where they elicit microbicidal activity against *M. tb* and *M. smeg* by forming pores that increase the permeability of the bacteria (Alonso *et al.* 2007). This is important in early infection and is facilitated by histones, the ribosomal proteins L30, S30 and S19. Both LAM and *M. smeg* caused the dysregulation of histone H4 in the secretome, and ribosomal L30 was upregulated by the *M. smeg* infection. Thus, *M. tb* may circumvent lysosomal killing by upregulating other ribosomal proteins rather than the aforementioned.

Analysis of the time point harvests by zymography suggested that there is a switch in the proteolytic repertoire of the macrophages between the 6- and 18-hour time points to one that causes a decrease in the fold difference between infected and uninfected secretome. It is also possible that this leads to generation of the same degradation products between infected and uninfected macrophages minimising the positive loop mechanism that leads to chronic expression and activity of MMPs. Further investigation needs to be done to conclude. The postulated upstream factors that regulate MMPs during infection were not enhanced by LAM treatment somewhat validating their role in activating and/or inactivating MMPs. Expression of MMP-9 in *M. smeg* infected macrophages could be regulated by IL-1β in a COX-prostaglandin synthase-dependent manner, and also via alternative splicing which was also indicated by western blotting. Its secretion was possibly regulated and facilitated by exosomal compartmentalisation, TIMP-1 and cytoskeletal-related proteins including tubulins, actins and adenylyl cyclase-associated protein 1. Finally, the activation of MMP-9

may be regulated in the secretome by downregulating cathepsins and via redox control by secreting PDI, HMGB1 and ribonuclease T2. Also, by scavenging reactive oxygen species through the superoxide dismutase and nucleotide de novo biosynthesis II pathway in the lysate.

The current study suggests that the potential serine protease activity of MMP-9 may have implications for drug design. For example, inhibiting its serine protease activity may lead to decreased degradation of pro-inflammatory cytokines, whilst chelating the active site zinc abolishes the formation of aggNETS only but does not prevent the degradation of the pro-inflammatory cytokines. Reduced formation of aggNETS which may trap LAM preventing its transportation across the GBM, this could have potential implications for urine-LAM detection kits.

References

Abe, Y., Nakamura, M., Oshika, Y., Hatanaka, H., Tokunaga, T., Ohkubo, Y., Hashizume, T., Suzuki, K. & Fujino, T. 2001. Serum levels of vascular endothelial growth factor and cavity formation in active pulmonary tuberculosis. *Respiration,* 68**,** 496-500.

Abromaitis, S. & Stephens, R. S. 2009. Attachment and entry of Chlamydia have distinct requirements for host protein disulfide isomerase. *PLoS Pathog,* 5**,** e1000357.

Aebersold, R. & Mann, M. 2003. Mass spectrometry-based proteomics. *Nature,* 422**,** 198-207.

Aebersold, R. & Mann, M. 2016. Mass-spectrometric exploration of proteome structure and function. *Nature,* 537**,** 347.

Ahidjo, B. A., Maiga, M. C., Ihms, E. A., Maiga, M., Ordonez, A. A., Cheung, L. S., Beck, S., Andrade, B. B., Jain, S. & Bishai, W. R. 2016. The antifibrotic drug pirfenidone promotes pulmonary cavitation and drug resistance in a mouse model of chronic tuberculosis. *JCI Insight,* 1**,** e86017.

Alagarasu, K., Selvaraj, P., Swaminathan, S., Raghavan, S., Narendran, G. & Narayanan, P. R. 2007. Mannose binding lectin gene variants and susceptibility to tuberculosis in HIV-1 infected patients of South India. *Tuberculosis,* 87**,** 535-543.

Alatas, F., Alatas, ö., Metintas, M., özarslan, A., Erginel, S. & Yildirim, H. 2004. Vascular Endothelial Growth Factor Levels in Active Pulmonary Tuberculosis. *Chest,* 125**,** 2156-2159.

Ali Khan, H. & Mutus, B. 2014. Protein disulfide isomerase a multifunctional protein with multiple physiological roles. *Frontiers in Chemistry,* 2.

Alonso, S., Pethe, K., Russell, D. G. & Purdy, G. E. 2007. Lysosomal killing of Mycobacterium mediated by ubiquitin-derived peptides is enhanced by autophagy. *Proc Natl Acad Sci U S A,* 104**,** 6031-6.

Altaf, M., Miller, C. H., Bellows, D. S. & O'Toole, R. 2010. Evaluation of the Mycobacterium smegmatis and BCG models for the discovery of Mycobacterium tuberculosis inhibitors. *Tuberculosis (Edinb),* 90**,** 333-7.

Angala, S. K., McNeil, M. R., Shi, L., Joe, M., Pham, H., Zuberogoitia, S., Nigou, J., Boot, C. M., Lowary, T. L., Gilleron, M. & Jackson, M. 2017. Biosynthesis of the Methylthioxylose Capping Motif of Lipoarabinomannan in Mycobacterium tuberculosis. *ACS Chem Biol,* 12**,** 682-691.

Antoine, D. J., Harris, H. E., Andersson, U., Tracey, K. J. & Bianchi, M. E. 2014. A systematic nomenclature for the redox states of high mobility group box (HMGB) proteins. *Mol Med,* 20**,** 135-7.

Appelmelk, B. J., den Dunnen, J., Driessen, N. N., Ummels, R., Pak, M., Nigou, J., Larrouy-Maumus, G., Gurcha, S. S., Movahedzadeh, F., Geurtsen, J., Brown, E. J., Smeets, M. M. E., Besra, G. S., Willemsen, P. T. J., Lowary, T. L., van Kooyk, Y., Maaskant, J. J., Stoker, N. G., van der Ley, P., Puzo, G., Vandenbroucke-Grauls, C. M. J. E., Wieland, C. W., van der Poll, T., Geijtenbeek, T. B. H., van der Sar, A. M. & Bitter, W. 2008. The mannose cap of mycobacterial

lipoarabinomannan does not dominate the Mycobacterium-host interaction. *Cellular Microbiology,* 10**,** 930-944.

Ashley, S. L., Pretto, C. D., Stier, M. T., Kadiyala, P., Castro-Jorge, L., Hsu, T.-H., Doherty, R., Carnahan, K. E., Castro, M. G., Lowenstein, P. R. & Spindler, K. R. 2017. Matrix Metalloproteinase Activity in Infections by an Encephalitic Virus, Mouse Adenovirus Type 1. *Journal of Virology,* 91.

Atay, S. & Godwin, A. K. 2014. Tumor-derived exosomes: A message delivery system for tumor progression. *Commun Integr Biol,* 7**,** e28231.

Atta, S., Kassem, A., Elhadidi, A. & El Esawy, H. 2015. The diagnostic value of adenosine deaminase activity in pulmonary tuberculosis: Comparison between sputum and serum. *Egyptian Journal of Chest Diseases and Tuberculosis,* 64**,** 103-107.

Baba, K., Hoosen, A. A., Langeland, N. & Dyrhol-Riise, A. M. 2008. Adenosine deaminase activity is a sensitive marker for the diagnosis of tuberculous pleuritis in patients with very low CD4 counts. *PLoS One,* 3**,** e2788.

Bakker, W. W., Borghuis, T., Harmsen, M. C., van den Berg, A., Kema, I. P., Niezen, K. E. & Kapojos, J. J. 2005. Protease activity of plasma hemopexin. *Kidney Int,* 68**,** 603-10.

Banki, K., Hutter, E., Colombo, E., Gonchoroff, N. J. & Perl, A. 1996. Glutathione Levels and Sensitivity to Apoptosis Are Regulated by Changes in Transaldolase Expression. *Journal of Biological Chemistry,* 271**,** 32994-33001.

Bannikov, G. A., Karelina, T. V., Collier, I. E., Marmer, B. L. & Goldberg, G. I. 2002. Substrate binding of gelatinase B induces its enzymatic activity in the presence of intact propeptide. *J Biol Chem,* 277**,** 16022-7.

Beatty, W. L., Rhoades, E. R., Hsu, D. K., Liu, F. T. & Russell, D. G. 2002. Association of a macrophage galactoside-binding protein with Mycobacterium-containing phagosomes. *Cell Microbiol,* 4**,** 167-76.

Benjamin, M. M. & Khalil, R. A. 2012. Matrix Metalloproteinase Inhibitors as Investigative Tools in the Pathogenesis and Management of Vascular Disease. *Exs,* 103**,** 209-279.

Bildyug, N. 2016. Matrix metalloproteinases: an emerging role in regulation of actin microfilament system. *Biomol Concepts,* 7**,** 321-329.

Boon, L., Ugarte-Berzal, E., Vandooren, J. & Opdenakker, G. 2016. Glycosylation of matrix metalloproteases and tissue inhibitors: present state, challenges and opportunities. *Biochemical Journal,* 473**,** 1471-1482.

Bouchet, S. & Bauvois, B. 2014. Neutrophil Gelatinase-Associated Lipocalin (NGAL), Pro-Matrix Metalloproteinase-9 (pro-MMP-9) and Their Complex Pro-MMP-9/NGAL in Leukaemias. *Cancers,* 6**,** 796-812.

Bracher, M., Bezuidenhout, D., Lutolf, M. P., Franz, T., Sun, M., Zilla, P. & Davies, N. H. 2013. Cell specific ingrowth hydrogels. *Biomaterials,* 34**,** 6797-803.

Burg-Roderfeld, M., Roderfeld, M., Wagner, S., Henkel, C., Grotzinger, J. & Roeb, E. 2007. MMP-9-hemopexin domain hampers adhesion and migration of colorectal cancer cells. *Int J Oncol,* 30**,** 985-92.

Burgess, J. K., Ge, Q., Poniris, M. H., Boustany, S., Twigg, S. M., Black, J. L. & Johnson, P. R. 2006. Connective tissue growth factor and vascular endothelial growth factor from airway smooth muscle interact with the extracellular matrix. *Am J Physiol Lung Cell Mol Physiol,* 290**,** L153-61.

Cao, J., Rehemtulla, A., Pavlaki, M., Kozarekar, P. & Chiarelli, C. 2005. Furin directly cleaves proMMP-2 in the trans-Golgi network resulting in a nonfunctioning proteinase. *J Biol Chem,* 280**,** 10974-80.

Carroll, C. W. & Straight, A. F. 2007. Centromeric chromatin gets loaded. *The Journal of cell biology,* 176**,** 735-736.

Case, E. D. R. & Samuel, J. E. 2016. Contrasting Lifestyles Within the Host Cell. *Microbiology spectrum,* 4**,** 10.1128/microbiolspec.VMBF-0014-2015.

Chang, J. C., Wysocki, A., Tchou-Wong, K. M., Moskowitz, N., Zhang, Y. & Rom, W. N. 1996. Effect of Mycobacterium tuberculosis and its components on macrophages and the release of matrix metalloproteinases. *Thorax,* 51**,** 306-11.

Chen, C. K. M., Chan, N.-L. & Wang, A. H. J. 2011. The many blades of the β-propeller proteins: conserved but versatile. *Trends in Biochemical Sciences,* 36**,** 553-561.

Chen, H. Y., Weng, I. C., Hong, M. H. & Liu, F. T. 2014. Galectins as bacterial sensors in the host innate response. *Curr Opin Microbiol,* 17**,** 75-81.

Chennathukuzhi, V. M., Kurihara, Y., Bray, J. D., Yang, J. & Hecht, N. B. 2001. Altering the GTP binding site of the DNA/RNA-binding protein, Translin/TB-RBP, decreases RNA binding and may create a dominant negative phenotype. *Nucleic Acids Res,* 29**,** 4433-40.

Chintala, S. K., Sawaya, R., Aggarwal, B. B., Majumder, S., Giri, D. K., Kyritsis, A. P., Gokaslan, Z. L. & Rao, J. S. 1998. Induction of matrix metalloproteinase-9 requires a polymerized actin cytoskeleton in human malignant glioma cells. *J Biol Chem,* 273**,** 13545-51.

Christensen, J. & Shastri, V. P. 2015. Matrix-metalloproteinase-9 is cleaved and activated by Cathepsin K. *BMC Research Notes,* 8**,** 322.

Chung, C., Dinakarpandian, D., Yoshida, N., Lauer-Fields, J. L., Fields, G. B., Visse, R. & Nigasse, H. 2004. Collagenase unwinds triple-helical collagen prior to peptide bond hydrolysis. *The EMBO Journal* 23**,** 3020.

Chung, C., Mader, C., Protiva, P., Schmitz, J., Koleske, A., Crawford, S. & Gorelick, F. 2010. The Vacuolar-ATPase (v-ATPase) Confers Invasive Properties to Human Pancreatic Cancer by Modulating Mmps. *Pancreas,* 39**,** 1315-1315.

Chung, C., Mader, C. C., Schmitz, J. C., Atladottir, J., Fitchev, P., Cornwell, M. L., Koleske, A. J., Crawford, S. E. & Gorelick, F. 2011. The vacuolar-ATPase modulates matrix metalloproteinase isoforms in human pancreatic cancer. *Laboratory Investigation,* 91**,** 732-743.

Converse, P. J., Dannenberg, A. M., Jr., Estep, J. E., Sugisaki, K., Abe, Y., Schofield, B. H. & Pitt, M. L. 1996. Cavitary tuberculosis produced in rabbits by aerosolized virulent tubercle bacilli. *Infect Immun,* 64**,** 4776-87.

Cox, J., Hein, M. Y., Luber, C. A., Paron, I., Nagaraj, N. & Mann, M. 2014. Accurate proteome-wide label-free quantification by delayed normalization and maximal peptide ratio extraction, termed MaxLFQ. *Mol Cell Proteomics,* 13**,** 2513-26.

Cox, J. A., Lukande, R. L., Kalungi, S., Van Marck, E., Van de Vijver, K., Kambugu, A., Nelson, A. M., Colebunders, R. & Manabe, Y. C. 2015. Is Urinary Lipoarabinomannan the Result of Renal Tuberculosis? Assessment of the Renal Histology in an Autopsy Cohort of Ugandan HIV-Infected Adults. *PLoS One,* 10**,** e0123323.

Crabbe, T., Kelly, S. M. & Price, N. C. 1996. An analysis of the conformational changes that accompany the activation and inhibition of gelatinase A. *FEBS Lett,* 380**,** 53-7.

Dartois, V. 2014. The path of anti-tuberculosis drugs: from blood to lesions to mycobacterial cells. 12**,** 159.

Davidson, J. M. 1990. BIOCHEMISTRY AND TURNOVER OF LUNG INTERSTITIUM. *European Respiratory Journal,* 3**,** 1048-1068.

Davis, J. M. & Ramakrishnan, L. 2009. The Role of the Granuloma in Expansion and Dissemination of Early Tuberculous Infection. *Cell,* 136**,** 37-49.

Depraetere, S., Vanhaesebroeck, B., Fiers, W., Willems, J. & Joniau, M. 1995. Polar agents with differentiation inducing capacity potentiate tumor necrosis factor-mediated cytotoxicity in human myeloid cell lines. *J Leukoc Biol,* 57**,** 141-51.

Dheda, K., Schwander, S. K., Zhu, B., van Zyl-Smit, R. N. & Zhang, Y. 2010. The immunology of tuberculosis: from bench to bedside. *Respirology,* 15**,** 433-50.

Di Liegro, C. M., Schiera, G. & Di Liegro, I. 2017. Extracellular Vesicle-Associated RNA as a Carrier of Epigenetic Information. *Genes (Basel),* 8.

Domon, B. & Aebersold, R. 2010. Options and considerations when selecting a quantitative proteomics strategy. *Nat Biotechnol,* 28**,** 710-21.

Duellman, T., Burnett, J. & Yang, J. 2015. Functional roles of N-linked glycosylation of human matrix metalloproteinase 9. *Traffic (Copenhagen, Denmark),* 16**,** 1108-1126.

Duncan, M. E., Richardson, J. P., Murray, G. I., Melvin, W. T. & Fothergill, J. E. 1998. Human matrix metalloproteinase-9: activation by limited trypsin treatment and generation of monoclonal antibodies specific for the activated form. *Eur J Biochem,* 258**,** 37-43.

Eckhard, U., Huesgen, P. F., Brandstetter, H. & Overall, C. M. 2014. Proteomic protease specificity profiling of clostridial collagenases reveals their intrinsic nature as dedicated degraders of collagen()(). *Journal of Proteomics,* 100**,** 102-114.

Ecroyd, H., Thorn, David C., Liu, Y. & Carver, John A. 2010. The dissociated form of κ-casein is the precursor to its amyloid fibril formation. *Biochemical Journal,* 429**,** 251-260.

Eliuk, S. & Makarov, A. 2015. Evolution of Orbitrap Mass Spectrometry Instrumentation. *Annu Rev Anal Chem (Palo Alto Calif),* 8**,** 61-80.

Elkington, P., Shiomi, T., Breen, R., Nuttall, R. K., Ugarte-Gil, C. A., Walker, N. F., Saraiva, L., Pedersen, B., Mauri, F., Lipman, M., Edwards, D. R., Robertson, B. D., D'Armiento, J. & Friedland, J. S. 2011a. MMP-1 drives immunopathology in human tuberculosis and transgenic mice. *J Clin Invest,* 121**,** 1827-33.

Elkington, P. T., Green, J. A., Emerson, J. E., Lopez-Pascua, L. D., Boyle, J. J., O'Kane, C. M. & Friedland, J. S. 2007. Synergistic up-regulation of epithelial cell matrix metalloproteinase-9 secretion in tuberculosis. *Am J Respir Cell Mol Biol,* 37**,** 431-7.

Elkington, P. T., Nuttall, R. K., Boyle, J. J., O'Kane, C. M., Horncastle, D. E., Edwards, D. R. & Friedland, J. S. 2005a. Mycobacterium tuberculosis, but not vaccine BCG, specifically upregulates matrix metalloproteinase-1. *Am J Respir Crit Care Med,* 172**,** 1596-604.

Elkington, P. T., Ugarte-Gil, C. A. & Friedland, J. S. 2011b. Matrix metalloproteinases in tuberculosis. *Eur Respir J,* 38**,** 456-64.

Elkington, P. T. G., O'Kane, C. M. & Friedland, J. S. 2005b. The paradox of matrix metalloproteinases in infectious disease. *Clinical and Experimental Immunology,* 142**,** 12-20.

Elkins, P. A., Ho, Y. S., Smith, W. W., Janson, C. A., D'Alessio, K. J., McQueney, M. S., Cummings, M. D. & Romanic, A. M. 2002. Structure of the C-terminally truncated human ProMMP9, a gelatin-binding matrix metalloproteinase. *Acta Crystallogr D Biol Crystallogr,* 58**,** 1182-92.

Feeley, E. M., Pilla-Moffett, D. M., Zwack, E. E., Piro, A. S., Finethy, R., Kolb, J. P., Martinez, J., Brodsky, I. E. & Coers, J. 2017. Galectin-3 directs antimicrobial guanylate binding proteins to vacuoles furnished with bacterial secretion systems. *Proceedings of the National Academy of Sciences,* 114**,** E1698-E1706.

Fingleton, B. 2008. MMPs as therapeutic targets--still a viable option? *Semin Cell Dev Biol,* 19**,** 61-8.

Flannagan, R. S., Cosio, G. & Grinstein, S. 2009. Antimicrobial mechanisms of phagocytes and bacterial evasion strategies. *Nat Rev Microbiol,* 7**,** 355-66.

Flo, T. H., Smith, K. D., Sato, S., Rodriguez, D. J., Holmes, M. A., Strong, R. K., Akira, S. & Aderem, A. 2004. Lipocalin 2 mediates an innate immune response to bacterial infection by sequestrating iron. *Nature,* 432**,** 917-921.

Freire-de-Lima, L., da Fonseca, L. M., da Silva, V. A., da Costa, K. M., Morrot, A., Freire-de-Lima, C. G., Previato, J. O. & Mendonca-Previato, L. 2016. Modulation of Cell Sialoglycophenotype: A Stylish Mechanism Adopted by Trypanosoma cruzi to Ensure Its Persistence in the Infected Host. *Front Microbiol,* 7**,** 698.

Freire-de-Lima, L., Fonseca, L. M., Oeltmann, T., Mendonca-Previato, L. & Previato, J. O. 2015. The trans-sialidase, the major Trypanosoma cruzi virulence factor: Three decades of studies. *Glycobiology,* 25**,** 1142-9.

Friedland, J. S., Shaw, T. C., Price, N. M. & Dayer, J. M. 2002. Differential regulation of MMP-1/9 and TIMP-1 secretion in human monocytic cells in response to Mycobacterium tuberculosis. *Matrix Biol,* 21**,** 103-10.

Friggeri, A., Yang, Y., Banerjee, S., Park, Y.-J., Liu, G. & Abraham, E. 2010. HMGB1 inhibits macrophage activity in efferocytosis through binding to the alphavbeta3-integrin. *American journal of physiology. Cell physiology,* 299**,** C1267-C1276.

Fry, S. A., Van den Steen, P. E., Royle, L., Wormald, M. R., Leathem, A. J., Opdenakker, G., McDonnell, J. M., Dwek, R. A. & Rudd, P. M. 2006. Cancer-associated glycoforms of gelatinase B exhibit a decreased level of binding to galectin-3. *Biochemistry,* 45**,** 15249-58.

Fu, X., Kassim, S. Y., Parks, W. C. & Heinecke, J. W. 2001. Hypochlorous Acid Oxygenates the Cysteine Switch Domain of Pro-matrilysin (MMP-7): A MECHANISM FOR MATRIX METALLOPROTEINASE ACTIVATION AND ATHEROSCLEROTIC PLAQUE RUPTURE BY MYELOPEROXIDASE. *Journal of Biological Chemistry,* 276**,** 41279-41287.

Fukuda, T., Matsumura, T., Ato, M., Hamasaki, M., Nishiuchi, Y., Murakami, Y., Maeda, Y., Yoshimori, T., Matsumoto, S., Kobayashi, K., Kinoshita, T. & Morita, Y. S. 2013. Critical Roles for Lipomannan and Lipoarabinomannan in Cell Wall Integrity of Mycobacteria and Pathogenesis of Tuberculosis. *mBio,* 4**,** e00472-12.

Galazka, G., Windsor, L. J., Birkedal-Hansen, H. & Engler, J. A. 1996. APMA (4-aminophenylmercuric acetate) activation of stromelysin-1 involves protein interactions in addition to those with cysteine-75 in the propeptide. *Biochemistry,* 35**,** 11221-7.

Gallina, A., Hanley, T. M., Mandel, R., Trahey, M., Broder, C. C., Viglianti, G. A. & Ryser, H. J. 2002. Inhibitors of protein-disulfide isomerase prevent cleavage of disulfide bonds in receptor-bound glycoprotein 120 and prevent HIV-1 entry. *J Biol Chem,* 277**,** 50579-88.

Gao, N., Huang, J., He, W., Zhu, M., Kamm, K. E. & Stull, J. T. 2013. Signaling through myosin light chain kinase in smooth muscles. *J Biol Chem,* 288**,** 7596-605.

Garamszegi, N., Garamszegi, S. P. & Scully, S. P. 2012. Matrix metalloproteinase-1 contribution to sarcoma cell invasion. *J Cell Mol Med,* 16**,** 1331-41.

Gogly, B., Groult, N., Hornebeck, W., Godeau, G. & Pellat, B. 1998. Collagen Zymography as a Sensitive and Specific Technique for the Determination of Subpicogram Levels of Interstitial Collagenase. *Analytical Biochemistry,* 255**,** 211-216.

Goldberg, G. I., Strongin, A., Collier, I. E., Genrich, L. T. & Marmer, B. L. 1992. Interaction of 92-kDa type IV collagenase with the tissue inhibitor of metalloproteinases prevents dimerization, complex formation with interstitial collagenase, and activation of the proenzyme with stromelysin. *J Biol Chem,* 267**,** 4583-91.

Gross, J. & Lapiere, C. M. 1962. Collagenolytic activity in amphibian tissues: a tissue culture assay. *Proc Natl Acad Sci U S A,* 48**,** 1014-22.

Gu, Z., Kaul, M., Yan, B., Kridel, S. J., Cui, J., Strongin, A., Smith, J. W., Liddington, R. C. & Lipton, S. A. 2002. S-Nitrosylation of Matrix Metalloproteinases: Signaling Pathway to Neuronal Cell Death. *Science,* 297**,** 1186-1190.

Halawani, D., Gogonea, V., DiDonato, J. A., Pipich, V., Yao, P., China, A., Topbas, C., Vasu, K., Arif, A., Hazen, S. L. & Fox, P. L. 2018. Structural control of caspase-generated glutamyl-tRNA synthetase by appended noncatalytic WHEP domains. *J Biol Chem,* 293**,** 8843-8860.

Hamze, A. B., Wei, S., Bahudhanapati, H., Kota, S., Acharya, K. R. & Brew, K. 2007. Constraining specificity in the N-domain of tissue inhibitor of metalloproteinases-1; gelatinase-selective inhibitors. *Protein Sci,* 16**,** 1905-13.

Hanania, R., Sun, H. S., Xu, K., Pustylnik, S., Jeganathan, S. & Harrison, R. E. 2012. Classically activated macrophages use stable microtubules for matrix metalloproteinase-9 (MMP-9) secretion. *J Biol Chem,* 287**,** 8468-83.

Hashimoto, G., Inoki, I., Fujii, Y., Aoki, T., Ikeda, E. & Okada, Y. 2002. Matrix metalloproteinases cleave connective tissue growth factor and reactivate angiogenic activity of vascular endothelial growth factor 165. *J Biol Chem,* 277**,** 36288-95.

Heussen, C. & Dowdle, E. B. 1980. Electrophoretic analysis of plasminogen activators in polyacrylamide gels containing sodium dodecyl sulfate and copolymerized substrates. *Anal Biochem,* 102**,** 196-202.

Hodge, K., Have, S. T., Hutton, L. & Lamond, A. I. 2013. Cleaning up the masses: exclusion lists to reduce contamination with HPLC-MS/MS. *Journal of proteomics,* 88**,** 92-103.

Hrabec, E., Strek, M., Zieba, M., Kwiatkowska, S. & Hrabec, Z. 2002. Circulation level of matrix metalloproteinase-9 is correlated with disease severity in tuberculosis patients. *Int J Tuberc Lung Dis,* 6**,** 713-9.

Inoki, I., Shiomi, T., Hashimoto, G., Enomoto, H., Nakamura, H., Makino, K., Ikeda, E., Takata, S., Kobayashi, K. & Okada, Y. 2002. Connective tissue growth factor binds vascular endothelial growth factor (VEGF) and inhibits VEGF-induced angiogenesis. *Faseb j,* 16**,** 219-21.

Ishibuchi, H., Abe, M., Yokoyama, Y. & Ishikawa, O. 2010. Induction of matrix metalloproteinase-1 by small interfering RNA targeting connective tissue growth factor in dermal fibroblasts from patients with systemic sclerosis. *Exp Dermatol,* 19**,** e111-6.

Jacob, A. & Prekeris, R. 2015. The regulation of MMP targeting to invadopodia during cancer metastasis. *Frontiers in Cell and Developmental Biology,* 3.

Jung, M., Brüne, B., Hotter, G. & Sola, A. 2016. Macrophage-derived Lipocalin-2 contributes to ischemic resistance mechanisms by protecting from renal injury. *Scientific Reports,* 6**,** 21950.

Kaewseekhao, B., Naranbhai, V., Roytrakul, S., Namwat, W., Paemanee, A., Lulitanond, V., Chaiprasert, A. & Faksri, K. 2015. Comparative Proteomics of Activated THP-1 Cells Infected with Mycobacterium tuberculosis Identifies Putative Clearance Biomarkers for Tuberculosis Treatment. *PLoS One,* 10**,** e0134168.

Kanwar, Y. S., Linker, A. & Farquhar, M. G. 1980. Increased permeability of the glomerular basement membrane to ferritin after removal of glycosaminoglycans (heparan sulfate) by enzyme digestion. *J Cell Biol,* 86**,** 688-93.

Kaplan, G., Post, F. A., Moreira, A. L., Wainwright, H., Kreiswirth, B. N., Tanverdi, M., Mathema, B., Ramaswamy, S. V., Walther, G., Steyn, L. M., Barry, C. E. & Bekker, L. G. 2003. Mycobacterium tuberculosis Growth at the Cavity Surface: a Microenvironment with Failed Immunity. *Infection and Immunity,* 71**,** 7099-7108.

Kapojos, J. J., van den Berg, A., van Goor, H., te Loo, M. W., Poelstra, K., Borghuis, T. & Bakker, W. W. 2003. Production of hemopexin by TNF-alpha stimulated human mesangial cells. *Kidney Int,* 63**,** 1681-6.

Kerkvliet, E. H., Jansen, I. C., Schoenmaker, T., Beertsen, W. & Everts, V. 2003. Collagen type I, III and V differently modulate synthesis and activation of matrix metalloproteinases by cultured rabbit periosteal fibroblasts. *Matrix Biol,* 22**,** 217-27.

Khan, M. M., Simizu, S., Suzuki, T., Masuda, A., Kawatani, M., Muroi, M., Dohmae, N. & Osada, H. 2012. Protein disulfide isomerase-mediated disulfide bonds regulate the gelatinolytic activity and secretion of matrix metalloproteinase-9. *Exp Cell Res,* 318**,** 904-14.

Khan, Z., Shen, X. Z., Bernstein, E. A., Giani, J. F., Eriguchi, M., Zhao, T. V., Gonzalez-Villalobos, R. A., Fuchs, S., Liu, G. Y. & Bernstein, K. E. 2017. Angiotensin-converting enzyme enhances the oxidative response and bactericidal activity of neutrophils. *Blood,* 130**,** 328-339.

Klein, T. & Bischoff, R. 2011. Physiology and pathophysiology of matrix metalloproteases. *Amino Acids,* 41**,** 271-90.

Kolonko, M., Geffken, A. C., Blumer, T., Hagens, K., Schaible, U. E. & Hagedorn, M. 2014. WASH-driven actin polymerization is required for efficient mycobacterial phagosome maturation arrest. *Cellular Microbiology,* 16**,** 232-246.

Koo, I. C., Ohol, Y. M., Wu, P., Morisaki, J. H., Cox, J. S. & Brown, E. J. 2008. Role for lysosomal enzyme β-hexosaminidase in the control of mycobacteria infection. *Proceedings of the National Academy of Sciences,* 105**,** 710-715.

Korb, V., Chuturgoon, A. & Moodley, D. 2016. Mycobacterium tuberculosis: Manipulator of Protective Immunity. *International Journal of Molecular Sciences,* 17**,** 131.

Kotra, L. P., Zhang, L., Fridman, R., Orlando, R. & Mobashery, S. 2002. N-Glycosylation pattern of the zymogenic form of human matrix metalloproteinase-9. *Bioorg Chem,* 30**,** 356-70.

Krey, J. F., Wilmarth, P. A., Shin, J.-B., Klimek, J., Sherman, N. E., Jeffery, E. D., Choi, D., David, L. L. & Barr-Gillespie, P. G. 2014. Accurate label-free protein quantitation with high- and low-resolution mass spectrometers. *Journal of proteome research,* 13**,** 1034-1044.

Kridel, S. J., Chen, E., Kotra, L. P., Howard, E. W., Mobashery, S. & Smith, J. W. 2001. Substrate hydrolysis by matrix metalloproteinase-9. *J Biol Chem,* 276**,** 20572-8.

Kubler, A., Luna, B., Larsson, C., Ammerman, N. C., Andrade, B. B., Orandle, M., Bock, K. W., Xu, Z., Bagci, U., Mollura, D. J., Marshall, J., Burns, J., Winglee, K., Ahidjo, B. A., Cheung, L. S., Klunk, M., Jain, S. K., Kumar, N. P., Babu, S., Sher, A., Friedland, J. S., Elkington, P. T. & Bishai, W. R. 2015. Mycobacterium tuberculosis dysregulates MMP/TIMP balance to drive rapid cavitation and unrestrained bacterial proliferation. *J Pathol,* 235**,** 431-44.

LaFever, K. S., Wang, X., Page-McCaw, P., Bhave, G. & Page-McCaw, A. 2017. Both Drosophila matrix metalloproteinases have released and membrane-tethered forms but have different substrates. 7**,** 44560.

Lasa, M., Marin, O. & Pinna, L. A. 1997. Rat liver Golgi apparatus contains a protein kinase similar to the casein kinase of lactating mammary gland. *Eur J Biochem,* 243**,** 719-25.

Lawn, S. D. & Gupta-Wright, A. 2016. Detection of lipoarabinomannan (LAM) in urine is indicative of disseminated TB with renal involvement in patients living with HIV and advanced immunodeficiency: evidence and implications. *Transactions of the Royal Society of Tropical Medicine and Hygiene,* 110**,** 180-185.

Li, A., Dawson, J. C., Forero-Vargas, M., Spence, H. J., Yu, X., König, I., Anderson, K. & Machesky, L. M. 2010. The Actin-Bundling Protein Fascin Stabilizes Actin in Invadopodia and Potentiates Protrusive Invasion. *Current Biology,* 20**,** 339-345.

Lombard, C., Saulnier, J. & Wallach, J. 2005. Assays of matrix metalloproteinases (MMPs) activities: a review. *Biochimie,* 87**,** 265-72.

Ludwig, C., Gillet, L., Rosenberger, G., Amon, S., Collins, B. C. & Aebersold, R. 2018. Data-independent acquisition-based SWATH-MS for quantitative proteomics: a tutorial. *Molecular systems biology,* 14**,** e8126-e8126.

Luhtala, N. & Parker, R. 2010. T2 Family ribonucleases: ancient enzymes with diverse roles. *Trends Biochem Sci,* 35**,** 253-9.

Marakalala, M. J., Raju, R. M., Sharma, K., Zhang, Y. J., Eugenin, E. A., Prideaux, B., Daudelin, I. B., Chen, P.-Y., Booty, M. G., Kim, J. H., Eum, S. Y., Via, L. E., Behar, S. M., Barry Iii, C. E., Mann, M., Dartois, V. & Rubin, E. J. 2016. Inflammatory signaling in human tuberculosis granulomas is spatially organized. *Nat Med,* 22**,** 531-538.

Marwick, J. A., Stevenson, C. S., Giddings, J., MacNee, W., Butler, K., Rahman, I. & Kirkham, P. A. 2006. Cigarette smoke disrupts VEGF165-VEGFR-2 receptor signaling complex in rat lungs and patients with COPD: morphological impact of VEGFR-2 inhibition. *Am J Physiol Lung Cell Mol Physiol,* 290**,** L897-908.

Mauk, M. R., Smith, A. & Mauk, A. G. 2011. An alternative view of the proposed alternative activities of hemopexin. *Protein Sci,* 20**,** 791-805.

Mecham, R. P., Broekelmann, T. J., Fliszar, C. J., Shapiro, S. D., Welgus, H. G. & Senior, R. M. 1997. Elastin degradation by matrix metalloproteinases. Cleavage site specificity and mechanisms of elastolysis. *J Biol Chem,* 272**,** 18071-6.

Mehta, K. & Lopez-Berestein, G. 1986. Expression of Tissue Transglutaminase in Cultured Monocytic Leukemia (THP-1) Cells during Differentiation. *Cancer Research,* 46**,** 1388-1394.

Melander, M. C., Jurgensen, H. J., Madsen, D. H., Engelholm, L. H. & Behrendt, N. 2015. The collagen receptor uPARAP/Endo180 in tissue degradation and cancer (Review). *Int J Oncol,* 47**,** 1177-88.

Menges, D. A., Ternullo, D. L., Tan-Wilson, A. L. & Gal, S. 1997. Continuous assay of proteases using a microtiter plate fluorescence reader. *Anal Biochem,* 254**,** 144-7.

Mhawech, P. 2005. 14-3-3 proteins--an update. *Cell Res,* 15**,** 228-36.

Michalski, A., Damoc, E., Hauschild, J. P., Lange, O., Wieghaus, A., Makarov, A., Nagaraj, N., Cox, J., Mann, M. & Horning, S. 2011. Mass spectrometry-based proteomics using Q Exactive, a high-performance benchtop quadrupole Orbitrap mass spectrometer. *Mol Cell Proteomics,* 10**,** M111.011015.

Miharada, K., Hiroyama, T., Sudo, K., Danjo, I., Nagasawa, T. & Nakamura, Y. 2008. Lipocalin 2-mediated growth suppression is evident in human erythroid and monocyte/macrophage lineage cells. *J Cell Physiol,* 215**,** 526-37.

Mikesh, L. M., Ueberheide, B., Chi, A., Coon, J. J., Syka, J. E. P., Shabanowitz, J. & Hunt, D. F. 2006. The Utility of ETD Mass Spectrometry in Proteomic Analysis: BIOCHIMICA ET BIOPHYSICA ACTA Proteins and Proteomics Posttranslational Modifications in Proteomics Special Issue. *Biochimica et biophysica acta,* 1764**,** 1811-1822.

Miner, J. H. 2011. Glomerular basement membrane composition and the filtration barrier. *Pediatr Nephrol,* 26**,** 1413-7.

Miner, J. H. 2012. The glomerular basement membrane. *Exp Cell Res,* 318**,** 973-8.

Mori, H., Tomari, T., Koshikawa, N., Kajita, M., Itoh, Y., Sato, H., Tojo, H., Yana, I. & Seiki, M. 2002. CD44 directs membrane-type 1 matrix metalloproteinase to lamellipodia by associating with its hemopexin-like domain. *Embo j,* 21**,** 3949-59.

Morimoto, S., Yamamoto, Y., O'Brien, J. S. & Kishimoto, Y. 1990. Distribution of saposin proteins (sphingolipid activator proteins) in lysosomal storage and other diseases. *Proc Natl Acad Sci U S A,* 87**,** 3493-7.

Morrison, C. J., Butler, G. S., Rodriguez, D. & Overall, C. M. 2009. Matrix metalloproteinase proteomics: substrates, targets, and therapy. *Curr Opin Cell Biol,* 21**,** 645-53.

Mthembu, N. N., Mbita, Z., Hull, R. & Dlamini, Z. 2017. Abnormalities in alternative splicing of angiogenesis-related genes and their role in HIV-related cancers. *HIV AIDS (Auckl),* 9**,** 77-93.

Munthali, L., Khan, P. Y., Mwaungulu, N. J., Chilongo, F., Floyd, S., Kayange, M., Glynn, J. R., French, N. & Crampin, A. C. 2014. The effect of HIV and antiretroviral therapy on characteristics of pulmonary tuberculosis in northern Malawi: a cross-sectional study. *BMC Infect Dis,* 14**,** 107.

Nagase, H., Visse, R. & Murphy, G. 2006. Structure and function of matrix metalloproteinases and TIMPs. *Cardiovasc Res,* 69**,** 562-73.

Nedeltchev, G. G., Raghunand, T. R., Jassal, M. S., Lun, S., Cheng, Q. J. & Bishai, W. R. 2009. Extrapulmonary dissemination of Mycobacterium bovis but not Mycobacterium tuberculosis in a bronchoscopic rabbit model of cavitary tuberculosis. *Infect Immun,* 77**,** 598-603.

Niikura, Y., Kitagawa, R. & Kitagawa, K. 2016. The inheritance of centromere identity. *Molecular & cellular oncology,* 3**,** e1188226-e1188226.

Nishino, M., Cryer, S. K., Okajima, Y., Sholl, L. M., Hatabu, H., Rabin, M. S., Jackman, D. M. & Johnson, B. E. 2012. Tumoral cavitation in patients with non-small-cell lung cancer treated with antiangiogenic therapy using bevacizumab. *Cancer Imaging,* 12**,** 225-35.

O'Connor, C. M. & FitzGerald, M. X. 1994. Matrix metalloproteases and lung disease. *Thorax,* 49**,** 602-9.

O'Kane, C. M., Elkington, P. T. & Friedland, J. S. 2008. Monocyte-dependent oncostatin M and TNF-alpha synergize to stimulate unopposed matrix metalloproteinase-1/3 secretion from human lung fibroblasts in tuberculosis. *Eur J Immunol,* 38**,** 1321-30.

Ochieng, J., Fridman, R., Nangia-Makker, P., Kleiner, D. E., Liotta, L. A., Stetler-Stevenson, W. G. & Raz, A. 1994. Galectin-3 Is a Novel Substrate for Human Matrix Metalloproteinases-2 and -9. *Biochemistry,* 33**,** 14109-14114.

Oehlers, S. H., Cronan, M. R., Scott, N. R., Thomas, M. I., Okuda, K. S., Walton, E. M., Beerman, R. W., Crosier, P. S. & Tobin, D. M. 2015. Interception of host angiogenic signalling limits mycobacterial growth. *Nature,* 517**,** 612-615.

Ogata, Y., Enghild, J. J. & Nagase, H. 1992. Matrix metalloproteinase 3 (stromelysin) activates the precursor for the human matrix metalloproteinase 9. *J Biol Chem,* 267**,** 3581-4.

Ogata, Y., Itoh, Y. & Nagase, H. 1995. Steps involved in activation of the pro-matrix metalloproteinase 9 (progelatinase B)-tissue inhibitor of metalloproteinases-1 complex by 4-aminophenylmercuric acetate and proteinases. *J Biol Chem,* 270**,** 18506-11.

Ordonez, A. A., Tasneen, R., Pokkali, S., Xu, Z., Converse, P. J., Klunk, M. H., Mollura, D. J., Nuermberger, E. L. & Jain, S. K. 2016. Mouse model of pulmonary cavitary tuberculosis and expression of matrix metalloproteinase-9. *Dis Model Mech,* 9**,** 779-88.

Overall, C. M. 2002. Molecular determinants of metalloproteinase substrate specificity: matrix metalloproteinase substrate binding domains, modules, and exosites. *Mol Biotechnol,* 22**,** 51-86.

Ozaki, N. K., Beharry, K. D., Nishihara, K. C., Akmal, Y., Ang, J. G., Sheikh, R. & Modanlou, H. D. 2002. Regulation of Retinal Vascular Endothelial Growth Factor and Receptors in Rabbits Exposed to Hyperoxia. *Investigative Ophthalmology & Visual Science,* 43**,** 1546-1557.

Pandie, S., Peter, J. G., Kerbelker, Z. S., Meldau, R., Theron, G., Govender, U., Ntsekhe, M., Dheda, K. & Mayosi, B. M. 2016. The diagnostic accuracy of pericardial and urinary lipoarabinomannan (LAM) assays in patients with suspected tuberculous pericarditis. *Sci Rep,* 6**,** 32924.

Paracuellos, P., Briggs, D. C., Carafoli, F., Loncar, T. & Hohenester, E. 2015. Insights into Collagen Uptake by C-type Mannose Receptors from the Crystal Structure of Endo180 Domains 1-4. *Structure,* 23**,** 2133-42.

Pardo, A. & Selman, M. 2005. MMP-1: the elder of the family. *Int J Biochem Cell Biol,* 37**,** 283-8.

Pavan Kumar, N., Anuradha, R., Andrade, B. B., Suresh, N., Ganesh, R., Shankar, J., Kumaraswami, V., Nutman, T. B. & Babu, S. 2013. Circulating biomarkers of pulmonary and extrapulmonary tuberculosis in children. *Clin Vaccine Immunol,* 20**,** 704-11.

Piccard, H., Van den Steen, P. E. & Opdenakker, G. 2007. Hemopexin domains as multifunctional liganding modules in matrix metalloproteinases and other proteins. *J Leukoc Biol,* 81**,** 870-92.

Pieters, J. & Gatfield, J. 2002. Hijacking the host: survival of pathogenic mycobacteria inside macrophages. *Trends Microbiol,* 10**,** 142-6.

Pires, D., Marques, J., Pombo, J. P., Carmo, N., Bettencourt, P., Neyrolles, O., Lugo-Villarino, G. & Anes, E. 2016. Role of Cathepsins in Mycobacterium tuberculosis Survival in Human Macrophages. *Sci Rep,* 6**,** 32247.

Poincloux, R., Lizárraga, F. & Chavrier, P. 2009. Matrix invasion by tumour cells: a focus on MT1-MMP trafficking to invadopodia. *Journal of Cell Science,* 122**,** 3015-3024.

Polena, H., Boudou, F., Tilleul, S., Dubois-Colas, N., Lecointe, C., Rakotosamimanana, N., Pelizzola, M., Andriamandimby, S. F., Raharimanga, V., Charles, P., Herrmann, J.-L., Ricciardi-Castagnoli, P., Rasolofo, V., Gicquel, B. & Tailleux, L. 2016. Mycobacterium tuberculosis exploits the formation of new blood vessels for its dissemination. *Scientific Reports,* 6**,** 33162.

Prabakaran, S., Lippens, G., Steen, H. & Gunawardena, J. 2012. Post-translational modification: nature's escape from genetic imprisonment and the basis for dynamic information encoding. *Wiley Interdiscip Rev Syst Biol Med,* 4**,** 565-83.

Qin, Z. 2012. The use of THP-1 cells as a model for mimicking the function and regulation of monocytes and macrophages in the vasculature. *Atherosclerosis,* 221**,** 2-11.

Quesada, A. R., Barbacid, M. M., Mira, E., Fernandez-Resa, P., Marquez, G. & Aracil, M. 1997. Evaluation of fluorometric and zymographic methods as activity assays for stromelysins and gelatinases. *Clin Exp Metastasis,* 15**,** 26-32.

Ra, H. J. & Parks, W. C. 2007. Control of matrix metalloproteinase catalytic activity. *Matrix Biol,* 26**,** 587-96.

Ramos-DeSimone, N., Hahn-Dantona, E., Sipley, J., Nagase, H., French, D. L. & Quigley, J. P. 1999. Activation of Matrix Metalloproteinase-9 (MMP-9) via a Converging Plasmin/Stromelysin-1 Cascade Enhances Tumor Cell Invasion. *Journal of Biological Chemistry,* 274**,** 13066-13076.

Ray, P. S. & Fox, P. L. 2014. Origin and Evolution of Glutamyl-prolyl tRNA Synthetase WHEP Domains Reveal Evolutionary Relationships within Holozoa. *PLOS ONE,* 9**,** e98493.

Raymond, B. B. A., Madhkoor, R., Schleicher, I., Uphoff, C. C., Turnbull, L., Whitchurch, C. B., Rohde, M., Padula, M. P. & Djordjevic, S. P. 2018. Extracellular Actin Is a Receptor for Mycoplasma hyopneumoniae. *Front Cell Infect Microbiol,* 8**,** 54.

Reece, S. T. & Kaufmann, S. H. 2012. Floating between the poles of pathology and protection: can we pin down the granuloma in tuberculosis? *Curr Opin Microbiol,* 15**,** 63-70.

Remacle, A., Murphy, G. & Roghi, C. 2003. Membrane type I-matrix metalloproteinase (MT1-MMP) is internalised by two different pathways and is recycled to the cell surface. *J Cell Sci,* 116**,** 3905-16.

Ren, Z., Chen, J. & Khalil, R. A. 2017. Zymography as a Research Tool in the Study of Matrix Metalloproteinase Inhibitors. *Methods in molecular biology (Clifton, N.J.),* 1626**,** 79-102.

Ressad, F., Didry, D., Egile, C., Pantaloni, D. & Carlier, M. F. 1999. Control of actin filament length and turnover by actin depolymerizing factor (ADF/cofilin) in the presence of capping proteins and ARP2/3 complex. *J Biol Chem,* 274**,** 20970-6.

Reyrat, J. M. & Kahn, D. 2001. Mycobacterium smegmatis: an absurd model for tuberculosis? *Trends Microbiol,* 9**,** 472-4.

Riendeau, C. J. & Kornfeld, H. 2003. THP-1 cell apoptosis in response to Mycobacterial infection. *Infect Immun,* 71**,** 254-9.

Roderfeld, M., Graf, J., Giese, B., Salguero-Palacios, R., Tschuschner, A., Muller-Newen, G. & Roeb, E. 2007. Latent MMP-9 is bound to TIMP-1 before secretion. *Biol Chem,* 388**,** 1227-34.

Rodríguez, D., Morrison, C. J. & Overall, C. M. 2010. Matrix metalloproteinases: What do they not do? New substrates and biological roles identified by murine models and proteomics. *Biochimica et Biophysica Acta (BBA) - Molecular Cell Research,* 1803**,** 39-54.

Roeb, E., Schleinkofer, K., Kernebeck, T., Potsch, S., Jansen, B., Behrmann, I., Matern, S. & Grotzinger, J. 2002. The matrix metalloproteinase 9 (mmp-9) hemopexin domain is a novel gelatin binding domain and acts as an antagonist. *J Biol Chem,* 277**,** 50326-32.

Rosewell, K., Al-Alem, L., Li, F., Kelty, B. & Curry, T. E. 2011. Identification of Hepsin and Protein Disulfide Isomerase A3 as Targets of Gelatinolytic Action in Rat Ovarian Granulosa Cells During the Periovulatory Period. *Biology of Reproduction,* 85**,** 858-866.

Rossano, R., Larocca, M., Riviello, L., Coniglio, M. G., Vandooren, J., Liuzzi, G. M., Opdenakker, G. & Riccio, P. 2014. Heterogeneity of serum gelatinases MMP-2 and MMP-9 isoforms and charge variants. *J Cell Mol Med,* 18**,** 242-52.

Sakamoto, K. 2012. The pathology of Mycobacterium tuberculosis infection. *Vet Pathol,* 49**,** 423-39.

Salgame, P. 2011. MMPs in tuberculosis: granuloma creators and tissue destroyers. *J Clin Invest,* 121**,** 1686-8.

Sano, H., Hsu, D. K., Apgar, J. R., Yu, L., Sharma, B. B., Kuwabara, I., Izui, S. & Liu, F. T. 2003. Critical role of galectin-3 in phagocytosis by macrophages. *J Clin Invest,* 112**,** 389-97.

Santos, C. X., Stolf, B. S., Takemoto, P. V., Amanso, A. M., Lopes, L. R., Souza, E. B., Goto, H. & Laurindo, F. R. 2009. Protein disulfide isomerase (PDI) associates with NADPH oxidase and is required for phagocytosis of Leishmania chagasi promastigotes by macrophages. *J Leukoc Biol,* 86**,** 989-98.

Saunders, W. B., Bayless, K. J. & Davis, G. E. 2005. MMP-1 activation by serine proteases and MMP-10 induces human capillary tubular network collapse and regression in 3D collagen matrices. *J Cell Sci,* 118**,** 2325-40.

Scannevin, R. H., Alexander, R., Mezzasalma Haarlander, T., Burke, S. L., Singer, M., Hou, C., Zhang, Y. M., Maguire, D., Spurlino, J., Deckman, I., Carroll, K. I., Lewandowski, F., Devine, E., Dzordzorme, K., Tounge, B., Milligan, C., Bayoumy, S., Williams, R., Schalk-Hihi, C., Leonard, K., Jackson, P., Todd, M., Kuo, L. C. & Rhodes, K. J. 2017. Discovery of a highly selective chemical inhibitor of matrix metalloproteinase-9 (MMP-9) that allosterically inhibits zymogen activation. *J Biol Chem*.

Schauer, C., Janko, C., Munoz, L. E., Zhao, Y., Kienhofer, D., Frey, B., Lell, M., Manger, B., Rech, J., Naschberger, E., Holmdahl, R., Krenn, V., Harrer, T., Jeremic, I., Bilyy, R., Schett, G., Hoffmann, M. & Herrmann, M. 2014. Aggregated neutrophil extracellular traps limit inflammation by degrading cytokines and chemokines. *Nat Med,* 20**,** 511-517.

Schröpfer, A., Kammerer, U., Kapp, M., Dietl, J., Feix, S. & Anacker, J. 2010. Expression pattern of matrix metalloproteinases in human gynecological cancer cell lines. *BMC Cancer,* 10**,** 553-553.

Senior, R. M., Griffin, G. L., Fliszar, C. J., Shapiro, S. D., Goldberg, G. I. & Welgus, H. G. 1991. Human 92- and 72-kilodalton type IV collagenases are elastases. *Journal of Biological Chemistry,* 266**,** 7870-7875.

Shamamian, P., Schwartz, J. D., Pocock, B. J., Monea, S., Whiting, D., Marcus, S. G. & Mignatti, P. 2001. Activation of progelatinase A (MMP-2) by neutrophil elastase, cathepsin G, and proteinase-3: a role for inflammatory cells in tumor invasion and angiogenesis. *J Cell Physiol,* 189**,** 197-206.

Shapiro, S. D., Fliszar, C. J., Broekelmann, T. J., Mecham, R. P., Senior, R. M. & Welgus, H. G. 1995. Activation of the 92-kDa gelatinase by stromelysin and 4-aminophenylmercuric acetate. Differential processing and stabilization of the carboxyl-terminal domain by tissue inhibitor of metalloproteinases (TIMP). *J Biol Chem,* 270**,** 6351-6.

Shiloh, M. U. & Champion, P. A. 2010. To catch a killer. What can mycobacterial models teach us about Mycobacterium tuberculosis pathogenesis? *Curr Opin Microbiol,* 13**,** 86-92.

Spiller, F., Costa, C., Souto, F. O., Vinchi, F., Mestriner, F. L., Laure, H. J., Alves-Filho, J. C., Freitas, A., Rosa, J. C., Ferreira, S. H., Altruda, F., Hirsch, E., Greene, L. J., Tolosano, E. & Cunha, F. Q. 2011. Inhibition of neutrophil migration by hemopexin leads to increased mortality due to sepsis in mice. *Am J Respir Crit Care Med,* 183**,** 922-31.

Stokes, R. W. & Doxsee, D. 1999. The receptor-mediated uptake, survival, replication, and drug sensitivity of Mycobacterium tuberculosis within the macrophage-like cell line THP-1: a comparison with human monocyte-derived macrophages. *Cell Immunol,* 197**,** 1-9.

Tandon, A. & Sinha, S. 2011. Structural insights into the binding of MMP9 inhibitors. *Bioinformation,* 5**,** 310-314.

Tate, S., Larsen, B., Bonner, R. & Gingras, A. C. 2013. Label-free quantitative proteomics trends for protein-protein interactions. *J Proteomics,* 81**,** 91-101.

Theus, S. A., Cave, M. D. & Eisenach, K. D. 2004. Activated THP-1 cells: an attractive model for the assessment of intracellular growth rates of Mycobacterium tuberculosis isolates. *Infect Immun,* 72**,** 1169-73.

Thomas, S. G., Huang, S., Li, S., Staiger, C. J. & Franklin-Tong, V. E. 2006. Actin depolymerization is sufficient to induce programmed cell death in self-incompatible pollen. *The Journal of Cell Biology,* 174**,** 221-229.

Tokito, A. & Jougasaki, M. 2016. Matrix Metalloproteinases in Non-Neoplastic Disorders. *International Journal of Molecular Sciences,* 17**,** 1178.

Tominaga, T., Suzuki, M., Saeki, H., Matsuno, S., Tachibana, T. & Kudo, T. 1998. Establishment of an activated macrophage cell line, A-THP-1, and its properties. *Tohoku J Exp Med,* 186**,** 99-119.

Toshima, M., Ohtani, Y. & Ohtani, O. 2004. Three-dimensional architecture of elastin and collagen fiber networks in the human and rat lung. *Arch Histol Cytol,* 67**,** 31-40.

Tsuchiya, S., Yamabe, M., Yamaguchi, Y., Kobayashi, Y., Konno, T. & Tada, K. 1980. Establishment and characterization of a human acute monocytic leukemia cell line (THP-1). *Int J Cancer,* 26**,** 171-6.

Ugarte-Berzal, E., Vandooren, J., Bailon, E., Opdenakker, G. & Garcia-Pardo, A. 2016. Inhibition of MMP-9-dependent Degradation of Gelatin, but Not Other MMP-9 Substrates, by the MMP-9 Hemopexin Domain Blades 1 and 4. *J Biol Chem,* 291**,** 11751-60.

van Crevel, R., Ottenhoff, T. H. M. & van der Meer, J. W. M. 2002. Innate Immunity to Mycobacterium tuberculosis. *Clinical Microbiology Reviews,* 15**,** 294-309.

van den Hoven, M. J., Wijnhoven, T. J., Li, J. P., Zcharia, E., Dijkman, H. B., Wismans, R. G., Rops, A. L., Lensen, J. F., van den Heuvel, L. P., van Kuppevelt, T. H., Vlodavsky, I., Berden, J. H. & van der Vlag, J. 2008. Reduction of anionic sites in the glomerular basement membrane by heparanase does not lead to proteinuria. *Kidney Int,* 73**,** 278-87.

Van Doren, S. R., Marcink, T. C., Koppisetti, R. K., Jurkevich, A. & Fulcher, Y. G. 2017. Peripheral membrane associations of matrix metalloproteinases. *Biochimica et Biophysica Acta (BBA) - Molecular Cell Research*.

Velegraki, M., Papakonstanti, E., Mavroudi, I., Psyllaki, M., Tsatsanis, C., Oulas, A., Iliopoulos, I., Katonis, P. & Papadaki, H. A. 2013. Impaired clearance of apoptotic cells leads to HMGB1 release in the bone marrow of patients with myelodysplastic syndromes and induces TLR4-mediated cytokine production. *Haematologica,* 98**,** 1206-1215.

Vemula, M. H., Ganji, R., Sivangala, R., Jakkala, K., Gaddam, S., P S, R. & Banerjee, S. 2016. Mycobacterium tuberculosis Zinc Metalloprotease-1 Elicits Tuberculosis-specific Humoral Immune Response Independent of Mycobacterial Load in Pulmonary and Extra-Pulmonary Tuberculosis Patients. *Frontiers in Microbiology,* 7.

Via, L. E., England, K., Weiner, D. M., Schimel, D., Zimmerman, M. D., Dayao, E., Chen, R. Y., Dodd, L. E., Richardson, M., Robbins, K. K., Cai, Y., Hammoud, D., Herscovitch, P., Dartois, V., Flynn, J. L. & Barry, C. E., 3rd 2015. A sterilizing tuberculosis treatment regimen is associated with faster clearance of bacteria in cavitary lesions in marmosets. *Antimicrob Agents Chemother,* 59**,** 4181-9.

Vinchi, F., Costa da Silva, M., Ingoglia, G., Petrillo, S., Brinkman, N., Zuercher, A., Cerwenka, A., Tolosano, E. & Muckenthaler, M. U. 2016. Hemopexin therapy reverts heme-induced proinflammatory phenotypic switching of macrophages in a mouse model of sickle cell disease. *Blood,* 127**,** 473-486.

Volkman, H. E., Pozos, T. C., Zheng, J., Davis, J. M., Rawls, J. F. & Ramakrishnan, L. 2010. Tuberculous granuloma induction via interaction of a bacterial secreted protein with host epithelium. *Science,* 327**,** 466-9.

Walker, N. F., Clark, S. O., Oni, T., Andreu, N., Tezera, L., Singh, S., Saraiva, L., Pedersen, B., Kelly, D. L., Tree, J. A., D'Armiento, J. M., Meintjes, G., Mauri, F. A., Williams, A., Wilkinson, R. J., Friedland, J. S. & Elkington, P. T. 2012. Doxycycline and HIV infection suppress tuberculosis-induced matrix metalloproteinases. *American journal of respiratory and critical care medicine,* 185**,** 989-997.

Wang, X., Li, Y., Luo, D., Wang, X., Zhang, Y., Liu, Z., Zhong, N., Wu, M. & Li, G. 2017. Lyn regulates mucus secretion and MUC5AC via the STAT6 signaling pathway during allergic airway inflammation. *Sci Rep,* 7**,** 42675.

Watanabe, A., Hosino, D., Koshikawa, N., Seiki, M., Suzuki, T. & Ichikawa, K. 2013. *Critical Role of Transient Activity of MT1-MMP for ECM Degradation in Invadopodia*.

Watanabe, Y., Hirakawa, K., Haruyama, T. & Akaike, T. 2001. Direct production of an activated matrix metalloproteinase-9 (gelatinase B) from mammalian cells. *FEBS Letters,* 502**,** 63-67.

Weinkauf, C., Salvador, R. & Pereiraperrin, M. 2011. Neurotrophin receptor TrkC is an entry receptor for Trypanosoma cruzi in neural, glial, and epithelial cells. *Infect Immun,* 79**,** 4081-7.

Wilczynska, K. M., Gopalan, S. M., Bugno, M., Kasza, A., Konik, B. S., Bryan, L., Wright, S., Griswold-Prenner, I. & Kordula, T. 2006. A novel mechanism of tissue inhibitor of metalloproteinases-1 activation by interleukin-1 in primary human astrocytes. *J Biol Chem,* 281**,** 34955-64.

Wisniewski, J. R., Zougman, A., Nagaraj, N. & Mann, M. 2009. Universal sample preparation method for proteome analysis. *Nat Methods,* 6**,** 359-62.

Withrock, I. C., Anderson, S. J., Jefferson, M. A., McCormack, G. R., Mlynarczyk, G. S. A., Nakama, A., Lange, J. K., Berg, C. A., Acharya, S., Stock, M. L., Lind, M. S., Luna, K. C., Kondru, N. C., Manne, S., Patel, B. B., de la Rosa, B. M., Huang, K.-P., Sharma, S., Hu, H. Z., Kanuri, S. H. & Carlson, S. A. 2015. Genetic diseases conferring resistance to infectious diseases. *Genes & Diseases,* 2**,** 247-254.

Wolf, B. B., Schuler, M., Echeverri, F. & Green, D. R. 1999. Caspase-3 is the primary activator of apoptotic DNA fragmentation via DNA fragmentation factor-45/inhibitor of caspase-activated DNase inactivation. *J Biol Chem,* 274**,** 30651-6.

Wolf, J., Lachmann, I., Wagner, U., Osman, A. & Mothes, T. 2011. Immunoassay of in vitro activated human tissue transglutaminase. *Anal Biochem,* 411**,** 10-5.

Wong, D., Li, W., Chao, J. D., Zhou, P., Narula, G., Tsui, C., Ko, M., Xie, J., Martinez-Frailes, C. & Av-Gay, Y. 2018. Protein tyrosine kinase, PtkA, is required for Mycobacterium tuberculosis growth in macrophages. *Sci Rep,* 8**,** 155.

Wood, R. C., Luabeya, A. K., Weigel, K. M., Wilbur, A. K., Jones-Engel, L., Hatherill, M. & Cangelosi, G. A. 2015. Detection of Mycobacterium tuberculosis DNA on the oral mucosa of tuberculosis patients. *Sci Rep,* 5**,** 8668.

Wu, Y. I., Munshi, H. G., Sen, R., Snipas, S. J., Salvesen, G. S., Fridman, R. & Stack, M. S. 2004. Glycosylation broadens the substrate profile of membrane type 1 matrix metalloproteinase. *J Biol Chem,* 279**,** 8278-89.

Yamaguchi, H., Takeo, Y., Yoshida, S., Kouchi, Z., Nakamura, Y. & Fukami, K. 2009. Lipid rafts and caveolin-1 are required for invadopodia formation and extracellular matrix degradation by human breast cancer cells. *Cancer Res,* 69**,** 8594-602.

Yan, L., Borregaard, N., Kjeldsen, L. & Moses, M. A. 2001. The High Molecular Weight Urinary Matrix Metalloproteinase (MMP) Activity Is a Complex of Gelatinase B/MMP-9 and Neutrophil Gelatinase-associated Lipocalin (NGAL): MODULATION OF MMP-9 ACTIVITY BY NGAL. *Journal of Biological Chemistry,* 276**,** 37258-37265.

Zeng, X. & Carlin, C. R. 2013. Host cell autophagy modulates early stages of adenovirus infections in airway epithelial cells. *J Virol,* 87**,** 2307-19.

Zhang, M., Gong, J., Lin, Y. & Barnes, P. F. 1998a. Growth of Virulent and Avirulent Mycobacterium tuberculosis Strains in Human Macrophages. *Infection and Immunity,* 66**,** 794-799.

Zhang, S., Wu, Q., Shan, Y., Zhao, Q., Zhao, B., Weng, Y., Sui, Z., Zhang, L. & Zhang, Y. 2016. Fast MS/MS acquisition without dynamic exclusion enables precise and accurate quantification of proteome by MS/MS fragment intensity. *Scientific Reports,* 6**,** 26392.

Zhang, Y., McCluskey, K., Fujii, K. & Wahl, L. M. 1998b. Differential regulation of monocyte matrix metalloproteinase and TIMP-1 production by TNF-alpha, granulocyte-macrophage CSF, and IL-1 beta through prostaglandin-dependent and -independent mechanisms. *J Immunol,* 161**,** 3071-6.

Zhao, P., Elks, C. M. & Stephens, J. M. 2014. The Induction of Lipocalin-2 Protein Expression in Vivo and in Vitro. *Journal of Biological Chemistry,* 289**,** 5960-5969.

Zhou, H. W., DeLoid, G., Browning, E., Gregory, D. J., Tan, F. X., Bedugnis, A. S., Imrich, A., Koziel, H., Kramnik, I., Lu, Q. & Kobzik, L. 2012. Genome-Wide RNAi Screen in IFN-gamma-Treated Human Macrophages Identifies Genes Mediating Resistance to the Intracellular Pathogen Francisella tularensis. *Plos One,* 7**,** 15.

Zhou, M., Zhang, Y., Ardans, J. A. & Wahl, L. M. 2003. Interferon-gamma differentially regulates monocyte matrix metalloproteinase-1 and -9 through tumor necrosis factor-alpha and caspase 8. *J Biol Chem,* 278**,** 45406-13.

Zielonka, T. M., Demkow, U., Michalowska-Mitczuk, D., Filewska, M., Bialas, B., Zycinska, K., Obrowski, M. H., Kus, J. & Skopinska-Rozewska, E. 2011. Angiogenic activity of sera from pulmonary tuberculosis patients in relation to IL-12p40 and TNFalpha serum levels. *Lung,* 189**,** 351-7.

Zucchi, F. C., Tsanaclis, A. M., Moura-Dias, Q., Jr., Silva, C. L., Pelegrini-da-Silva, A., Neder, L. & Takayanagui, O. M. 2013. Modulation of angiogenic factor VEGF by DNA-hsp65 vaccination in a murine CNS tuberculosis model. *Tuberculosis (Edinb),* 93**,** 373-80.

Zughaier, S. M., Stauffer, B. B. & McCarty, N. A. 2014. Inflammation and ER Stress Downregulate BDH2 Expression and Dysregulate Intracellular Iron in Macrophages. *Journal of Immunology Research,* 2014**,** 140728.

Appendix 1

Western blotting

SDS-PAGE

The stacking and separating gels were prepared to final concentrations of 4% and 10% polyacrylamide gels, respectively. Samples were prepared by diluting in sample buffer which contained β-mercaptoethanol and then boiled for 5 minutes, unless otherwise stated. Electrophoresis was carried out at 40 mA for two gels using 1 X electrophoresis buffer. Following that, the protein bands were either visualised by using Coomassie-blue staining or transferred to a Hybond C nitrocellulose membrane as required for western blotting analysis.

Table 6-1: SDS-PAGE buffer recipes

	Components
Stacking gel	4% Acrylamide 0.125 M Tris-HCL pH 6.8, 0.1% SDS and 150 µl of 10% ammonium persulfate (APS) and 20 µl TEMED
Separating gel	10% Acrylamide 0.375 M Tris-HCL pH 8.8; 0.1% SDS, 150 µl of 10% ammonium persulfate (APS) and 15 µl TEMED
Electrophoresis buffer	192 mM glycine, 1% (w/v) SDS and 25 mM Tris, pH 8.5
3X Sample loading buffer	10% glycerol, 0.01% bromophenol blue, 1% SDS and 50 mM Tris-HCL, pH 6.8

Protein transfer

Transfer of protein to the Hybond C nitrocellulose membrane was done using the Biorad transfer apparatus. The Whatman papers, sponges and gel were soaked in ice-cold blotting buffer for 15 minutes prior assembling the transfer sandwich. This was done to minimise bubble formation during assembly and protein transfer. The transfer sandwich was assembled appropriately also ensuring exclusion of bubbles that may interfere with the blotting procedure. Blotting was carried out at 300 mA for about an hour with constant

stirring of the blotting buffer. To keep the buffer cool, an ice pack was placed in the slot provided in the apparatus.

Table 6-2: Western blotting buffers

	Buffer components
Transfer buffer	0.025 M Tris-HCL, 0.192 M Glycine, 20% Methanol, pH 8.2
Blocking buffer	5% Skim milk, 0.1% Tween-20, 0.2 M NaCl, 0.05 M Tris-HCL, pH 7.4
10X TBS buffer	2 M NaCl, 0.5 M Tris-HCL, pH 7.4
TBS-T buffer	0.1% Tween-20, 0.2 M NaCl, 0.05 M Tris-HCL, pH 7.4

Zymography

Table 6-3: Zymography buffer components

	Components
Stacking buffer	4% Acrylamide 0.125 M Tris-HCL pH 6.8, 0.1% SDS and 150 µl of 10% ammonium persulfate (APS) and 20 µl TEMED
Separating buffer	10% Acrylamide 0.462 M Tris-HCL pH 8.8, 1.5 mg/ml substrate, 0.1% SDS, 150 µl of 10% ammonium persulfate (APS) and 15 µl TEMED
Substrate preparation (1.5 mg/ml)	1.5 mg gelatin, 1 ml dH_2O, dissolve at 60 ˚C 1.5 mg casein, 1 ml dH2O 1.5 mg collagen, 0.1 M Acetic acid, dissolve by agitation
10X Electrophoresis buffer	1.92 M glycine, 1% (w/v) SDS and 0.25 M Tris, pH 8.5
Renaturation buffer	2.5% TritonX-100 (make up with distilled water)
Activation buffer	50 mM Tris-HCL pH 7.6, 0.2 NaCl, 5 mM $CaCl_2$

Appendix 2

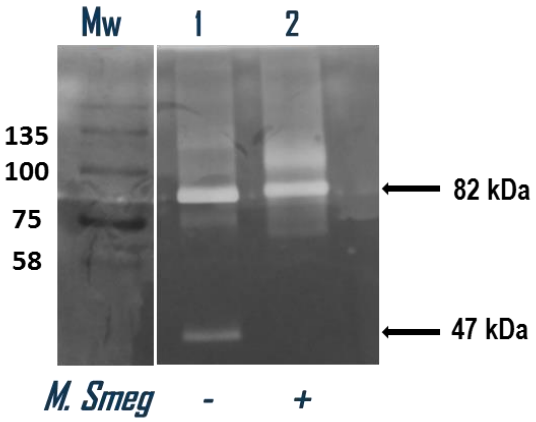

Figure 6-1: Gelatinase activity of the 72-hour <u>secretome</u> at higher protein concentration. The uninfected (Lane 1) and infected (Lane 2) secretome was loaded at a higher total protein concentration. Clear bands representing MMP-9 (82 kDa) and MMP-1 (47 kDa) hydrolysis are indicated.

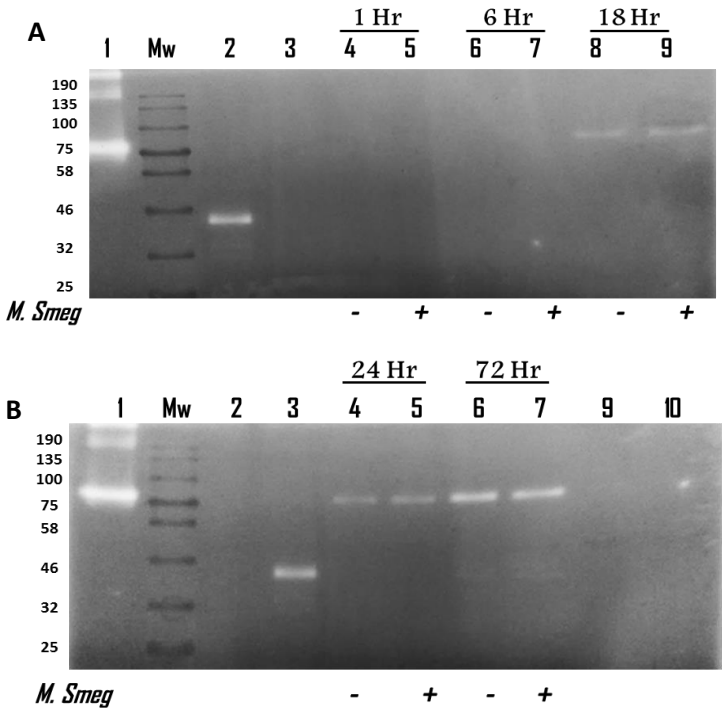

Figure 6-2: Casein hydrolysis by the <u>secretome</u>. The secretome from the second biological replicate of the M. smeg infections was analysed. MMP-9 (Lane 1) and MMP-1 (Lane 2 in gel A and Lane 3 in gel B) were loaded as controls.

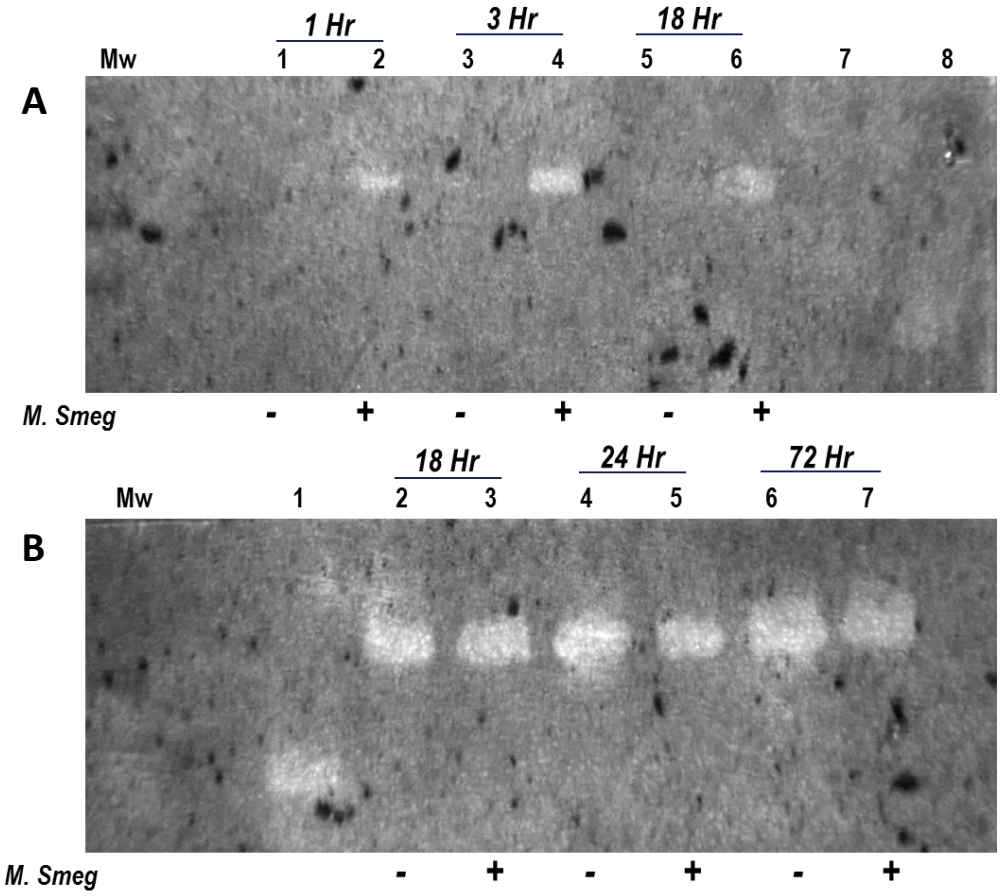

Figure 6-3: Collagenase activity of the secretome. The secretome samples from the second biological replicate of the *M. smeg* infection time point experiments were evaluated by collagen zymography. MMP-1 was loaded as a positive control in lanes 8 and 1 for gel A and B, respectively.

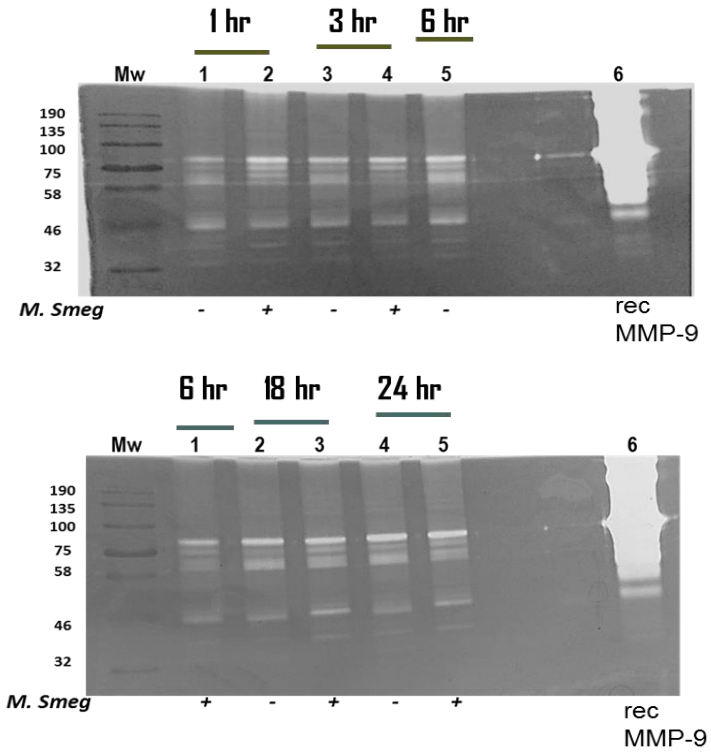

Figure 6-4: Gelatinase activity of the lysate. The lysate samples from the 2nd biological replicate of the *M. smeg* infection time point experiments. Recombinant MMP-9 (Lane 6) was loaded as a control.

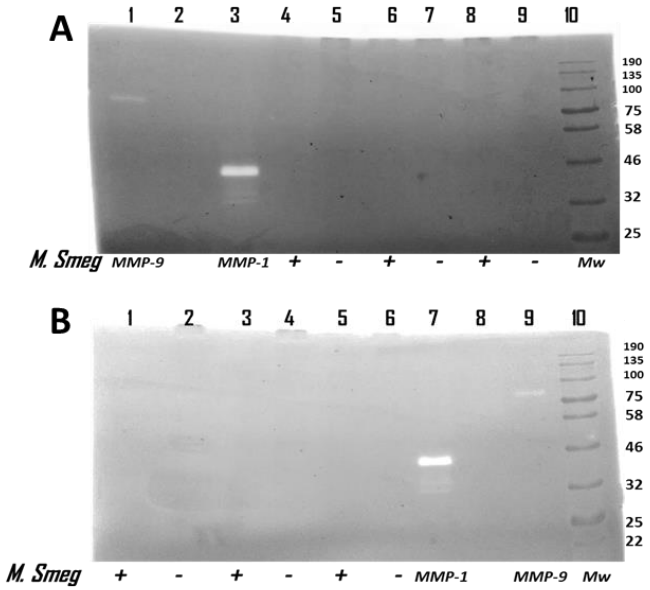

Figure 6-5: Analysis of casein hydrolysis by the lysate. The lysate from the second biological replicate of the *M. smeg* infection time point harvests were loaded in gels A and B. The recombinant MMP-9 and MMP-1 were loaded as controls in lanes 1 and 3 (**A**) and in lanes 9 and 7 (**B**) , respectively.

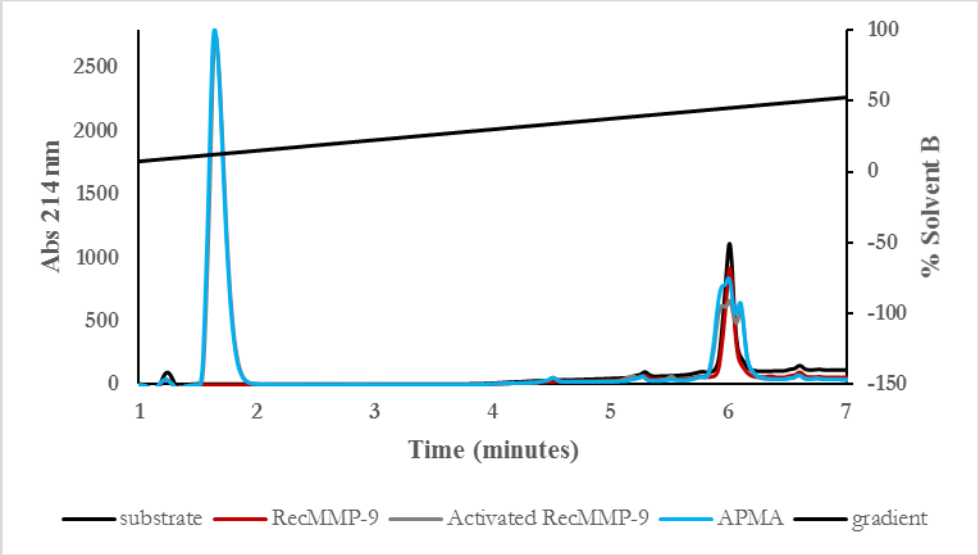

Figure 6-6: HPLC trace of samples used for MALDI analysis. The full chromatograph is represented where the substrate was either incubated with non-activated recombinant MMP-9 (RecMMP-9), APMA-activated MMP-9 (Activated RecMMP-9) or APMA.

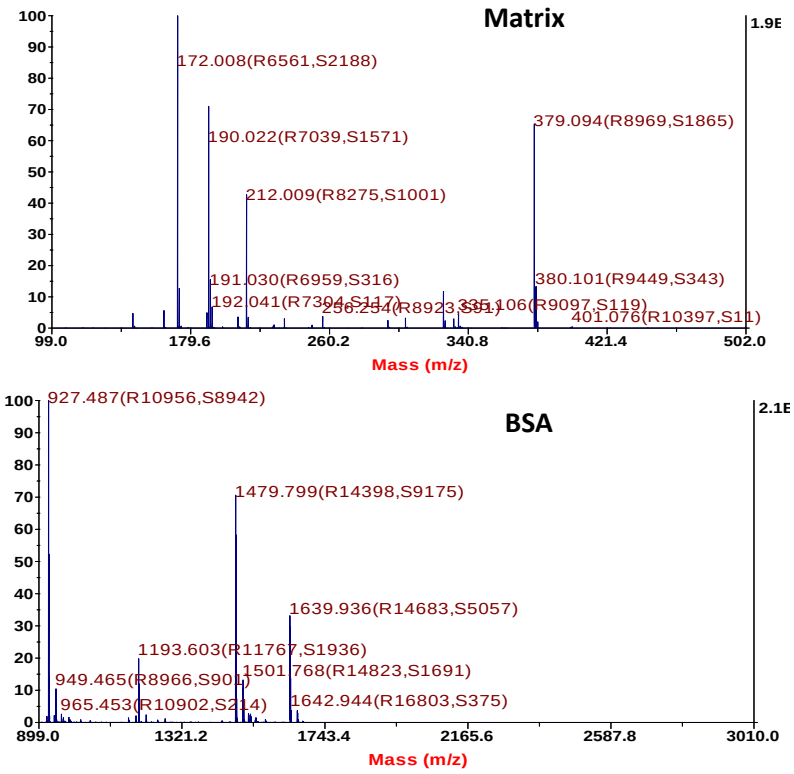

Figure 6-7: Representative MALDI spectra of the matrix and BSA. The α-Cyano-4-hydroxyccinamic acid (α-CHCA) and BSA were included as controls in the analysis of the MMP-9 cleavage products experiment.

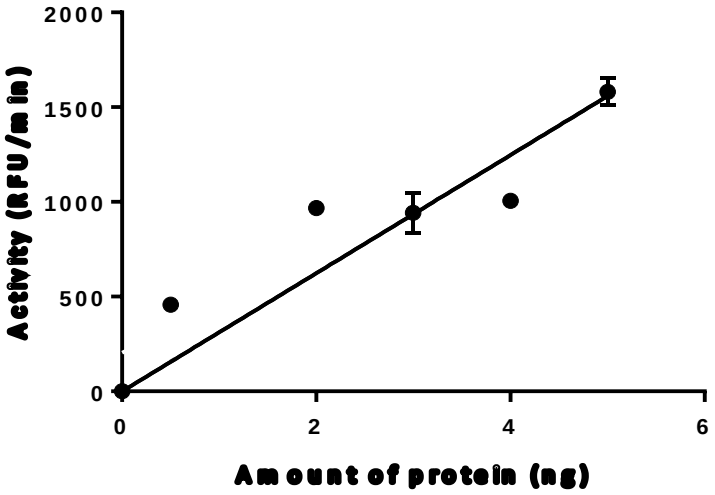

Figure 6-8: MMP-1 standard curve from activity assays.
The R^2 value of the linear regression curve was 0. 82, with standard deviation of ± 539 and y = 311.8x.

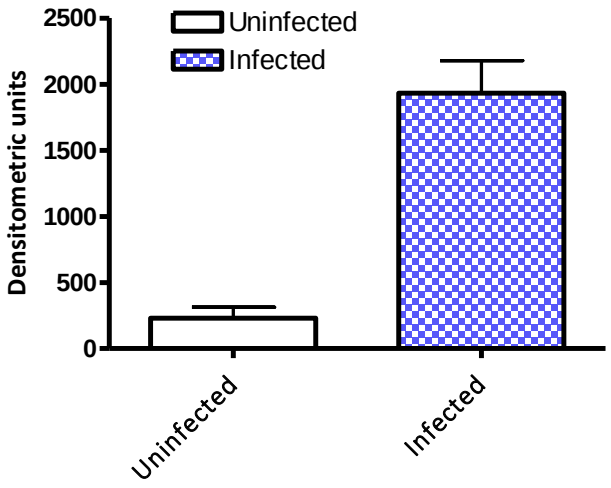

Figure 6-9: Densitometric analysis of the Intracellular MMP-1 western blot. The 72-hour time point lysate was loaded using non-reduced sample buffer. The 47 kDa form was then compared between infected and uninfected by densitometry.

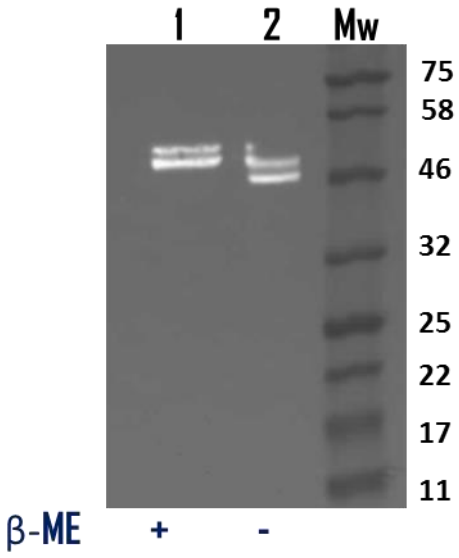

Figure 6-10: Migration pattern of MMP-1 prepared under reducing versus no-reducing conditions. MMP-1 antibody was used to probe the recombinant MMP-1 prepared with reducing (Lane 1) and non-reducing (Lane 2) sample buffer.

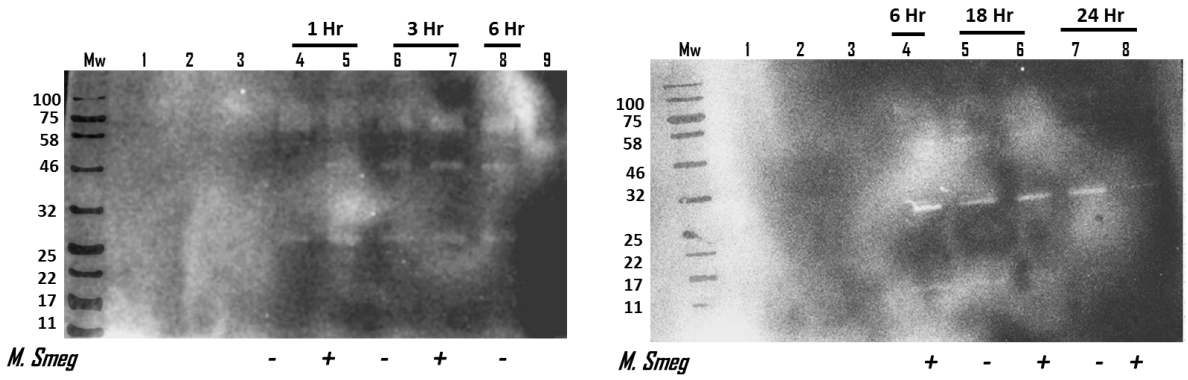

Figure 6-11: Western blot analysis of the <u>intracellular expression</u> of MMP-9. The lysate from the *M. smeg* uninfected and infected lysate time point harvests were prepared using non-reducing sample buffer. The blots were then probed using the proMMP-9 primary antibody. Different time points are indicated with proMMP-9 loaded as a positive control in lanes 1 and 2.

Appendix 3

Proteomics

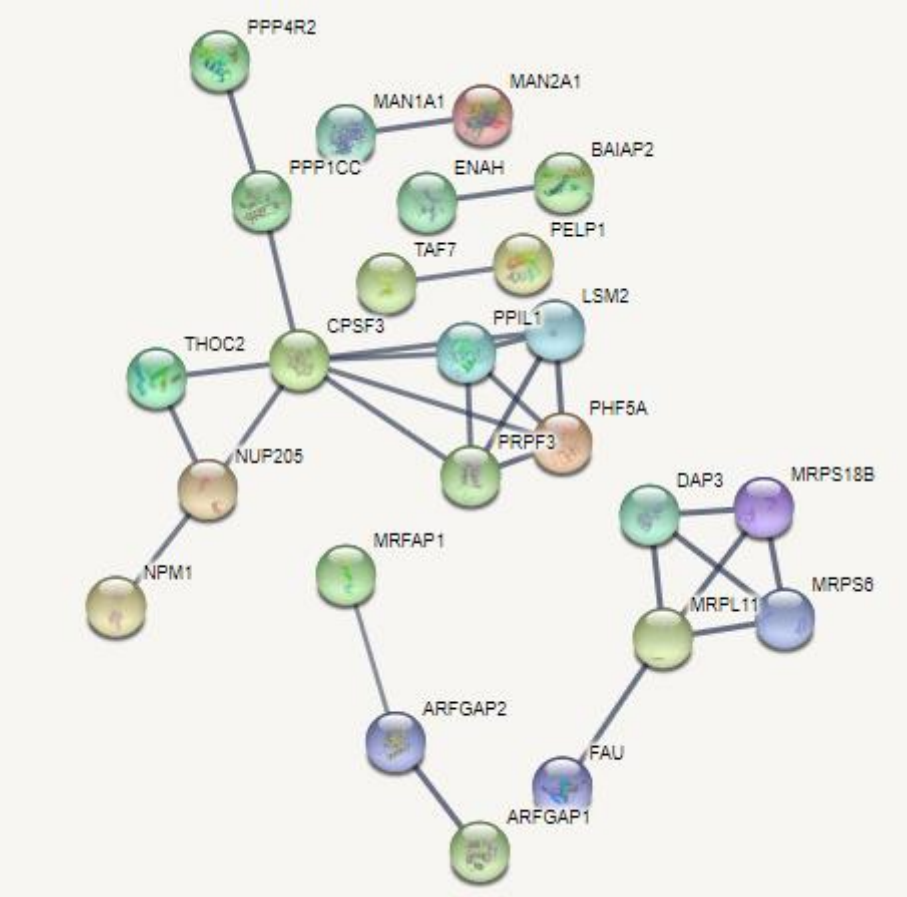

Figure 6-12: The uninfected <u>intracellular proteome</u> forms fewer interactions. The colour coding indicates the different types of proteins.

Table 6-4: Dysregulated proteins secreted by *M. smeg* infected macrophages (two-sample t-test).

These were computed using the two-sample t-test.

Protein ID	Protein Name	Unique Peptides	q-value	Fold Change	Sequence Coverage (%)
O00115	Deoxyribonuclease-2-alpha	2	0	-3.07	6.4
O00584	Ribonuclease T2	8	0	-1.09	38.3
P01023	Alpha-2-macroglobulin	14	0	-1.97	11.1
P06865	Beta-hexosaminidase	5	0	-3.77	9.6
P07355	Annexin A2	11	0	-3.06	50.4
P07686	Beta-hexosaminidase subunit beta	10	0	-3.75	21.9
P08670	Vimentin OS=Homo sapiens G	37	0	-4.25	65.5
P11279	Lysosome-associated membrane glycoprotein 1	1	0	-2.17	2.2
P12109	Collagen alpha-1(VI) chain	14	0	-7.94	16.9
P14780	Matrix metalloproteinase-9	18	0	3.41	28.1
P34741	Syndecan-2	2	0	-4.23	10.9
P36222	Chitinase-3-like protein 1	8	0	-2.83	41.3
P62805	Histone H4	7	0	-6.08	49.5
P62937	Peptidyl-prolyl cis-trans isomerase A	12	0	3.06	70.9
P63313	Thymosin beta-10	2	0	-3.15	63.6
P68104	Putative elongation factor 1-alpha-like 3	22	0	-3.04	53
Q9UBR2	Cathepsin Z	6	0	-2.35	21.8
P06753	Tropomyosin alpha-3 chain	10	0	4.24	39.6

Table 6-5: Dysregulated proteins from the lysate of *M. smeg* infected macrophages (two-sample t-test).

These were computed using the two-sample t-test.

Protein ID	Protein Name	Unique Peptides	q-value	Fold change	Sequence Coverage (%)
P01584	Interleukin-1 beta	7	0	7.12	27.3
P43490	Nicotinamide phosphoribosyltransferase	11	0	5.04	12
P11166	Solute carrier family 2. facilitated glucose transporter member 1	6	0	5.01	3.2
P04179	Superoxide dismutase [Mn]. mitochondrial	4	0	4.50	66.8
A8MVU1	Putative neutrophil cytosol factor 1C	7	0	3.92	21.8
Q96RQ9	L-amino-acid oxidase	5	0	3.17	6.4
B7Z5P7	Leupaxin	3	0	3.05	17.2
B7Z3Z9	Long-chain-fatty-acid--CoA ligase 1	4	0	3.02	9.4
P05362	Intercellular adhesion molecule 1	11	0	2.8	11.8
E5RIJ3	Tumor necrosis factor alpha-induced protein 8	1	0	2.75	23.5
Q9ULC4	Malignant T-cell-amplified sequence 1	3	0	2.73	18.6
P07948	Tyrosine-protein kinase Lyn	7	0	2.63	16.7
P10124	Serglycin	3	0	2.56	35.4
C9JRH2	Regulator of chromosome condensation	3	0	2.55	20.3
O00410	Importin-5	4	0	2.55	33.9
Q9NY12	H/ACA ribonucleoprotein complex subunit 1	3	0	2.54	34.5
Q9NQR4	Omega-amidase NIT2	3	0	2.54	11.3
Q9H4M9	EH domain-containing protein 1	12	0	2.3	3.8
Q03405	Urokinase plasminogen activator surface receptor	8	0	2.21	7.3
A0A087X1W8	Cell adhesion molecule 1	2	0	2.20	35
Q9Y512	Sorting and assembly machinery	4	0	2.17	11.3

	component 50 homolog				
Q13303	Voltage-gated potassium channel subunit beta-2	4	0	2.08	10.9
E5RJ98	Protein NDRG1 OS	1	0	2.05	23.3
P29966	Myristoylated alanine-rich C-kinase substrate	5	0	2.04	47.4
P61224	Ras-related protein Rap-1b	1	0	2.01	15.9
P49915	GMP synthase [glutamine-hydrolyzing]	7	0	2.00	26.3
P13674	Prolyl 4-hydroxylase subunit alpha-1	8	0	1.98	24.5
G3XAJ6	Raft-linking protein. isoform CRA	7	0	1.97	32
Q12913	Receptor-type tyrosine-protein phosphatase eta	4	0	1.97	5.1
S4R456	40S ribosomal protein S15	3	0	1.91	14.9
Q99878	Histone H2A type 1-J	2	0	1.89	29.4
Q8NBZ7	UDP-glucuronic acid decarboxylase 1	1	0	1.88	16.6
O00303	Eukaryotic translation initiation factor 3 subunit F	6	0	1.87	34.6
Q9Y5X1	Sorting nexin-9	6	0	1.86	58
H3BTA2	Serine/threonine-protein phosphatase	3	0	1.85	30.1
E9PEP6	Neuropilin	13	0	1.83	32
Q96P48	Arf-GAP with Rho-GAP domain. ANK repeat and PH domain-containing protein 1	2	0	1.82	28.1
H0YDT8	ER membrane protein complex subunit 7	2	0	1.79	9.1
P40306	Proteasome subunit beta type-10	2	0	1.65	23
P06756	Integrin alpha-V	13	0	1.64	23
P08240	Signal recognition particle receptor subunit alpha	7	0	1.63	45.1
P55795	Heterogeneous nuclear ribonucleoprotein H2	4	0	1.62	12.7
P28482	Mitogen-activated protein kinase 1	3	0	1.59	22.8
Q92769	Histone deacetylase 2	4	0	1.58	15.8

Q96HE7	ERO1-like protein alpha	11	0	1.57	24.8
H0Y4R1	Inosine-5-monophosphate dehydrogenase 2	8	0	1.54	34.4
D6RD47	40S ribosomal protein S23	2	0	1.54	66.9
Q9P2J5	Leucine--tRNA ligase. cytoplasmic	7	0	1.52	18.5
P09543	2.3-cyclic-nucleotide 3-phosphodiesterase	2	0	1.52	12.7
P08754	Guanine nucleotide-binding protein G(k) subunit alpha	3	0	1.50	45.2
P18510	Interleukin-1 receptor antagonist protein	3	0	1.50	21.9
P17858	ATP-dependent 6-phosphofructokinase. liver type	5	0	1.47	23.5
P10155	60 kDa SS-A/Ro ribonucleoprotein	5	0	1.44	15.8
Q15393	Splicing factor 3B subunit 3	9	0	1.44	14.3
P46778	60S ribosomal protein L21	4	0	1.44	37.1
P21964	Catechol O-methyltransferase	4	0	1.43	21.1
Q8WYA6	Beta-catenin-like protein 1	4	0	1.42	12
P08567	Pleckstrin OS	7	0	1.41	15.5
Q96JB2	Conserved oligomeric Golgi complex subunit 3	1	0.0004	1.40	8.6
P31150	Rab GDP dissociation inhibitor alpha	6	0	1.36	26.5
P22102	Trifunctional purine biosynthetic protein adenosine-3	7	0	1.34	23.4
Q4KMQ2	Anoctamin-6	1	0	1.32	29.7
Q96AH8	Ras-related protein Rab-7b	4	0	1.28	11.7
P49354	Protein farnesyltransferase/geranylgeranyltransferase type-1 subunit alpha	9	0	1.28	13
P14780	Matrix metalloproteinase-9	18	0	1.28	14.6
P27701	CD82 antigen	3	0	1.28	14.8
P43034	Platelet-activating factor acetylhydrolase IB subunit alpha	3	0	1.27	23
H7C2R7	Spermine synthase (Fragment)	1	0	1.27	29.9

P07602	Prosaposin	19	0	1.26	19.1
P46977	Dolichyl-diphosphooligosaccharide--protein glycosyltransferase subunit STT3A	5	0	1.25	16.9
P31949	Protein S100-A11	4	0	1.25	9.2
P61020	Ras-related protein Rab-5B	3	0	1.25	28.1
D6RD63	COP9 signalosome complex subunit 4 (Fragment)	3	0	1.24	30.5
D6RFL4	Monocyte differentiation antigen CD14 (Fragment)	3	0	1.24	6.8
O00116	Alkyldihydroxyacetonephosphate synthase. peroxisomal	5	0	1.23	20.2
O00743	Serine/threonine-protein phosphatase 6 catalytic subunit	3	0	1.23	29.5
A0A0A0MR02	Voltage-dependent anion-selective channel protein 2 (Fragment)	12	0	1.21	40
P16278	Beta-galactosidase	3	0	1.21	23.4
Q9Y263	Phospholipase A-2-activating protein OS	2	0	1.20	16.1
Q9Y696	Chloride intracellular channel protein 4	10	0	1.20	8.8
P13995	Bifunctional methylenetetrahydrofolate dehydrogenase/cyclohydrolase. mitochondrial	4	0	1.20	23.2
O00442	RNA 3-terminal phosphate cyclase	4	0	1.20	22.2
O43447	Peptidyl-prolyl cis-trans isomerase H	5	0	1.19	7
P34897	Serine hydroxymethyltransferase. mitochondrial	14	0	1.18	25.7
O43598	2-deoxynucleoside 5-phosphate N-hydrolase 1	4	0	1.16	68.6
A0A087WSW9	Thioredoxin reductase 1. cytoplasmic	11	0	1.16	25.1
B0QYV8	ADP-ribosylation factor GTPase-activating protein 3 (Fragment)	2	0.0004	1.15	10.4
E9PJK1	Tetraspanin OS	3	0	1.15	33.7
E5RHW4	Erlin-2 (Fragment)	9	0	1.14	26.9

P55735	Protein SEC13 homolog	5	0	1.12	36.7
O00186	Syntaxin-binding protein 3	2	0.0004	1.12	27
Q8WX92	Negative elongation factor B	2	0.0004	1.11	7.4
P05141	ADP/ATP translocase 2	4	0	1.11	43.6
P21796	Voltage-dependent anion-selective channel protein 1	16	0	1.11	44.2
Q9HCC0	Methylcrotonoyl-CoA carboxylase beta chain. mitochondrial	5	0	1.10	21.3
O00560	Syntenin-1	2	0	1.09	13.5
Q9BXD5	N-acetylneuraminate lyase	1	0.000	1.09	18
X1WI28	60S ribosomal protein L10 (Fragment)	1	0	1.08	11.4
Q99459	Cell division cycle 5-like protein	5	0	1.07	24.4
Q14566	DNA replication licensing factor MCM6	6	0	1.06	30.4
P56134	ATP synthase subunit f. mitochondrial	3	0	1.05	35.2
Q13573	SNW domain-containing protein 1	4	0	1.05	48.9
P00338	L-lactate dehydrogenase A chain	9	0	1.05	23.1
Q9BUF5	Tubulin beta-6 chain	6	0	1.03604	17.8
Q9Y277	Voltage-dependent anion-selective channel protein 3	6	0	1.02	18.8
H9KV28	Protein diaphanous homolog 1	10	0	1.02	32.9
Q13423	NAD(P) transhydrogenase. mitochondrial	9	0	1.01	40
Q9H7D7	WD repeat-containing protein 26	11	0	1.00	41
P40939	Trifunctional enzyme subunit alpha. mitochondrial	17	0	1.00	7.6
P62995	Transformer-2 protein homolog beta	2	0	0.99	32.1
Q9BX68	Histidine triad nucleotide-binding protein 2. mitochondrial	2	0	0.99	34.6
P04150	Glucocorticoid receptor OS	5	0	0.97	22
Q9UNM6	26S proteasome non-ATPase regulatory subunit 13	10	0	0.97	13.6
P51659	Peroxisomal multifunctional enzyme type 2	16	0	0.97	35.4

P07814	Bifunctional glutamate/proline--tRNA ligase	24	0	0.97	16
A0A087WUD3	Oligosaccharyltransferase complex subunit OSTC	1	0	0.96	11
Q13501	Sequestosome-1	11	0	0.96	15
P31939	Bifunctional purine biosynthesis protein PURH	15	0	0.96	32.6
Q9BW60	Elongation of very long chain fatty acids protein 1	2	0	0.95	32.8
P62081	40S ribosomal protein S7	6	0	0.95	61
I3L1I0	Glyoxalase domain-containing protein 4 (Fragment)	1	0	0.94	25
A0A1W2PNM1	Hydroxyacyl-coenzyme A dehydrogenase. mitochondrial	4	0	0.94	6.5
P07686	Beta-hexosaminidase subunit beta	10	0	0.94	16.2
Q16186	Proteasomal ubiquitin receptor ADRM1	3	0	0.93	15.9
Q15185	Prostaglandin E synthase 3	3	0	0.93	62.1
P62304	Small nuclear ribonucleoprotein E	1	0	0.92	29
K7EK60	Formin-like protein 1	1	0.0004	0.92	44.7
Q8NBS9	Thioredoxin domain-containing protein 5	6	0	0.92	29.4
P35232	Prohibitin	7	0	0.91	21.7
Q13148	TAR DNA-binding protein 43	4	0	0.90	14.4
P48147	Prolyl endopeptidase	8	0	0.90	30.6
P43686	26S proteasome regulatory subunit 6B	11	0	0.89	33.8
P14618	Pyruvate kinase PKM	3	0	0.88	21.2
A6NLH6	Protein cornichon homolog 4	1	0	0.88	5.8
P30520	Adenylosuccinate synthetase isozyme 2	5	0	0.88	7.6
P51571	Translocon-associated protein subunit delta	4	0	0.87	40.2
P05091	Aldehyde dehydrogenase. mitochondrial	8	0	0.87	26.6
P22695	Cytochrome b-c1 complex subunit 2. mitochondrial	8	0	0.87	52.7

E7EVZ5	Prenylcysteine oxidase-like	1	0	0.86	24.8
J3KNF8	Cytochrome b5 type B	4	0	0.86	26.6
Q16658	Fascin	14	0	0.86	13.8
Q9UHA4	Regulator complex protein LAMTOR3	2	0.0004	0.85	36.4
P01034	Cystatin-C	3	0	0.85	39.4
E7EQJ3	HLA class II histocompatibility antigen gamma chain	2	0	0.85	56.7
O43312	Metastasis suppressor protein 1	9	0	0.85	12.6
Q9Y265	RuvB-like 1	18	0	0.85	35.8
H0YKT8	Proteasome subunit beta type (Fragment)	5	0	0.84	18
K7EJE8	Lon protease homolog. mitochondrial	13	0	0.84	39.4
Q8NCW5	NAD(P)H-hydrate epimerase	3	0	0.83	21.9
G3V4W0	Heterogeneous nuclear ribonucleoproteins C1/C2 (Fragment)	4	0	0.82	20.5
P49591	Serine--tRNA ligase. cytoplasmic	15	0	0.82	14.1
P31930	Cytochrome b-c1 complex subunit 1. mitochondrial	10	0	0.82	15.3
M0QZS6	SUMO-activating enzyme subunit 1	7	0	0.82	47.4
P61026	Ras-related protein Rab-10	4	0	0.82	28.4
P25205	DNA replication licensing factor MCM3	5	0	0.81	12
Q5T6H7	Xaa-Pro aminopeptidase 1	7	0	0.81	24.4
P14868	Aspartate--tRNA ligase. cytoplasmic	12	0	0.81	47.1
P30084	Enoyl-CoA hydratase. mitochondrial	7	0	0.81	51.8
E9PMW2	Dr1-associated corepressor	2	0	0.80	10.4
P62820	Ras-related protein Rab-1A	3	0	0.80	57.1
P30101	Protein disulfide-isomerase A3	20	0	0.80	55.3
Q9P0J0	NADH dehydrogenase [ubiquinone] 1 alpha subcomplex subunit 13	4	0	0.80	22.7
Q9BXY0	Protein MAK16 homolog	1	0	0.80	14.4
Q15029	116 kDa U5 small nuclear ribonucleoprotein component	12	0	0.79	10.7

O15126	Secretory carrier-associated membrane protein 1	4	0	0.79	39.1
Q96JJ7	Protein disulfide-isomerase TMX3	6	0	0.79	44.6
Q9BQE3	Tubulin alpha-1C chain	1	0	0.79	33.8
Q86Y82	Syntaxin-12	5	0	0.79	5.9
P30153	Serine/threonine-protein phosphatase 2A 65 kDa regulatory subunit A alpha isoform	9	0	0.78	4.5
A0A286YF22	D-3-phosphoglycerate dehydrogenase	13	0	0.78	12.9
Q9Y6M1	Insulin-like growth factor 2 mRNA-binding protein 2	5	0	0.77	12.1
P55072	Transitional endoplasmic reticulum ATPase	23	0	0.77	23.4
B4DY09	Interleukin enhancer-binding factor 2	8	0	0.77	17.5
O75487	Glypican-4	9	0	0.77	23.5
A0A0A0MS41	Sideroflexin	6	0	0.76	10.3
P43304	Glycerol-3-phosphate dehydrogenase. mitochondrial	8	0	0.76	53
P12236	ADP/ATP translocase 3	4	0	0.75	12.1
A0A087X1W2	Protein arginine N-methyltransferase 1	1	0	0.75	5
Q13043	Serine/threonine-protein kinase 4	5	0	0.74	32.7
O43615	Mitochondrial import inner membrane translocase subunit	4	0	0.74	11.1
Q5JP53	Tubulin beta chain	3	0	0.74	20
P55084	Trifunctional enzyme subunit beta. mitochondrial	10	0	0.74	8.5
Q9BTV4	Transmembrane protein 43	5	0	0.74	2.8
Q96HQ2	CDKN2AIP N-terminal-like protein	1	0	0.74	24
P00558	Phosphoglycerate kinase 1	20	0	0.73	6.1
P57737	Coronin-7	7	0	0.73	4.7
F8VY35	Nucleosome assembly protein 1-like 1 (Fragment)	7	0	0.73	21.7

P16435	NADPH--cytochrome P450 reductase	9	0	0.73	19.9
G3V126	ATPase. H+ transporting. lysosomal 50/57kDa. V1 subunit	2	0	0.72	34.1
Q15758	Neutral amino acid transporter B(0)	4	0	0.72	16.2
Q92598	Heat shock protein 105 kDa	23	0	0.72	23.8
P42025	Beta-centractin	3	0	0.72	20.9
E7EQ72	Transmembrane emp24 domain-containing protein 2 (Fragment)	2	0	0.71	16.9
P49411	Elongation factor Tu. mitochondrial	15	0	0.71	13.7
Q13405	39S ribosomal protein L49. mitochondrial	3	0	0.71	11.3
P55957	BH3-interacting domain death agonist	4	0	0.70	0.4
P04899	Guanine nucleotide-binding protein G(i) subunit alpha	3	0	0.70	10.5
P04406	Glyceraldehyde-3-phosphate dehydrogenase	12	0	0.68	10.6
Q15366	Poly(rC)-binding protein 2	3	0	0.68	42.8
P16615	Sarcoplasmic/endoplasmic reticulum calcium ATPase 2	20	0	0.67	3.2
F5H6X6	Neutral alpha-glucosidase AB	4	0	0.67	21.3
P60900	Proteasome subunit alpha type-6	7	0	0.67	34.1
P78371	T-complex protein 1 subunit beta	22	0	0.67	6.4
P23381	Tryptophan--tRNA ligase. cytoplasmic	9	0	0.67	2.4
E5RI99	60S ribosomal protein L30 (Fragment)	5	0	0.65	18.8
O60506	Heterogeneous nuclear ribonucleoprotein Q	13	0	0.65	14.9
E9PBS1	Multifunctional protein ADE2 (Fragment)	10	0	0.65	24.6
P05388	60S acidic ribosomal protein P0	7	0	0.65	26.4
V9GY93	Transmembrane protein 165 (Fragment)	2	0	0.64	10.5
O95373	Importin-7	11	0	0.64	5.3
F5GZG1	Ras-related protein Rap-1b (Fragment)	1	0	0.64	5.9

P23141	Liver carboxylesterase 1	17	0	0.63	10.3
Q9BS26	Endoplasmic reticulum resident protein 44	11	0	0.63	2.7
Q15019	Septin-2	7	0	0.63	18.8
Q96K17	Transcription factor BTF3 homolog 4	6	0	0.62	4
P56537	Eukaryotic translation initiation factor 6	8	0	0.61	14.6
P08648	Integrin alpha-5	9	0	0.60	3.4
Q04837	Single-stranded DNA-binding protein. mitochondrial	5	0	0.60	7.8
Q16659	Mitogen-activated protein kinase 6	2	0.0003	0.60	16.8
P06576	ATP synthase subunit beta. mitochondrial	22	0	0.60	38.9
O15355	Protein phosphatase 1G	7	0	0.59	11.9
Q13595	Transformer-2 protein homolog alpha	1	0	0.59	8.8
Q9Y6N5	Sulfide:quinone oxidoreductase. mitochondrial	17	0	0.57	8.2
P25705	ATP synthase subunit alpha. mitochondrial	19	0	0.57	25.1
P29350	Tyrosine-protein phosphatase non-receptor type 6	11	0	0.56	24.7
F5H3X6	Prohibitin-2 (Fragment)	3	0	0.56	35.7
P61225	Ras-related protein Rap-2b	2	0	0.56	15.5
P13010	X-ray repair cross-complementing protein 5	16	0	0.56	14.5
O95831	Apoptosis-inducing factor 1. mitochondrial	7	0	0.55	1.8
Q53H82	Endoribonuclease LACTB2	4	0	0.55	18.3
Q15746	Myosin light chain kinase. smooth muscle	1	0.0022	0.54	41.1
G5EA31	Protein transport protein Sec24C	5	0	0.53	1.7
O00299	Chloride intracellular channel protein 1	12	0	0.53	12.2
P26639	Threonine--tRNA ligase. cytoplasmic	12	0	0.53	9.7
Q9H2U2	Inorganic pyrophosphatase 2. mitochondrial	8	0	0.52	17.8

H0YL19	WD repeat-containing protein 61	3	0	0.49	15.6
Q14012	Calcium/calmodulin-dependent protein kinase type 1	9	0	0.49	5.3
P48444	Coatomer subunit delta	7	0	0.46	37.7
O75436	Vacuolar protein sorting-associated protein 26A	6	0	0.42	15.3
H0YE97	Phosphatidylinositol-binding clathrin assembly protein	1	0	0.41	17.8
Q9NR30	Nucleolar RNA helicase 2 OS	11	0	0.37	21.5
P09960	Leukotriene A-4 hydrolase OSB228B227:B243B244B22B103	11	0	0.36	9.7
B0QY90	Eukaryotic translation initiation factor 3 subunit L	5	0	0.24	24.9
Q92896	Golgi apparatus protein 1	7	0	-0.30	21.5
Q15006	ER membrane protein complex subunit 2	4	0	-0.42	3.4
Q8IVJ8	AP20 region protein 1	1	0.0037	-0.45	4.3
Q13347	Eukaryotic translation initiation factor 3 subunit I	3	0	-0.45	11.9
P52292	Importin subunit alpha-1	8	0	-0.51	22.6
A0A0A0MRV0	Ribosome-binding protein 1	12	0	-0.58	37.4
A0A087WWC8	Myelin expression factor 2	1	0.0004	-0.60	32
Q9UJU6	Drebrin-like protein	8	0	-0.60	23.3
O75312	Zinc finger protein ZPR1	7	0	-0.66	23.4
A0A024R4E5	High density lipoprotein binding protein (Vigilin). isoform CRA	11	0	-0.67	11.3
M0QXH0	Thioredoxin. mitochondrial	1	0.0004	-0.72	13.7
Q96I24	Far upstream element-binding protein 3	5	0	-0.73	11.8
Q7Z5R6	Amyloid beta A4 precursor protein-binding family B member 1-interacting protein	11	0	-0.73	10.9
Q92974	Rho guanine nucleotide exchange	6	0	-0.77	14.9

	factor 2				
A0A087X0G7	NF-kappa-B essential modulator	2	0	-0.78	17.2
E9PGC0	Ras GTPase-activating protein 1	5	0	-0.79	18
Q8N573	Oxidation resistance protein 1	6	0	-0.81	14.5
J3KS31	BUB3-interacting and GLEBS motif-containing protein ZNF207 (Fragment)	1	0.0003	-0.87	15.7
F5GWX5	Chromodomain-helicase-DNA-binding protein 4	7	0	-0.94	14.6
Q12965	Unconventional myosin-Ie	4	0	-0.97	37.5
F5H0W4	Bridging integrator 2	7	0	-0.98	13.8
P49006	MARCKS-related protein	4	0	-0.99	8.6
P67809	Nuclease-sensitive element-binding protein 1	10	0	-1.0	19
O60361	Putative nucleoside diphosphate kinase	1	0.0033	-1.05	41.1
B5MCT7	Protein phosphatase 1F	4	0	-1.07	28.8
Q3KQU3	MAP7 domain-containing protein 1	3	0	-1.10	21
E9PKP7	Nucleolar transcription factor 1	9	0	-1.10	6.8
O95104	Splicing factor. arginine/serine-rich 15	3	0	-1.12	27.4
O75368	SH3 domain-binding glutamic acid-rich-like protein	5	0	-1.15	26.5
P11234	Ras-related protein Ral-B	4	0	-1.16	27.7
Q9Y3B9	RRP15-like protein	2	0	-1.20	35.6
H3BRD2	Sulfhydryl oxidase (Fragment)	2	0.0044	-1.20	4.3
Q96FJ2	Dynein light chain 2. cytoplasmic	1	0	-1.23	14.4
H7C2F2	CD99 antigen (Fragment)	2	0	-1.28	4
B0S8I6	Protein FAM50A	4	0	-1.28	59.2
Q9ULZ3	Apoptosis-associated speck-like protein containing a CARD	5	0	-1.32	31.8
B0QYK0	RNA-binding protein EWS	4	0	-1.32	6.4
A2A2D0	Stathmin (Fragment)	3	0	-1.41	9.8
P98082	Disabled homolog 2	12	0	-1.42	15
M0R088	Serine/arginine repetitive matrix	4	0	-1.44	59.7

	protein 1 (Fragment)				
Q7L014	Probable ATP-dependent RNA helicase DDX46	11	0	-1.55	5.4
A0A0U1RQL8	Gelsolin (Fragment)	1	0	-1.56	10.9
Q9UQ35	Serine/arginine repetitive matrix protein 2	7	0	-1.59	40.2
B1AMS2	Septin 6. isoform CRA	2	0	-1.61	10.9
P21757	Macrophage scavenger receptor types I and II	8	0	-1.65	6.5
O75410	Transforming acidic coiled-coil-containing protein 1	7	0	-1.70	20.6
E7ETA6	Pericentriolar material 1 protein	17	0	-1.76	13
Q8IVD9	NudC domain-containing protein 3	2	0	-1.89	14
H3BV80	RNA-binding protein with serine-rich domain 1	4	0	-2.06	20.9
J3QQK6	Myelin basic protein	3	0	-2.36	23.4
Q14814	Myocyte-specific enhancer factor 2D	3	0	-2.43	53.3
P17096	High mobility group protein HMG-I/HMG-Y	5	0	-4.03	1.8

Table 6-6: Dysregulated proteins from *M. smeg* infected macrophages (volcano plots).
These were computed using volcano plots.

	Protein ID	Protein Name	Unique Peptides	q-value	Fold Change	Sequence Coverage (%)
Media	P62805	Histone H4	7	0	-6.08	49.5
Lysate	**Protein ID**	**Protein Name**	**Unique Peptides**	**q-value**	**Fold Change**	**Sequence Coverage (%)**
	E9PEP6	Neuropilin	13	0	1.83	23.5
	P05362	Intercellular adhesion molecule 1	11	0	2.81	24.8
	P07602	Prosaposin	19	0	1.27	45.2
	P14780	Matrix metalloproteinase-9	18	0	1.28	28.1
	P18510	Interleukin-1 receptor antagonist protein	3	0	1.51	23.2
	Q03405	Urokinase plasminogen activator surface receptor	8	0	2.21	39.1

Table 6-7: Dysregulated proteins secreted by LAM-stimulated macrophages (two-sample t test).
These were computed using the two-sample t-test.

Protein ID	Protein Name	Unique Peptides	q-value	Fold Change	Sequence Coverage (%)
Q00610	Clathrin heavy chain 1	42	0	3.3	36.9
P78527	DNA-dependent protein kinase catal	76	0	2.55	24.4
P25705	ATP synthase subunit alpha. mitochondrial	21	0	2.54	49.2
P62979	Ubiquitin-40S ribosomal protein S2	6	0	2.2	40.4
P04406	Glyceraldehyde-3-phosphate dehydrogenase	14	0	2.19	63.6
P19105	Myosin regulatory light chain 12A	3	0	2.09	24
P05107	Integrin beta	26	0	1.67	48.5
P62753	40S ribosomal protein S6	4	0	1.64	18.9
Q99832	T-complex protein 1 subunit eta	21	0	1.42	56.2

P62241	40S ribosomal protein S8	7	0	1.29	41.3
P13639	Elongation factor 2	38	0	1.2	55
P61158	Actin-related protein 3	17	0	1.13	47.8
Q09666	Neuroblast differentiation-associated protein	108	0	1.1	40.2
P02751	Fibronectin	22	0	0.99	13.3
P18084	Integrin beta-5	4	0	0.94	6.6
A0A087WXM6	60S ribosomal protein L17	4	0	0.92	29.6
P62805	Histone H4	9	0	0.83	49.5
O15511	Actin-related protein 2/3 complex	5	0	0.81	52.3
P11413	Glucose-6-phosphate 1-dehydrogenase	16	0	0.81	40
O75367	Core histone macro-H2A.1	12	0	0.79	38.2
P08238	Heat shock protein HSP 90-beta	21	0	0.77	33.3
P38571	Lysosomal acid lipase/cholesteryl ester hydrolase	3	0	0.76	14.1
P52565	Rho GDP-dissociation inhibitor 1	6	0	0.68	39.9
E9PQQ4	Heat shock cognate 71 kDa protein	1	0	0.48	6.6
P00918	Carbonic anhydrase 2	13	0	0.46	55.8
Q12906	Interleukin enhancer-binding factor 3	18	0	-0.76	27.4
P06454	Prothymosin alpha	4	0	-0.91	26.2
Q9BT09	Protein canopy homolog 3	5	0	-1.39	19.4

Table 6-8: Dysregulated lysate proteins harvested from LAM-stimulated macrophages (two-sample t-test).
These were computed using the two-sample t-test.

Protein ID	Protein Name	q-value	Fold Change	Unique Peptides	Sequence Coverage (%)
Q6DKJ4	Nucleoredoxin	0	4.17	3	11
Q9Y277	Voltage-dependent anion-selective channel protein 3	0	3.72	8	43.5
Q01970	1-phosphatidylinositol 4.5-bisphosphate phosphodiesterase beta-3	0	3.67	3	4.6
O60784	Target of Myb protein 1	0	3.50	8	32.1
Q9C0H2	Protein tweety homolog 3	0	3.41	1	2.7
Q99436	Proteasome subunit beta type-7	0	3.37	2	10.8
O43592	Exportin-T	0	3.37	5	7.2
P54725	UV excision repair protein RAD23 homolog A	0	3.32	2	15.2
Q9HBI0	Gamma-parvin	0	3.31	5	20.2
P61586	Transforming protein RhoA	0	3.26	2	18.7
S4R456	40S ribosomal protein S15 (Fragment)	0	3.16	1	27.9
K7EJ57	Mitochondrial import receptor subunit TOM40 homolog (Fragment)	0	3.12	3	36
Q9NRX4	14 kDa phosphohistidine phosphatase	0	3.11	2	25.6
Q92890	Ubiquitin recognition factor in ER-associated degradation protein 1	0	3.09	3	16.9
E9PJ81	UBX domain-containing protein 1 (Fragment)	0	3.06	3	22.1
Q7L1Q6	Basic leucine zipper and W2 domain-containing protein 1	0	3.01	5	13.1
P45880	Voltage-dependent anion-selective channel protein 2	0	3.00	13	61.6
E7ETC2	Serine/threonine-protein phosphatase	0	2.99	2	9
Q8N6M0	OTU domain-containing protein 6B	0	2.94	2	10.2

P49721	Proteasome subunit beta type-2	0	2.86	7	41.3
Q9NR31	GTP-binding protein SAR1a	0	2.86	3	27.8
Q5T0R9	Adenylyl cyclase-associated protein 1 (Fragment)	0	2.81	1	8.4
P61224	Ras-related protein Rap-1b	0	2.80	1	14.1
D6RG39	OCIA domain-containing protein 1 (Fragment)	0	2.79	2	17.5
Q96HQ2	CDKN2AIP N-terminal-like protein	0	2.79	1	15.5
Q9H0U4	Ras-related protein Rab-1B	0	2.78	4	31.3
Q9P0J7	E3 ubiquitin-protein ligase KCMF1	0	2.75	1	4.5
Q9BW60	Elongation of very long chain fatty acids protein 1	0	2.74	2	9.7
F8W1W1	WASH complex subunit 4 (Fragment)	0	2.70	2	23.3
P20645	Cation-dependent mannose-6-phosphate receptor	0	2.69	2	11.6
A0A087WU65	Vacuolar protein sorting-associated protein 45	0	2.69	3	7.6
Q96CN7	Isochorismatase domain-containing protein 1	0	2.67	5	24.2
P04632	Calpain small subunit 1	0	2.63	7	34.7
P49407	Beta-arrestin-1	0	2.63	3	12.7
Q99943	1-acyl-sn-glycerol-3-phosphate acyltransferase alpha	0	2.63	1	7.4
M0R1B5	Acetolactate synthase-like protein (Fragment)	0	2.61	2	21.8
Q9BRF8	Serine/threonine-protein phosphatase CPPED1	0	2.59	6	26.8
E9PKH6	NADH dehydrogenase [ubiquinone] iron-sulfur protein 8. mitochondrial	0	2.59	2	19.6
Q05639	Elongation factor 1-alpha 2	0	2.58	1	6
Q96S44	TP53-regulating kinase	0	2.56	2	15.4
P62314	Small nuclear ribonucleoprotein Sm D1	0	2.55	4	54.6
E7EQ72	Transmembrane emp24 domain-containing protein 2 (Fragment)	0	2.53	2	16.9

E9PJ95	COMM domain-containing protein 9	0	2.51	1	8.6
P35270	Sepiapterin reductase	0	2.48	2	13
P30153	Serine/threonine-protein phosphatase 2A 65 kDa regulator	0	2.43	11	26.5
Q9ULZ3	Apoptosis-associated speck-like protein containing a CAR	0	2.42	6	28.2
P45974	Ubiquitin carboxyl-terminal hydrolase 5	0	2.42	9	16
P48163	NADP-dependent malic enzyme	0	2.41	6	14.9
A0A024RA52	Proteasome subunit alpha type	0	2.40	3	23.9
F8VZN8	Protein phosphatase 1 regulatory subunit 12A (Fragment)	0	2.38	3	7.4
Q05209	Tyrosine-protein phosphatase non-receptor type 12	0	2.37	5	11.9
C9JDE9	3-ketoacyl-CoA thiolase. peroxisomal	0	2.37	4	18
Q93009	Ubiquitin carboxyl-terminal hydrolase 7	0	2.35	13	19.4
P46821	Microtubule-associated protein 1B	0	2.35	11	7.1
A0A1B0GWF8	Adenylosuccinate lyase (Fragment)	0	2.34	3	12.7
D6RD69	GTP-binding protein SAR1b (Fragment)	0	2.33	2	25.3
E7EMB1	Switch-associated protein 70	0	2.31	7	21.6
P49354	Protein farnesyltransferase/geranylgeranyltransferase type-1 subunit alpha	0	2.31	6	22.7
P48059	LIM and senescent cell antigen-like-containing domain protein 1	0	2.30	5	18.8
P47813	Eukaryotic translation initiation factor 1A. X-chromosome	0	2.29	2	17.4
A0A1B0GTK8	Tumor necrosis factor alpha-induced protein 8-like protein 3	0	2.29	4	26.5
P46734	Dual specificity mitogen-activated protein kinase kinase	0	2.28	2	9.2
P60953	Cell division control protein 42 homolog	0	2.27	2	14.7
Q16762	Thiosulfate sulfur transferase	0	2.27	2	10.8
Q96A33	Coiled-coil domain-containing protein 47	0	2.26	6	20.1
D6RIZ4	Major facilitator superfamily domain-	0.000	2.26	1	3.7

	containing protein	4			
P21796	Voltage-dependent anion-selective channel protein 1	0	2.25	14	64
F8VXI1	NADH dehydrogenase [ubiquinone] 1 alpha subcomplex subunit	0.0021	2.25	1	14.5
J3KS22	L-xylulose reductase (Fragment)	0	2.24	6	39
F5H6Y0	Vacuolar protein sorting-associated protein 33A	0	2.23	1	8.6
O43920	NADH dehydrogenase [ubiquinone] iron-sulfur protein 5	0	2.22	1	11.3
E9PQX9	Dr1-associated corepressor	0	2.22	4	30.8
P07204	Thrombomodulin	0	2.22	3	11.1
Q13740	CD166 antigen	0	2.22	13	32.9
Q96AQ6	Pre-B-cell leukemia transcription factor-interacting protein 1	0	2.21	3	5.1
O94826	Mitochondrial import receptor subunit TOM70	0	2.19	11	35.2
Q5T196	FAD synthase	0	2.19	3	9.6
H7C5S0	Actin-like protein 6A (Fragment)	0	2.18	4	39.8
C9JP16	Cartilage-associated protein	0	2.18	3	10.6
P62266	40S ribosomal protein S23	0	2.17	3	34.3
P61758	Prefoldin subunit 3	0	2.17	3	21.3
O60711	Leupaxin	0	2.15	3	11.4
Q13185	Chromobox protein homolog 3	0	2.15	5	36.1
A0A087X1K9	Acyl-protein thioesterase 1S	0	2.14	4	33.7
P08758	Annexin A5	0	2.12	11	50
P62081	40S ribosomal protein S7	0	2.11	6	46.9
Q15121	Astrocytic phosphoprotein PEA-15	0	2.08	5	60
J3QL26	Serine/threonine-protein phosphatase 4 regulatory subuni	0	2.07	2	18.5
Q8TBQ9	Protein kish-A OS	0.0013	2.07	1	12.5
P20701	Integrin alpha-L	0	2.07	5	6.8

P15289	Arylsulfatase A	0	2.05	4	12.6
Q15555	Microtubule-associated protein RP/EB family member 2	0	2.05	3	14.7
P18031	Tyrosine-protein phosphatase non-receptor type 1	0	2.04	4	11
Q13636	Ras-related protein Rab-31	0	2.02	4	32
P31949	Protein S100-A11	0	2.01	3	32.4
P43304	Glycerol-3-phosphate dehydrogenase. mitochondrial	0	2.01	8	15
O14933	Ubiquitin/ISG15-conjugating enzyme E2 L6	0	1.99	1	9.8
C9J8R4	DCN1-like protein (Fragment)	0	1.99	2	26.6
X6RDA4	Paraspeckle component 1 (Fragment)	0	1.99	3	21.8
P61289	Proteasome activator complex subunit 3	0	1.99	4	22.8
Q08J23	tRNA (cytosine(34)-C(Khan1 et al.))-methyltransferase	0	1.98	7	14.7
O14617	AP-3 complex subunit delta-1	0	1.97	5	7.3
Q10471	Polypeptide N-acetylgalactosaminyltransferase 2	0	1.96	5	15.4
A6PVH9	Copine-1	0	1.94	6	19.1
Q02750	Dual specificity mitogen-activated protein kinase kinase	0	1.93	4	22.1
P48960	CD97 antigen	0	1.92	7	16.2
M0R0F0	40S ribosomal protein S5 (Fragment)	0	1.92	5	37
Q86UP2	Kinectin	0	1.91	13	14.8
B0QY91	MICAL-like protein 1 (Fragment)	0	1.90	1	7
P47985	Cytochrome b-c1 complex subunit Rieske. mitochondrial	0	1.90	3	21.5
A0A087WUN7	SRA stem-loop-interacting RNA-binding protein. mitochondrial	0	1.90	3	41.3
P61026	Ras-related protein Rab-10	0	1.86	4	24.5
O00264	Membrane-associated progesterone receptor component 1	0	1.85	3	27.2
Q6XQN6	Nicotinate phosphoribosyltransferase	0	1.85	8	25.3

P63104	14-3-3 protein zeta/delta	0	1.84	14	62
H7C0V0	m-AAA protease-interacting protein 1. mitochondrial (Fragment)	0	1.84	1	4.4
P61421	V-type proton ATPase subunit d 1	0	1.83	6	30.8
F8VYE8	Serine/threonine-protein phosphatase	0	1.82	2	12.2
P60228	Eukaryotic translation initiation factor 3 subunit E	0	1.81	7	20.9
P07355	Annexin A2	0	1.80	17	55.8
Q9UJY5	ADP-ribosylation factor-binding protein GGA1	0	1.75	3	10.3
Q15067	Peroxisomal acyl-coenzyme A oxidase 1	0	1.75	11	29.4
P13861	cAMP-dependent protein kinase type II-alpha regulatory s	0	1.74	7	24.8
O75663	TIP41-like protein	0	1.74	2	10.7
Q07666	KH domain-containing. RNA-binding. signal transduction-associated protein 1	0	1.73	3	9.7
P01023	Alpha-2-macroglobulin	0	1.73	18	15.2
Q10567	AP-1 complex subunit beta-1	0	1.73	8	12.8
O75607	Nucleoplasmin-3	0	1.73	2	17.4
Q5T8U5	Surfeit 4	0	1.72	4	26.9
Q5R3B4	Mitochondrial pyruvate carrier (Fragment)	0.0013	1.72	1	9.5
P30084	Enoyl-CoA hydratase. mitochondrial	0	1.72	9	45.2
Q16666	Gamma-interferon-inducible protein 16	0	1.72	5	11.3
P38606	V-type proton ATPase catalytic subunit A	0	1.71	15	40
O00764	Pyridoxal kinase	0	1.69	6	30.4
B4E0K5	Mitogen-activated protein kinase	0	1.68	6	34.6
G3V1U5	Golgi transport 1 homolog B (S. cerevisiae). isoform CRA	0	1.67	1	18.9
O75915	PRA1 family protein 3	0	1.67	3	20.7
Q9BWF3	RNA-binding protein 4	0	1.66	3	14.3
O75947	ATP synthase subunit d. mitochondrial	0	1.66	7	59

Q93034	Cullin-5	0	1.65	2	4.9
H7C089	Tetratricopeptide repeat protein 38 (Fragment)	0.0021	1.64	1	7.6
Q15397	Pumilio homolog 3	0	1.64	2	4.2
P32119	Peroxiredoxin-2	0	1.64	8	48.5
P27348	14-3-3 protein theta	0	1.63	9	45.3
P52888	Thimet oligopeptidase	0	1.63	13	26.3
J3KMY5	Epididymal secretory protein E1	0	1.63	5	46.6
Q9Y678	Coatomer subunit gamma-1	0	1.62	23	42.2
Q14240	Eukaryotic initiation factor 4A-II	0	1.62	9	30.5
J3QQK6	Myelin basic protein	0	1.62	2	15.8
Q9H4M9	EH domain-containing protein 1	0	1.62	6	17.8
P05455	Lupus La protein	0	1.60	13	37.5
Q969S3	Zinc finger protein 622	0	1.59	2	6.5
Q9P0J0	NADH dehydrogenase [ubiquinone] 1 alpha subcomplex subunit	0	1.59	2	20.1
P09543	2.3-cyclic-nucleotide 3-phosphodiesterase	0	1.58	4	14.7
A0A0B4J2A4	3-ketoacyl-CoA thiolase. mitochondrial	0	1.58	5	26.4
Q13724	Mannosyl-oligosaccharide glucosidase	0	1.58	5	8.2
P06748	Nucleophosmin	0	1.57	9	41.8
P61981	14-3-3 protein gamma	0	1.57	5	33.2
P30085	UMP-CMP kinase	0	1.56	6	35.7
A5YKK6	CCR4-NOT transcription complex subunit 1	0.0059	1.55	2	0.9
H7C3C4	Anion exchange protein (Fragment)	0	1.55	2	5.1
O15145	Actin-related protein 2/3 complex subunit 3	0	1.54	4	32
P31946	14-3-3 protein beta/alpha	0	1.53	7	46.7
P62191	26S proteasome regulatory subunit 4	0	1.52	11	34.8
A0A1W2PRL9	Transcription elongation factor A protein 1	0	1.52	5	28.6

Q9Y263	Phospholipase A-2-activating protein	0	1.51	4	8.3
Q9Y371	Endophilin-B1	0	1.49	2	7.1
P49756	RNA-binding protein 25	0	1.48	4	6.8
P05362	Intercellular adhesion molecule 1	0	1.47	8	20.3
Q96HY6	DDRGK domain-containing protein 1	0	1.47	5	30.9
P04179	Superoxide dismutase [Mn]. mitochondrial	0	1.45	4	19.8
P61769	Beta-2-microglobulin	0	1.44	3	35.3
P62834	Ras-related protein Rap-1A OS	0	1.43	4	29.3
P62258	14-3-3 protein epsilon	0	1.43	16	64.3
P00403	Cytochrome c oxidase subunit 2	0	1.42	4	24.7
Q9UL46	Proteasome activator complex subunit 2	0	1.42	8	48.1
Q15050	Ribosome biogenesis regulatory protein homolog	0	1.40	3	14.5
H3BQZ7	HCG2044799	0	1.40	10	22
Q99878	Histone H2A type 1-J	0	1.40	1	14.8
Q27J81	Inverted formin-2	0	1.39	16	22.4
Q9Y376	Calcium-binding protein 39	0	1.39	6	20.5
Q8TAQ2	SWI/SNF complex subunit SMARCC2	0	1.39	6	7
P28070	Proteasome subunit beta type-4	0	1.38	6	37.9
Q9ULV4	Coronin-1C	0	1.36	11	33.8
P33241	Lymphocyte-specific protein 1	0	1.35	4	26.3
Q9UL25	Ras-related protein Rab-21	0	1.34	4	25.3
P31146	Coronin-1A	0	1.34	10	31.7
Q00722	1-phosphatidylinositol 4.5-bisphosphate phosphodiesteras beta-2	0	1.33	7	7.9
X1WI28	60S ribosomal protein L10 (Fragment)	0	1.32	1	13.5
P55072	Transitional endoplasmic reticulum ATPase	0	1.31	28	50
P35637	RNA-binding protein FUS	0	1.30	5	18.6
P55957	BH3-interacting domain death agonist	0	1.29	5	44.1

K7EJE8	Lon protease homolog. mitochondrial	0	1.29	17	31.1
Q05823	2-5A-dependent ribonuclease	0	1.28	1	1.2
Q8WX92	Negative elongation factor B	0	1.28	1	1.7
A0A0A0MTI6	Elongation of very long chain fatty acids protein	0	1.26	1	5
P56134	ATP synthase subunit f. mitochondrial	0	1.25	3	39.4
P08133	Annexin A6	0	1.25	13	25
P11234	Ras-related protein Ral-B	0	1.25	4	14.6
P50552	Vasodilator-stimulated phosphoprotein	0	1.24	10	32.4
Q13148	TAR DNA-binding protein 43	0	1.23	5	25.6
D6R9P3	Heterogeneous nuclear ribonucleoprotein A/B	0	1.22	5	21.8
C9J3L8	Translocon-associated protein subunit alpha	0	1.22	3	12.8
Q9Y679	Ancient ubiquitous protein 1	0	1.22	4	12.8
Q9P0L0	Vesicle-associated membrane protein-associated protein	0	1.22	2	13.7
M0QZS6	SUMO-activating enzyme subunit 1	0	1.21	6	40.4
A8MVU1	Putative neutrophil cytosol factor 1C	0	1.20	2	9.3
Q9BWD1	Acetyl-CoA acetyltransferase. cytosolic	0	1.20	6	30.2
P27797	Calreticulin	0	1.18	19	68.1
O14773	Tripeptidyl-peptidase 1	0	1.18	9	23.6
H3BUX2	Cytochrome b5 type B	0	1.18	4	52.9
Q9NY65	Tubulin alpha-8 chain	0	1.16	3	10.9
P35268	60S ribosomal protein L22	0	1.15	3	39.1
P54578	Ubiquitin carboxyl-terminal hydrolase 14	0	1.15	6	19
A0A1W2PR68	Malic enzyme	0	1.15	10	27.7
P31939	Bifunctional purine biosynthesis protein PURH	0	1.13	20	51.5
P60174	Triosephosphate isomerase	0	1.13	12	58.7
P50995	Annexin A11	0	1.11	8	19.8
Q9BR76	Coronin-1B	0	1.10	8	23.1

A0A087X1W2	Protein arginine N-methyltransferase 1	0	1.08	1	10.9
Q32Q12	Nucleoside diphosphate kinase	0	1.08	4	18.2
Q9BXP5	Serrate RNA effector molecule homolog	0	1.07	6	12.6
Q86UE4	Protein LYRIC	0	1.07	10	28.7
P12277	Creatine kinase B-type	0	1.06	10	44.9
B4DY09	Interleukin enhancer-binding factor 2	0	1.06	11	48
Q14690	Protein RRP5 homolog	0	1.06	4	2.9
Q9Y3L3	SH3 domain-binding protein 1	0	1.06	1	2.6
O14828	Secretory carrier-associated membrane protein 3	0	0.99	2	8.6
P13498	Cytochrome b-245 light chain	0	0.98	1	15.9
O95433	Activator of 90 kDa heat shock protein ATPase homolog 1	0	0.96	8	38.5
O14579	Coatomer subunit epsilon	0	0.93	8	51
Q9Y4E8	Ubiquitin carboxyl-terminal hydrolase 15	0	0.89	3	4
P61009	Signal peptidase complex subunit 3	0	0.84	2	12.8
Q02218	2-oxoglutarate dehydrogenase. mitochondrial	0	0.84	18	24.6
P12955	Xaa-Pro dipeptidase	0	0.75	7	18.1
P08708	40S ribosomal protein S17	0	0.71	4	41.5
P55210	Caspase-7	0	0.69	2	10.9
Q96KC8	DnaJ homolog subfamily C member 1	0.0029	0.63	2	4.2
Q6P2E9	Enhancer of mRNA-decapping protein 4	0	-0.36	8	9
P06730	Eukaryotic translation initiation factor 4E	0	-0.85	5	29.5
A0A087X2D0	Serine/arginine-rich-splicing factor 3	0	-0.91	2	22.1
P08621	U1 small nuclear ribonucleoprotein 70 kDa	0	-0.92	5	19
P50416	Carnitine O-palmitoyltransferase 1. liver isoform	0	-1.03	7	10.2
Q71UI9	Histone H2A.V	0	-1.16	2	18.8
P26447	Protein S100-A4	0	-1.27	4	35.6

F5GWH5	Transmembrane protein 258	0.0044	-1.33	1	16.3
P37837	Transaldolase	0	-1.39	10	30.3
Q8TCJ2	Dolichyl-diphosphooligosaccharide--protein glycosyltransferase subunit STT3B	0	-1.43	4	5.1
A0A024R4M0	40S ribosomal protein S9	0	-1.44	6	26.3
Q9HAB8	Phosphopantothenate--cysteine ligase	0	-1.48	8	26.7
E7ETA6	Pericentriolar material 1 protein	0	-1.53	11	7.9
Q9Y3C8	Ubiquitin-fold modifier-conjugating enzyme 1	0	-1.72	2	11.4
Q8TEM1	Nuclear pore membrane glycoprotein 210	0	-1.92	7	5.7
P21266	Glutathione S-transferase Mu 3	0	-1.96	5	28
P04181	Ornithine aminotransferase. mitochondrial	0	-2.02	8	25.1
H0YN26	Acidic leucine-rich nuclear phosphoprotein 32 family member A	0	-2.18	3	18.6
Q8N573	Oxidation resistance protein 1	0	-2.24	4	7.3
P62851	40S ribosomal protein S25	0	-2.30	4	24
P05386	60S acidic ribosomal protein P1	0	-2.39	2	36.8
Q9NRH3	Tubulin gamma-2 chain	0	-2.55	3	13.1
C9JA28	Translocon-associated protein subunit gamma	0	-2.60	1	8
Q16401	26S proteasome non-ATPase regulatory subunit 5	0	-2.63	4	10.5
P11142	Heat shock cognate 71 kDa protein	0	-2.63	2	5.1
Q5T0I0	Gelsolin (Fragment)	0	-3.02	2	3.8

Table 6-9: Dysregulated proteome from LAM-stimulated macrophages (volcano plots).
These were calculated using the volcano plots.

	Protein ID	Protein Name	Unique Peptides	q-value	Fold Change	Sequence Coverage (%)
Media	P62979	Ubiquitin-40S ribosomal protein S27a	6	0	2.20	40.4
	P78527	DNA-dependent protein kinase catalytic subunit	76	0	2.55	24.4
	Q00610	Clathrin heavy chain 1	42	0	3.30	44.5
Lysate	**Protein ID**	**Protein Name**	**Unique Peptides**	**q-value**	**Fold Change**	**Sequence Coverage (%)**
	P45880	Voltage-dependent anion-selective channel protein 2	13	0	3.00	61.6
	P54725	UV excision repair protein RAD23 homolog A	2	0	3.32	15.2
	P61586	Transforming protein RhoA	2	0	3.26	18.7
	Q16401	26S proteasome non-ATPase regulatory subunit 5	4	0	-2.63	10.5
	C9JA28	Translocon-associated protein subunit gamma	1	0	-2.60	8
	Q5T0I0	Gelsolin (Fragment)	2	0	-3.02	3.8